Inhibition of Ras using Affimer reagents

Katarzyna Zaneta Haza

Submitted in accordance with the requirements for the degree of
Doctor of Philosophy

The University of Leeds
Faculty of Biological Sciences
School of Molecular and Cellular Biology

June 2019

The candidate confirms that the work submitted is his/her own and that appropriate credit has been given where reference has been made to the work of others.

This copy has been supplied on the understanding that it is copyright material and that no quotation from the thesis may be published without proper acknowledgement.

Acknowledgements

Abstract

Ras proteins are small GTPases that are mutationally activated in around 30% of all human cancers. Oncogenic mutations in Ras trigger uncontrolled cellular differentiation and division through uninhibited Ras-GTP signalling. Despite major efforts in developing inhibitors, lack of treatments directly targeting Ras in cancer led to the current assumption that Ras is undruggable. A new approach, which involves use of biologics, have shown great potential for development of Ras inhibitors, as demonstrated by recent increase in the number of antibody mimetic reagents targeting Ras, including single domain antibodies, monobodies and DARPins. Research presented in this thesis has developed modulators of Ras activity using novel artificial binding proteins, termed Affimers. Affimer reagents are small 91 amino acid scaffold proteins that constrain one or two randomised nine amino acid loop regions for molecular recognition. Affimers isolated against KRas, the most commonly mutated Ras family member, were shown to be effective at inhibiting nucleotide exchange and blocked interaction between Ras and its effector Raf. When expressed in mammalian cells, Affimers bound with endogenous Ras and inhibited Ras-mediated signalling. Site-directed mutagenesis of the Affimer variable regions revealed three residues critical for binding and inhibition. X-ray crystal structure of Affimer in complex with KRas demonstrated that these residues bind into a hydrophobic pocket on Ras, previously described with small molecules. Molecular docking was used to generate mimics of the Affimer residues, therefore providing insights into new mode of therapeutic development. These Affimer-derived compounds were shown to be effective in biochemical and cell-based assays, with comparable properties to previously published small molecule inhibitors of Ras, but without any optimisation of the compounds. Therefore, these molecules hold great potential for development of even more potent inhibitors through employment of medicinal chemistry. The work presented in this thesis established a novel use of Affimer reagents as valuable tools for the development of small molecule inhibitors.

Table of Contents

List of Tables

List of Figures

List of Abbreviations

A280	absorbance at 280 nm
ABP	artificial binding protein
ADAs	anti-drug antibodies
ANOVA	Analysis of variance
ATP	Adenosine triphosphate
BAP	biotin acceptor protein
BCA	bicinchoninic acid
BCL-6	B-cell lymphoma 6 protein
BRET	bioluminescent resonance energy transfer
CRC	colon and rectal carcinoma
DARPins	Designed Ankyrin Repeat Proteins
DD	Destabilisation domain
DMEM	Dulbecco's Modified Eagle Medium
DMSO	Dimethyl sulfoxide
DNA	Deoxyribonucleic acid
DPBS	Dulbecco's Phosphate-Buffered Saline
DTT	Dithiothreitol
E. coli	Escherichia coli
EDTA	Ethylenediaminetetraacetic acid
EGF	Epidermal growth factor
EGFR	epidermal-growth factor receptor
ELISA	enzyme-linked immunosorbent assay
EM	electron microscopy
ERK	Extracellular signal-regulated kinase
FACS	fluorescent activated cell sorting
FBS	fetal bovine serum
FcɣRIIIa	Fc gamma receptor IIIa
FDA	Food and Drug Administration agency
FRET	fluorescent resonance energy transfer
FTI	farnesyltransferase inhibitor
GAP	GTPase activating protein
GDP	Guanosine diphosphate

GEF	Guanine nucleotide exchange factor
GF	growth factor
GFP	green fluorescent protein
GPCR	G-protein coupled receptor
GST	Glutathione S-transferase
GTP	Guanosine triphosphate
HEPES	(4-(2-hydroxyethyl)-1-piperazineethanesulfonic acid
HRP	Horseradish peroxidase
HTS	high throughput screening
HVR	Hypervariable region
IAC	Intracellular antibody capture
IC50	half maximal inhibitory concentration
IPTG	isopropyl-β-D-thio-galactopyranoside
ITC	isothermal titration calorimetry
kDa	Kilodaltons
mAbs	monoclonal antibodies
MANT	2'-(or-3')-O-(N-Methylanthraniloyl)
MAPK	Mitogen-activated protein kinase
MPD	2-Methyl-2,4-pentanediol
mRNA	messenger RNA
MW	molecular weight
MWCO	molecular weight cut off
NADPH	nicotinamide adenine dinucleotide phosphate
Ni-NTA	Nickel-nitrilotriacetic acid
NMR	Nuclear magnetic resonance
NSCLC	non-small-cell lung cancer
PAINS	Pan-assay interference compounds
PBMC	peripheral blood mononuclear cells
PBS	phosphate buffered saline
PCR	polymerase chain reaction
PDAC	pancreatic ductal adenocarcinoma
PDB	Protein data bank

PDE6δ	Phosphodiesterase 6δ
PEG	Polyethylene glycol
PI3K	phosphatidylinositol-4,5-bisphosphate 3-kinase
PPI	protein-protein interactions
RBD	Ras binding domain
RMSD	root mean square deviation
RNA	Ribonucleic acid
ROCS	rapid overlay of chemical structure
RPMI	Roswell Park Memorial Institute 1640 Medium
RTK	Receptor tyrosine kinase
scFv	single chain variable fragment
SDS-PAGE	Sodium dodecyl sulphate polyacrylamide gel
SEC	size exclusion chromatography
SEM	standard error of the mean
SHG s	second-harmonic generation
siRNA	short interfering RNA
SOE	splice overlap extension
Sos1	Son of Sevenless
SPR	surface plasmon resonance
SUMO	Small ubiquitin-like modifier
TCEP	tris(2-carboxyethyl)phosphine
tGFP	turbo-green fluorescent protein
TMB	3,3',5,5'-Tetramethylbenzidine
TNF-α	tumour-necrosis factor-α
VR	variable region
VS	Virtual screening

Chapter 1

Introduction

Chapter 1
Introduction

1.1 Ras history

Ras research dates back to studies in 1960s, which identified transforming retroviruses: Harvey murine sarcoma and Kirsten murine sarcoma viruses. These viruses caused rapid formation of sarcomas and potently transformed cells in culture (Harvey, 1964, Scolnick, 1982, Scolnick et al., 1979, Tsuchida et al., 1982, Cox and Der, 2010). Further studies on these cancer-causing viruses identified the genetic elements responsible for the oncogenic transformation, which were initially referred to as *src* oncogenes (Cox and Der, 2010). These are now known as *Ras* oncogenes, due to their ability to cause <u>ra</u>t <u>s</u>arcomas, and are differentiated according to which retrovirus these originated from, i.e. *HRas* identified from Harvey murine sarcoma virus and *KRas* from Kirsten murine sarcoma virus (Cox and Der, 2010). Later, a third homolog: *NRas* of the *Ras* oncogenes was identified from neuroblastoma cells (Shimizu et al., 1983). Isolation of mutationally activated and potently transforming *Ras* from human cancer cell lines drove intensive research to expand understanding of Ras structure and functioning, in order to provide clues for development of Ras inhibitors for cancer therapy (Cox and Der, 2010, Baines et al., 2011). This search continues to this day, however despite academic and industrial effort, there has been limited success so far (Cox et al., 2014). Nevertheless, recent developments in understanding Ras function, along with advances in strategies and technologies, bring hope for development of novel anti-Ras treatments for cancer therapy (Cox et al., 2014).

1.2 Ras superfamily structure

The three *Ras* genes encode four structurally and biochemically highly related monomeric proteins (HRas, NRas, KRas4A and KRas4B) of approximately 21 kDa (Friday and Adjei, 2005, Colicelli, 2004). *KRas* encodes two proteins, due to alternative splicing of fourth exon (Capon et al., 1983, Tsai et al., 2015). These four Ras proteins display more than 90% amino acid sequence identity in the G

domain (Hobbs et al., 2016a). The G domain is composed of five α-helices with central β-sheet (Wittinghofer, 2014). The G proteins are characterised by conserved G box sequence motifs (Wennerberg et al., 2005, Bourne et al., 1991), consisting of: G1 (GXXXXGKS/T) responsible for phosphate binding; G2 (T), also referred to as switch I region, responsible for effector binding; G3 (DXXGQ/H/T) involved in binding a nucleotide-associated Mg^{2+} ion; G4 (T/NKXD) responsible for contact with the guanine ring via hydrogen bonds and G5 box (C/SAK/L/T) involved in indirect interaction with guanine nucleotide (Figure 1.1) (Wennerberg et al., 2005, Wittinghofer, 2014, Colicelli, 2004).
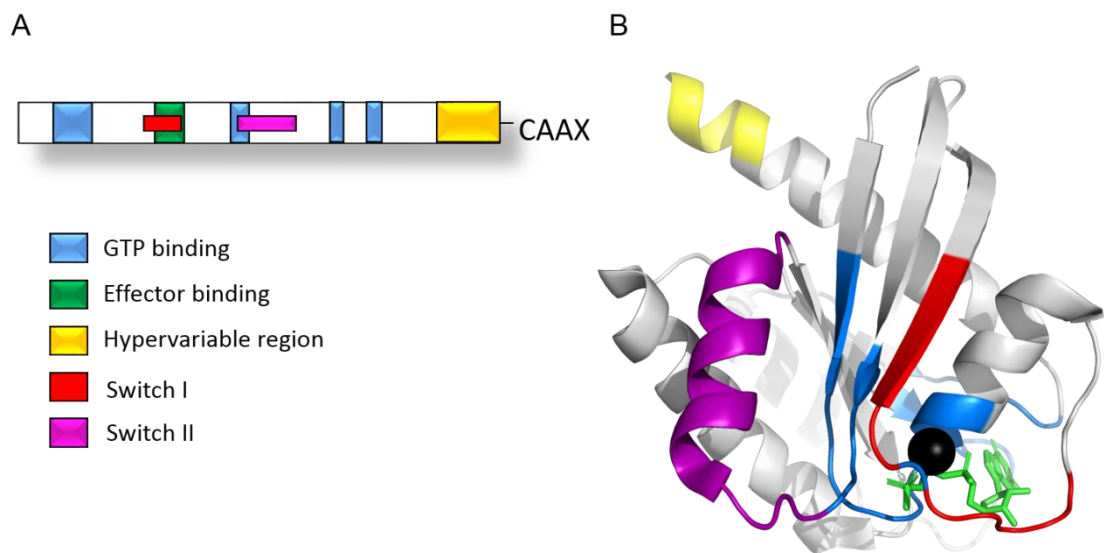
Figure 1.1 Schematic representation of functional domains in Ras structure. A) Coloured boxes indicate regions participating in GTP and effector binding, as well as switch I and II regions and terminal CAAX sequence for post-translational modifications. B) The regions indicated in A) highlighted on the KRas structure (PDB: 6GOD). GPPNHP is shown in green and magnesium in black. Image was generated in PyMOL.

Ras GTPases cycle between GDP- and GTP-bound states (Friday and Adjei, 2005) and comparison of structures of Ras with either GDP or GTP bound, identified large conformational changes within all members of the Ras superfamily (Figure 1.2). Regions undergoing these conformations are referred to as ''switch'' regions. The switch I region is responsible for effector binding in the GTP-bound state. This region also possesses a highly conserved threonine residue, which is essential for detecting the GTP ɣ-phosphate and for contacting Mg^{2+} ion. Similarly, the switch II region, adjacent to G3 motif, also senses the ɣ-phosphate and is involved in effector interactions, but it does not contain a conserved sequence motif. Moreover, the switch II region is crucial for interactions with guanine nucleotide exchange factors (GEFs) responsible for nucleotide exchange, and GTPase activating proteins (GAPs) that stimulate GTP hydrolysis. In the presence of GTP, the switch I and switch II regions adopt positions close to the nucleotide, forming a 'closed' conformation (Wittinghofer, 2014). Upon ɣ-phosphate cleavage and release, the switch regions become disordered, forming an 'open' GDP-bound state. This form does not have a defined conformation, instead the switch regions dynamically fluctuate on a nanosecond scale, as evidenced by NMR spectroscopy (Wittinghofer, 2014, Kraulis et al., 1994).
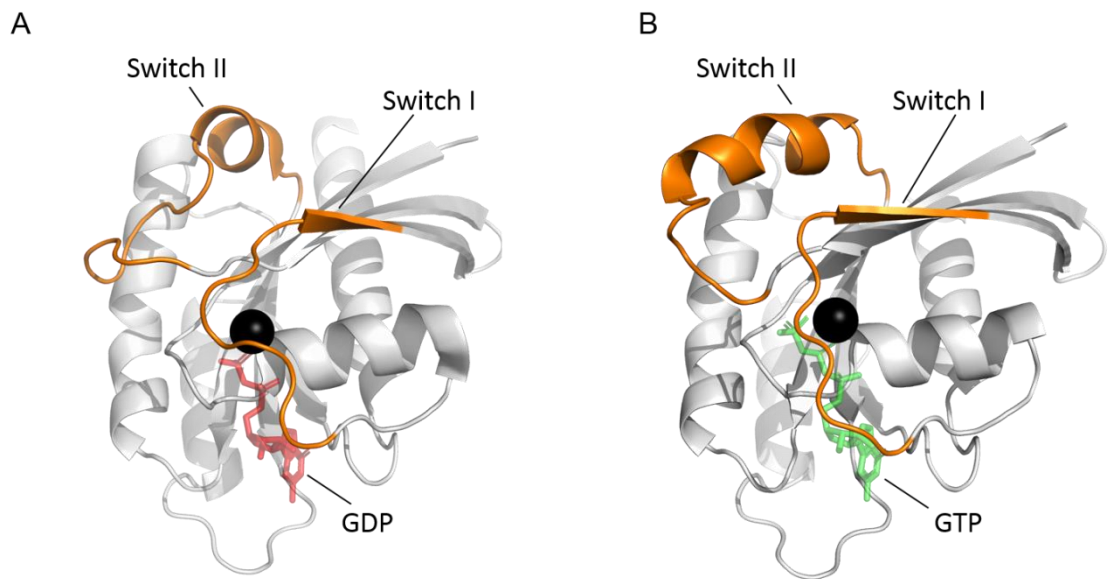
Figure 1.2 Conformational changes between the active and inactive Ras structures. Crystal structures of A) inactivated Ras-GDP (PDB: 1Q21) and B) activated Ras-GTP (PDB: 5P21). The flexible switch I and switch II regions are shown in orange, the coordinated magnesium in black and the nucleotides are coloured in red (GDP) and green (GTP). Images were generated in PyMOL software.

Historically, high sequence similarity coupled with expression in all cell lineages and organs, high conservation across different species and activation of the same effector proteins led to the assumption that all four Ras proteins are functionally similar (Leon et al., 1987b, Furth et al., 1987, Fiorucci and Hall, 1988). Consequently, the majority of the early studies on Ras proteins were carried out with HRas only, with expectations that biological functions of Ras isoforms are interchangeable (Castellano and Santos, 2011). In contrast, the C-terminal hyper variable regions (HVR) of Ras isoforms share only 8% sequence identity (Tsai et al., 2015). These regions dictate Ras intracellular trafficking and membrane interactions, which in turn contribute to distinct biological functions of Ras isoforms (Bos, 1989, Lowy and Willumsen, 1993, Colicelli, 2004, Friday and Adjei, 2005). The multi-stage lipid modifications of Ras proteins include prenylation at the terminal CAAX motif by farnesyltransferase, proteolytic cleavage of AAX motif by Rce1 or Afc1 proteases, carboxymethylation and finally

5

palmitoylation of the SH group. Exception is the KRas4B isoform, which omits the palmitoylation and associates with the membrane via electrostatic interactions (Figure 1.3) (Jackson et al., 1994, Buday and Downward, 2008).
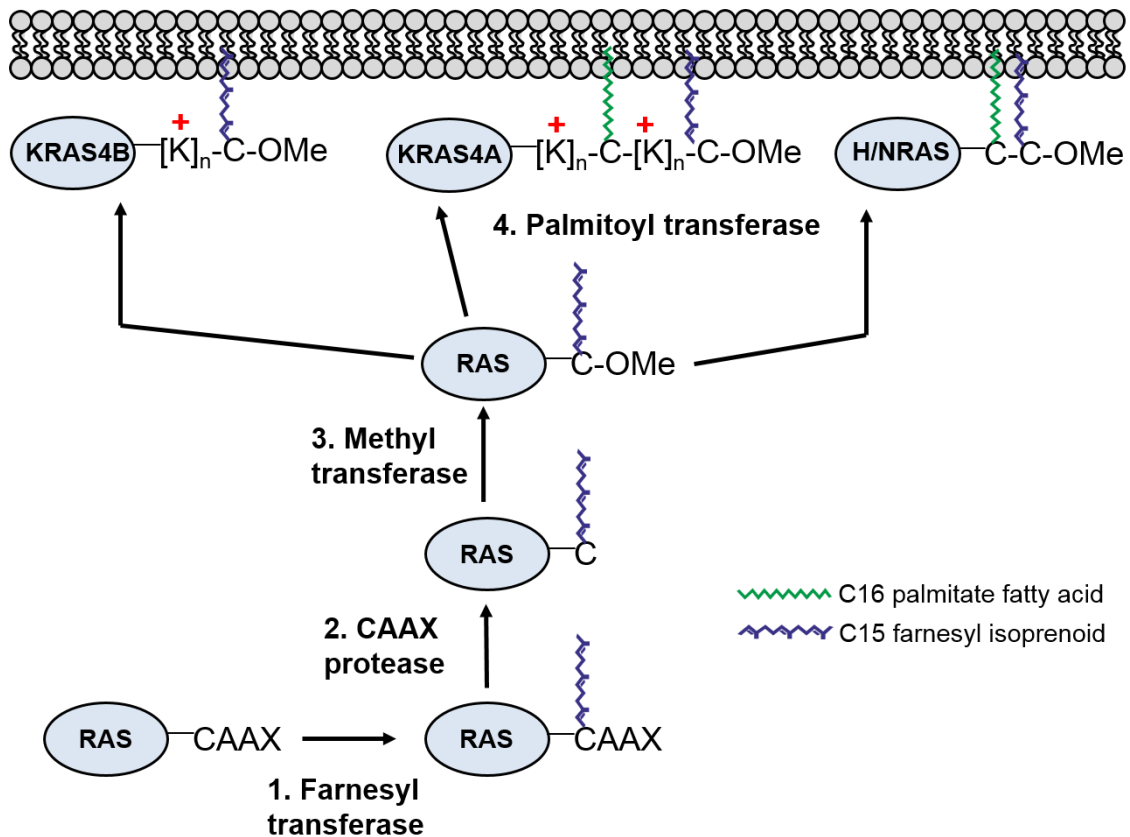
Figure 1.3 Ras plasma membrane targeting via post-translational modifications. All Ras isoforms are firstly farnesylated on the cysteine residue, following by cleavage of the terminal AAX tripeptide and methylation of the terminal cysteine. Finally, Ras proteins, except KRas-4B are palmitylated at the cysteine residue close to the carboxy terminus. KRas-4B isoform associates with the membrane via electrostatic interactions mediated by cluster of lysine residues.

1.3 Ras biochemistry and function

Proteins from the Ras superfamily are small guanosine triphosphatases (GTPases), that function as 'molecular switches' by transmitting extracellular signals to intracellular environment (Friday and Adjei, 2005). Because of their function, small GTPases are important modulators of a great range of cellular processes, including cell growth, differentiation and survival, as these processes occur through linking of extracellular signals to intracellular signalling cascades (Friday and Adjei, 2005, Wennerberg et al., 2005).

Ras signalling is initiated by activation of receptor tyrosine kinase (RTK) by its appropriate growth factor, which then results in receptor's autophosphorylation of tyrosine residues. This initiates binding of adaptor proteins, such as Grb2, via their SH2 domains, which in turn recruit guanine nucleotide exchange factors such as Son of Sevenless 1 (Sos1) or CDC25. These then interact with Ras (Friday and Adjei, 2005). GEFs catalyse the release of GDP and GTP loading, which is the rate-limiting step in Ras activation (Figure 1.4) (Colicelli, 2004). The bound GTP is then hydrolysed to GDP by Ras which is enhanced by GTPase activating proteins such as p120-GAP, to prevent prolonged signal transduction. Thus, because of the low intrinsic GTPase activity and stimulation by GAPs, the Ras signalling is normally transient. However, prolonged Ras signalling due to *ras* mutations, inactivation of GAPs or Ras overexpression is the key element in Ras-induced cancers (Friday and Adjei, 2005, Colicelli, 2004).
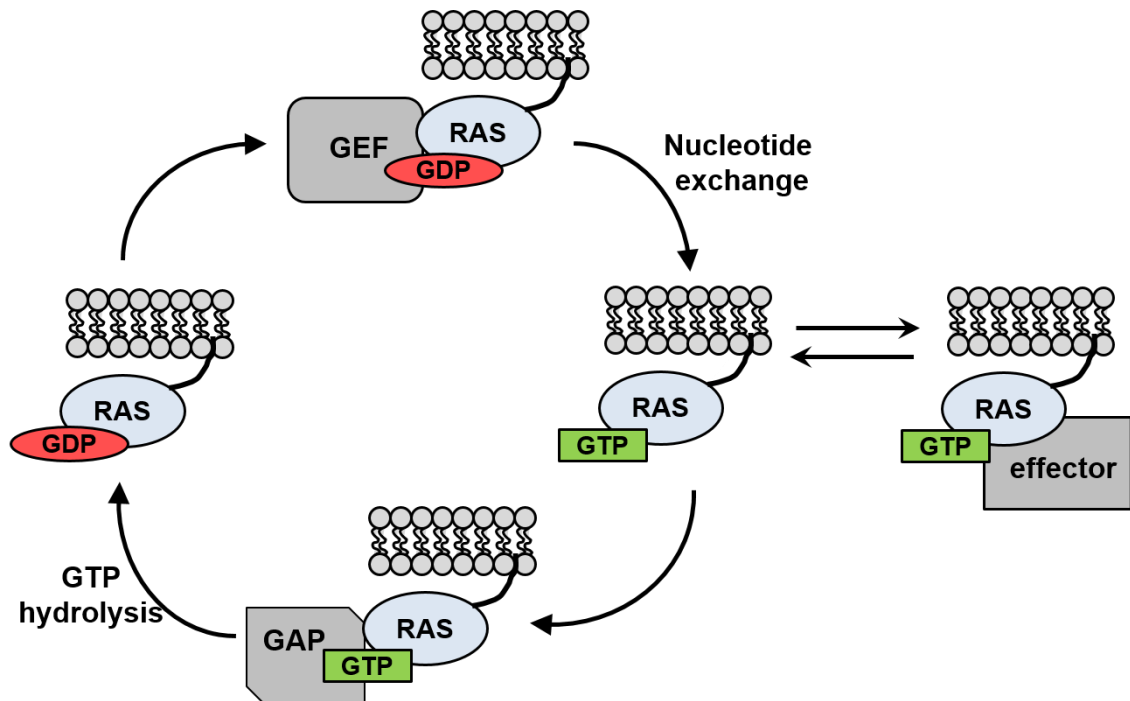
Figure 1.4 Activation/inactivation cycle of Ras. Ras activation is initiated by interaction with guanine nucleotide exchange factors (GEFs), which catalyse the release of GDP and GTP loading. Once activated, Ras binds to its effector protein. Ras signalling is terminated by GTP hydrolysis catalysed by GTPase activating proteins (GAPs) to prevent prolonged signal transduction.

Once activated, Ras displays high affinity binding with a wide range of effectors, which are involved in number of signalling pathways regulating a variety of cellular processes (summarised in Figure 1.5) (Friday and Adjei, 2005). Of these effectors, Raf is the most studied, due to its involvement in the classical mitogen-activated protein kinase (MAPK) signal transduction pathway (Figure 1.6) (Friday and Adjei, 2005, Colicelli, 2004). Active Ras promotes recruitment of Raf to the membrane and its dimerization and activation. This in turn phosphorylates and activates MEK kinase, which then activates ERK kinase by phosphorylation. Activated ERK phosphorylates and activates a number of transcription factors and kinases, which regulate wide range of fundamental cellular processes, including cell cycle progression, differentiation, protein translation, cell survival and death (Friday and Adjei, 2005, Samatar and Poulikakos, 2014).
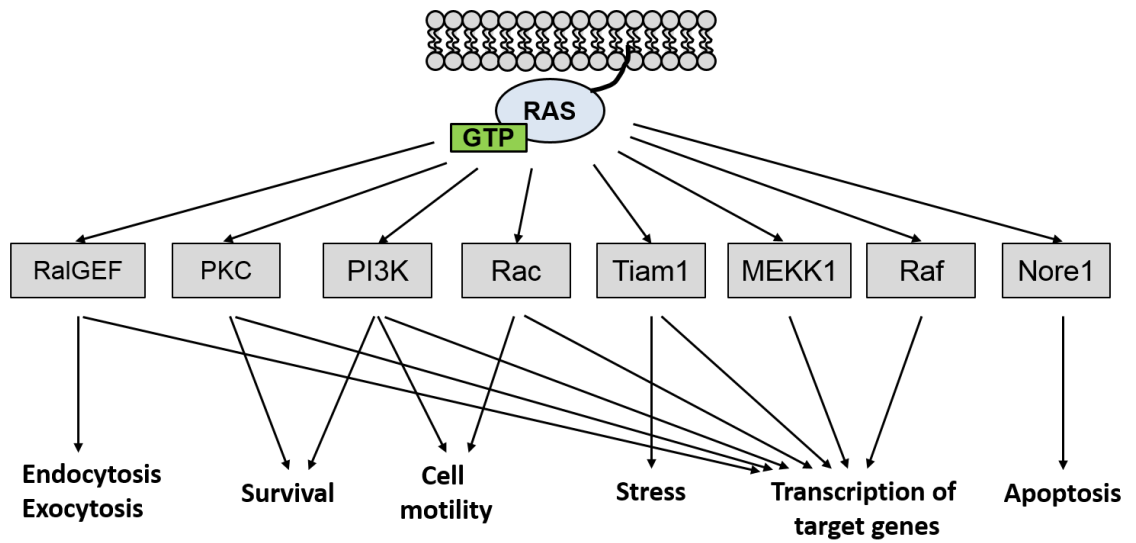
Figure 1.5 Ras effectors and signalling pathways. Activated, GTP-bound Ras proteins signal through multiple effector pathways, which are involved in processes regulating cell proliferation, differentiation and survival.
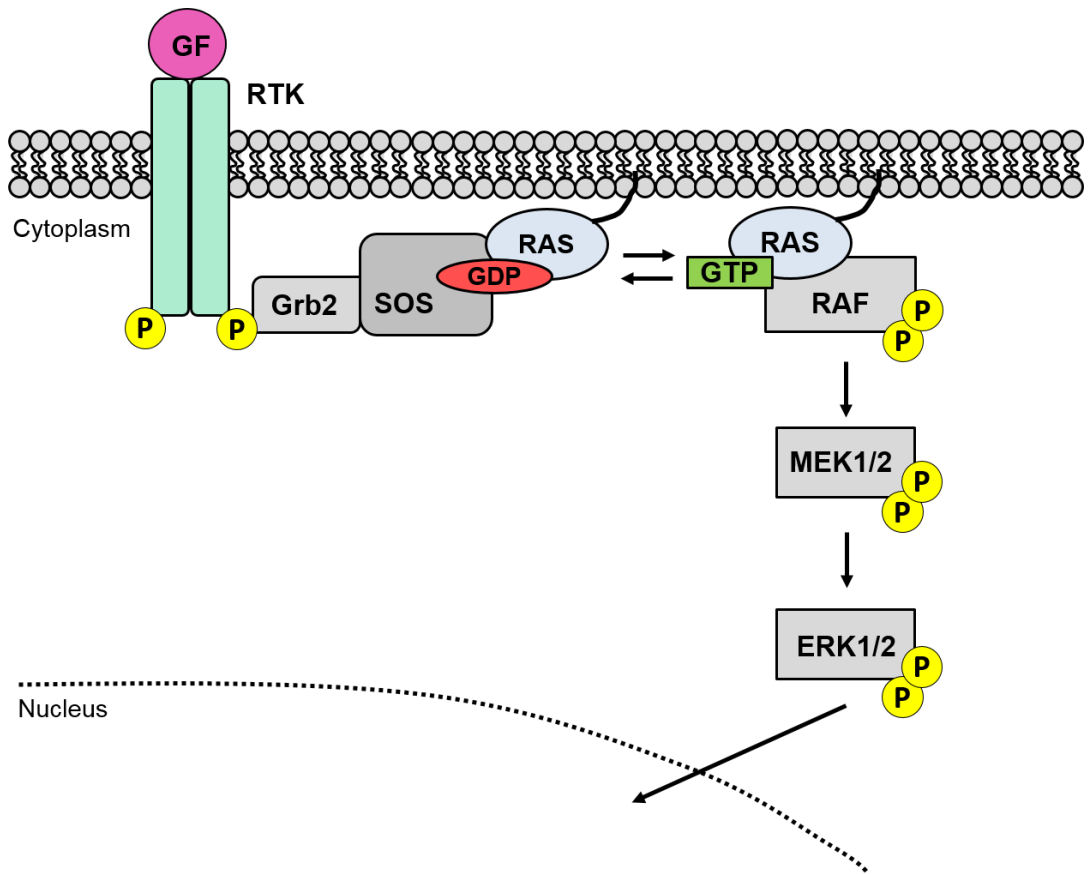
Figure 1.6 Simplified model of Ras signalling cascade. Ras signalling is initiated by activation of receptor tyrosine kinase (RTK) by its growth factor (GF), resulting in receptor's autophosphorylation. Adaptor proteins, such as Grb2 are recruited to the receptor. These adaptor proteins mediate membrane localisation of guanine nucleotide exchange factor, such as Sos, which catalyses nucleotide exchange to activate Ras. Once active, Ras recruits Raf kinases to the plasma membrane, where they become phosphorylated. Active Raf acts as MAP kinase kinase kinase (MAPKKK) and catalyses activation of MEK1/MEK2 by phosphorylation, which in turn catalyse activation of ERK1/ERK2. Activated ERK1 and ERK2 phosphorylate a plethora of cytoplasmic and nuclear substrates involved in diverse array of cellular responses.

The above signalling pathway applies to all four Ras proteins (KRas4A, KRas4B, HRas and NRas). Although, Ras isoforms activate a common set of effectors with varying efficiencies, leading to differential signalling outputs (Hancock, 2003). For example, signalling through Raf-1 is more potently activated by KRas, while HRas is more potent activator of phosphatidylinositol-4,5-bisphosphate 3-kinase (PI3K) (Yan et al., 1998, Voice et al., 1999). This differential signalling is mainly modulated by different membrane microenvironments of the isoforms, which in turn is regulated by the hypervariable region (Willumsen et al., 1984), described above. There is now a vast amount of data providing evidence for additional factors contributing to biochemical as well as biological differences between Ras isoforms. These include: 1) high sequence conservation in the HVR of the different isoform (Tsai et al., 2015, Castellano and Santos, 2011), 2) different frequencies, at which Ras proteins are mutated in human cancers (Mitsuuchi and Testa, 2002, Grady and Markowitz, 2002, Jaffee et al., 2002, Rodenhuis and Slebos, 1992, Hobbs et al., 2016b), 3) different patterns of expression (Leon et al., 1987a, Su et al., 2004), 4) differential sensitivities for modulation by GEFs or GAPs (Bollag and McCormick, 1991, Jones and Jackson, 1998, Matallanas et al., 2003), 5) distinct transforming potential of each isoform (Cheng et al., 2011, Maher et al., 1995, Pulciani et al., 1985) and 6) evident phenotypes of knock-out animal models for each isoform (O'Hagan and Heyer, 2011, Singh et al., 2010, Esteban et al., 2001).

1.4 Ras proteins and cancer

Aberrant Ras signalling occurs due to increased upstream signalling, Ras overexpression, deregulation of GAPs or activating mutations, resulting in deregulated cellular processes and leading to disease (Burns et al., 2014). Indeed, aberrant Ras signalling has been identified to play a role in more than 30% of all human cancers (Baines et al., 2011).

The highest incidence of aberrant Ras signalling is due to single base missense mutations, most frequently occurring in codons 12, 13 and 61. These mutations impair GAP-induced GTP hydrolysis, thus prolonging signalling from active Ras (Friday and Adjei, 2005). Mutations in Ras are found in 63–90% of pancreas, 36–50% of colon and 19–30% of lung cancers (Burns et al., 2014). These are amongst the deadliest cancers, with mutations in KRas alone accounting for one

million deaths per year (Cox et al., 2014, McCormick, 2016). Moreover, activating mutations in Ras are related to poor prognosis and chemo-resistance (Leshchiner et al., 2015).

It is now well known that the three *Ras* genes are not mutated at equal frequencies. KRas is the most predominantly mutated isoform, found in 86% of Ras-driven cancers, followed by NRas (11%) and HRas (3%) (Papke and Der, 2017). Mutations at residue G12 are most common in KRas and HRas, while Q61 mutations are predominantly found in NRas (Cox et al., 2014). In addition to isoform specificity, *Ras* mutations show remarkable tissue-specific preferences. For example, in pancreatic ductal adenocarcinoma (PDAC) and colon and rectal carcinoma (CRC) G12D is the dominating substitution. Conversely, G12C mutation is most common in non-small-cell lung cancer (NSCLC).

Ras mutations initiate tumour formation, and continuous expression of mutant Ras is required for tumour maintenance. This is due to requirement of downstream signalling leading to cell proliferation, evasion of cell death, altered metabolism, induced angiogenesis, increased invasion and metastasis and evasion of immune destruction – the capabilities that represent hallmarks of cancer (Burns et al., 2014, Cox et al., 2014).

1.5 Ras as therapeutic target

The critical role that Ras plays in cell transformation (the high incidence of aberrant Ras signalling and its effects) illustrates that development of Ras inhibitors as anti-cancer therapeutics is of the highest priority in cancer research (Colicelli, 2004, Leshchiner et al., 2015). However, since more than 30 years of efforts to develop Ras inhibitors have not yielded clinically relevant compounds, Ras proteins have been considered as 'undruggable' targets. This is mainly due to their simple protein structure with no distinct binding cavities and high affinity for GTP (Cromm et al., 2015, Fang, 2016). Nevertheless, advanced understanding of Ras function as well as novel technologies for direct targeting of small GTPases bring hope for development of anti-Ras therapeutics (Cox et al., 2014, Thompson, 2013).

1.6 Strategies for targeting Ras

Detailed understanding of Ras structure and function is essential for development of a Ras antagonist. However, it is also crucial to remember that Ras does not function in isolation, rather it is involved in a multi-protein signalling cascade (De Las Rivas and Fontanillo, 2010). For example, 375 proteins and more than 1000 protein-protein interactions (PPIs) are involved in the epidermal-growth factor receptor (EGFR) signalling pathway, which adds the complexity to design and development of novel anti-Ras therapeutics (Saafan et al., 2016). Therefore, numerous strategies to target Ras have been employed over the past three decades. These include: inhibiting protein expression (Gray et al., 1993, Duursma and Agami, 2003, Brummelkamp et al., 2002), inhibiting membrane localisation (Sun et al., 1995, End et al., 2001, Zimmermann et al., 2013), direct Ras inhibition (Cromm et al., 2015), blocking interaction with GEFs (Leshchiner et al., 2015, Maurer et al., 2012, Patgiri et al., 2011, Sun et al., 2012) and inhibiting downstream effectors (Friday and Adjei, 2005, Britten, 2013, Cheng and Tian, 2017, Cox and Der, 2010, Durrant and Morrison, 2018, Freeman et al., 2013).
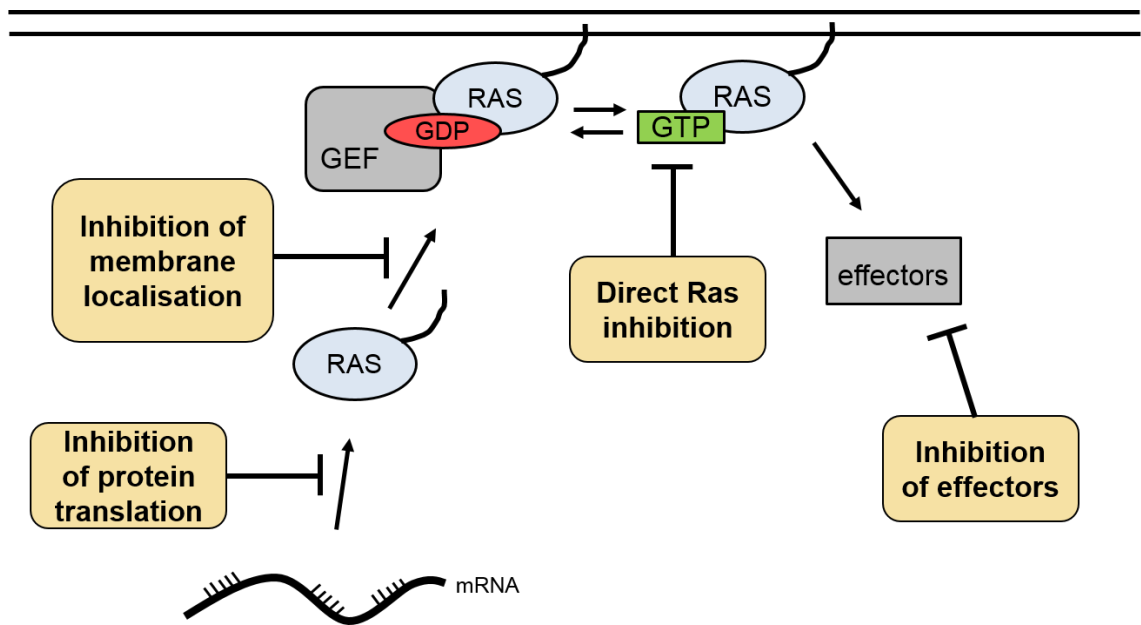
Figure 1.7 Approaches for discovery and development of Ras inhibitors.
Inhibition of protein expression, membrane localisation, Ras effectors and direct Ras targeting has been investigated as strategies for development of Ras inhibitors.

1.6.1 Inhibiting Ras protein expression

Numerous studies have shown that mutant Ras proteins have potent cancer-inducing capabilities and that continued expression of Ras mutants is essential for tumour maintenance (Cox et al., 2014). This, therefore, initiated research to develop inhibitors of Ras expression. The first approach included introduction of antisense Ras oligonucleotide into tumour cells, to hinder protein translation. Despite reduced Ras protein expression by 90% in Ras-transformed cells and anti-tumour effects in mouse models, the success of this approach was restricted by inability to safely and effectively introduce antisense oligonucleotides and considerable toxicity in clinical evaluation (Duursma and Agami, 2003, Gray et al., 1993).

The second approach to inhibit Ras expression involved gene silencing by short interfering RNAs (siRNA) containing complementary sequence to target gene

mRNA. Recognition of mRNA complementary to the siRNA results in mRNA degradation. Importantly, this strategy allows specific targeting of mutant Ras over wild-type Ras, since even a single base mismatch between siRNA and target mRNA reduces siRNA-mediated mRNA degradation (Friday and Adjei, 2005). Indeed, RNA interference reduced mutant Ras expression in human cancer cell lines (Brummelkamp et al., 2002). However, this approach, similarly to antisense oligonucleotides approach, is limited by safe and effective delivery (Friday and Adjei, 2005).

1.6.2 Inhibiting membrane localisation

A strong relationship between membrane localisation and Ras function has been extensively described in literature. Therefore, inhibition of steps during the post-translational lipid modifications of Ras proteins could theoretically inhibit Ras activity (Ahearn et al., 2012). Since prenylation, mediated by farnesyltransferase enzyme, is the rate-limiting step in Ras lipid modification, extensive effort has been put into development of farnesyltransferase inhibitors (FTIs) (Friday and Adjei, 2005). As a result, numerous potent FTIs have been tested in preclinical mouse studies, which have shown effective growth inhibition of Ras-induced cancers (Cox et al., 2014, End et al., 2001, Sun et al., 1995). Two of these FTIs, namely lonafarnib and tipifarnib were tested in clinical trials, but with limited success due to compensatory activities of geranylgeranyl transferase, and thus alternative Ras prenylation and membrane localisation (Cromm et al., 2015, Cox et al., 2014). The disappointing outcome of these studies had decreased interest in inhibiting membrane localisation as a valid approach to target Ras. Recent years, however, have witnessed a growing interest in targeting proteins that selectively target farnesylated forms of Ras. Phosphodiesterase 6δ (PDE6δ) is one example of such a protein. PDE6δ recognise KRas4B and other prenylated proteins and facilitate their localisation to membrane compartments (Chandra et al., 2011). PDE6δ small molecule inhibitor Deltarasin and its derivatives were shown to impair KRas localisation and oncogenic signalling and reduce the growth of tumour cells harbouring KRas mutations (Martin-Gago et al., 2017, Zimmermann et al., 2013). Despite promising results, questions regarding the degree of KRas dependency on PDE6δ will need to be answered, before the therapeutic potential of these inhibitors can be evaluated (Cox et al., 2014).

1.6.3 Direct Ras inhibition

One of the obvious strategies to inhibit oncogenic Ras is its direct targeting. However, this has proven to be very challenging, mainly due to the lack of distinct binding pockets. In addition, Ras signalling is mediated by PPIs, which are often intractable to small molecules (Nero et al., 2014). Nevertheless, computational approaches along with new crystal structures in previously unidentified conformations highlighted novel transient binding pockets that could be targeted (Spoerner et al., 2004). Likewise, advancements in technologies expanded the available approaches for direct targeting of small GTPases (Cromm et al., 2015).

1.6.3.1 Interference with nucleotide binding

Ras-driven tumours arise as a result of prolonged signalling from activated GTP-bound Ras protein. Thus, initial studies of direct Ras targeting aimed to interfere with nucleotide binding (Cromm et al., 2015). ATP-competitive inhibitors, which have been successively used as antagonists of protein kinases, have been used as a guide for development of GTP-competitive inhibitors. However, ATP exhibits low micromolar affinity for kinases, as compared to GTP binding with picomolar affinity to Ras, which thus prevented development of potent inhibitors (Cox et al., 2014).

1.6.3.2 Irreversible covalent modification

In order to overcome restrictions of GTP-competitive inhibitors, efforts have been made to inhibit small GTPases by irreversible covalent modifications (Cromm et al., 2015). Molecular docking studies have been used to design GDP analogue SML-8-73-1, which covalently attached to KRas^{G12C} mutant, thus stabilising the inactive GDP-bound form of Ras. Further derivative of this analogue has been shown to impair phosphorylation of downstream Ras effectors as well as proliferation of KRas^{G12C} cell lines. However, these studies were conducted with nucleotide-free Ras, and therefore it is unclear if the inhibitor would have the ability to compete with cellular nucleotide (Lim et al., 2014). Additionally, a tethering approach yielded another set of covalent inhibitors, which were shown to specifically target KRas^{G12C} mutant but not wild-type, and bound to KRas at a novel binding site, termed S-IIP. These compounds reduced activated KRas-GTP levels, abolished Sos-catalysed nucleotide exchange and promoted apoptosis of

KRas[G12C] cell lines (Lim et al., 2014, Janes et al., 2018). Further derivatives were shown to be effective across KRas G12C mutant cell lines and *in vivo* tumour models, therefore demonstrating therapeutic potential of KRas G12C covalent inhibitors (Janes et al., 2018, Zeng et al., 2017). Success of these studies inspired development of MRTX849 small molecule inhibitor of KRas G12C, that has now entered phase I/II clinical trials (MiratiTherapeutics, 2018).

1.6.3.3 Inhibition of GTPase-GEF interaction

To become active, GTPases have to firstly release GDP to vacate the binding site for GTP. Since this release is catalysed by GEFs, interfering with GTPase-GEF interaction constitutes another strategy for Ras inhibition (Cromm et al., 2015).

The Ras-Sos interaction comprises insertion of Sos α-helix into Ras binding pocket between switch I and II regions (Cromm et al., 2015). Thus, the Sos α-helix was used as a basis for development of peptide inhibitors of the Ras-Sos interaction (Patgiri et al., 2011, Leshchiner et al., 2015). Stabilised α-helices with a hydrogen bond surrogate approach yielded peptide HBS3, which inhibited Sos-mediated nucleotide exchange with micromolar potency (IC_{50}= 25µM), and was shown to impair ERK activation (Patgiri et al., 2011). Interestingly, stabilisation of α-helix with stapling approach yielded SAH-SOS1$_a$ peptide, which inhibited both wild-type and mutant KRas with low micromolar potency (IC_{50}= 5-15µM) and reduced KRas downstream signalling and viability of KRas-dependent cancer cell lines (Leshchiner et al., 2015).

Computational studies and molecular dynamics simulations identified novel transient pockets on Ras, which could be capable of binding small molecules (Gorfe et al., 2008, Grant et al., 2011). Docking studies identified binding of anticancer agent Andrographolide to these transient pockets on Ras, which in turn resulted in inhibition of Ras activation. Moreover, derivatives of Andrographolide were shown to reduce Ras-GTP levels and impair ERK phosphorylation (Hocker et al., 2013). In addition to computational approaches, fragment-based ligand discovery identified small molecule DCAI, which bound to novel hydrophobic pocket between switch I and II regions and demonstrated Sos-mediated nucleotide exchange inhibition with moderate potency (IC_{50}= 342µM)

(Maurer et al., 2012). This pocket has been also utilised by others to develop small molecule inhibitors of Ras (Sun et al., 2012, Quevedo et al., 2018). On the other hand, the Ras-GEF interaction has also been blocked by small molecule inhibitors targeting the catalytic site of Sos1 (Evelyn et al., 2014). Altogether, these compounds provide starting point for development of potent inhibitors of Ras-GEF interaction and can be used as a tools to dissect Ras signalling, but further optimisations are required before these can progress into the clinic (Sun et al., 2012).

1.6.3.4 Inhibition of GTPase-effector interaction

The most universal approach for targeting Ras GTPases include interfering with GTPase-effector interaction, as the inhibition of signal propagation would be irrespective of the cause of constitutively active GTPase (i.e. mutation, overexpression or loss of GAP activity). However, development of such inhibitors is challenging due to high binding affinity of effectors to GTPases as well as no well-defined binding pockets (Cromm et al., 2015). Nonetheless, several approaches have yielded GTPase-effector interaction inhibitors, for example: small molecules based on the Kobe family scaffold, peptide inhibitors such as cyclorasin 9A5, engineered protein R11.1.6 and organometallic complexes acting as allosteric inhibitors (Cromm et al., 2015, Kauke et al., 2017). Further studies of the above compound classes are required before proceeding into clinical trials, due to problems associated with low potency, off-target activity and low binding selectivity for some of these agents (Cox et al., 2014).

1.6.3.5 Stabilisation of GTPase-protein complexes

An opposite approach to inhibiting GTPase-protein interactions, is stabilisation of these PPIs and therefore trapping GTPases in non-functional conformations. Advantages of this strategy include targeting potential novel binding sites at the interface of GTPase-protein complex and eliminated competition with high affinity GTPase binders (Cromm et al., 2015). Example of such stabilisation is seen with fungal metabolite Brefeldin A, which binds to and stabilises small GTPase Arf in complex with its GEF, resulting in impaired Arf-signalling (Zeeh et al., 2006). This has driven further research to develop PPI stabilisers, with AstraZeneca successfully developing compounds targeting KRas-GDP-Sos complex, which

inhibited KRas activation (Winter et al., 2015). However, further developments of these compounds are required to achieve higher affinity binding (Cromm et al., 2015).

1.6.4 Effector inhibition

Engagement of the effector proteins that transmit the signal downstream is a key requirement for Ras function. In addition, cancer-driving roles of at least six Ras effectors have been previously described (Cox and Der, 2010). As a result, the majority of efforts to develop therapies for Ras-driven cancers have focused on inhibition of effector signalling, as described below (Cox et al., 2014).
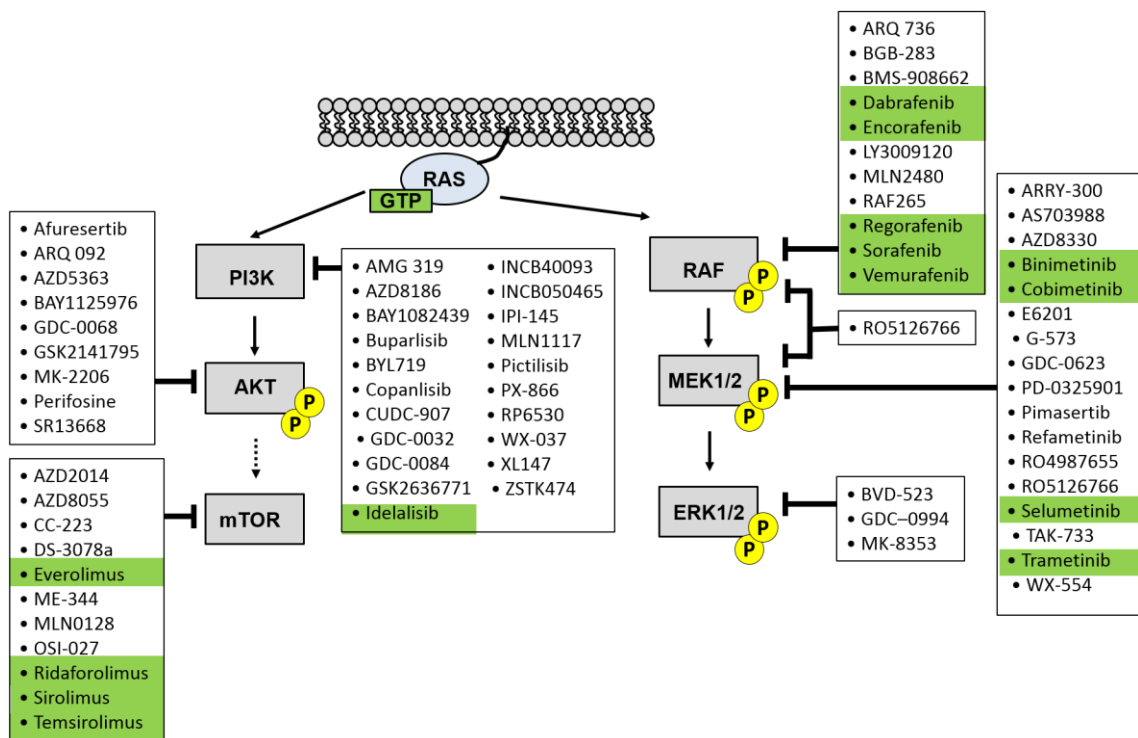
Figure 1.8 Inhibitors of Ras effectors under clinical evaluation. Approved inhibitors are highlighted in green. Adapted from (Cox et al., 2014, Ryan and Corcoran, 2018).

1.6.4.1 Raf-MEK-ERK inhibitors

The Raf-MEK-ERK pathway is one of the best characterised signalling cascades downstream of Ras. Historically, it was perceived as a linear and unidirectional pathway, however the complexity of this signalling cascade is now well-established, with numerous feedback mechanisms and regulators (Roskoski, 2012). Therefore, initial assumptions that inhibition of either Raf, MEK or ERK would have equivalent results on mutant Ras-driven signalling was proven to be incorrect (Cox et al., 2014).

Numerous Raf inhibitors are under clinical investigation (Figure 1.8), with four approved by the US Food and Drug Administration (FDA) agency. Although impressive responses with these inhibitors were observed in the clinic, drug resistance has been detected (Lito et al., 2013). In addition, Raf inhibitors triggered paradoxical activation of downstream signalling, by promoting Raf dimerization, which resulted in formation of secondary malignancies (Su et al., 2012, Lacouture et al., 2012). Hence, second-generation inhibitors that do not cause Raf dimerization are under evaluation (Freeman et al., 2013, Durrant and Morrison, 2018).

In recent years, there has been an increasing amount of discovery and development of MEK inhibitors, with many under clinical evaluation and trametinib and cobimetinib approved for treatment of *BRAF*-mutant melanoma (Figure 1.8) (Grimaldi et al., 2017, Cheng and Tian, 2017). However, the main obstacles with MEK inhibitors concern their toxicity (Cheng and Tian, 2017). To overcome this, dual inhibition of Raf and MEK have been evaluated in the clinic, which demonstrated increased efficacy and minimised toxicity. Indeed, this combined treatment is now considered best practice for *BRAF*-mutant melanoma patients (Hauschild et al., 2018, Planchard et al., 2017, Simeone et al., 2017). Therefore, the dual inhibition of Raf and MEK is believed to be the prospective strategy for inhibition of the MAPK pathway (Cheng and Tian, 2017).

ERK inhibitors have also been investigated, with three compounds under clinical evaluation (Figure 1.8) (Morris et al., 2013). However, similarly to MEK inhibitors, drug resistance and enhanced MEK activation due to feedback mechanisms were observed (Cox et al., 2014).

1.6.4.2 PI3K-AKT-mTOR inhibitors

The second best characterised signalling cascade downstream of Ras is the PI3K-AKT-mTOR pathway. Numerous studies, including mouse model analyses have described the role that the p110 catalytic subunits (α-, ɣ- and δ-subunits) of PI3Ks play in Ras-dependent cancer growth, however to a lesser extent than the components of MAPK pathway (Gupta et al., 2007, Castellano et al., 2013). Nonetheless, inhibition of the PI3K pathway holds therapeutic potential (Cox et al., 2014).

A plethora of PI3K-AKT-mTor pathway inhibitors are under clinical evaluation (Figure 1.8) (Cox et al., 2014). These inhibitors, when used as a single agent, have not shown anti-tumour effects in Ras-mutant cancers. However, because resistance to MAPK cascade inhibitors can be mediated by activation of PI3K-AKT-mTOR pathway, combined inhibition of both pathways has been evaluated (Papke and Der, 2017). Disappointingly, results from clinical trials did not reflect those observed in mouse models. This was partially due to toxicity in human patients not detected in mouse studies (Engelman et al., 2008). As a result, ongoing research intends to determine the combinations of inhibitors with reduced toxicity (Britten, 2013).

1.6.5 Inhibition of synthetic lethal interactions

Another indirect strategy for inhibition of mutant Ras aims to define synthetic lethal interaction partners for Ras oncogene. These are genes, whose functioning is required in mutant Ras but not wild-type Ras cells (Kaelin, 2005). Several synthetic lethal interactors of mutant Ras have been previously identified. These included genes associated with cell cycle and mitosis (e.g. survivin), cell survival (BCL-X_L), transcriptional programmes (GATA2) and parallel growth and survival (TBK1) (Luo et al., 2009, Kumar et al., 2012, Barbie et al., 2009, Steckel et al., 2012). However, the overlap between identified genes from different studies was small and subsequent research failed to validate these as potential therapeutic targets. The limiting factors contributing to disappointing results of those studies include poor RNAi libraries validation, resulting in false-negative results and off-target activities (Cox et al., 2014). Use of small number of *KRAS*-mutant cell lines in those screens is another limitation, due to heterogeneity in tumours arising from different organs, despite bearing similar oncogenic mutations (Garraway

and Sellers, 2006). To overcome some of these obstacles, Wang *et al.* recently employed CRISPR-Cas9 methodology, which have less off-target activities compared to RNAi screens, and used larger panel of Ras-mutant and wild-type cell lines to identify synthetic lethal genes (Wang et al., 2017). Further improvements to the synthetic lethal screen could include use of three-dimensional culture models and *in vivo* assays (Papke and Der, 2017, Cox et al., 2014).

1.6.6 Inhibitors of metabolism

Cancer cells need to reprogram cell metabolism in order to obtain energy required for increased proliferation. These metabolic adaptations constitute one of the hallmarks of cancer (Hanahan and Weinberg, 2011). There is an increasing number of reports describing the role of mutant Ras in regulation of various metabolic processes. For example, it has been shown that mutant Ras drives macropinocytosis, a process of internalisation of plasma membrane to acquire nutrients (Commisso et al., 2013). Albumin is one example of component obtained through macropinocytosis. Hijacking this process with albumin-bound chemotherapy drug paclitaxel is considered as standard of care for PDAC (Giordano et al., 2017). Ras-mutant cancers were also characterised by increased autophagy. Chloroquine, an autophagy inhibitor, was shown to impair tumour growth in mice and its derivative is under clinical evaluation for PDAC (Yang et al., 2011, Boone et al., 2018). Other metabolic processes directed by mutant Ras include elevated glucose metabolism and nucleotide and lipid biosynthesis by up-regulation of key enzymes, and increased flux through non-canonical pathway to produce nicotinamide adenine dinucleotide phosphate (NADPH) to maintain redox balance (Ying et al., 2012, Son et al., 2013). In summary, understanding the involvement of Ras in metabolic processes broadens the therapeutic opportunities for Ras-driven cancers, by defining new targets (Papke and Der, 2017).

1.7 Artificial binding proteins

Despite promising results of many of the Ras inhibitors outlined above, none of them have been approved as anti-cancer therapeutics. Considering the high incidence of Ras-mediated oncogenesis as well as poor prognosis for Ras-driven

cancers, novel approaches for development of successful Ras inhibitors are required. Engineered proteins are becoming increasingly prevalent in biotechnology and clinical applications. Not surprisingly, over last two decades around 50 different engineered proteins have been developed, with some reaching clinical evaluation and several being available commercially (Table 1.1) (Wurch et al., 2012).

Until recently, antibodies have been the most commonly used binding proteins in scientific research, diagnostics and therapy. However, as the development of novel applications progressed, certain drawbacks became apparent. These include large size, expensive manufacturing process and complex patent situation (Skerra, 2007). To overcome these limitations, the concept of universal binding site has been combined with robust protein framework, also termed 'scaffold', to generate novel artificial binding proteins (ABPs) (Hey et al., 2005). An advantage of ABPs includes use of combinatorial mutagenesis of the variable binding region to generate diverse libraries of the scaffolds. Currently, a broad range of artificial binding site architectures are employed to mimic the binding principle of conventional antibodies. These include single or multiple loops presented on the scaffold or surface-exposed side chains of secondary structure elements (Hey et al., 2005). Screening of those diverse libraries allows selection of variants with desired binding to a pre-defined target via phage display or related techniques. Importantly, the *in vitro* selection process allows for fine-tuning of the biomolecular characteristics to improve target affinity and selectivity, thermodynamic and chemical stability, shelf life and solubility as well as protease resistance (Skerra, 2007). A further advantage of ABPs is high production yield in bacterial systems, thus a cost-effective manufacturing process (Hey et al., 2005).

Many of the ABPs target disease-related proteins and display potential for development of binding molecules for therapeutic and diagnostic applications (Wurch et al., 2012, Hey et al., 2005). Therefore, it is not surprising that some of these scaffolds have been used to target Ras.

Scaffold	Target	Drug	Disease	Phase
Adnectin (Hooper and Burnett, 2013, Mullard, 2012, Tolcher et al., 2011)	VEGFR2 PCSK9 Myostatin	Angiocept BMS-962476. BMS-986089	Cancer Hypercholesterolemia Cachexia	Phase II Phase I Phase I
Affibody (Lofblom et al., 2010a, Ahlgren et al., 2010)	HER2 Complement protein C5	ABY-025 SOBI002	Cancer inflammation	Phase I/II Phase I
Affilin (Ebersbach et al., 2007)	VEGF-A	PRS-050	Cancer	Phase I
Anticalin (Richter et al., 2014)	Hepcidin	PRS-080	Anaemia	Phase I
Avimer (Silverman et al., 2005)	IL-6	AMG220	Crohn's disease	Phase I
DARPin (Stumpp et al., 2008, Wolf et al., 2011)	VEGF-A VEGF-A VEGF/HGF HER2	MP0112 Abicipar MP0250 MP0274	Macular degeneration Macular degeneration Cancer Cancer	Phase II Phase III Phase I Phase I
Fynomer (Silacci et al., 2016)	TNF/IL-17A	COVA322	Plaque psoriasis	Phase I/II
Knottin (S Smith and Deer, 2009, Mascarenhas-Saraiva and Mascarenhas-Saraiva, 2018)	N-type calcium channels Guanylate cyclase C receptor	Ziconotide Linaclotide	Neuropathic pain Irritable bowel disease	FDA approval 2004 FDA approval 2012
Kunitz Domains (Dunlevy et al., 2012, Lehmann, 2008)	Plasma kallikrein Neutrophil elastase	DX-88 DX-890	Hereditary angioedema Acute respiratory distress syndrome	FDA approval 2012 Phase II

Table 1.1 Scaffold binding proteins currently approved or in clinical trials.

1.7.1 Intrabody

To overcome the limitations of intracellular expression of antibodies, and thus targeting of intracellular targets, antibody fragments, such as single chain variable fragments (scFv), also termed intrabodies, have been engineered. ScFvs comprise heavy and light chain variable domains. The two chains are linked with flexible peptide linker, therefore eliminating the requirement for the inter-chain disulphide bond. This, coupled with small size makes the scFv form suitable for intracellular expression (Tanaka and Rabbitts, 2003). Intracellular antibody capture (IAC) technology, which combines *in vitro* phage selection and *in vivo* antibody-antigen interaction assay, has been developed to isolate intrabodies that are functional intracellularly (Tse et al., 2002, Visintin et al., 2002).

Since their creation in 1980s, scFvs have been extensively characterised as research and imaging tools and in therapeutic applications (Wheeler et al., 2003). For example, intracellular expression of intrabody targeting receptor tyrosine kinase ErbB-2 was shown to impair downstream signalling, cause specific cytotoxicity in ovarian tumour cells and prolonged survival of mice with human ovarian carcinoma tumours (Beerli et al., 1994, Deshane et al., 1995, Wheeler et al., 2003). Not surprisingly then, an anti-ErbB2 intrabody has reached clinical evaluation (Alvarez et al., 2000).

Intrabodies were the first engineered scaffold proteins used to target Ras. Anti-Ras scFvs were shown to inhibit oncogenic HRas G12V-mediated transformation of NIH 3T3 cells (Tanaka and Rabbitts, 2003). Further studies using intracellular single variable domain (iDab) format, isolated iDab6 intrabody, which specifically bound to active Ras and impaired Ras-dependent tumorigenesis in a mouse model. The X-ray crystal structure (Figure 1.9A) demonstrated that the interaction interface between iDab6 and HRas (discussed in more detail in section 5.1) overlapped with that of HRas and its effector Raf1, which provided evidence that iDab6 functions by impairing Ras-effectors interaction (Tanaka and Rabbitts, 2010, Tanaka et al., 2007, Tanaka et al., 2003). In addition, an anti-Ras intrabody was recently used in a competition assay to screen for small molecules that target the same location on Ras (discussed in more detail in section 6.1) (Quevedo et

al., 2018). Altogether, these findings demonstrated the use of ABPs as a valid approach to develop Ras inhibitors.
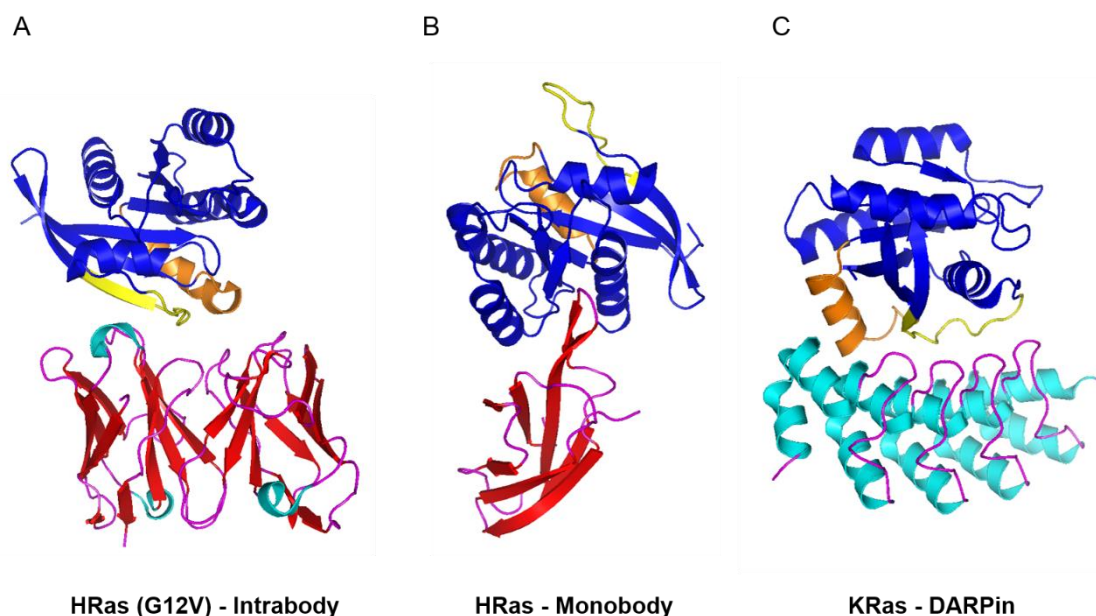
Figure 1.9 Co-crystal structures of Ras and Ras-binding scaffold proteins. Structures of A) HRas and intrabody iDab6 complex (PDB: 2UZI), B) HRas and monobody NS1 complex (PDB: 5E95) and C) KRas and DARPin K27 complex (PDB: 5O2S). Ras is shown in blue with switch I and switch II regions in yellow and orange, respectively. Images were generated in PyMOL.

1.7.2 Affibody

Affibodies are examples of non-immunoglobulin based scaffold proteins, derived from the Z domain of immunoglobulin-binding protein A from *Staphylococcus aureus* (Lofblom et al., 2010a). The affibody structure is composed of three α-helices, with 13 randomised amino acids exposed on surface of two of the α-helices (Lofblom et al., 2010b). Phage display techniques have been used to screen Affibody libraries to select high affinity and specificity Affibodies against variety of targets, including human insulin, CD28, apolipoprotein A-1 and HER2 (Skerra, 2007). Isolated Affibodies have proven applications in therapy, imaging

and biotechnology, with some under clinical evaluation (Table 1.1) (Lofblom et al., 2010b).

Specific Affibodies against HRas and Raf1 were also selected, which displayed micro- and nanomolar affinities towards Ras and Raf, respectively. Only the Raf-specific Affibody was capable of inhibiting Ras:Raf interaction in a dose-dependent manner, however with little effect on ERK activity. In contrast, the Ras-specific Affibody, was shown to impair tumour-necrosis factor-α (TNF-α)-stimulated ERK activation, but had no effect at inhibiting the Ras:Raf interaction. Further studies are required to determine mode of inhibition of these proteins. Nevertheless, use of Affibodies expanded the available approaches to target members of the MAPK signalling pathway (Grimm et al., 2010).

1.7.3 Sso7d scaffold

The Ras:Raf interaction has also been targeted by another engineered scaffold protein, based on the Sso7d DNA-binding protein from hyperthermophilic archaeon *Sulfolobus solfataricus.* Sso7d is a suitable protein for development of binding scaffold due to its small size (7kDa), high stability and lack of cysteines and glycosylation sites (Gera et al., 2011). Charge-neutralisation of this highly positively charged protein eliminated problems with non-specific interactions, while maintaining thermostability (Traxlmayr et al., 2016). Yeast display isolated binders with low nanomolar affinities towards variety of targets such as mouse serum albumin, growth factor receptor, small organic molecule and Notch1 receptor (Traxlmayr et al., 2016, Gocha et al., 2017).

The Sso7d library was screened against KRas to isolate R11.1.6 protein. Interestingly, R11.1.6 displayed preferential binding towards KRas G12D over wild-type KRas. R11.1.6 was also shown to directly block interaction with Raf, which in turn resulted in impaired downstream signalling through MAPK pathway. Structural studies of R11.1.6 in complex with KRas wild-type or G12D mutant provided insights into the basis for specificity. The major defining element in the specificity was the different conformation of switch I between the two structures. Therefore, this study highlighted the importance of consideration of switch I states during development of mutant-specific Ras inhibitors. Additionally, the R11.1.6-KRas structure revealed an extensive hydrophobic interaction surface, which

could be exploited for future development of oncogenic Ras inhibitors (Kauke et al., 2017).

1.7.4 Monobody

The fibronectin type III domain was used to develop monobody scaffold proteins (Koide et al., 1998). These are immunoglobulin-like domains, which adopt a β-fold with randomised loops for molecular recognition. Properties of monobodies include high thermostability, lack of cysteine residues and post-translational modifications, high affinity and specificity of binding and minimal potential of immunogenicity, due to high concentration of fibronectin in human plasma. Various display systems, including phage, mRNA, yeast and yeast two-hybrid, have been used to isolate binders against variety of targets including growth factor receptors, SH2 and SH3 domains and kinases (Bloom and Calabro, 2009).

A Monobody isolated against Ras, NS1, displayed binding to HRas and KRas isoforms irrespective of their nucleotide bound forms. Moreover, NS1 potently inhibited growth factor signalling and HRas and KRas-mediated oncogenic transformation. Structural studies demonstrated binding to a novel allosteric site, α4-β5-α6 (Figure 1.9B, discussed in more detail in section 5.1). This region was shown to be crucial for Ras dimerization and nanoclustering, which in turn is required for CRaf-BRaf heterodimerisation and activation (Spencer-Smith et al., 2017a). In addition, recent studies demonstrated ability of NS1 to inhibit KRas-driven tumour growth *in vivo* (Khan et al., 2018). In summary, these findings established the importance of the allosteric regulatory site in Ras-mediated signalling and provided an invaluable tool for studying Ras dimerization and nanoclustering.

1.7.5 DARPin

Designed Ankyrin Repeat Proteins (DARPins) are another example of engineered proteins currently under clinical evaluation (Table 1.1). DARPins are derived from ankyrin repeat proteins, elementary binding proteins for numerous biological processes. Single ankyrin repeat structure consists of β-turn followed by two antiparallel α-helices. DARPins usually contain four to six repeats, yielding a solenoid-shaped structure with hydrophobic core and large interaction surface (discussed in more detail in section 5.1) (Pluckthun, 2015). Libraries of DARPins

are generated by sequence alignments of natural ankyrin repeat motifs along with structural analysis (Binz et al., 2003). Using ribosome display, variants with picomolar binding affinities were selected against variety of targets, including maltose-binding proteins and ERK. Interestingly, ERK-specific DARPins were able to distinguish between the inactive and active (doubly phosphorylated, p-ERK) forms. Moreover, fusion of p-ERK-specific DARPin with fluorescent dye allowed real-time visualisation of active ERK in mouse embryo fibroblasts (Kummer et al., 2013). Thus, demonstrating that DARPins could be also used as biosensors of protein active states. The potential of using DARPins as therapeutic agents is currently evaluated in clinical trials with VEGF-A specific DARPin for treatment of advanced solid tumours, age-related macular degeneration and diabetic macular edema (Pluckthun, 2015, Rodon et al., 2015).

DARPins have been also used to target Ras. Interestingly, DARPin K27 isolated against KRas (Figure 1.9C), was shown to target the inactive Ras-GDP form and inhibited nucleotide exchange of Ras. This translated into inhibition of downstream activation of ERK and AKT and impairment of Ras-mediated transformation. Structural studies demonstrated that K27 interaction interface on Ras overlaps with that of Sos, however without the conformational change in switch I required for nucleotide release. Therefore, K27 trapped KRas in inactive conformation. These findings established inhibition of nucleotide exchange as a promising new approach to block Ras-mediated signalling, and provided novel tools for better understanding of this mechanism of inhibition (Guillard et al., 2017).

In contrast, DARPin K55 inhibited Ras:Raf interaction, by binding to a region where Raf binds, therefore directly competing with Raf binding to Ras. Similarly to K27, DARPin K55 was shown to impair Ras-mediated downstream signalling and transformation (Guillard et al., 2017). Along with iDab6, R11.1.6 and Ras:Raf Affibodies, these findings further highlight the importance of Ras:Raf PPI for inhibition of Ras-driven signalling (Martin et al., 2018).

1.7.6 Affimer

Recently, a novel artificial binding protein, termed Affimer, was developed (Tiede et al., 2017, Tiede et al., 2014). Two types of the Affimer scaffold are available, and these are described below.

1.7.6.1 Type I Affimer

The Type I Affimer scaffold is based on the human protease inhibitor Stefin A (Stadler et al., 2011). It is a 98 amino acids, single-chain protein, which uses exposed peptide loops to bind its target (Figure 1.10A). Site-directed mutagenesis abolished binding to Stefin A natural substrates (cathepsins) and allowed insertion of randomised peptides into the N-terminal and two hairpin loop regions (herein termed variable regions). This scaffold was termed Stefin A Quadrupole Mutant-Tracy, and successful expression has been obtained from *E. coli*, yeast and human cells and on the surface of the phage (Stadler et al., 2011).

Yeast-two hybrid libraries were created, using the scaffold with randomised either 10 residues in variable region 1 (VR1) or 12 residues in variable region 2 (VR2) or with simultaneously randomised 6 residues in VR1 and 12 residues in VR2. These libraries, comprising ~ 10^7 clones each, were screened to identify specific binders for the POZ domain of B-cell lymphoma 6 protein (BCL-6) and for the peptide derived from the penicillin binding protein PBP2' (Stadler et al., 2011). Since the initial screens, phage display libraries of this scaffold have been created and are used for screening.

1.7.6.2 Type II Affimer

The Type II Affimer scaffold, originally termed the Adhiron, is related in structure to the Type I scaffold (Tiede et al., 2014). It is based on a consensus sequence of plant-derived phytocystatin, encoding four-strand β-sheet core with central α-helix and two randomised 9 amino acid loop regions for specific molecular recognition (Figure 1.10B) (Tiede et al., 2014). Similarly to the Type I, the Type II Affimer scaffold's properties include small size, high solubility and stability, high-affinity target binding as well as lack of disulphide bonds and glycosylation sites, thus matching the criteria for engineered therapeutic proteins (Carter, 2011). Specific Affimers are isolated by employing phage display technique to screen the Affimer library. Since the initial proof-of-concept study, which isolated highly

specific Affimers against yeast SUMO protein (Tiede et al., 2014), specific Affimers displaying nanomolar binding affinities were selected for more than 350 diverse targets, including modular domains, growth factor receptors, ion channels and small organic compounds. The extent to which Affimers can be used in applications such as dissection of intracellular pathways, inhibition of extracellular receptor function, modulation of ion channel function, *in vivo* imaging, affinity fluorescence, super-resolution microscopy, diagnostics and in drug discovery has been evaluated (Tiede et al., 2014, Tiede et al., 2017). For example, Affimer targeting glypican-3, a marker for hepatocellular carcinoma, have been used in combination with antibody to develop immunological diagnosis kit (Xie et al., 2017a). In addition, Affimer specifically binding to anti-myc tag antibody was integrated into electrochemical biosensor, generating label-free, high sensitivity biosensor. This demonstrated that use of Affimers as the capture molecules, which offer high stability, specificity and affinity, is a suitable approach for label-free detection of biomarkers (Raina et al., 2015). Noteworthy, Affimers have also been used to gain new insights into the HIF-1α/p300 protein–protein interaction, which plays an important role in tumour metabolism. Affimers were shown to inhibit this interaction with low micromolar affinity and indicated important binding regions on p300 surface, yielding information that could inform novel inhibitor design and development (Kyle et al., 2015). Importantly, Affimers have been also used to target members of the PI3K signalling cascade. This pathway is parallel to MAPK signalling, that can be activated by oncogenic Ras. Affimers against p85, a regulatory subunit of PI3K, blocked p85 function and effected downstream AKT phosphorylation. These findings therefore, demonstrated Affimers as valuable tools to study intracellular signalling (Tiede et al., 2017).
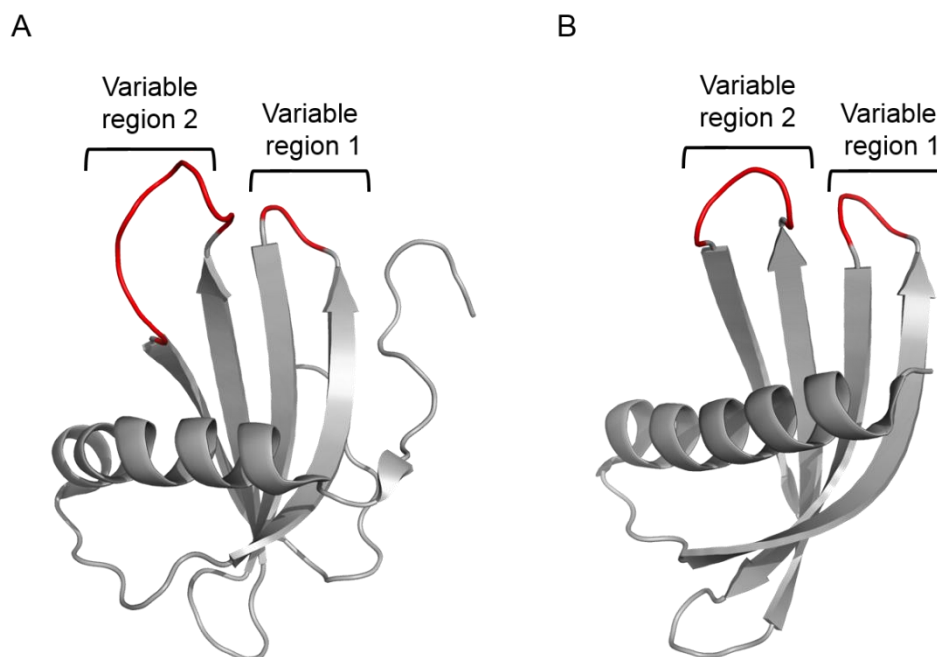
Figure 1.10 Structures of the Affimer scaffolds. Crystal structures of A) Affimer Type I (PDB: 1NB5) and B) Affimer Type II (PDB: 4N6U) with variable regions indicated in red. Images generated in PyMOL.

1.8 Objectives

The overall aim of this project was to investigate the suitability of Affimer reagents as new Ras-targeting molecular biology tools to study Ras function. Affimer reagents targeting Ras have previously been isolated, and preliminary experiments demonstrated the ability of these to modulate Ras activity. This project aimed to characterise selected Affimers, to develop new tools to study Ras function. Biochemical and structural characterisation of isolated binders were employed to understand the mode of action of these Affimers. Further characterisation of selected Affimers involved investigating their ability to block oncogenic Ras signalling in mammalian cells. This biochemical, structural and cellular understanding of Affimers action on Ras function could be used to inform development of new anti-Ras therapeutics. If successful, this strategy may be applied to screen for unique binding proteins against other disease-related targets, which are currently considered as 'undruggable'.

Chapter 2

Materials and Methods

Chapter 2

Materials and Methods

2.1 Materials

2.1.1 General materials

Primers used for sub-cloning (sequences shown in Table 2.2) and site-directed mutagenesis (sequences shown in Table 2.3) were obtained from Sigma-Aldrich. Primary and secondary antibodies were used as described in Table 2.4. Plasmids pFLAG-CMV-hErk1 (#49328) and pBabe-puro (#1764) were purchased from Addgene. Affimer-mimicking compounds were supplied by Dr Richard Foster, University of Leeds. Compounds 8-10 were purchased from ChemDiv.

2.1.2 Bacterial strain genotypes

BL21 Star™ (DE3) *E. coli* cells were purchased from Invitrogen (Life Technologies) and were used for protein production. XL-1 Blue supercompetent *E. coli* cells were purchased from Stratagene (Agilent Technologies) and were used for replication of plasmid DNA. The genotypes of each strain are shown in Table 2.1.

E.coli strain	Genotype
BL21 Star™ (DE3)	F- *ompT hsdS*$_B$ (r$_B^-$, m$_B^-$) *gal dcm rne*131 (DE3)
XL1-Blue Supercompetent	*recA1 endA1 gyrA96 thi-1 hsdR17 supE44 relA1 lac* [F´ *proAB lacI*^{q} *Z∆M15* Tn*10* (Tet^r)]

Table 2.1 Genotypes of competent bacterial strains used in this project.

2.1.3 Primers used for sub-cloning

Primers were used in the amplification of Ras or Affimer DNA from parent vectors by polymerase chain reaction (PCR), for sub-cloning into destination vectors.

Primer name	Primer sequence (5' – 3')
GST-KRas forward	TCGCGGATCCACCGAATATAAACTGGTGGTTG
GST-KRas reverse	CGTTGGGAATTCTTATTTATGTTTGCGAATTTCACG
KRas-forward	CGCGCTAGCATGACCGAATATAAACTGGTGG
KRas-reverse	CGTTGGCGGCCGCTTATTTATGTTTGCGAATTTCACG
DD-Affimer forward	GAACTGAGATCTCTGCTAGCAACTCCCTGGAAATC
DD-Affimer reverse	GTCATCCCATGGCTAAGCGTCACCAACCGGTTTGAAC
Affimer-His forward	ATGGATCCGCCACCATGGCCGCTACCGGTGTTCGTG
Affimer-His reverse	GTTTGGCCAACCACTGCGACTAATATTTCTACTGCTACTGTT CGTAGTAGTAGTAGTAGTAATCCCATTCGCCGGCGATTACG
Affimer-GFP forward	TATACTCGAGGCCACCATGGCTAGCAACTCCCTGG
Affimer-GFP reverse	ATAACGCGTGTCACCAACCGGTTTGAACTC
Affimer-VR1 forward	ATGGCTAGCAACTCCCTGGAAATCGAAG
Affimer-VR1 reverse	CACCGTCTTTAGCTTCCAGG
Affimer-VR2 forward	CCTGGAAGCTAAAGACGGTG
Affimer-VR2 reverse	TACCCTAGTGGTGATGATGGTGATGC

Table 2.2 List and sequences of primers used for sub-cloning.

Primer name	Primer sequence
K6-VR1.1 forward	TGTTAAAGCGAAAGAACAGGCTTTCACTCCGTGGTTCCAG
K6-VR1.1 reverse	CTGGAACCACGGAGTGAAAGCCTGTTCTTTCGCTTTAACA
K6-VR1.2 forward	TCGTGTTGTTAAAGCGAAAGAACAGCATGCTACTCCGTGGTTCCAG
K6-VR1.2 reverse	CTGGAACCACGGAGTAGCATGCTGTTCTTTCGCTTTAACAACACGA
K6-VR1.3 forward	GAAAGAACAGCATTTCGCTCCGTGGTTCCAGCG
K6-VR1.3 reverse	CGCTGGAACCACGGAGCGAAATGCTGTTCTTTC
K6-VR1.4 forward	TAAAGCGAAAGAACAGCATTTCACTGCTTGGTTCCAGCGTA
K6-VR1.4 reverse	TACGCTGGAACCAAGCAGTGAAATGCTGTTCTTTCGCTTTA
K6-VR1.5 forward	AAAGAACAGCATTTCACTCCGGCTTTCCAGCGTAACACCATGTAC
K6-VR1.5 reverse	GTACATGGTGTTACGCTGGAAAGCCGGAGTGAAATGCTGTTCTTT
K6-VR1.6 forward	GAACAGCATTTCACTCCGTGGGCTCAGCGTAACACCATGTACTAC
K6-VR1.6 reverse	GTAGTACATGGTGTTACGCTGAGCCCACGGAGTGAAATGCTGTTC
K6-VR1.7 forward	CAGCATTTCACTCCGTGGTTCGCTCGTAACACCATGTACTACCTG
K6-VR1.7 reverse	CAGGTAGTACATGGTGTTACGAGCGAACCACGGAGTGAAATGCTG
K6-VR1.8 forward	CACTCCGTGGTTCCAGGCTAACACCATGTACTACC
K6-VR1.8 reverse	GGTAGTACATGGTGTTAGCCTGGAACCACGGAGTG
K6-VR1.9 forward	CATTTCACTCCGTGGTTCCAGCGTGCTACCATGTACTACCTGACC
K6-VR1.9 reverse	GGTCAGGTAGTACATGGTAGCACGCTGGAACCACGGAGTGAAATG
K6-VR2.1 forward	CTGTACGAAGCGAAAGTTTGGGTTAAGGCTATTATGGTTACCGATAAA ATGAGAAAC
K6-VR2.1 reverse	GTTTCTCATTTTATCGGTAACCATAATAGCCTTAACCCAAACTTTCGC TTCGTACAG
K6-VR2.2 forward	GAAGCGAAAGTTTGGGTTAAGAGAGCTATGGTTACCGATAAAATGAGA AAC
K6-VR2.2 reverse	GTTTCTCATTTTATCGGTAACCATAGCTCTCTTAACCCAAACTTTCGC TTC
K6-VR2.3 forward	TGTACGAAGCGAAAGTTTGGGTTAAGAGAATTGCTGTTACCGATAAAA TGAGAAACT
K6-VR2.3 reverse	AGTTTCTCATTTTATCGGTAACAGCAATTCTCTTAACCCAAACTTTCG CTTCGTACA
K6-VR2.4 forward	AAAGTTTGGGTTAAGAGAATTATGGCTACCGATAAAATGAGAAACTTC
K6-VR2.4 reverse	GAAGTTTCTCATTTTATCGGTAGCCATAATTCTCTTAACCCAAACTTT
K6-VR2.5 forward	AAAGTTTGGGTTAAGAGAATTATGGTTGCTGATAAAATGAGAAACTTC AAAGAACTG
K6-VR2.5 reverse	CAGTTCTTTGAAGTTTCTCATTTTATCAGCAACCATAATTCTCTTAAC CCAAACTTT
K6-VR2.6 forward	GGTTAAGAGAATTATGGTTACCGCTAAAATGAGAAACTTCAAAGAAC
K6-VR2.6 reverse	GTTCTTTGAAGTTTCTCATTTTAGCGGTAACCATAATTCTCTTAACC
K6-VR2.7 forward	GGGTTAAGAGAATTATGGTTACCGATGCTATGAGAAACTTCAAAGAAC TGCAGG
K6-VR2.7 reverse	CCTGCAGTTCTTTGAAGTTTCTCATAGCATCGGTAACCATAATTCTCT TAACCC
K6-VR2.8 forward	GAAAGTTTGGGTTAAGAGAATTATGGTTACCGATAAAGCTAGAAACTT CAAAGAACTGC
K6-VR2.8 reverse	GCAGTTCTTTGAAGTTTCTAGCTTTATCGGTAACCATAATTCTCTTAA CCCAAACTTTC
K6-VR2.9 forward	AAGAGAATTATGGTTACCGATAAAATGGCTAACTTCAAAGAACTGCAG GAGTTCAAA
K6-VR2.9 reverse	TTTGAACTCCTGCAGTTCTTTGAAGTTAGCCATTTTATCGGTAACCAT AATTCTCTT

Table 2.3 Sequences of primers used for site-directed mutagenesis of Affimer K6.

Antigen	Species	Concentration (mg/ml)	Dilution factor	Source	Catalogue number
Ras	Rabbit	1.175	IB: 1:1000	Abcam	EPR18713-13
6xHis (HRP)	Rabbit	0.100	IB: 10 000 ELISA: 1:5000	Abcam	ab1187
Phospho ERK	Mouse	0.200	IB: 1:1000	Santa Cruz Antibodies	C2618
Phospho ERK	Rabbit	0.500	IF: 1:100	Cell Signalling Technology	4370L
ERK	Rabbit	1.078	IB:1:1000	Abcam	ab184699
Tubulin	Rat	1.000	IB:1:3000	BioRad	MCA77G
Destabilisation domain (DD)	Mouse	0.125	IB: 1:2000	Takara Bio	631073
GST (HRP)	Rabbit	0.178	IB: 1:5000	GeneTex	GTX114099
Rabbit IgG	Goat	0.065	IB: 1:10 000	Cell Signalling Technology	7074S
Rabbit IgG	Goat, AlexaFluor 568	2.000	IF: 1:10 000	Life Technologies	A11011
Mouse IgG	Goat	0.500	IB: 1:10 000	Abcam	ab97040
Rat IgG	Goat	1.000	IB: 1:10 000	Abcam	ab97057

Table 2.4 Primary and secondary antibodies. Details of antibodies species, concentration, dilution factor and source. IB: immunoblot, IF: immunofluorescence, ELISA: enzyme-linked immunosorbent assay.

2.1.4 Cell lines

Cell lines HEK293, Phoenix A, U2-OS, were maintained in Dulbecco's Modified Eagle Medium (DMEM), high glucose, GlutaMAX medium (Thermo Fisher, cat. no. 10569010) + 10% fetal bovine serum (FBS, Thermo Fisher, cat. No. 10270). Cell line Panc 10.05 was maintained in Roswell Park Memorial Institute (RPMI) 1640 Medium, GlutaMAX (Thermo Fisher, cat. No. 61870044) +15% FBS, 10U insulin. Cell lines DLD-1 and SW620 were maintained in RPMI +10% FBS. Panc 10.05 cell line was purchased from ATCC (CRL-2547). HEK293, Phoenix A and U2-OS cells were obtained from Dr Heather Martin, Leeds. DLD-1 and SW620 cells were obtained from prof. Mark Hull, St. James's University Hospital, Leeds. All cell lines used were mycoplasma-free.

2.2 Methods

2.2.1 DNA protocols and molecular sub-cloning

2.2.1.1 Polymerase Chain Reaction (PCR)

The DNA sequences used during sub-cloning into various expression vectors were amplified by the polymerase chain reaction (PCR). The primers used in each reaction were dependent upon the parent and recipient vectors, and are detailed in the relevant method sections describing protein production and mammalian cell line production. The reactions were performed in 200 µl PCR tubes, using a G-Storm™ GS2 thermal cycler. Reactions were carried out with Phusion® High-Fidelity DNA polymerase (New England Biolabs; NEB) using the components supplied with the polymerase. Reaction components and thermocycling conditions are detailed in Table 2.5 and Table 2.6. Following thermocycling, the template methylated DNA was digested by 10 U *Dpn I* (NEB) for 1 h at 37 °C. The PCR product was then purified using a NucleoSpin® Gel and PCR Clean-up kit (Macherey-Nagel), according to the manufacturer's instructions. DNA was eluted using 50 µl nuclease-free water.

Component	25 µl Reaction	Final Concentration
Sterile Water	13.8 µl	
5X Phusion HF Buffer	5 µl	1X
dNTP Mix, 25 mM	0.2 µl	200 µM each
DMSO	0.75 µl	3%
Forward Primer, 10 µM	2 µl	0.8 µM
Reverse Primer, 10 µM	2 µl	0.8 µM
Phusion DNA Polymerase	0.25 µl	0.02 units/µl
Template DNA	1 µl	

Table 2.5 Composition of thermal cycling reaction.

Cycle Step	Temperature	Time	Cycles
Initial Denaturation	98°C	30 seconds	1
Denaturation	98°C	20 seconds	
Annealing	54°C	20 seconds	30
Extension	72°C	20 seconds	
Final Extension	72°C	10 minutes	1
Hold	4°C	Hold	

Table 2.6 Cycling conditions for Phusion PCR method.

2.2.1.2 Agarose gel electrophoresis

Nine microliters of the PCR amplified and *Dpn I* digested DNA were mixed with 1 µl of the 10x DNA loading dye (30 % glycerol; 0.2 % Orange G; H_2O; final concentration 1x) and 5 µl of samples were loaded onto a 2 % (w/v) agarose gel in Tris-acetate-EDTA (TAE) buffer (40 mM Tris; 20 mM acetic acid, 1 mM EDTA, pH 8.0), containing 1X SYBR® Safe DNA Gel Stain. Quick-Load® Purple 2-log DNA Ladder (NEB) was loaded into a separate well. Electrophoresis was carried out in Mini-Sub® Cell GT apparatus (Bio-Rad) in TAE buffer at 100 V. DNA bands were visualised under UV light and imaged using an Amersham™ Imager 600 (GE Healthcare).

DNA purification from agarose gel was performed for the recipient vector DNA. After the electrophoresis, bands were excised from the gel using a scalpel. Extraction of the DNA was performed using a NucleoSpin® Gel and PCR Clean-up kit (Macherey-Nagel), according to the manufacturer's instructions. DNA was eluted using 50 µl nuclease-free water.

2.2.1.3 Restriction digestion

The restriction enzymes (purchased from NEB) used were dependent on the recipient vectors, and are detailed in the relevant method sections describing protein production and mammalian cell line production. The restriction digestion reactions were carried out in a total reaction volume of 50 µl containing 10 U restriction enzyme(s), 1 – 5 µg DNA and 1X CutSmart® Buffer (NEB) in nuclease-free water. The resulting fragments were purified using a NucleoSpin® Gel and

PCR Clean-up kit (Macherey-Nagel), according to the manufacturer's instructions. DNA was eluted using 50 µl nuclease-free water.

The recipient vector DNA was dephosphorylated to remove 5' phosphate and prevent self-ligation. Dephosphorylation was carried out using Antarctic Phosphatase in a total reaction volume of 60 µl, containing 5 U Antarctic Phosphatase (NEB), 5 µg vector DNA and 1X Antarctic Phosphatase Reaction Buffer (NEB) in nuclease-free water. After incubation for 15 min at 37 °C, Antarctic Phosphatase was heat inactivated by incubation at 65 °C for 5 mins.

2.2.1.4 DNA ligation

Ligation reactions were performed in a total volume of 20 µl, containing 25 ng vector DNA, 75 ng insert DNA, 1 U T4 DNA Ligase (Roche) and 1X T4 DNA Ligase Buffer (Roche), in nuclease-free water. Ligation reactions were incubated at 4 °C overnight, followed by transformation of XL-1 Blue supercompetent *E. coli* cells.

2.2.1.5 Transformation of *E. coli* bacterial strains with DNA

The appropriate competent cells for each construct were thawed on ice. 1 µl of DNA was aliquoted to microcentrifuge tube and pre-chilled on ice, following by addition of 10 µl of cells (per transformation). The cell/DNA mixture was mixed and incubated on ice for 30 minutes, followed by heat shock in a 42 ºC water bath for 45 seconds. Samples were then incubated for further 2 min on ice, before addition of 190 µl of SOC media (2% (w/v) tryptone, 0.5% (w/v) yeast extract, 10 mM NaCl, 2.5 mM KCl, 10 mM $MgCl_2$, 10 mM $MgSO_4$, and 20 mM glucose). Mixture was incubated at 37°C for 1 hour with shaking at 230 rpm. 100 µl of the transformation mixture was plated onto Lennox L agar plate (Invitrogen® Life Technologies, 10 g/L SELECT peptone 140; 5 g/L SELECT yeast extract; 5 g/L sodium chloride; 12 g/L SELECT agar) containing 100 µg/ml carbenicillin (LB-carb plate) and incubated overnight at 37°C.

2.2.1.6 Purification of plasmid DNA

The sub-cloned plasmid DNA was purified by QIAprep® Spin Miniprep Kit for use of the plasmid in bacterial production or HiSpeed® Plasmid Maxi Kit (Qiagen) for use in production of mammalian cell lines. A single bacterial colony from LB-carb

plate was inoculated into 5 ml of Lennox L Broth Base (LB media, Invitrogen™, cat. no. 12780-052) containing 100 µg/mL carbenicillin (LB-carb media) and incubated overnight at 37°C and 230 rpm. For minipreps, the overnight cultures were centrifuged at 4816 xg for 10 min at 4 °C and the plasmid DNA purified using the QIAprep Spin Miniprep kit, according to the manufacturer's instructions. For maxipreps, the overnight cultures were used to inoculate 150 ml LB-carb media and incubated overnight at 37 °C, 230 rpm. Cells were pelleted at 4816 xg for 20 min at 4 °C and plasmid DNA purified using the HiSpeed® Plasmid Maxi Kit, according to the manufacturer's instructions. DNA was eluted in nuclease-free water.

2.2.1.7 Determination of DNA concentration

The concentration of purified DNA was measured by a NanoDrop™ Lite spectrophotometer. The instrument was blanked with nuclease-free water, before taking measurements of the DNA samples. The absorbance at 260 nm has been used to calculate the DNA concentration using the Beer-Lambert Law ($A260 = \varepsilon cl$, where ε is the extinction coefficient, c is the DNA concentration in ng/µl and l is the path length in cm).

2.2.1.8 DNA sequencing

Sub-cloning was confirmed by DNA sequencing. The purified plasmid DNA was diluted to 100 ng/µl and sequencing was performed by Genewiz, using the primers detailed in Table 2.7.

Plasmid	Primer name	Primer DNA sequence (5'-3')
pET11a	T7	TAATACGACTCACTATAGGG
pGEX-6P-2	5GEX	GGGCTGGCAAGCCACGTTTGGTG
pcDNA5	BGHR	TAGAAGGCACAGTCGAGG
pRetroX-PTuner	pRetroX sequencing (custom)	CTGACTATATCTCCAGATTATG
pCMV6-AC-GFP	VP1.5	GGACTTTCCAAAATGTCG

Table 2.7 Primers used for DNA sequencing of plasmids.

2.2.1.9 Construction of K6ΔVR2 mutant

To generate Affimer K6ΔVR2 mutant, residues of the K6 variable region 2 were replaced with these from the Alanine Affimer (AAE). Affimer K6 variable region 1 was amplified by Phusion PCR (as detailed in 2.2.1.1), using 1 µl of Affimer K6 DNA, Affimer-VR1 forward and reverse primers (Table 2.2) and reaction components outlined in Table 2.5. Thermal cycling was performed using parameters outlined in Table 2.6. The same approach was used to amplify Alanine Affimer variable region 2 DNA sequence, but using Alanine Affimer DNA and Affimer-VR2 forward and reverse primers (Table 2.2) instead. PCR products were purified by PCR clean-up kit and subjected to splice overlap extension (SOE) PCR (as detailed in 2.2.1.1 but without any primers used) to anneal the two fragments together, followed by normal Phusion PCR with Affimer-His forward and reverse primers (Table 2.2). The spliced product was digested with *Nhe I* and *Not I* overnight at 37ºC. The digestion products were purified using Qiagen Gel and PCR Clean up kit and according to the manufacturer's instructions and sub-cloned into the pET11a vector double digested with *Nhe I* and *Not I*. Ligated DNA was transformed into XL-1 Blue super-competent cells for culturing and DNA extracted by mini-preparation. Resulting DNA was sent for sequencing to confirm successful ligation. On return of sequencing data, correctly sub-cloned DNA was transformed into BL21 Star™ DE3 cells for protein expression.

2.2.1.10 Alanine scanning by site directed mutagenesis

Mutagenic primers were designed using QuikChange primer design online tool (https://www.chem.agilent.com/store/primerDesignProgram.jsp) to substitute variable regions' residues to alanine (shown in Table 2.3). The reactions containing 1x KOD Polymerase reaction buffer, 0.2 mM dNTP 2 mM $MgSO_4$, 0.3 µM of forward and reverse primers, 10 ng DNA template and 1 U KOD polymerase in a total of 50 µl were subjected to thermal cycling using parameters shown in Table 2.8. Following thermal cycling, samples were digested with *Dpn I* for 1 h at 37ºC. XL1-Blue supercompetent cells were transformed with *Dpn I* treated samples, as outlined in section 2.2.1.5. Sub-cloned plasmid DNA was extracted using QIAprep Spin Miniprep Kit. Mutagenesis was confirmed by sequencing (Genewiz).

Cycle Step	Temperature	Time	Cycles
Initial Denaturation	98°C	2 minutes	1
Denaturation	98°C	20 seconds	
Annealing	68°C	10 seconds	30
Extension	70°C	3.5 minutes	
Final Extension	70°C	5 minutes	1

Table 2.8 Cycling conditions for site-directed mutagenesis protocol.

2.2.2 Protein analysis

2.2.2.1 Protein concentration determination

The concentration of purified proteins was measured using a NanoDrop™ Lite spectrophotometer. The instrument was blanked with the appropriate sample buffer before sample reading. Concentration was determined from the absorbance at 280 nm (A280) using the Beer-Lambert law (A280 = εcl, where ε is the extinction coefficient, c is the protein concentration in mg/ml and l is the path length in cm). Extinction coefficients for each protein were calculated using ExPASy ProtParam software.

Total protein concentration of cell lysates was determined by the bicinchoninic acid (BCA) assay. A Pierce™ BCA Protein Assay Kit was used, according to the manufacturer's instructions for 5 μl samples in a microplate format.

2.2.2.2 SDS-PAGE

Purified proteins or whole cell lysates were re-suspended in 4x SDS sample buffer (200mM Tris-HCl, 8% SDS, 20% glycerol, 20% mercaptoethanol, 0.1% (w/v) bromophenol blue) and incubated at 95ºC for 5 minutes. Samples were loaded onto 12.5% or 15% (w/v) SDS-polyacrylamide resolving gel (1.5 M Tris-HCl, 0.4 % (w/v) SDS, pH 8.9) with 7.5% (w/v) SDS-polyacrylamide stacking gel (0.4M Tris-HCl, 0.4 % (w/v) SDS, pH 6.7) and run at 150 V for 60 minutes in SDS-running buffer (25 mM Tris, 192 mM glycine, 0.1% SDS). PageRuler™ Prestained Protein Ladder (10–180 kDa) was used as molecular weight marker. Gels were stained for 45 min in Coomassie Blue (45% methanol; 7% acetic acid; 0.25% Coomassie Brilliant Blue R-250 (Sigma-Aldrich)) and de-stained overnight in 25%

methanol and 7.5% acetic acid. Coomassie-stained gels were imaged using an Amersham™ Imager 600 (GE Healthcare).

2.2.2.3 Immunoblotting

Proteins subjected to SDS-PAGE were transferred onto nitrocellulose membrane in transfer buffer (100mM Tris, 191mM glycine, 20% (v/v) methanol) using the Turbo transblot. Membranes were incubated in 5 % (w/v) skimmed milk (in TBS-T (10mM Tris.HCl, 15mM NaCl, 0.1% Tween- 20 at pH7.5)) for 1 h on a rocker at room temperature. Membranes were then incubated with primary antibodies (Table 2.4) overnight at 4ºC and washed 3 times for 5 min in TBS-T prior to incubation with HRP-conjugated secondary antibodies (Table 2.4) in 5 % (w/v) skimmed milk in TBS-T for 1 h at room temperature. Membranes were then washed 3 times for 5 min in TBS-T followed by detection using the Immunoblot forte Western HRP substrate (Millipore), according to the manufacturer's instructions. Images were taken using an Amersham™ Imager 600 (GE Healthcare). Quantification of proteins was performed using densitometry on ImageQuant TL 8.1 analysis software (GE Healthcare) and quantities were corrected against loading controls.

2.2.3 Protein production

2.2.3.1 Affimers

His-tagged Affimers were produced in *E. coli* BL21 Star™ DE3 Star cells. Briefly, a single bacterial colony from transformed cells was used to inoculate a 5 ml LB media (Invitrogen) with 100 µg/mL carbenicillin (LB-carb media). Then 500 ml LB-carb media was inoculated with 5 ml of overnight culture and grown at 37°C and 230 rpm to an OD600 between 0.6–0.8, before addition of 0.5 mM isopropyl-β-D-thio-galactopyranoisde (IPTG) and further grown overnight at 25°C at 150 rpm. The cells were harvested by centrifugation at 4816 x g for 15 minutes. Cells were lysed in 50 mM NaH_2PO_4, 300 mM NaCl, 20 mM Imidazole and 10% Glycerol pH 7.4 supplemented with 0.1 mg/ml lysozyme, 1x Halt protease inhibitor cocktail and 10 U/ml Benzonase for 20 minutes at room temperature before heat denaturation at 50 °C for 20 minutes. The lysate was cleared by centrifugation at 4,816 x g for 20 minutes then 12,000 x g for a further 20 minutes, then incubated with 500 µl Ni-NTA resin at room temperature for 1h. Unbound proteins were

removed by centrifugation followed by extensive washing with 50 mM NaH_2PO_4, 500 mM NaCl and 20 mM Imidazole pH 7.4. His-tagged Affimers were eluted with 50 mM NaH_2PO_4, 500 mM NaCl, 500 mM imidazole and 10% glycerol pH 7.5. A280 was measured for the purified proteins, from which the protein concentration was calculated using the Beer-Lambert law. Protein purity was analysed by Coomassie staining on 15% SDS-PAGE.

2.2.3.2 KRas and HRas

Plasmids encoding N-terminally His-tagged and C-terminally biotin acceptor protein (BAP)-tagged KRas and HRas proteins were synthesised by GenScript. (Piscataway, USA). Plasmid encoding the wild-type (wt) KRas was used in a QuikChange™ mutagenesis to generate oncogenic KRas mutants: G12D, G12V and Q61H. These recombinant proteins were produced in *E. coli* BL21Star™ DE3 Star cells. A single bacterial colony from LB-carb plate was used to inoculate a 5 ml overnight culture in LB media (Invitrogen) with 100 µg/mL carbenicillin. Then 500 ml LB-carb media was inoculated with 5 ml of overnight culture and grown at 37°C and 230 rpm to an OD600 between 0.6–0.8, before addition of 0.5 mM IPTG and further grown overnight at 20 °C at 150 rpm. The cells were harvested by centrifugation at 4816 x g for 15 minutes. Cells were lysed in 50 mM Tris-HCl, 500 mM NaCl, 10 mM Imidazole, 5 mM $MgCl_2$, 5% Glycerol, pH 7.5 supplemented with 0.1 mg/ml lysozyme, 1x Halt protease inhibitor cocktail and 10 U/ml Benzonase for 20 minutes at 4 ºC. The lysates were cleared by centrifugation at 4,816 x g for 20 minutes then 12,000 x g for a further 20 minutes, then incubated with 500 µl Ni-NTA resin at 4 ºC for 1-2 h. Unbound proteins were removed by centrifugation followed by washing with 50 mM Tris-HCl, 500 mM NaCl, 20 mM Imidazole, 5 mM $MgCl_2$, 5% Glycerol, pH 7.5. His-tagged Ras proteins were eluted with 50 mM Tris-HCl, 500 mM NaCl, 300 mM Imidazole, 5 mM $MgCl_2$, 5% Glycerol, pH 7.5. OD280 was measured for the purified proteins, from which the protein concentration was calculated using the Beer-Lambert law. Protein purity was analysed by Coomassie staining on 15% SDS-PAGE.

2.2.3.3 GST-KRas

The KRas wt DNA sequence from expression vector pET11a was amplified by PCR (as detailed in 2.2.1.1) with GST-KRas forward and reverse primers

(Table 2.2). The PCR products were digested with *Bam HI* and *Eco RI* restriction enzymes at 37°C overnight (as described in 2.2.1.3). The digested products were purified using Qiagen Gel and PCR Clean up kit (Qiagen) according to the manufacturer's instructions and ligated with pGEX-6P-2 vector also digested with *Bam HI* and *Eco RI* restriction enzymes (as detailed in 2.2.1.4). Ligated DNA was transformed into XL-1 Blue super-competent cells (see 2.2.1.5) for culturing and DNA extracted by mini-preparation. Resulting DNA was sent for sequencing to confirm successful ligation. On return of sequencing data, correctly sub-cloned DNA was transformed into BL21 Star™ DE3 Star cells for protein production. Briefly, a single bacterial colony from LB-carb plate was used to inoculate a 5 ml overnight culture in LB media with 100 μg/mL carbenicillin. Then 500 ml LB-carb media was inoculated with 5 ml of overnight culture and grown at 37°C and 230 rpm to an OD600 between 0.6–0.8, before addition of 0.5 mM IPTG and further grown overnight at 20°C at 150 rpm. The cells were harvested by centrifugation at 4816 xg for 15 minutes. Cells were lysed in 50 mM Tris-HCl, 150 mM NaCl, 1 mM DTT, 5 mM MgCl2, 1% Triton X-100, pH 7.5 supplemented with 1mg/ml lysozyme, 1x Halt protease inhibitor cocktail and 3U/ml Benzonase for 30-60 minutes at 4°C. The lysates were cleared by centrifugation at 4,816xg for 20 minutes then 12,000 xg for a further 20 minutes, then incubated with 1 ml SuperGlu Agarose Affinity Resin (Generon, cat. no. SuperGlu 25A) at 4°C for 1-2h. Unbound proteins were removed by centrifugation followed by washing of the resin with 50 mM Tris-HCl, 150 mM NaCl, 1 mM DTT, 5 mM MgCl2, pH 7.5. GST-KRas was eluted with 50 mM Tris-HCl, 150 mM NaCl, 1 mM DTT, 5 mM MgCl2, 50 mM reduced glutathione, pH 7.5. Purified protein was dialysed into 50 mM Tris-HCl, 100 mM NaCl, 1 mM DTT, 5 mM MgCl2, 5% glycerol, pH 7.5 using Slide-A-Lyzer™ 10K MWCO dialysis cassette (Thermo Fisher). Protein concentration was measured using a BCA assay, as detailed in 2.2.2.1. Protein purity was analysed by Coomassie staining on 12.5% SDS-PAGE as described in 2.2.2.2.

2.2.3.4 Affimer-KRas complex

The KRas wt DNA sequence (without His- and BAP-tag) from expression vector pET11a was amplified by PCR (as detailed in 2.2.1.1) with KRas-forward and KRas-reverse primers (Table 2.2). The PCR products were digested with *Nhe I*

and *Not I* restriction enzymes at 37°C overnight (as described in 2.2.1.3). The digested products were purified using Qiagen Gel and PCR Clean up kit (Qiagen) according to the manufacturer's instructions and ligated with pET11a vector also digested with *Nhe I* and *Not I* restriction enzymes (as detailed in 2.2.1.4). Ligated DNA was transformed into XL-1 Blue super-competent cells (see 2.2.1.5) for culturing and DNA extracted by mini-preparation. Resulting DNA was sent for sequencing to confirm successful ligation. On return of sequencing data, correctly sub-cloned DNA was transformed into BL21 Star™ DE3 Star cells for protein production, as described in 2.2.3.2.

Affimer was produced and purified as outlined in 2.2.3.1. Purified Affimer was dialysed into phosphate buffered saline (PBS, 137 mM NaCl, 2.7 mM KCl, 8 mM Na_2HPO_4, and 2 mM KH_2PO_4) buffer using Slide-A-Lyzer™ 5K MWCO dialysis cassette (Thermo Fisher). A280 of the dialysed Affimer was measured, from which the protein concentration was calculated using the Beer-Lambert law. Ten milligrams of purified Affimer was mixed with KRas lysate and incubated on a roller overnight at 4 °C. Two hundred microliters of pre-washed Ni-NTA resin was added to Affimer-KRas lysate mixture and incubated on a roller for 1-2 h at 4 °C. Unbound proteins were removed by centrifugation followed by washing in 50 mM Tris, 150mM NaCl, 5mM $MgCl_2$, 1mM DTT, 20 mM Imidazole, 5% glycerol, pH 7.5. Complex was eluted with 50 mM Tris, 150mM NaCl, 5mM $MgCl_2$, 1mM DTT, 300 mM Imidazole, 5% glycerol, pH 7.5. Eluted proteins were analysed by Coomassie staining on 15 % SDS-PAGE. Affimer-KRas complex was further purified into 10mM Tris, 50 mM NaCl, 0.5mM TCEP, pH 8 by size exclusion chromatography, using HiPrep 16/60 Sephacryl S-100 column (GE Healthcare). Eluted proteins were analysed by Coomassie staining on 15 % SDS-PAGE. Purified complex was concentrated using Vivaspin 6 5K MWCO centrifugal concentrator (Sartorius) to 12 mg/ml as determined by the BCA protein assay.

2.2.3.5 Raf-RBD-GST expression

The GST-tagged Ras binding domain (RBD) of Raf1 in pGEX vector (Addgene) was used to transform BL21 Star™ DE3 cells for protein production. A single bacterial colony from LB-carb plate was used to inoculate a 5 ml overnight culture in LB media with 100 µg/mL carbenicillin. Then 500 ml LB-carb media was inoculated with 5 ml of overnight culture and grown at 37°C and 230 rpm to an

OD600 between 0.6–0.8, before addition of 0.5 mM IPTG and further grown overnight at 20°C at 150 rpm. The cells were harvested by centrifugation at 4816 xg for 15 minutes. Cells were lysed in 50 mM Tris-HCl, 150 mM NaCl, 1 mM DTT, 1% Triton X-100, pH 7.5 supplemented with 1mg/ml lysozyme, 1x Halt^{TM} protease inhibitor cocktail and 3U/ml Benzonase for 30-60 minutes at 4ºC. The lysates were cleared by centrifugation at 4,816xg for 20 minutes then 12,000 xg for a further 20 minutes and the cleared cell lysates were used for subsequent assays.

2.2.4 Ras nucleotide loading

Prior to nucleotide loading, 50 µM Ras protein was desalted into nucleotide loading buffer (25mM Tris-HCL, 50mM NaCl, 0.5mM MgCl$_2$ pH 7.5) using a Zeba^{TM} spin desalting column (Thermo Fisher) equilibrated with buffer according to the manufactures instructions. MANT-GDP or GTP was added in a 20 fold excess over Ras as well as 1mM DTT and 5mM EDTA in a final volume of 130 µl and incubated at 4 °C for 1h. After incubation MgCl$_2$ was added in a 2 fold excess over EDTA and incubated for a further 30 minutes at 4 °C. Ras-mGDP or Ras-GTP was then desalted using a Zeba spin column into nucleotide exchange (NE) buffer (20mM HEPES pH 7.5, 150mM NaCl, 10mM MgCl$_2$). Nucleotide loading was confirmed by native mass-spectrometry by Dr Kevin Tipping.

2.2.5 Guanine nucleotide exchange assay

Nucleotide exchange buffer was supplemented with 0.4 mM GTP and 0.5 µM Sos-cat (produced by Dr Kevin Tipping) for experiments involving wt Ras or 2µM Sos-cat for experiments involving mutant Ras proteins. The Affimers were diluted with this buffer to make 20 µM stock solutions, which were then used to make serial dilutions of the Affimers by diluting each new concentration of Affimer 2-fold with nucleotide exchange buffer supplemented with Sos-cat and GTP. A 1µM stock of the WT or mutant Ras-mGDP protein was made by diluting the stock Ras in nucleotide exchange buffer supplemented with 2 mM DTT. Solutions were incubated at 30°C for 10 min prior to the assay. The reaction was initiated by addition of Affimer/Sos-cat/GTP solution to Ras/DTT containing solution. Changes in fluorescence were measured by a fluorescence spectrometer (Tecan Spark) in a Corning black, flat-bottomed, non-binding 384 well plate at 440 nm

every minute for 90 minutes. The data was then normalised to Ras-only control and fit to a single exponential decay using OriginPro software. The derived rates were normalised to these of Ras-Sos and Ras-only samples and fit to Hill equation (y = START + (END – START) (xn / kn + xn) from which the IC$_{50}$ values were calculated.

2.2.6 Ras-Raf interaction assay

Glutathione magnetic agarose beads (Thermo Scientific, Cat. No. 78601) were blocked with 2x blocking buffer (Sigma, Cat. No. B6429) overnight at 4º C. Beads were then washed with Binding/Wash (B/W) buffer (125mM Tris, 150mM NaCl, 5mM MgCl$_2$, 1mM DTT, 0.01% Tween-20, pH 8.0) and incubated with Raf-RBD-GST soluble cell lysate for 1h at room temperature on a roller. At the same time, 1 µg of KRas-GTP (in B/W buffer) was incubated with 10 µg of Affimers (in PBS) or PBS (no Affimer control) for 1 h at room temperature on a roller. Beads were washed 3x with B/W buffer and mixed with KRas-Affimer solutions. The pulldown was performed on KingFisher, programmed to incubate Raf-RBD-GST bound beads with KRas-Affimers for 1 h at room temperature, followed by 4x washes with B/W buffer, 15 sec each and elution of pulled down proteins into SDS-PAGE sample buffer (200mM Tris-HCl, 8% SDS, 20% glycerol, 20% mercaptoethanol, 0.1% (w/v) bromophenol blue, pH 7). Proteins were then analysed by western blot with anti-GST and anti-Ras antibodies (Table 2.4).

2.2.7 ELISA

Maxisorp Nunc-Immuno strips (Sigma, Cat. No. Z755273-60EA) were coated with 100 µl of 1 µM GST-KRas and incubated overnight at 4 ºC on a shaker. Strips were then washed 3 times with PBST (137 mM NaCl, 8 mM Na$_2$HPO$_4$, 2 mM KH$_2$PO$_4$, 2.7 mM KCl, 0.1 % Tween-20, pH 7.4) on a plate washer (TECAN HydroSpeed), following by blocking with 10x Blocking Buffer (Sigma, Cat. No. B6429) for 3 h at 37º C. Strips were washed 3 x with PBST and incubated with dilutions of Affimers (in PBS) for 1 h at room temperature on a shaker. Wells were washed 3x with PBST, following incubation with anti-Hisx6-HRP antibody (Table 2.4) for 1 h at room temperature on a shaker. Antibody was washed off 3x with PBST and signal was developed with TMB substrate (Cat. No. S-001-TMB)

for 10 min at room temperature. Reaction was stopped by addition of H_2SO_4. Absorbance was measured at 450nm using plate reader.

2.2.8 Protein crystallisation

2.2.8.1 Initial screening

Crystallisation experiments were initiated with commercial crystal screens, JCSG Core I-IV (Qiagen). Using the NT8 drop setter robot (Formulatrix), the Affimer-KRas complex in 10mM Tris, 50 mM NaCl, 0.5mM TCEP, pH 8 at protein concentration of 12 mg/ml was mixed in 1:1 ratio with mother liquor, utilising the sitting-drop vapour diffusion technique. The plates were sealed and stored at room temperature. Crystal formation was monitored with the Rock Imager (Formulatrix) using visible light. In addition, the absorption of aromatic residues at 280nm (UV) has been employed in order to differentiate protein crystals from salt crystals and second-harmonic generation (SHG) microscopy has been used to detect crystal form.

2.2.8.2 Optimisation of crystallisation

Alterations of crystallisation conditions were made by changing the precipitant concentrations by 5% and the pH of the buffer by 0.5 unit. Hanging drops comprising 1 µl of Affimer-KRas protein complex with 1 µl of customized buffer were set up on cover slides, which were placed on top of the silliconised wells (Hampton Research) facing the buffer. Plates were incubated at room temperature and crystal formation was observed with a light microscope. Crystals were obtained in 0.1M Na acetate pH 5, 25% w/v PEG 4K, 0.2M $(NH_4)_2SO_4$, 5% MPD. Crystals were frozen in 30% w/v PEG 4K, 0.1M Na acetate, pH 5, 0.2M $(NH_4)_2SO_4$, 20mM $MgCl_2$, 5% PEG 400, 5% MPD, 5% ethylene glycol and 5% glycerol.

2.2.8.3   Crystal diffraction and structure determination

X-ray diffraction data was collected at the Diamond Light Source. The structure of KRas-K6 complex was solved by molecular replacement using Protein Data Bank (PDB) codes 4OBE for the KRas and 4N6U for the Affimer with the program Phaser (McCoy et al., 2007). Structures were refined using REFMAC5 (Murshudov et al., 1997), followed by iterative cycles of manual model building

using COOT (Emsley and Cowtan, 2004). Data collection and refinement statistics are summarized in Table 2.9. Data collection, processing and structure determination were carried out Dr Chi Trinh.

	KRas – Affimer K6
Data collection	
Beamline	I04-1 (Diamond Light Source)
Wavelength (Å)	0.9159
Space group	$I\,4_1$
a, b, c (Å)	71.6, 71.6, 144.4
α, β, γ (°)	90.0, 90.0, 90.0
Resolution (Å)	64.12 - 1.90 (1.95-1.90)
R_{merge}	0.084 (2.565)
R_{meas}	0.091 (2.828)
$R_{p.i.m}$	0.035 (1.17)
$\langle I/\sigma(I)\rangle$	13.3 (0.6)
CC(1/2)	1.00 (0.799)
No. of observed reflections	379142 (24154)
No. of unqiue reflections	28572 (2116)
Completeness (%)	100.0 (100.0)
Multiplicity	13.3 (11.4)
Refinement	
Resolution for refinement (Å)	64.12 - 1.90
R_{work}	0.232
R_{free}	0.268
Total No. of protein non-H atoms	1969
No. of ligands	1
No. of metal ions	1
No of water molecules	97
Wilson B factor ($Å^2$)	49.8
Bond lengths (Å)	0.013
Bond angles (°)	1.913
Average overall *B* factor ($Å^2$)	
Protein	25.7
Ligand	26.4
Water	39.8
Ramachandran analysis, the percentage of residues in the regions of plot (%) ξ	
Favoured	98.0
Allowed	1.6
Outliers	1

Table 2.9 X-ray crystallographic data collection, processing and refinement statistics for Affimer K6-KRas complex. Values given in parentheses correspond to those in the outermost shell of the resolution range.

$$R_{merge} = \sum_{hkl}\sum_{i}\left|I_i(hkl) - \langle I(hkl)\rangle\right| / \sum_{hkl}\sum_i I_i(hkl)$$

$$R_{pim} = \sum_{hkl}\{1/[N(hkl)-1]\}^{1/2}\sum_i\left|I_i(hkl) - \langle I(hkl)\rangle\right| / \sum_{hkl}\sum_i I_i(hkl)$$

R_{free} was calculated with 5% of the reflections set aside randomly.

ξ Ramachandran analysis using the program MolProbity (Chen et al., 2010).

2.2.9 Thawing cell lines

Cells were thawed at 37 ºC in water bath and transferred to 25 cm^2 flask containing 5 ml of pre-warmed growth medium. Cells were incubated at 37 °C for 1–2 days to allow attachment to the flask and passaged once reached 70-80% confluency.

2.2.10 Passaging cells

Cells were washed twice with Dulbecco's Phosphate-Buffered Saline (DPBS) (Corning) and incubated with 2 ml trypsin-EDTA (Gibco^{TM}) at 37 °C for 5 min to detach cells. Trypsin was neutralised by addition of 10 ml growth medium, and cells were pelleted by centrifugation at 1500 rpm for 5 min. Pelleted cells were re-suspended in growth medium and cell solution was distributed to new flasks and incubated at 37 °C, 5% CO_2.

2.2.11 Transient transfection of HEK293 cells

For transient transfection optimisation trials and immunofluorescence studies Affimer-tGFP constructs were used. Affimer DNA was amplified from the pET11a vector using the Affimer-GFP forward and reverse primers (Table 2.2) in PCR with an exception that annealing temperature of 60 ºC was used. The products were digested with *Asi SI* and *Mlu I.* The digested DNA fragments were ligated into *Asi SI* and *Mlu I* digested pCMV6-AC-GFP vector (Origene). The ligated plasmids were transformed into XL1-Blue cells and DNA extracted by mini-preparation. Resulting DNA was sent for sequencing to confirm successful sub-cloning. On return of sequencing data, DNA was transformed into XL-1 Blue cells for culturing and DNA was maxi-prepared (2.2.1.6) for transfection of HEK293 cells.

In addition, constructs encoding His-tagged Affimers were also generated and subsequently used in transient transfections of HEK293 cells. Affimer DNA was amplified from the pET11a vector using the Affimer-His forward and reverse primers (Table 2.2) in PCR with an exception that annealing temperature of 60ºC was used. The products were digested with *Bam HI* and *Not I.* The digested DNA fragments were ligated into *Bam HI* and *Not I* digested pcDNA5/FRT/TO vector (Thermo Fisher). The ligated plasmids were transformed into XL1-Blue cells and

DNA extracted by mini-preparation. Resulting DNA was sent for sequencing to confirm successful sub-cloning. On return of sequencing data, DNA was transformed into XL-1 Blue cells for culturing and DNA was maxi-prepared (2.2.1.6) for transfection of HEK293 cells.

400 000 HEK293 cells were seeded per well of 6-well plate and incubated for 24 h at 37º C, 5 % CO_2. 150 µl of Opti-MEM media (Thermo Fisher, cat. No. 31985070) was mixed with 6 µl of Lipofectamine 2000 (Thermo Fisher, 11668027), and incubated at room temperature for 5 min. 3 µg of plasmid was mixed with 150 µl of Opti-MEM media and mixed with 150 µl of media/Lipofectamine mix and incubated on a shaker at room temperature for 20 min. Media from cells was aspirated and replaced with 2 ml of Opti-MEM media. 250 µl of media/Lipofectamine/plasmid mix was added dropwise to cells and plates were incubated for either 24 h at 37º C, 5 % CO_2.

2.2.12   Ras immunoprecipitation

400 000 HEK293 cells in 1 ml of DMEM +10% FBS were seeded per well in a 12 well plate (Sarstedt). Following culturing for 24 h at 37º C, 5 % CO_2, cells were transiently transfected with plasmids encoding Affimer-His constructs using the Lipofectamine 2000 reagent as outlined in 2.2.11. Twenty-four hours post transfection, media was aspirated, cells were washed with ice cold Dulbecco's Phosphate-Buffered Saline (DPBS, Corning, cat. No. 21-031-cvr) and cells were lysed in 50 mM Tris, 150 mM NaCl, 1% NP-40 (v/v), 1x Halt™ protease inhibitor cocktail (Thermo Fisher), 1x Phosphatase inhibitor cocktail (Sigma Aldrich), pH 7.5. Cell lysates were centrifuged at 13 000 rpm for 10 min at 4° C to remove cell debris and the supernatant was incubated overnight at 4°C with Ni-NTA resin. After washing 5x with 500 µl of lysis buffer, pulled down proteins were eluted in 40 µl SDS sample buffer (200mM Tris-HCl, 8% SDS, 20% glycerol, 20% mercaptoethanol, 0.1% (w/v) bromophenol blue, pH 7) and detected in a western blot with an anti-KRAS+HRAS+NRAS antibody or with anti-6X His tag antibody (HRP) (Table 2.4).

2.2.13 ERK immunoprecipitation

400 000 HEK293 cells, maintained in DMEM +10% FBS were seeded per well of 12 well plate. Following culturing for 24 h at 37ºC, 5% CO_2, cells were transiently co-transfected with plasmids encoding FLAG-ERK and Affimer-His constructs using the Lipofectamine 2000 reagent as outlined in 2.2.11. Twenty-four hours post transfection, cells were serum starved for 1 h and then signalling was stimulated with 25 ng/µl EGF (BD Biosciences, 354010) for 5 minutes. Media was aspirated, cells were washes with ice cold DPBS and lysed in 50 mM Tris, 150 mM NaCl, 1% NP-40 (v/v), 1x Halt™ protease inhibitor cocktail, 1x Phosphatase inhibitor cocktail, pH 7.5. Cell lysates were centrifuged at 13 000 rpm for 10 min at 4° C to remove cell debris and the supernatants were incubated overnight at 4° C with anti-FLAG M2 magnetic beads (Sigma Aldrich, M8823-1ML). After washing the beads 5x with 500 µl of TBS (50 mM Tris HCl,150 mM NaCl, pH 7.4), pulled down proteins were eluted in 40 µl SDS sample buffer (200mM Tris-HCl, 8% SDS, 20% glycerol, 20% mercaptoethanol, 0.1% (w/v) bromophenol blue, pH 7) and detected in a western blot with an anti-phosphoERK and anti-ERK antibody (Table 2.4).

2.2.14 Generation of stable cell lines

Affimer DNA was amplified from the pET11a vector using the DD-Affimer forward and reverse primers (Table 2.2) in PCR and the products were digested with *Nco I* and *Bgl II.* The digested DNA fragments were ligated into *Nco I* and *Bgl II* digested puromycin-resistant retroviral vector pRetroX-PTuner (ClonTech, cat. no. 632171). The ligated plasmids were transformed into XL1-Blue cells and DNA extracted by mini-preparation. Resulting DNA was sent for sequencing to confirm successful sub-cloning. On return of sequencing data, DNA was transformed into XL-1 Blue cells for culturing and DNA was maxi-prepared (2.2.1.6) for transfection of Phoenix cells.

Phoenix A packaging cells were plated in T25 flask at $2x10^6$ cells/ml. Six hours later the cells were transfected in serum-free media with 2 µg of pRetroX-PTuner plasmids using 8 µl TransIT-293 (Mirus, MIR 2704) in serum-free DMEM. Media was replaced with DMEM +10% FBS every 24h post-transfection. Virus supernatant was harvested at 72 h and 96 h post-transfection, filtered through

0.45µm filter and stored at 4ºC until retroviral transduction. U2-OS cells were plated in T25 flask to 50% confluency and transduced with 2 ml viral supernatant with 2 ml serum-free media and 8 µg/ml polybrene (Sigma Aldrich) or 4 ml serum-free media only (control transduction). The following morning, the media was replaced with DMEM +10% FBS and cells were incubated for 48 h at 37º C, 5 % CO_2, before selection with 2 µg/ml puromycin (Sigma Aldrich). When cells reached confluency, cells were passaged. To examine expression of DD-Affimers, cells were lysed in 50 mM Tris, 150 mM NaCl, 1% NP-40 (v/v), 1x Halt^{TM} protease inhibitor cocktail, 1x Phosphatase inhibitor cocktail, pH 7.5. Cell lysates were centrifuged at 13 000 rpm for 10 min at 4° C to remove cell debris and the supernatants were subjected to SDS-PAGE and western blotting analysis with anti-DD antibody (Table 2.4).

2.2.15 Treatment of cells with small molecules

300 000 HEK293 cells or 800 000 Panc 10.05 cells were seeded per well of 12-well plates and incubated for 24 h at 37º C, 5 % CO_2. Cells were incubated with serum-free media supplemented with indicated concentration of compounds or 0.6% DMSO for 3 h. Signalling was stimulated with 25 ng/µl EGF (BD Biosciences, cat. No. 354010) for 5 minutes. Media was aspirated, cells were washed with ice cold DPBS and lysed in 50 mM Tris, 150 mM NaCl, 1% NP-40 (v/v), 1x Halt protease inhibitor cocktail, 1x Phosphatase inhibitor cocktail, pH 7.5. Cell lysates were centrifuged at 12,000 xg for 10 minutes at 4 ºC to pellet cell debris. Supernatants were then mixed with SDS sample buffer and samples were analysed by western blot with an anti-phosphoERK and anti-tubulin antibodies (Table 2.4).

2.2.16 Viability test

20 000 cells were seeded per well of opaque walled 96-well plate and incubated overnight at 37º C, 5 % CO_2. Cell were treated with indicated concentration of compounds in complete growth media for 72 h. Plates were equilibrated at room temperature for 30 min before mixing with 90 µl of the CellTitre-Glo® reagent (Promega, cat. No. G7571) and incubated on a shaker for 5 min. Plates were incubated at room temperature for 10 min and luminescence was measured using Tecan Spark plate reader. Background luminescence (from media only samples)

was subtracted from all samples and the luminescence was normalised to that of DMSO samples.

2.2.17   Statistical analysis

Statistical analysis was performed using one-way analysis of variance (ANOVA) and Tukey's post-test analysis for multiple comparisons using OriginPro software. Significant differences between control and test groups were evaluated with p values less than 0.05 (*), 0.005 (**), 0.001 (***) and 0.0001 (****) indicated on the graphs. Error bars in graphs denote ± standard error of the mean (SEM) from results of at least three independent experiments.

Chapter 3

Biochemical characterisation of KRas-binding Affimers

Chapter 3

Biochemical characterisation of KRas-binding Affimers

3.1 Introduction

The initial production of monoclonal antibodies (mAbs) using hybridoma technology was reported over four decades ago (Kohler and Milstein, 1975). Since then antibodies have been the most commonly used binding proteins in scientific research. Advances in antibody engineering have enabled a striking transformation from scientific tools to human therapeutics, with over 30 therapeutic antibodies reaching the market (Buss et al., 2012). However, as the development of novel applications progressed, certain drawbacks became apparent. These include large size, expensive manufacturing process and complex patent situation (Skerra, 2007). Moreover, there have been concerns regarding lack of validation and renewability of antibodies (Bradbury and Pluckthun, 2015, Bordeaux et al., 2010). Notably, one study demonstrated that more than 50% of 6000 commercially available antibodies failed to recognise their target (Berglund et al., 2008). Not surprisingly, there is a growing need to develop innovative strategies to overcome these limitations. As a result, engineered binding proteins, which combine the concept of universal binding site with robust protein framework, are becoming increasingly prevalent in biotechnology and clinical applications (Hey et al., 2005). The properties of these engineered proteins include small size, high thermostability, lack of cysteine residues and post-translational modifications, high affinity and specificity of binding and high production yield in bacterial system, thus a cost-effective manufacturing process (Hey et al., 2005, Skerra, 2007).

Many of the engineered protein scaffolds target disease-related proteins and display potential for development of binding molecules for therapeutic and diagnostic applications (Wurch et al., 2012, Hey et al., 2005). This approach is especially promising in cases, where other strategies to develop therapeutics have failed to deliver. An example of such case is targeting of the Ras protein, which led to isolation of Ras-binding single domain intrabody. iDab6 intrabody

specifically bound to the active Ras and impaired Ras-dependent tumorigenesis in a mouse model (Tanaka and Rabbitts, 2003, Tanaka et al., 2007, Tanaka and Rabbitts, 2010). Since then, a number of other scaffolds have been used to target Ras, with some being evaluated *in vivo* (discussed in chapter 1.7) (Grimm et al., 2010, Kauke et al., 2017, Spencer-Smith et al., 2017a, Khan et al., 2018, Guillard et al., 2017). These findings, therefore further supported the use of engineered binding proteins as a valid approach to target Ras. However, despite displaying potent inhibition of Ras, these proteins cannot be used as biotherapeutics yet, due to limited intracellular delivery. Moreover, it is unlikely that these will be converted into small molecules, due to large interaction surfaces. In contrast, novel non-immunoglobulin scaffold protein, called Affimer, exploits a smaller binding interface (Kyle et al., 2015). This inspired the work presented in this thesis to test the use of Affimers to target and modulate Ras activity, and to investigate whether the smaller binding interface of Affimers can be used to inform development of novel Ras inhibitors.

Affimers are small (12 kDa) synthetic proteins comprising of a scaffold based on a consensus sequence of plant-derived phytocystatin and one or two variable regions for specific molecular recognition. To date, specific Affimers displaying nanomolar binding affinities were selected for more than 350 targets, and the extent to which Affimers can be used as research reagents, diagnostics and in drug discovery has been evaluated (discussed in chapter 1.7.6) (Tiede et al., 2017, Kyle et al., 2015, Rawlings et al., 2015, Xie et al., 2017b, Sharma et al., 2016, Koutsoumpeli et al., 2017).

3.1.1 Preliminary results

The Affimer phage library (Tiede et al., 2014) has been screened against wild-type KRas-GDP to identify KRas binding reagents. Ninety-six randomly selected colonies, each representing one Affimer clone, were tested for their ability to bind to the immobilised KRas, loaded with either GDP or GTP, by phage ELISA (Figure 3.1). The majority of isolated Affimers displayed little or no binding to control. Interestingly, similar to the anti-Ras monobody NS1 (Spencer-Smith et al., 2017b), Affimers displayed binding to KRas, irrespective of the nucleotide bound form. This therefore, demonstrated that Affimers can bind to KRas in both

the active and inactive conformations. The screening work was carried out by Dr Christian Tiede.
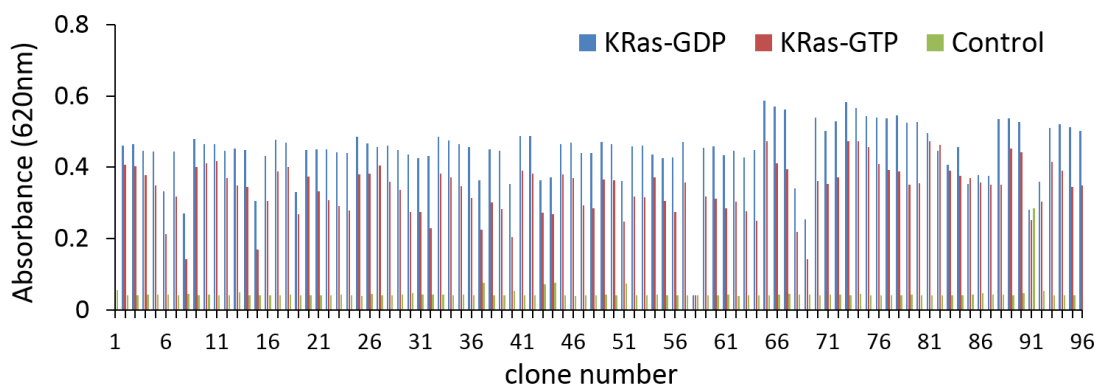
Figure 3.1 Phage ELISA for 96 Affimer clones isolated against KRas wild-type. Biotinylated wild-type KRas was immobilised on streptavidin-coated plates and incubated with phage, each expressing one Affimer clone. Following washing, bound phage was detected with HRP-conjugated anti-phage antibody and measured by absorbance to select positive clones. Binding selectivity was tested against GDP- and GTP loaded KRas. Streptavidin-only wells were used as negative control.

Sequencing analysis of these clones identified seven unique Affimers, with the amino acid sequences of variable regions and the number of appearances indicated in Table 3.1. Affimer K3 was the most abundant Affimer clone in a pool of 96 binders sequenced. The remaining Affimers appeared less frequently in sequencing data.

Affimer	Variable Region 1	Variable Region 2	Number of appearances
K3	HSIDIWYDF	KLNNSHTYK	80
K6	HFTPWFQRN	RIMVTDKMR	2
K19	FFYLWLAPG	AANSPMYHE	1
K37	QYNPWFQTN	VIHGTRWGN	5
K68	VYNPWYQVN	NMRVDMIVH	1
K69	WHFDYQQYN	RQLRMGSMN	1
K91	WDFSAWWKY	RNRYFKFPN	1

Table 3.1 Variable regions amino acid sequences and number of appearances of seven unique Affimers against KRas wild-type.

Further analysis of variable regions amino acid sequences revealed specific sequence patterns, diagrammed in Figure 3.2. In variable region one, a hydrophobic motif with tryptophan at residues 1, 5 and 6 was observed. In contrast, in variable region two, a charged and polar amino acids were the most frequent at residues 1, 3 and 9, respectively. To investigate the contribution of these particular residues to binding and inhibition and whether these motifs can be exploited for the development of novel anti-Ras inhibitors, further biochemical and structural characterisation of Affimers has been done (discussed in chapter 5).
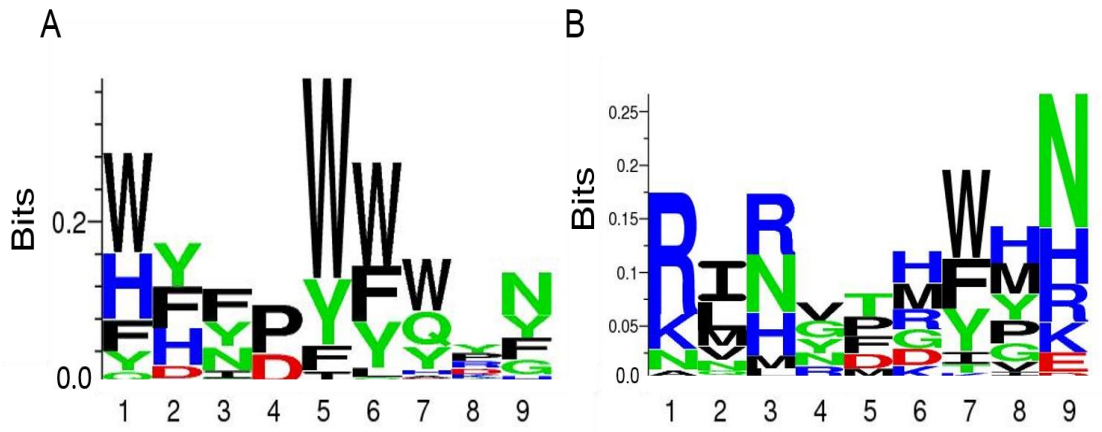
Figure 3.2 Analysis of motifs in variable region sequences of isolated Affimers. Web-based Seq2Logo representation of amino acids frequency at A) variable region 1 and B) variable region 2. The x-axis represents the position in the variable regions, while the y-axis represent the frequency at which the amino acid is observed at that position. Large letters represent frequently observed amino acids, big stacks of letters represents conserved positions and small stacks represents variable positions.

To identify inhibitors of Ras from the pool of isolated Affimers, their ability to inhibit nucleotide exchange reaction – a primary process in Ras activation, was assayed using nucleotide exchange assay (Figure 3.3). KRas, loaded with fluorescent N-methylanthraniloyl derivative of guanosine diphosphate nucleotide (mGDP) was incubated with GEF Sos, excess of unlabelled GTP and each Affimer. Sos-catalysed nucleotide exchange was monitored by decrease in fluorescence intensity of mGDP observed upon nucleotide release from KRas. The reaction was monitored over course of 90 minutes and data was normalised to Ras-only control and fit to a single exponential decay model (Figure 3.4). This work was carried out by Dr Kevin Tipping.
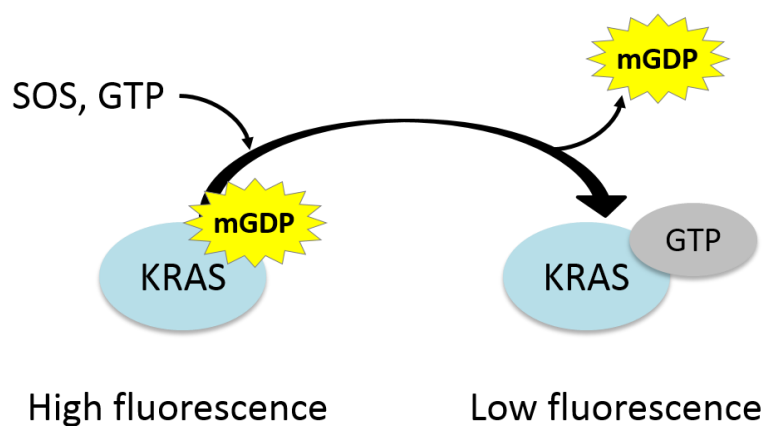
Figure 3.3 Diagram of the nucleotide exchange assay. KRas, loaded with fluorescent N-methylanthraniloyl derivative of guanosine diphosphate nucleotide (mGDP) was incubated with GEF Sos and excess of unlabelled GTP. Sos-catalysed nucleotide exchange was monitored by decrease in fluorescence intensity of mGDP observed upon nucleotide release from KRas.

The observed results demonstrated differential ability of selected Affimers to inhibit Sos-cat-mediated nucleotide exchange reaction in a time-dependent fashion (Figure 3.4). Affimers K3, K6 and K37 displayed the most potent inhibition of this reaction, while Affimers K19 and K68 shown modest effect and Affimers K69 and K91 demonstrated the weakest inhibition. Interestingly, Affimer K3 also displayed inhibition of KRas intrinsic nucleotide release (Figure 3.4). This could indicate that K3 functions by allosterically inhibiting KRas, rather than directly competing with Sos-cat. Although, further characterisation is required to validate this hypothesis. Altogether, these findings have established the ability of Affimers to modulate Ras activation by inhibiting nucleotide exchange.
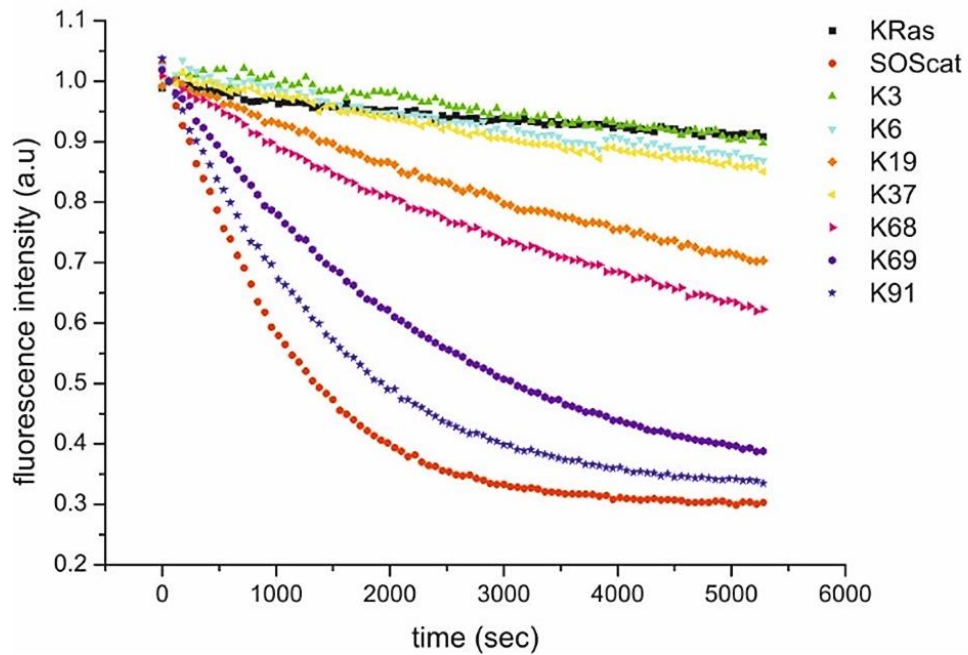
Figure 3.4 KRas-binding Affimers inhibited Sos-cat-catalysed nucleotide exchange reaction on KRas. Wild-type KRas protein, loaded with fluorescent nucleotide mGDP was incubated with either buffer only (black squares), Sos-cat (red circles) or Sos-cat and Affimers (coloured shapes) and the fluorescence was measured every 60 seconds for 90 minutes. Each Affimer inhibited the nucleotide exchange reaction with different potency. Results are representative of two biological replicates.

Work presented in this chapter examines the potencies of the three anti-Ras Affimers K3, K6 and K37 by nucleotide exchange with wild-type and clinically relevant KRas mutants as well as on HRas isoform. In addition, as number of previously reported Ras inhibitors were shown to affect interaction with Raf (Tanaka and Rabbitts, 2010, Kauke et al., 2017, Guillard et al., 2017), the capabilities of Affimers to impair the Ras-Raf binding were investigated.

3.2 Results

3.2.1 Expression and purification of Affimers and Ras proteins

The isolated Ras-binding Affimers and a control Affimer 10 (YS10) raised against yeast Sumo protein (Tiede et al., 2014), were previously sub-cloned into the pET11a expression vector. Affimer proteins with a C-terminal 6x Histidine (His) tag were produced in BL21 Star^{TM} (DE3) competent cells, as described in section 2.2.3.1. SDS-PAGE and Coomassie blue staining indicated sufficient production of Affimers, as compared to the non-transformed cells control (Figure 3.5A). The recombinant proteins were purified from bacterial cell lysates using nickel ion affinity chromatography, as described in section 2.2.3.1. Eluted fractions were analysed by SDS-PAGE and Coomassie staining, which indicated purification of proteins with the expected molecular weight (MW) of 12 kDa. Additionally, Coomassie analysis showed that 95% or more purity of the samples was obtained, which was sufficient for further assays (Figure 3.5B). Absorbance at 280 nm (A_{280}) was measured of each elution, and these values were used to calculate protein concentrations by using the Beer-Lambert law (molar extinction coefficients were determined using ExPASy ProtParam software). The maximal capacity of the amount of resin used was 25 mg and the typical yields of purified Affimers ranged from 10-25 mg of protein per 500 ml culture.
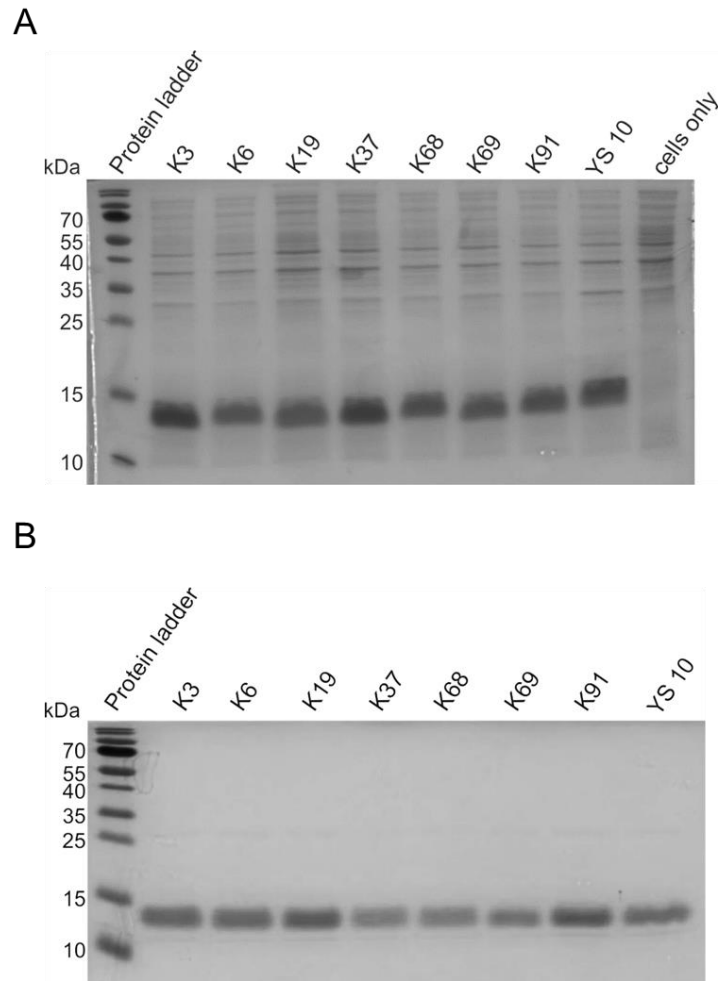
Figure 3.5 Production and purification of Affimers. A) Following IPTG-induced expression in BL21 Star™ DE3 cells, whole cell lysates were analysed by Coomassie staining, which demonstrated efficient production of Affimers, as compared to the whole cell lysate of non-transfected cells. B) Affimers were purified by His-tag affinity chromatography, and eluted proteins were analysed by Coomassie staining, which indicated 95% or more purity of the samples.

Plasmids encoding KRas and HRas proteins with and N-terminal His-tag and C-terminal biotin acceptor peptide (BAP)-tag were synthesised by GenScript (Piscataway, USA). These were sub-cloned in pET11a expression vector and produced in BL21 Star^{TM} (DE3) competent cells, as described in section 2.2.3.2. SDS-PAGE and Coomassie blue staining indicated sufficient production of Ras proteins, as compared to the non-transformed cells control (Figure 3.6A). The recombinant proteins were purified from bacterial cell lysates using nickel ion affinity chromatography, as described in section 2.2.3.2. Eluted fractions were analysed by SDS-PAGE and Coomassie staining, which indicated purification of proteins with the expected molecular weight (MW) of 21 kDa. Additionally, Coomassie analysis showed sufficient purity for downstream assays (Figure 3.6B). A_{280} was measured of each elution, and these values were used to calculate protein concentrations by using the Beer-Lambert law (molar extinction coefficients were determined using ExPASy ProtParam software). Typical yields ranged from 1-5 mg of protein per 1L culture.

QuikChange^{TM} mutagenesis was used to generate oncogenic KRas mutants, G12D, G12V and Q61H from the WT sequence. These variants were produced and purified as described above. The mutagenesis, production and purification of KRas mutants was carried out by Dr Kevin Tipping.
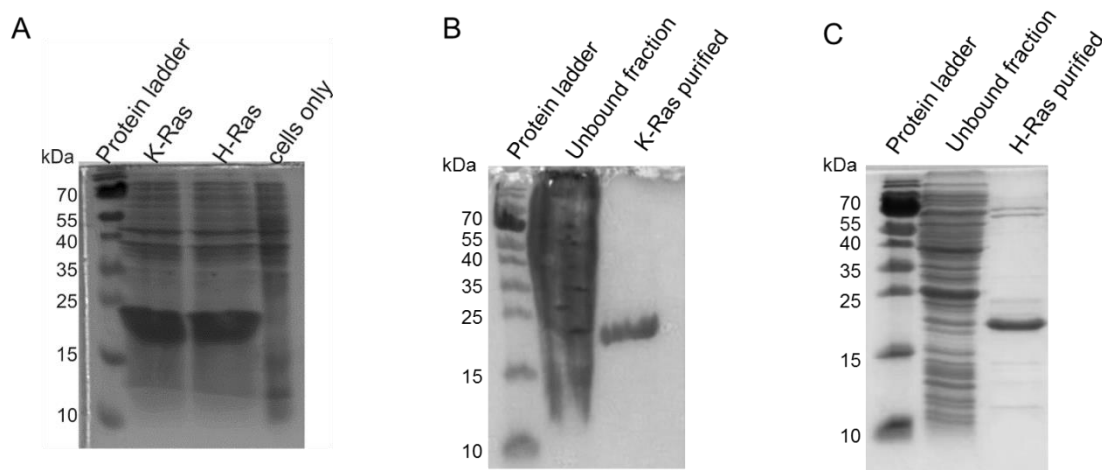
Figure 3.6 Production and purification of Ras. A) Following IPTG-induced expression in BL21 Star™ DE3 cells, whole cell lysates were analysed by Coomassie staining, which demonstrated efficient overexpression of KRas and HRas isoforms, as compared to whole cell lysate of non-transfected cells. Ras proteins were purified by His-tag affinity chromatography, and eluted B) KRas and C) HRas proteins were analysed by Coomassie staining, which indicated efficient purity for downstream assays.

3.2.2 Inhibition of nucleotide exchange of wild-type KRas and HRas proteins

To calculate the IC_{50}'s of Affimers K3, K6 and K37 on nucleotide exchange of wt KRas, selected Affimers were titrated into the assay from 5 nM to 10 µM. Dose-dependent inhibition of this reaction was observed, with highest Affimer concentrations displaying highest level of inhibition (Figure 3.7). To achieve an understanding of the effectiveness of the Affimers as inhibitors of nucleotide exchange, the initial reaction rates (V_0), were plotted against Affimer concentration. From obtained dose-response curves (Figure 3.8), the concentrations of Affimers required for 50% inhibition of the reaction were calculated and are shown in Table 3.2. Affimers K6 and K37 displayed moderate potency of inhibition, with IC_{50} values of 594 ± 271 and 697 ± 158 nM for wt KRas, respectively. In contrast, out of the three Affimers tested, K3 displayed the most potent inhibition of wt KRas, with IC_{50} of 144 ± 94 nM.

Ras isoforms are closely related with high amino acid sequence identity (Castellano and Santos, 2011), suggesting that KRas-binding Affimers may also have an effect on other Ras isoforms. To investigate this, wt HRas was tested with KRas-binding Affimers in nucleotide exchange assay. As expected, Affimers K3, K6 and K37 were also capable of inhibiting nucleotide exchange of HRas (Figure 3.8). Affimers K6 and K37 displayed similar inhibitory potencies towards wt HRas as towards wt KRas (Table 3.2) (p-value for K6 = 0.342, and for K37 = 0.752). This therefore, demonstrated that K6 and K37 do not show isoform specificity. Interestingly, significantly lower inhibition of HRas (IC_{50} of 2585 ± 335 nM, p-value = 0.006) in comparison to KRas has been observed with K3. From these findings, two conclusions were drawn. Firstly, K3 displayed potent inhibition of Ras activation in an isoform-specific manner. Secondly, because this isoform specificity has not been observed with K6 and K37, it is likely that these two Affimers have different mode of action than K3. However, structural characterisation of Affimer-Ras complexes would be required to provide definite answers.
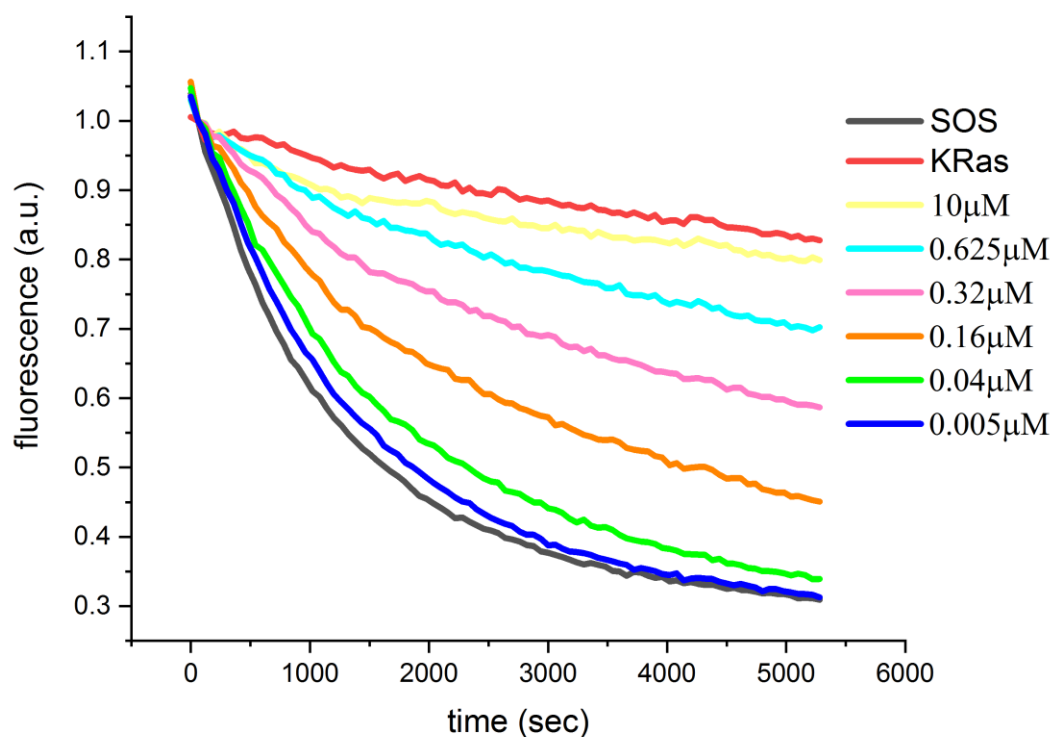
Figure 3.7 Affimers dose-responsively inhibited Sos-mediated nucleotide exchange reaction. Affimers were tested in nucleotide exchange at a range of concentrations between 5nM-10µM. Changes in the fluorescence intensity over time of Affimer K3 at different concentrations are shown. Similar results were obtained for Affimers K6 and K37 (data not shown). Results are representative of three biological replicates (n=3).
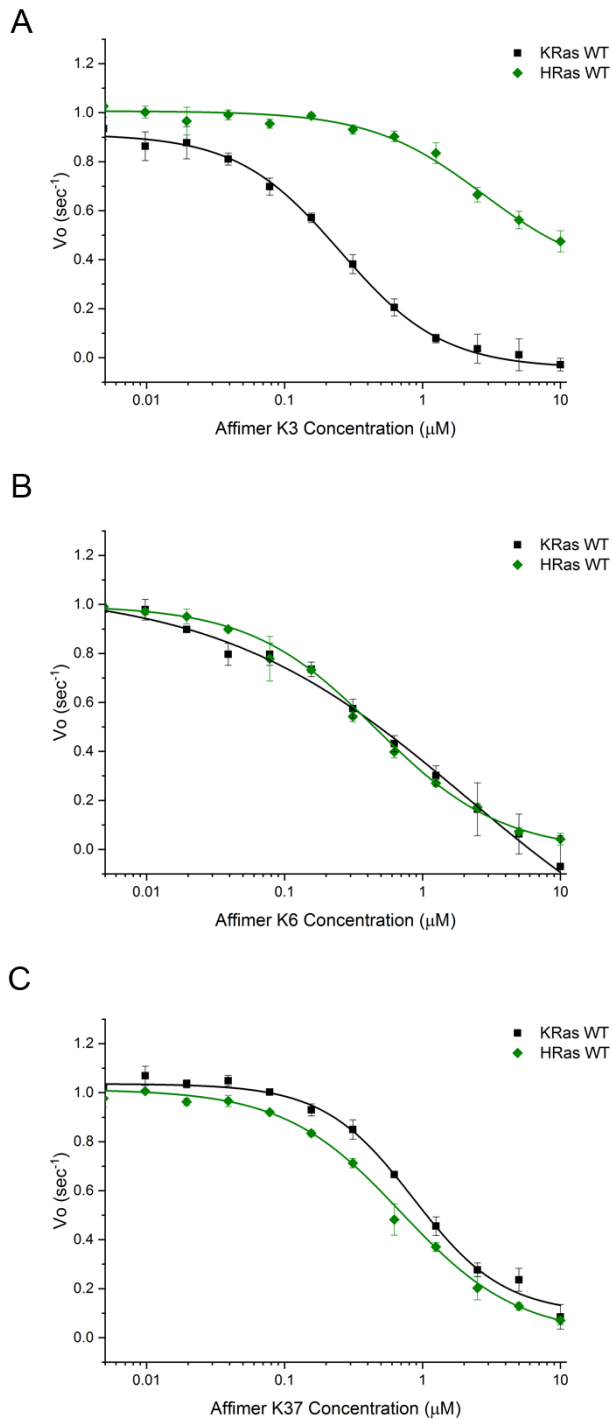
Figure 3.8 Affimers inhibited nucleotide exchange reaction on wild-type KRas and HRas. Dose-response curves for Affimers A) K3, B) K6 and C) K37 demonstrating inhibition of Sos-mediated nucleotide exchange of wild-type KRas (black) and wild-type HRas (green). The initial nucleotide exchange reaction rates were plotted against Affimer concentrations of 5 nM - 10 μM and fit to Hill model, which was used to calculate the IC_{50} values. Results are representative of three biological replicates (n=3). Error bars are ± SEM.

Affimer	IC$_{50}$ values (nM)	
	KRas wt	**HRas wt**
K3	144 ± 94	2585 ± 335
K6	594 ± 271	389 ± 187
K37	697 ± 158	626 ± 320

Table 3.2 Calculated IC$_{50}$ values for wt KRas and HRas. Values were calculated from the Hill equation, to which the data was fitted, and represent the averages from three biological repeats (n=3). Error bars are ± SEM.

3.2.3 Inhibition of nucleotide exchange of KRas mutants

To evaluate the effects of Affimers on mutant forms of KRas, nucleotide exchange assays with recombinant G12D, G12V and Q61H KRas mutant proteins were performed. Firstly, however, because Sos-cat is fivefold less effective at releasing the nucleotide from mutant KRas compared to wt KRas (Maurer et al., 2012), titration experiments with Sos-cat and KRas G12D were carried out (Figure 3.9). This was to determine the Sos-cat concentration to provide the optimal assay window for reactions with mutant KRas. Indeed, slower kinetics of the reaction were observed with the same Sos-cat concentration, which was used in assay with wt KRas. As a result, 4-fold increase in Sos-cat concentration was required (0.25 μM and 1 μM Sos-cat for assays with wild-type and mutant KRas, respectively).

Similarly to results obtained with wild-type KRas, co-incubation of mutant KRas-mGDP with Sos-cat and KRas-binding Affimers, dose-responsively inhibited nucleotide exchange, with IC$_{50}$ values shown in Table 3.3. Affimer K3 displayed similar potencies towards wt KRas and G12D and G12V mutants, while it was significantly less effective at inhibiting nucleotide exchange on Q61H mutant (Figure 3.10, p-value = 0.029). This therefore, indicated that K3 displayed not only isoform-specificity, but was also capable of discriminating between KRas mutants. Interestingly, Affimer K6 demonstrated marginally better inhibition of nucleotide exchange of the G12D mutant in comparison to other Ras mutants

and isoforms (Table 3.3). Likewise, K37 displayed lower IC_{50} value against G12D mutant, but it was less effective at blocking nucleotide exchange on Q61H KRas (Figure 3.10; Table 3.3).

Altogether, these findings conclude that Affimers isolated against wt KRas are also effective inhibitors of oncogenic mutants. Interestingly, mutant-selectivity was observed, which could be further explored for the isolation of mutant-specific inhibitors. Furthermore, differences in the IC_{50} values between those three Affimers, further supported the hypothesis that these binders could display different modes of inhibition.

Noteworthy, some of the dose-response curves did not reach plateau at the highest Affimer concentrations, which could have affected accurate determination of the IC_{50} values (Sebaugh, 2011). Therefore, further tests with broader Affimer concentration ranges would be required to determine the accuracy of obtained IC_{50}s. However, these assays aimed to determine whether isolated Affimers are effective against the clinically relevant KRas mutants, which was sufficiently demonstrated with the data presented.
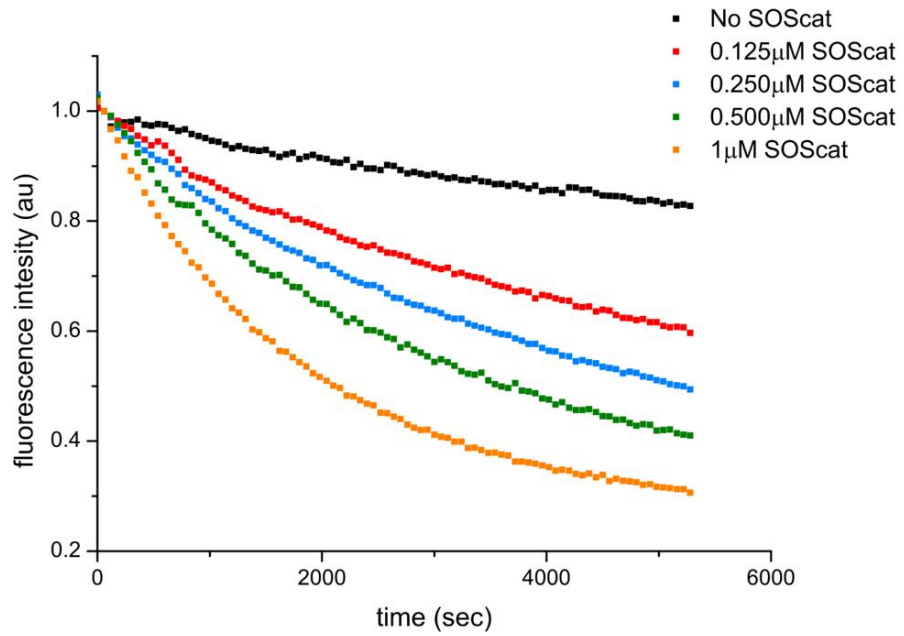
Figure 3.9 Titration of Sos-cat into the nucleotide exchange assay with KRas G12D mutant. Sos-cat was titrated into the assay from 125 nM to 1µM to determine the concentration for optimal assay window. As a result, 4-fold increase in Sos-cat concentration was required (final Sos-cat concentration of 1µM) to obtain similar kinetics as with the assay with wild-type KRas protein.
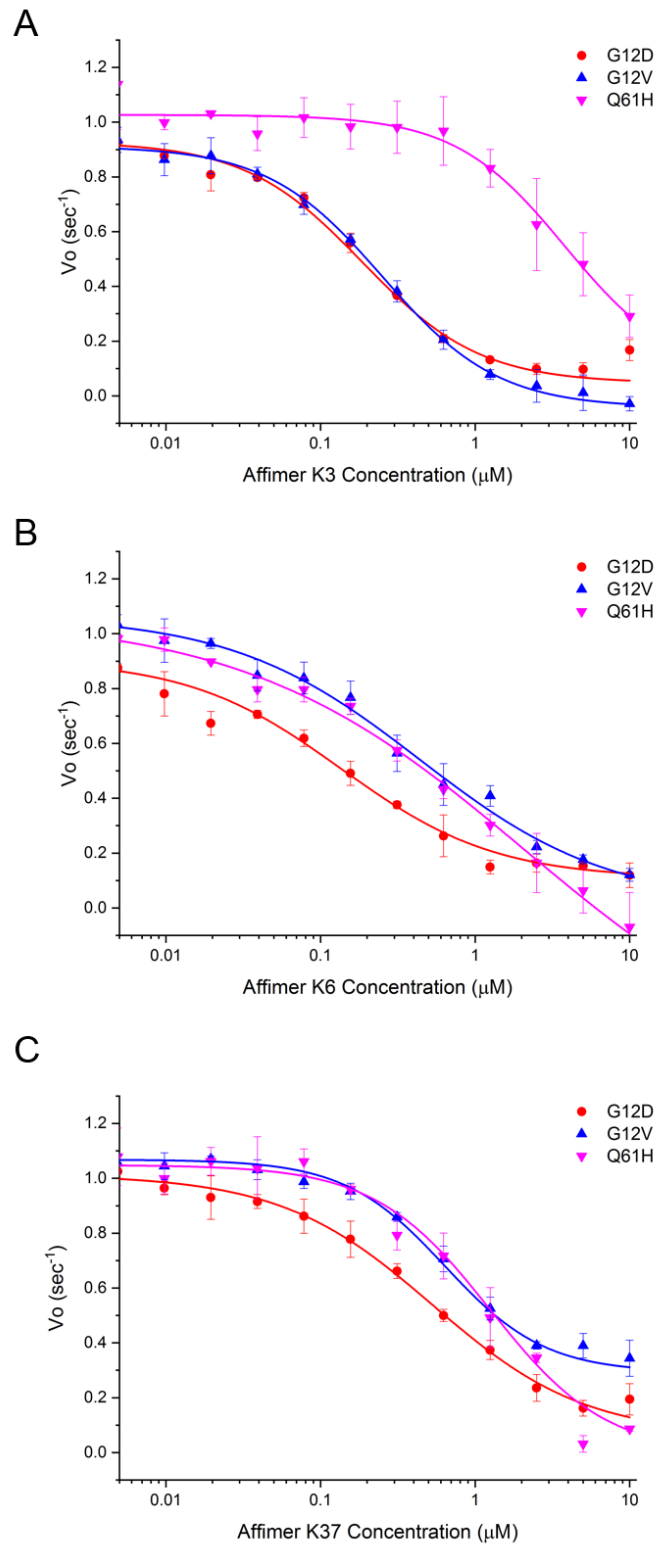
Figure 3.10 Affimers inhibited nucleotide exchange reaction of oncogenic mutant KRas proteins. Dose-response curves for A) Affimer K3, B) Affimer K6 and C) Affimer K37 demonstrating inhibition of nucleotide exchange of KRas G12D (red), KRas G12V (blue) and KRas Q61H (pink). Results are representative of three biological replicates (n=3). Error bars are ±SEM.

Affimer	IC$_{50}$ values (nM)		
	KRas G12D	KRas G12V	KRas Q61H
K3	144 ± 40	176 ± 115	3005 ± 865
K6	185 ± 46	571 ± 148	532 ± 165
K37	356 ± 161	640 ± 253	1075 ± 651

Table 3.3 Calculated IC$_{50}$ values for oncogenic KRas mutants. Values were calculated from the Hill equation, to which the data was fitted, and represent the averages from three biological repeats (n=3). Error bars are ± SEM.

3.2.4 Ras-Raf interaction assays

One of the strategies to block Ras function involves inhibition of the Ras-effector binding, with a number of previously reported Ras inhibitors demonstrating impairment of this interaction (Tanaka and Rabbitts, 2010, Kauke et al., 2017, Guillard et al., 2017). Therefore, the capabilities of Affimers to inhibit the Ras-Raf binding were also investigated. This was done by a pull down assay, as described in chapter 2.2.6, with recombinant Ras binding domain (RBD) of Raf1. Notably, although in the initial attempt only the three KRas-Affimers, described above, and a control YS10 Affimer have been used, in the optimised assay all seven anti-KRas Affimers were tested. This is because, in the initial phage-ELISA binding assay Affimers displayed binding to KRas, irrespective of the nucleotide bound form, which indicated the potential of Affimers binding to active, GTP-bound KRas and preventing interaction with its effector. Moreover, the fact that some of these did not display potent inhibition of nucleotide exchange, did not preclude them from blocking the Ras-RBD binding.

In this assay, a yeast-SUMO binding Affimer (YS10) was used as a negative control, along with Dynabeads^{TM} only sample. In contrast, no Affimer sample, comprising RBD-GST and KRas-GTP, was used as a positive control for the assay. In the initial attempt, a band in the beads only sample was observed (Figure 3.11A). This indicated non-specific binding of KRas-GTP to the beads.

To resolve this issue, the assay buffer was supplemented with 1mM dithiothreitol (DTT) and 0.1% Tween-20. While the reducing agent was used to disrupt non-specific interactions mediated by disulphide bridges, the Tween-20 detergent was added to prevent non-specific hydrophobic interactions (Johnson, 2013). In addition, a GST only sample was used as a negative control. This was a better negative control for this assay, as it demonstrated that the pulled down KRas was due to specific binding with RBD, rather than due to non-specific interactions with the GST-tag. As a result of these modifications, the non-specific binding to beads was reduced, as no detectable band at molecular weight of 21 kDa, corresponding to pulled down KRas, was observed in the GST-only sample (Figure 3.11B). In contrast, a strong band was detected in the no Affimer sample, signifying the successful binding and pulldown of KRas-GTP with RBD-GST. Interestingly, pre-incubation of K3 with KRas, blocked the KRas-RBD interaction almost completely, as demonstrated by hardly detectable levels of pulled down KRas-GTP in comparison to the amount of KRas-GTP in controls (Figure 3.11B). Affimers K19 and K37 also significantly impaired this interaction, although to a much lesser extent than K3 (Figure 3.11C). Affimer clones K6, K68, K69 and K91 along with the control Affimer YS10 had no effect on KRas binding to RBD.
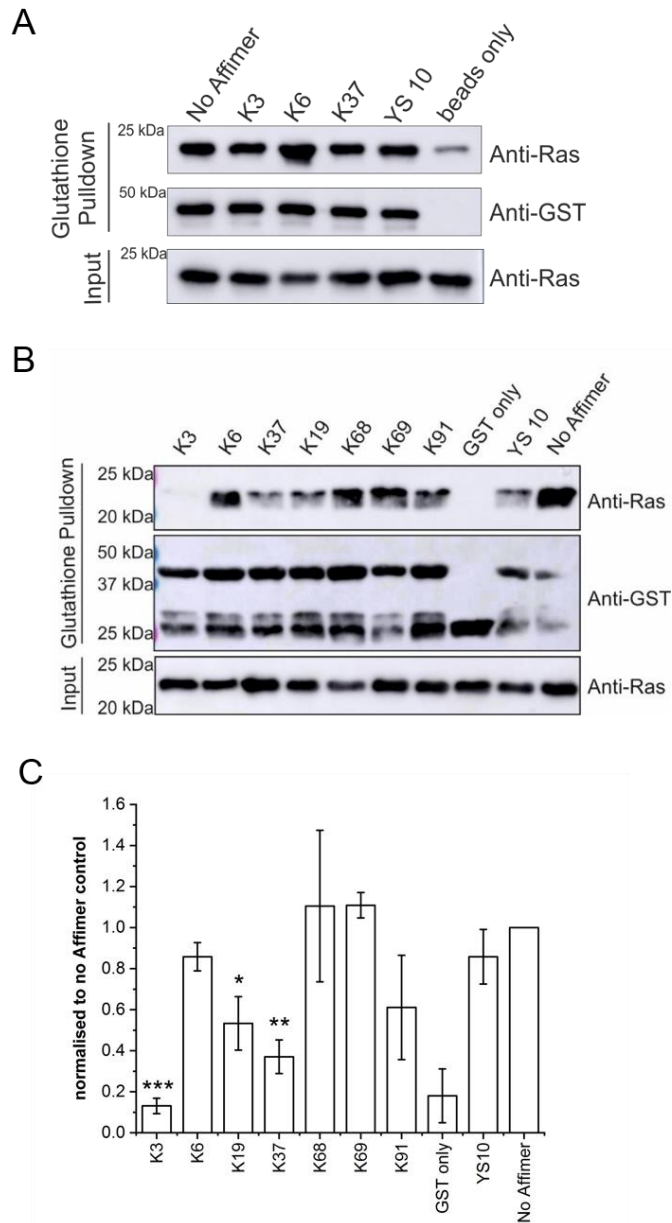
Figure 3.11 Effect of Affimers on KRas–GTP binding to Raf-RBD-GST. GST-tagged Ras binding domain (RBD) of Raf was added to KRas-GTP, which was pre-incubated with Affimers. RBD-GST was precipitated on glutathione Dynabeads™, and pulled down proteins were analysed by western blot with anti-Ras and anti-GST antibodies. A) Western blot analysis of precipitated protein from the initial attempt, demonstrating non-specific binding to beads. B) Western blot analysis of precipitated protein from the optimised method. C) Quantification of precipitated KRas-GTP. Relative KRas-GTP levels were normalised to levels of precipitated KRas from no Affimer sample. Affimers K3, K19 and K37 significantly inhibited the KRas-RBD interaction, as demonstrated by reduced pulldown of KRAS-GTP. GST only and Affimer YS10 were used as negative controls. Results are representative of three biological replicates. Error bars denote ± SEM. $p < 0.05$ (*), $p < 0.01$ (**), $p < 0.001$ (***).

3.3 Discussion

The Affimer library has been previously screened and seven unique KRas-binding clones have been isolated. In preliminary experiments, these Affimers were shown to bind to KRas, irrespective of the nucleotide bound form (Figure 3.1). This mode of binding is similar to previously reported anti-Ras monobody NS1. However, because of this insensitivity to the nucleotide state of Ras, NS1 did not block nucleotide exchange. Structural studies provided explanation for this, as NS1 monobody was shown to bind to the allosteric regulatory site, away from the switch I and II regions (Spencer-Smith et al., 2017a). Conversely, KRas binding Affimers were shown to inhibit nucleotide exchange (Figure 3.4). This therefore, could indicate that Affimers bind to a distant site away from the α4-β5-α6 interface. However, structural studies (discussed in more details in chapter 5) are required to provide definitive answers.

One of the strategies to directly modulate Ras function involves reducing the amount of active Ras by inhibiting nucleotide exchange. However, the effects of blocking nucleotide exchange were initially thought to be restricted by the impaired GTPase activity of Ras mutants. This dogma however, was challenged by studies, which provided the evidence for cycling of Ras nucleotide states (Patricelli et al., 2016). As a result, small molecules and peptides, which block nucleotide exchange have been reported. These were shown to inhibit the nucleotide exchange in dose-dependent manner with the half maximal inhibitory concentration (IC_{50}) ranging from mid- to low micromolar. Albeit those inhibitors showed only moderate effects on downstream signalling (Leshchiner et al., 2015, Maurer et al., 2012, Patgiri et al., 2011). Irreversible inhibition of nucleotide exchange on KRas G12C with a covalent inhibitor ARS-853 resulted in reduced levels of the active Ras and triggered apoptosis (Patricelli et al., 2016, Lito et al., 2016). Recently, Guillard *et al.* reported potent inhibition of nucleotide exchange with DARPin K27 as a valuable approach to affect active Ras levels and Ras function. DARPin K27 displayed low nanomolar IC_{50} and impaired Ras-mediated signalling and cell proliferation (Guillard et al., 2017). Altogether, these findings re-evaluated the potential of nucleotide exchange inhibition as promising approach to develop novel Ras inhibitors.

KRas labelled with fluorescently-tagged GDP nucleotide (mGDP) has been used to directly measure the effects of Affimers on nucleotide exchange. Properties of this fluorescent nucleotide include small fluorophore, therefore not causing major perturbation of protein-nucleotide interactions and significantly increased fluorescent signal when bound to the protein compared to unbound mGDP, which therefore allows for continuous monitoring of release and association of nucleotides from GTPases (Kanie and Jackson, 2018). Due to the very high affinity of Ras for guanine nucleotides, the slow intrinsic release rate needs to be enhanced by Sos, which lowers GTPase nucleotide affinity, allowing for rapid nucleotide exchange (Bos et al., 2007). Initial nucleotide exchange assays with seven KRas-binding Affimers, identified K3, K6 and K37 as the most potent inhibitors, with IC_{50} values ranging from 144 to 697 nM for wild-type KRas (Table 3.2). Notably, Affimers displayed a 1000-fold better inhibitory potency (Table 3.2) than small molecule Ras inhibitor DCAI (IC_{50}= 155 µM) (Maurer et al., 2012). Likewise, Affimers' IC_{50} values were significantly better to those of stabilised peptides SAH-SOS1$_A$ (IC_{50} = 5-15 µM) (Leshchiner et al., 2015) and HBS3 (IC_{50}= 25 µM) (Patgiri et al., 2011). However, inhibitory potencies of Affimers were two orders of magnitude lower than that of DARPin K27 (IC_{50} = 2.4 nM) (Guillard et al., 2017). Noteworthy, when interpreting data obtained from nucleotide exchange assays and comparing them to previously published data, the type of the assay and reaction conditions need to be considered, as different assay conditions could influence calculated IC_{50} values. Guillard et al. used fluorescent resonance energy transfer (FRET) biochemical assay, coupling nucleotide exchange with Ras-Raf binding, rather than direct measurement of the nucleotide exchange (Guillard et al., 2017). Additionally, the rate of heteronucleotide GDP → GTP exchange reaction is described to be 5-fold and 10-fold faster than homonucleotide GTP→ and GDP→ exchange reactions, respectively. This is due to higher affinity binding and activation of Sos-cat by Ras-GTP at the allosteric site and the stronger binding of Ras-GDP at the catalytic site (Vo et al., 2016). Nucleotide exchange assay employed in this study examined heteronucleotide mGDP→GTP exchange reaction, thus adequately representing Sos-cat-induced nucleotide exchange.

Ras isoforms, K-, H- and NRas are ubiquitously expressed and display 85% sequence identity. However, they exhibit different biological functions (Omerovic et al., 2008, Castellano and Santos, 2011), therefore isoform specificity of Ras inhibitors is highly desirable. Since, 86% of Ras-driven cancers carry KRas mutations (Downward, 2003), the majority of previously developed Ras inhibitors targeted the KRas isoform (Leshchiner et al., 2015, Lim et al., 2014, Maurer et al., 2012, Ostrem et al., 2013, Upadhyaya et al., 2015, Guillard et al., 2017), yet, their effects on other Ras isoforms have not been explored. Recently, selectivity towards KRas and HRas was shown with monobody NS1 due to single amino acid difference between Ras isoforms (Spencer-Smith et al., 2017a). Interestingly, Affimer K3 also demonstrated isoform-selectivity, as it displayed significantly lower inhibitory activity towards HRas (IC_{50} = 2585 ± 335 nM) in comparison to KRas (IC_{50} = 144 ± 94 nM). Therefore, K3 represents a valuable tool to study isoform-specific Ras inhibition. However, further tests including determination of binding affinities towards isoforms and structural characterisation of Ras-Affimer complexes are required to validate these results. Additionally, tests with the third isoform, NRas would be beneficial to further investigate isoform specificity. This however, was not performed due to problems with production of the soluble NRas protein (data not shown).

Ras mutations are one of the major driving forces in tumour development and progression, therefore identification of mutant specific inhibitors is highly desirable (Cox et al., 2014). The possibility of selective targeting of Ras mutants has been described with the KRas G12C inhibitors. These covalently attached to KRas via the mutant cysteine residue, therefore not affecting the wild-type protein (Patricelli et al., 2016, Lito et al., 2016, Ostrem et al., 2013, Janes et al., 2018). While other anti-Ras inhibitors, especially those inhibiting nucleotide exchange reactions, described above, were proven to be effective against oncogenic KRas mutants, the mutant-selectivity so far has not been described for any of them. In contrast, Affimer K3 has displayed strikingly better inhibition of KRas G12D and G12V (IC_{50} values of 144 ±40 and 176 ± 115 nM, respectively) in comparison to Q61H mutant (IC_{50} = 3005 ± 865 nM). Likewise, marginally better inhibition of KRas G12D was observed with K6 and K37 (Table 3.3). These findings demonstrated that Affimers isolated against wild-type KRas were also capable of

inhibiting clinically relevant mutants. Importantly, it also established those Affimers as valuable tools to study mutant-selectivity, which could lead to the development of mutant-specific inhibitors.

Perhaps the most interesting finding, described in this chapter, was that three out of the seven KRas-binding Affimers significantly impaired Ras-RBD binding, with K3 displaying the most potent inhibition (Figure 3.11). While number of Ras-targeting scaffold proteins were shown to function by inhibiting the Ras-Raf interaction (Tanaka et al., 2007, Kauke et al., 2017, Guillard et al., 2017), the ability to simultaneously block nucleotide exchange and Ras-effector binding has not been previously reported. This therefore, established a novel mode of Ras inhibition, which could be further explored for development of novel anti-Ras therapeutics.

Further characterisation of selected Affimers should involve assessment of the binding affinities towards wild-type KRas protein. Determination of the dissociation constants would allow to define whether these binders could compete with the interactions of Ras with its GEFs and effector proteins, such as Sos and Raf, for which the dissociation constants are 1.9 µM and 160 nM, respectively (Tanaka et al., 2007, Sondermann et al., 2004). Moreover, it would allow direct comparison to other anti-Ras scaffolds reported previously. One technique for measuring binding affinities is isothermal titration calorimetry (ITC). ITC is a well validated method, that has been extensively used to study protein-ligand, protein-protein, DNA-ligand and RNA-macromolecule interactions (Duff et al., 2011). ITC is a label-free technique, therefore eliminating the problems associated with molecular labels, such as steric hindrance or change of protein structure, which can in turn affect the measured affinity (Peters et al., 2009). Additionally, apart from the binding affinities, other useful information such as the stoichiometry and enthalpy, can be obtained from ITC experiments (Duff et al., 2011). Additionally, binding affinities towards GTP-bound KRas, as well as Ras isoforms and mutants could be investigated, as it would be interesting to see if these correlate with the isoform and mutant-selectivity observed in nucleotide exchange assays. Moreover, it could also provide evidence as to whether Affimers indeed do not discriminate between the nucleotide-bound forms of Ras, as indicated in the initial phage ELISA (Figure 3.1).

In conclusion, data presented in this chapter demonstrated anti-KRas Affimers as binding reagents displaying potent inhibition of nucleotide exchange on wild-type as well as on oncogenic KRas mutants and HRas isoform. Moreover, for the first time, dual inhibition of Ras activation and Ras-effector interaction has been described.

Chapter 4

Effects of Affimers on Ras-mediated signaling in cells

Chapter 4

Effects of Affimers on Ras-mediated signalling in cells

4.1 Introduction

During the development of protein inhibitors as potential therapeutics, it is important to remember that proteins in their native environment, within the cell, do not function in isolation, but are rather involved in multi-protein signalling cascades (De Las Rivas and Fontanillo, 2010). Indeed, the human protein-protein interactome is believed to contain between 130 000 to 650 000 protein interactions (Stumpf et al., 2008, Venkatesan et al., 2009). Most of the PPIs are usually intractable to small molecule inhibitors, due to large and flat interfaces (Cheng et al., 2007). This, has led to the development of macrodrugs, such as peptides (Fosgerau and Hoffmann, 2015) or antibodies (Perez-Martinez et al., 2010), and these biologics have become the fastest growing class of therapeutics (Aggarwal, 2010). However, the majority of these biotherapeutics, especially antibodies and their fragments, are only effective against extracellular targets, which represent only a small proportion of PPIs in signalling pathways (Tsomaia, 2015, Martin et al., 2018). In addition, antibodies are dependent on disulphide bond formation for stability, which is not possible in the reducing environment of the cytoplasm, thus leaving the intracellular targets out of their reach (Helma et al., 2015). Although intracellular antibodies, termed intrabodies (described in section 1.7.1) were shown to function in the cytoplasm, these usually require complex selection strategies to isolate clones that are indeed functional intracellularly and they often rely on localisation signals for efficient activity (Marschall et al., 2015). For instance, the anti-Ras intrabody iDab6 was shown to impair cancer cell proliferation and reverted the phenotype of Ras-transformed cancer cells only when the iDab6 expression was targeted to the plasma membrane (Tanaka et al., 2007). Therefore, non-immunoglobulin based artificial binding proteins offer an advantage to study intracellular targets in their native environment, as they lack disulphide bonds, therefore retain their full effectiveness in the cellular milieu.

A number of scaffold proteins have been examined in cell-based assays as well as in mouse models. For example, binders targeting individual SH2 domains allowed dissection of intracellular signalling pathways and identified new biological functions (Wojcik et al., 2010, Grebien et al., 2011, Sha et al., 2013, Tiede et al., 2017). The effects of binding proteins targeting Ras have also been evaluated in cellular assays. The Ras-binding monobody NS1 significantly reduced EGF-mediated ERK and AKT activation and inhibited transformation of NIH 3T3 cells by oncogenic KRas and HRas (Spencer-Smith et al., 2017b). Additionally, doxocycline-induced expression of NS1 reduced the growth of Ras tumour cells in nude mice (Khan et al., 2018). Likewise, intracellular expression of anti-Ras DARPins K27 and K55 reduced ERK and AKT phosphorylation in HEK 293 and HCT 116 cells and slowed anchorage-independent cell growth (Guillard et al., 2017). These findings therefore, demonstrated that scaffold proteins are effective intracellularly and are valuable tools to study signalling pathways in cells.

As mentioned earlier (chapter 1.7.6), the effects of Affimer reagents were also studied in cellular assays. Apart from being valuable tools for *in vivo* imaging, Affimer reagents have been also used to study signalling pathways. The isoform- and domain-specific Affimers targeting the SH2 domain of PI3K subunit p85, were shown to block the intracellular function of p85 in transiently transfected NIH 3T3 cells, which resulted in increased AKT phosphorylation (Tiede et al., 2017).

The abilities of isolated anti-KRas Affimers to function in the cytoplasmic environment and to modulate downstream signalling events were investigated and are described in this chapter. Firstly, the capability of intracellularly expressed Affimers to engage with the endogenous Ras has been evaluated, followed by examination of effects on Ras-mediated signalling by assaying the phosphorylation levels of downstream effectors ERK1 and 2.

4.2 Results

4.2.1 Optimisation of transient transfection of HEK 293 cells

Plasmids encoding recombinant proteins can be delivered into the cells by standard cell biology techniques including transient transfection or viral transduction (Deroo et al., 2016). Initially, transient transfection was chosen, because it is an easier, more rapid and less laborious method in comparison to generation of stable cell lines (Durocher et al., 2002) and high level of protein expression can be obtained (Subedi et al., 2015), which may be required for effective inhibition of Ras function.

Firstly, the sequences of Affimers K3, K6, K37 and YS10 were sub-cloned into the mammalian expression vectors pcDNA5 and pCMV6, to encode C-terminally 6xHis- and tGFP-tagged Affimers, respectively, as described in 2.2.11. The DNA sequences from bacterial expression vector pET11a were amplified by PCR, using primers designed to contain *Bam HI* and *Not I* restrictions sites for sub-cloning into pcDNA5 and *Sgf I* and *Mlu I* restrictions sites for sub-cloning into pCMV6. Obtained products of approximately 300 bp (Figure 4.1) were cloned into the desired vectors. Insertion of the genes was confirmed by sequencing (Genewiz).
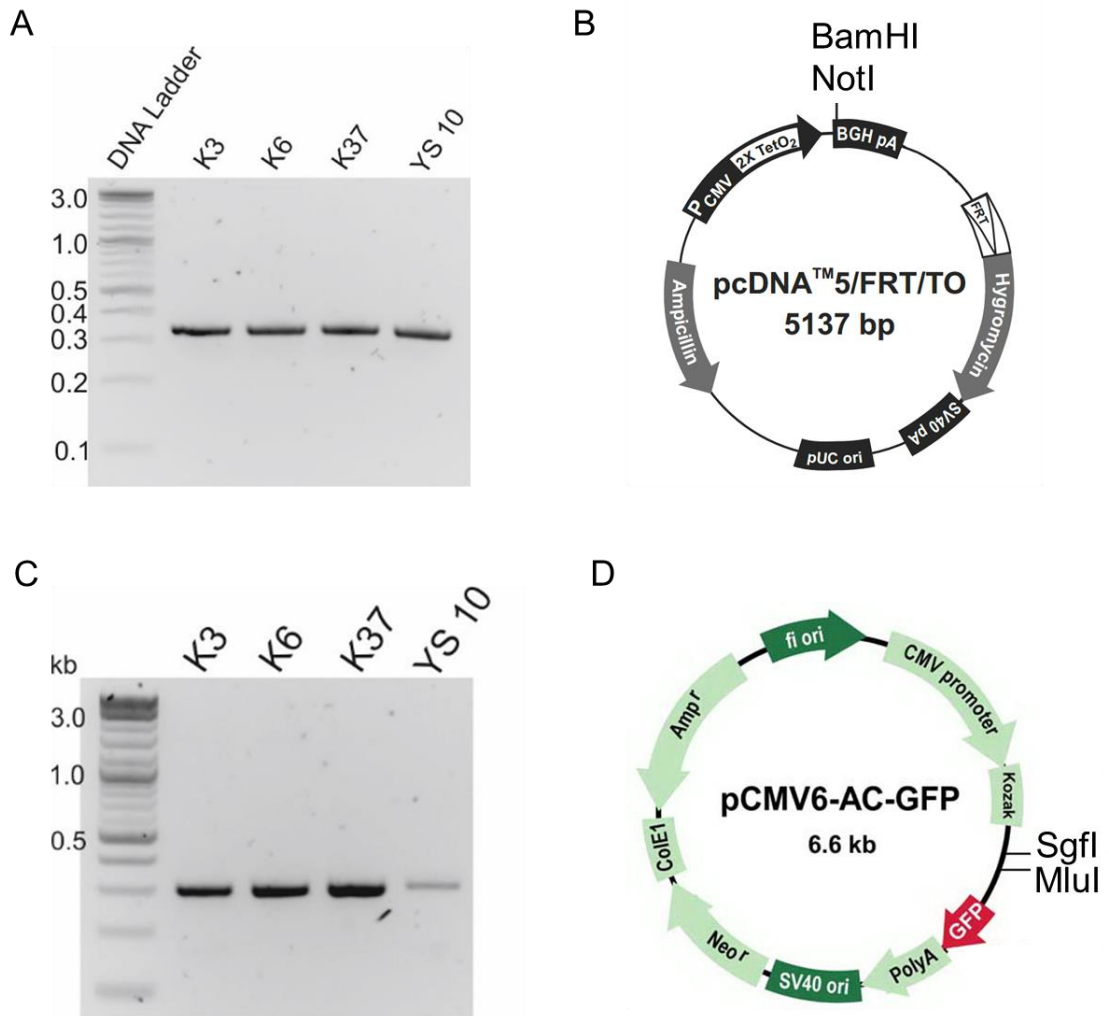
Figure 4.1 Cloning of Affimers into mammalian expression vector. A) Affimer DNA sequences were amplified from pET11a plasmid by PCR and the products were analysed by 2% agarose gel. PCR products were digested with *Bam HI* and *Not I* and ligated into pcDNA5/FRT/TO vector. B) Plasmid map of pcDNA5/FRT/TO with indicated position of restriction enzyme cleavage. C) Affimers' DNA sequences were amplified from pET11a plasmid by PCR and the products were analysed by 2% agarose gel. PCR products were digested with *Sgf II* and *Mlu I* and ligated into pCMV6-AC-GFP vector. D) Plasmid map of pCMV6-AC-GFP with indicated position of the restriction enzyme cleavage site.

Chemical transfection methods are the most commonly used techniques for introduction of plasmids into mammalian cells (Kim and Eberwine, 2010). Here, the cationic liposome based reagent Lipofectamine™ 2000 (LF2000) was used as a tool for DNA transfection. The transfection efficiency is largely dependent on the DNA/transfection reagent ratio (Kim and Eberwine, 2010). Additionally, high transfection reagent concentrations can cause cytotoxicity, due to accumulation of liposomes in the cytoplasm (Jäger et al., 2015). Therefore, transfection trials with different amounts of the LF2000 reagent were conducted to determine the optimal concentration for the highest transfection efficiency and the lowest cytotoxicity. Human embryonic kidney (HEK293) cells were transiently transfected with 1 µg of pCMV6 plasmid encoding turbo-green fluorescent protein (tGFP) tagged Affimer YS10 and with varying amounts of LF2000 reagent, as described in section 2.2.11. Turbo-GFP is a variant of the green fluorescent protein, displaying brighter green fluorescence, which is visible earlier in comparison to fluorescence of other GFPs (Shagin et al., 2004, Evdokimov et al., 2006). Live cells were imaged at 24 hours post-transfection (Figure 4.2), and the amount of viable cells expressing YS10-tGFP was used as a measure of transfection efficiency. Mock transfection with the LF2000 reagent only was used as a control. Highest transfection efficiency was observed with 2 µl of the reagent, as indicated by the highest proportion of green-fluorescent cells. Conversely, the highest amount of LF2000 used (5µl) resulted in the highest cell toxicity, as indicated by the largest proportion of rounded cells in the sample (Figure 4.2, bottom panels). Since, the amount of DNA was kept constant, the observed toxicity can be attributed to the effects of the transfection reagent. Noteworthy, expression of the Affimer YS10 did not appear to affect the phenotype of the cells, although this was not quantified in this assay. In summary, these findings have established the optimal transient transfection conditions, which were used for subsequent transfection assays.

Immunofluorescence on transiently transfected and fixed cells, with their nuclei stained could be performed to more quantitatively assay the transfection efficiency. Moreover, additional transfection trials using varying amounts of DNA and longer incubation time post-transfection could be performed to further optimise the protocol. Although, the levels of expressed protein in the transfected

cells appeared to be high, as indicated by the signal intensity in imaged cells. This was expected, due to expression of the adenovirus 13 S E1a protein in HEK293 cells, which increases transcription from the CMV promoter (Gorman et al., 1989), under which control was the production of Affimers in the vectors used. Therefore, further optimisation of transfection efficiency was not conducted.

	Phase	GFP	Merge
Mock			
2 μl LF2000			
3 μl LF2000			
4 μl LF2000			
5 μl LF2000			
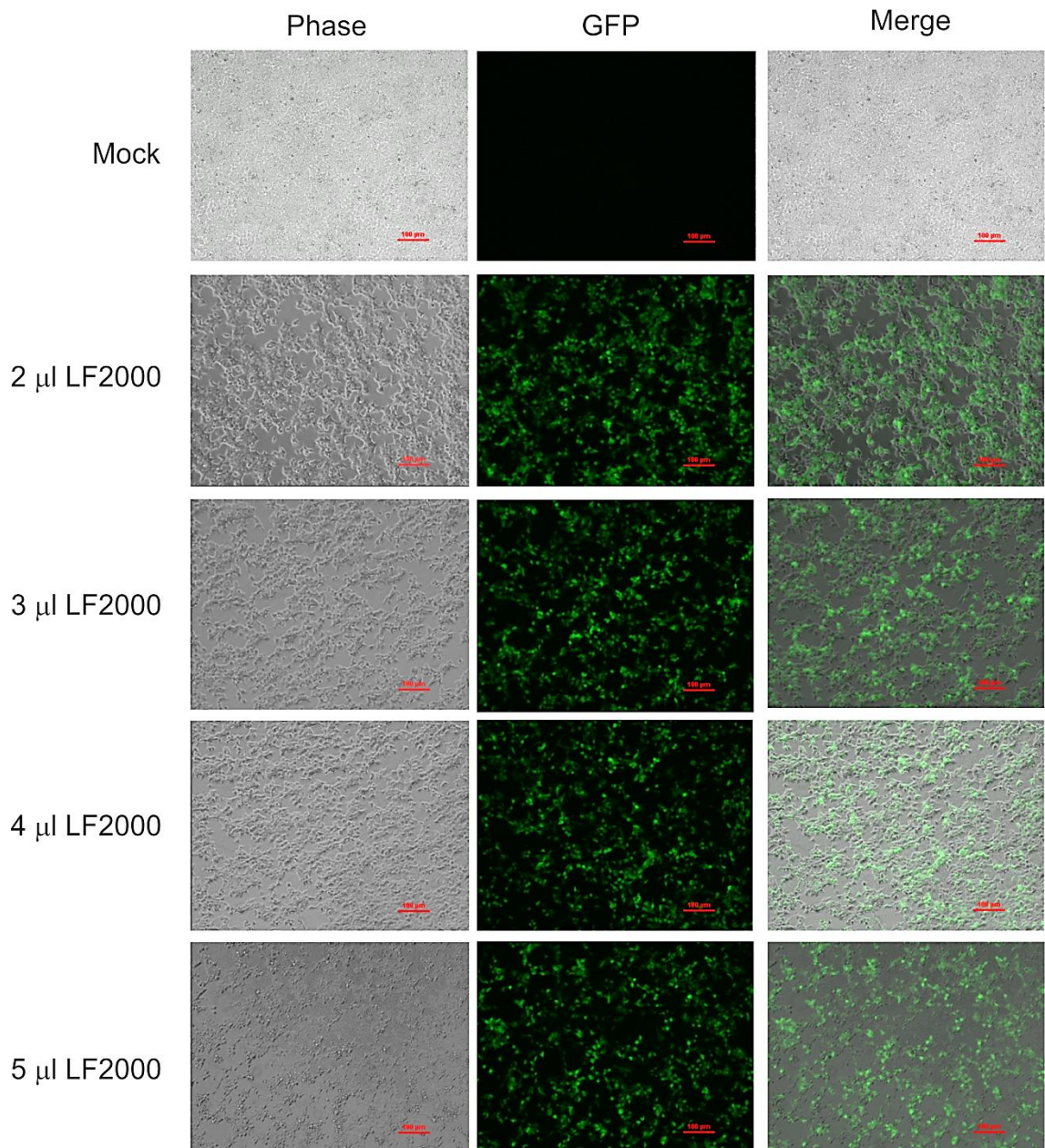
Figure 4.2 Optimisation of transient transfection conditions. 400 000 HEK293 cells were plated in 12 well-plate and incubated for 24h before transfection with 1µg of Affimer YS10-tGFP plasmid and with indicated amounts of Lipofectamine™ 2000 (LF2000) reagent. Cells were imaged at 24h post-transfection, and the visible light, GFP and merged images are shown. Highest transfection efficiency and lowest cell cytotoxicity was observed with 2µl LF2000 reagent. Scale bars are 100µm.

4.2.2 Intracellularly expressed Affimers engage with endogenous Ras

Next, the ability of intracellularly expressed Affimers to capture endogenous Ras was examined. Intracellular expression of Affimers was chosen over the use of purified proteins, as this would test whether the Affimers retain their ability to bind with the target protein in the reducing environment of the cytoplasm. This assay was also used to confirm Affimers binding to the native, full length form of Ras, as compared to the recombinant protein used in phage display. HEK293 cells were transiently transfected with pcDNA5 plasmids encoding His-tagged Affimers, as described in section 2.2.11. Twenty-four hours post-transfection cell lysates, containing expressed Affimers and endogenous Ras proteins were harvested and analysed by western blot to verify expression of Ras. Relatively equal levels of Ras proteins were seen in all samples, as indicated by detected bands at molecular weight of approximately 21 kDa (Figure 4.3, bottom panel). Remaining lysates were incubated with Ni-NTA resin. After washing the resin, pulled down proteins were eluted and analysed by western blot to detect resin bound Affimers and verify pulldown of endogenous Ras. Sufficient intracellular expression of Affimers was confirmed by detection of bands at the expected MW of 12 kDa with anti-His antibody (Figure 4.3). As visualised by western blotting analysis with the anti-Ras antibody, KRas-binding Affimers, but not the control YS10 Affimer, pulled down endogenous Ras (Figure 4.3). Additionally, binding to the resin only (labelled as HEK293 cells) was not observed, thus demonstrating, that Ras was precipitated due to specific interactions with Affimers, rather than to non-specific binding to resin. Relatively equal amounts of endogenous Ras were precipitated with the three KRas-binding Affimers tested, demonstrating similar binding capabilities of these reagents. Noteworthy, the immunoprecipitation assay employed here, detected levels of pulled down pan-Ras and did not discriminate between the Ras isoforms. Western blotting analysis with isoform-selective antibodies could be performed to determine if any of the Affimers preferentially precipitate specific isoforms. Although, the main purpose of this assay was to test Affimers ability to bind to endogenously expressed Ras in the intracellular environment, which was sufficiently demonstrated.
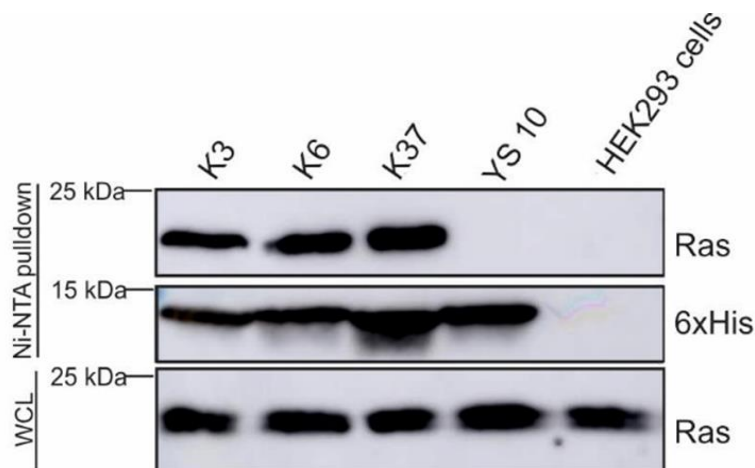
Figure 4.3 Precipitation of endogenous Ras with intracellularly expressed Affimers. Affimers were transiently expressed in HEK293 cells and precipitated via His-tag on Ni-NTA resin. Precipitated proteins were analysed by western blot with anti-His and anti-Ras antibodies. KRas-binding Affimers pulled down endogenously expressed wt Ras, as opposed to control Affimer YS10. Results are representative of three biological replicates (n=3). WCL: whole cell lysate.

4.2.3 Effects of Affimers on Ras-mediated signalling in transiently transfected HEK293 cells

Inhibition of Ras with Affimers was expected to modulate downstream signalling. To investigate this levels of ERK phosphorylation were measured, as an indicator of disruption of the Ras-mediated MAPK pathway. Firstly, however, the MAPK pathway needed to be initiated by stimulation of the epidermal growth factor receptor (EGFR) with the human epidermal growth factor (EGF). As this stimulation is known to be transient (Shah et al., 2003), a time-course of EGF-induced ERK phosphorylation was assayed to determine the optimum time point for harvesting the cells. HEK293 cells were firstly serum starved for 1h, to remove any effects of growth factors from the serum (Pirkmajer and Chibalin, 2011), following by treatment with 25 ng/ml EGF for 0-20 minutes. Cell lysates were subjected to western blotting analysis to detect phosphorylated-ERK1/2 (pERK) and tubulin as a loading control. EGF stimulation caused rapid ERK1/2 activation, reaching a peak in pERK between 2 and 5 minutes, as compared to the non-

stimulated control (Figure 4.4). Thereafter signal decline towards basal level was observed. Therefore, it was decided that 5 minutes stimulation would be used for subsequent assays, as any decrease in pERK levels could be readily observed.
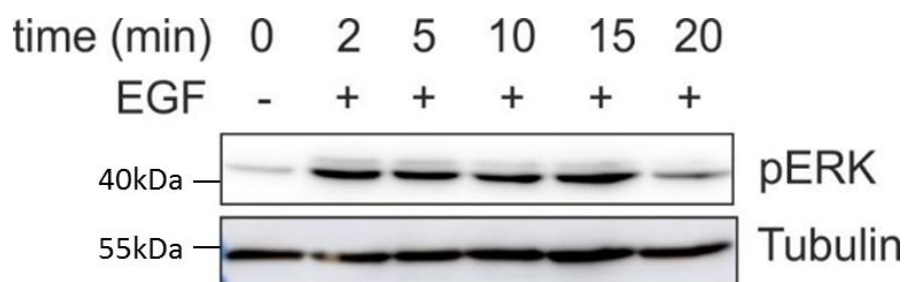
Figure 4.4 Time-course of EGF-induced ERK1/2 phosphorylation in HEK293 cells. HEK293 cells were starved in media without serum for 1h, then treated with 25 ng/ml EGF for the time periods indicated. Cell lysates were analysed by western blotting analysis with phospho-ERK specific antibody. Tubulin was used as a loading control. Results are representative of three biological replicates (n=3).

HEK293 cells were then transiently transfected with either empty pcDNA5 vector, used as a negative control, or plasmids encoding His-tagged Affimers. Twenty-four hours post transfection, cells were serum-starved, the MAPK pathway was stimulated with 25 ng/ml of EGF for 5 min, as described above, and cell lysates were subjected to western blotting analysis to detect levels of pERK and tubulin. As visualised in Figure 4.5, successful stimulation of cells was achieved, signified by the difference in ERK phosphorylation between stimulated and non-stimulated controls. However, neither of the KRas-binding Affimers nor the control YS10 Affimer had significant effect on ERK1/2 phosphorylation, when compared with the EGF-stimulated pcDNA5 vector only control. Sufficient Affimers expression was detected with anti-His western blot, therefore failure to detect effects on pERK cannot be attributed to the low levels of Affimer expression.
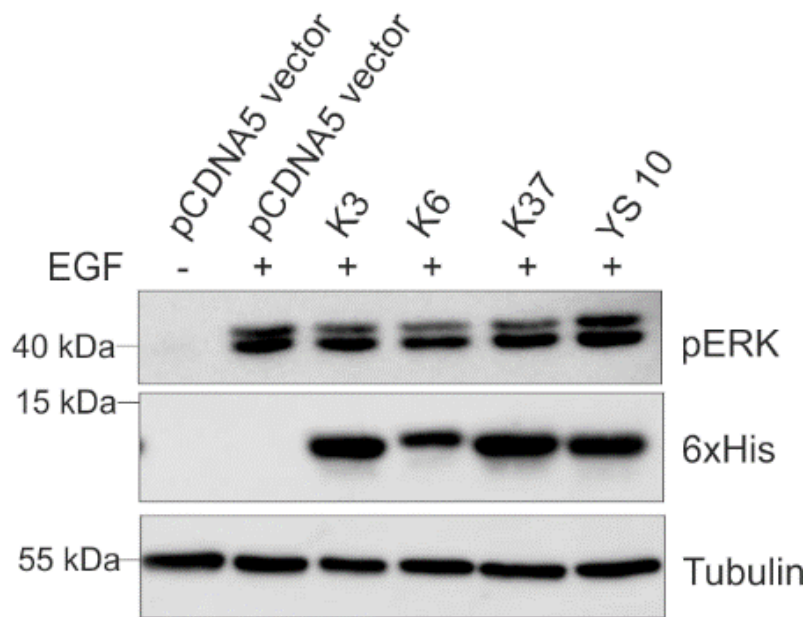
Figure 4.5 Effect of transiently expressed Affimers on EGF-induced ERK1/2 phosphorylation in HEK293 cells. HEK293 cells were transiently transfected with either empty pCDNA5 vector or encoding Affimers. Twenty-four hours post transfection, cells were starved in media without serum for 1h and signalling was stimulated with 25 ng/ml EGF for 5 min. Cell lysates were analysed by western blotting with phospho-ERK specific antibody. Tubulin was used as loading control. Results are representative of three biological replicates (n=3).

4.2.4 Transient expression of Affimers decreased ERK phosphorylation in co-transfected HEK293 cells

It was hypothesised that the lack of observed effects on ERK phosphorylation, described above, could have been due to lower than expected transfection efficiency. As a result, any changes to pERK levels caused by inhibition of Ras-mediated signalling by Affimers, could have been masked by the signal from non-transfected cells. Therefore, to assay the levels of ERK phosphorylation in cells producing Affimers, HEK293 cells were co-transfected with plasmids encoding His-tagged Affimers and FLAG-tagged ERK1. Twenty-four hours post transfection, cells were serum starved, followed by 5 min stimulation with 25 ng/ml EGF and the whole cell lysates were subjected to western blotting analysis

to detect endogenous pERK levels. Cells transfected with empty pcDNA5 vector and YS10 Affimer were used as controls. Similarly to results described above (Figure 4.5), no effect of Affimers on levels of endogenous pERK was observed. The remaining lysates were subjected to immunoprecipitation on anti-FLAG beads. After washing the beads, bound proteins were subjected to immunoblotting to detect levels of the recombinant pERK and total ERK as a loading control (Figure 4.6). As visualised by western blotting analysis, cells expressing Affimers K6 and K37 showed significantly reduced phosphorylation of the recombinant ERK1, as compared to the EGF-stimulated cells transfected with empty pcDNA5 vector. As expected, the control Affimer YS10 did not have an effect on pERK levels.

Rather surprising was the result obtained with Affimer K3, which did not reduce levels of pERK. As the binding between intracellularly expressed K3 and endogenous Ras was confirmed (Figure 4.3), it was expected that K3 would also affect Ras-mediated signalling. Since K3 displayed isoform-specific inhibition of nucleotide exchange (section 3.2.2), the Ras isoform expression levels in HEK293 cells were compared, which indicated over 3 fold higher expression of HRas over KRas (Uhlen et al., 2017, Human Protein Atlas). This therefore, indicated that effects of inhibition of KRas by K3 in HEK293 cells could have been masked by the signalling from uninhibited HRas. Thus providing explanation for the results observed here.

An alternative assay, based on immunofluorescence, was also performed, to further study the levels of ERK phosphorylation in cells expressing Affimers. In this case, the HEK293 cells were transiently transfected with pCMV6 plasmids encoding Affimers tagged with turbo green fluorescent protein (tGFP). Cells transfected with the transfection reagent only (cells) or the Affimer YS10 were used as controls. Twenty-four hours post-transfection cells were serum starved and stimulated with 25 ng/ml EGF for 5 min. Cells were fixed and stained with anti-pERK antibody and imaged with an Operetta HTS imaging system. Cells expressing Affimers were detected by green fluorescence. The advantage of this assay over the co-immunoprecipitation describe above, is that here the phosphorylation levels of the endogenous ERK were examined, as opposed to the recombinant protein detected above. Similarly to the results from the co-

immunoprecipitation, cells expressing Affimers K6 and K37 displayed significant reduction in pERK levels (Figure 4.7). As expected, the control Affimer YS10 did not affect ERK phosphorylation. Interestingly, significant effect of K3 on pERK levels was observed, although it was not as great as the effect of K6 or K37. Nevertheless, it demonstrated the ability of K3 to impair Ras-mediated signalling in HEK293 cells. Likewise, results obtained from this assay further supported the idea that the lack of effects observed on the global pERK in western blot analysis (section 4.2.3) was due to the lower than expected transfection efficiency. The immunofluorescence work was carried out by Dr Heather Martin.
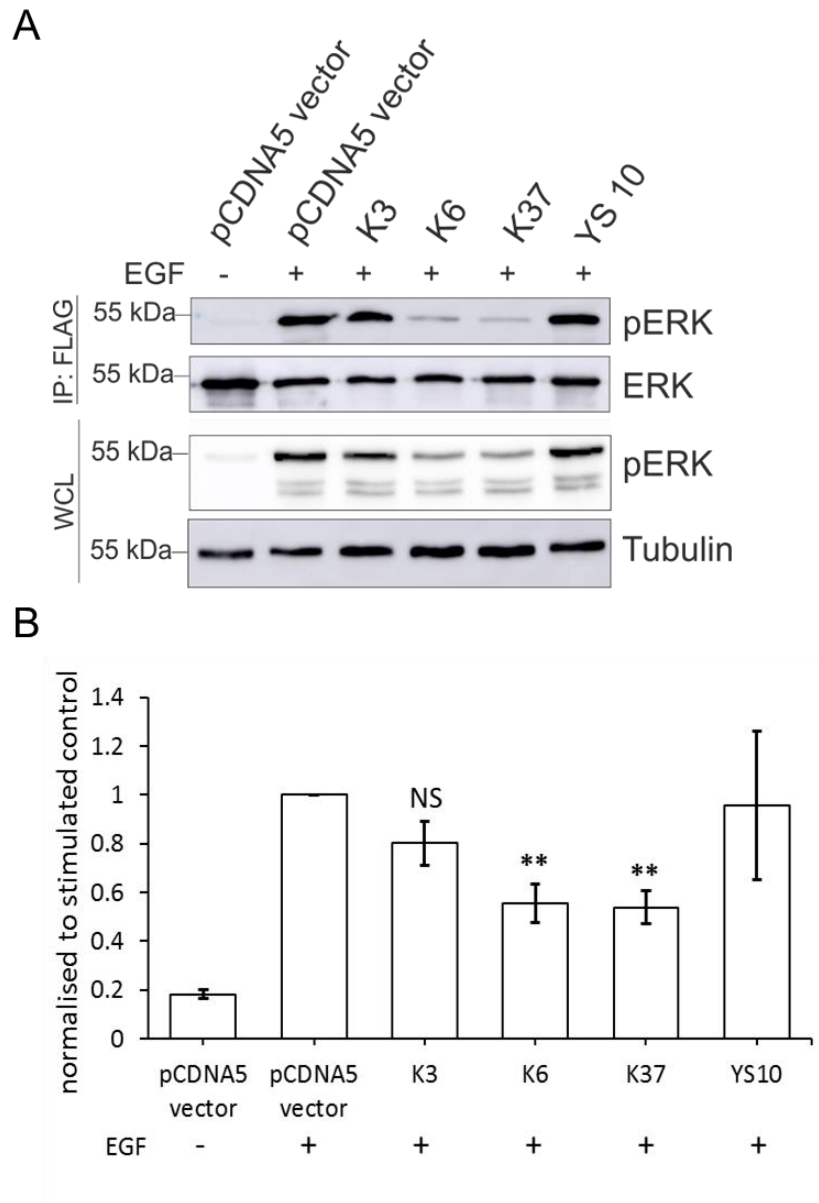
Figure 4.6 Immunoprecipitation of FLAG-ERK1 and effect on EGF-induced ERK phosphorylation in HEK293 cells. HEK293 cells were co-transfected with FLAG-ERK1 plasmid and either empty pcDNA5 or encoding Affimers. Twenty-four hours post transfection, cells were starved in media without serum for 1h then treated with 25 ng/ml EGF for 5 min. A) FLAG-ERK1 was precipitated from cell lysates using anti-FLAG beads and pulled down proteins were analysed by western blot with anti-ERK and anti-phospho-ERK antibodies. Tubulin was used as loading control. B) Quantification of results in A). Levels of phospho-ERK were divided by levels of ERK, and normalised to stimulated control (pCDNA5 vector + EGF). Results are representative of three biological replicates (n=3). Error bars denote SEM. $p < 0.05$ (*), $p < 0.01$ (**). IP: immunoprecipitation, WCL: whole cell lysate, NS: not significant.

A

B
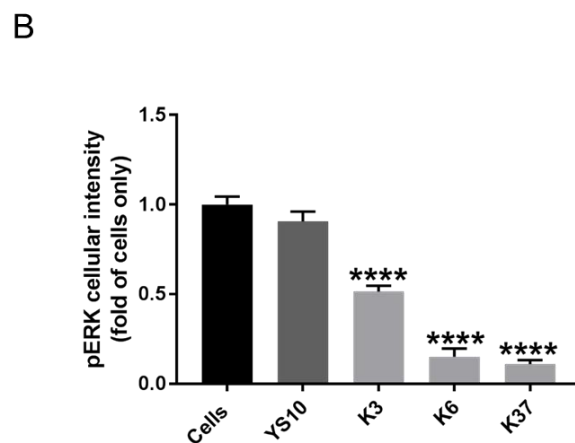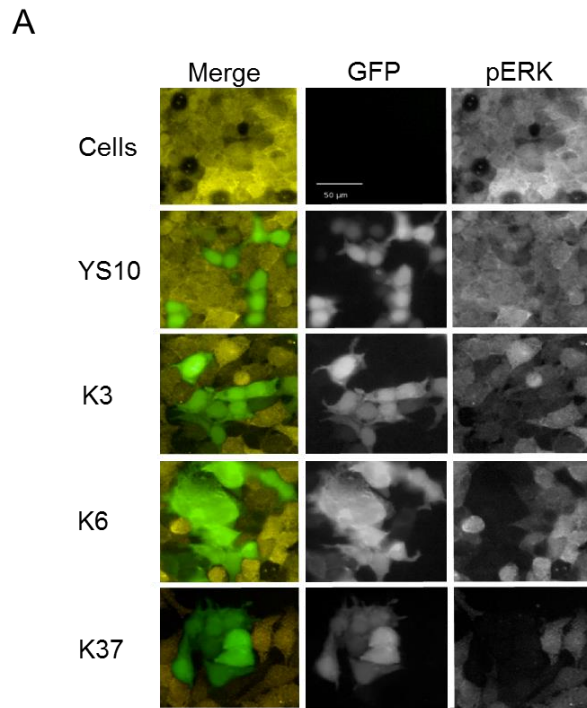
Figure 4.7 Ras binding Affimers inhibit EGF-induced phosphorylation of endogenous ERK in HEK293 cells. HEK293 cells were transfected with either empty pCMV6 plasmid or encoding Affimer-tGFP proteins. Twenty-four hours post transfection, cells were starved in media without serum for 1h then treated with 25 ng/ml EGF for 5 min. Cells were then fixed in 4% PFA, stained with anti-phospho-ERK antibody and imaged with an Operetta HTS imaging system. Images were then analysed with Columbus 2.7.1. A) Representative images of effects of Affimers on EGF-stimulated upregulation of pERK. Scale bar is 50µm. B) Quantification of cellular pERK intensity in Affimer positive cells as identified by GFP/well stimulated with EGF. Results are representative of three biological replicates (n=3). Error bars denote SEM. ANOVA with Dunnett's post-hoc test **** $p < 0.0001$. This work was carried out by Dr Heather Martin.

4.2.5 Effects of Affimers on Ras-mediated signalling in stably transduced U2OS cell lines

Since the transient transfection efficiency was not high enough to observe a significant change in the global pERK levels in western blotting analysis, it was decided to test stable transduction of Affimer DNA, as it ensures sustained transgene expression in 100% of cell population. The ProteoTuner™ technology (ClonTech) was employed. This system consists of a genetic fusion between the protein of interest and the destabilisation domain (DD). The DD is a FKBP12 protein (12 kDa), bearing destabilising mutation L106P, which leads to rapid proteasomal degradation of the fusion protein (Banaszynski et al., 2006). The stabilisation of DD-tagged protein, and thus accumulation in the cell, occurs in the presence of small molecule ligand Shield1™ (Figure 4.8). The amount of stabilised fusion protein is proportional to the amount of Shield1™ added, which allows tuneable stabilisation/destabilisation of the protein of interest. Use of this system, would therefore enable to study the dose-dependent effects of Affimer reagents in target cell lines. Besides, as the Affimers affect the MAPK signalling pathway that regulates cell growth, continuous expression of Affimers may lead to cell death. Therefore, it would be beneficial to 'switch off' Affimer expression during the propagation of the cell lines, to ensure healthy growth, and only stabilise the DD-Affimer fusion protein when performing signalling assays.

The Affimer coding sequences were cloned from the bacterial expression pET11a vector into the pRetroX-PTuner plasmid, to generate a genetic fusion between Affimers and the DD-tag (at the N-terminus). Thus produced plasmids were used to retrovirally transduce the human osteosarcoma U2OS cell line, as described in section 2.2.14. The U2OS cells are fast growing and display high transfection efficiency. Moreover, involvement of the MAPK pathway in osteosarcoma has been previously reported (Chandhanayingyong et al., 2012, Noh et al., 2011). Therefore it was decided, that U2OS is a suitable cell line to study the effects of Affimers on Ras-mediated signalling.

Retrovirally transduced U2OS cells were subjected to puromycin selection, to isolate only the successfully transduced cells. These cells were then seeded into 6-well plate and 2 hours later Shield1™ concentrations ranging from 50-500nM were added and the cells were incubated overnight. Cells were then starved in

media without serum and with Shield1™ for 1h, followed by stimulation with 25 ng/ml EGF for 5 min. Cell lysates were subjected to western blotting analysis with anti-pERK and anti-DD antibodies. Tubulin was used as loading control. As visualised by the western blotting analysis, stable expression of Affimers did not result in reduced ERK phosphorylation (Figure 4.9). This was also true for the control Affimer YS10, as expected. No detectable reduction in pERK cannot be attributed to the failure of Affimer expression, as dose-dependent DD-Affimer expression was observed for all constructs. However, the levels of fusion protein expression varied substantially between the constructs. While sufficient expression of DD-Affimer YS10 was detected, very low levels of KRas-binding Affimers, especially K6 and K37, were observed even at the highest Shield1™ concentration. This could lead to inefficient inhibition of Ras and therefore no observed effects on pERK levels.

Noteworthy, it was hypothesised that the N-terminal DD tag, which is in close proximity to the Affimers variable regions, could be obstructing Affimers binding to their target protein. Therefore, a helical linker sequence was introduced into the plasmid between the DD and the Affimer, to separate the two proteins, thereby making the Affimer variable regions more accessible for binding to the target protein. This strategy has proven successful in separating domains of bifunctional fusion proteins (Arai et al., 2001). However, it had no effect at improving the Affimers ability to affect Ras-mediated MAPK signalling, as reduction in pERK levels was not observed (data not shown). Since generation of stable cell lines is a laborious process, and the effects of Affimers on Ras-mediated signalling has been sufficiently demonstrated in transiently transfected cells, no further efforts were made to optimise the stable expression system.
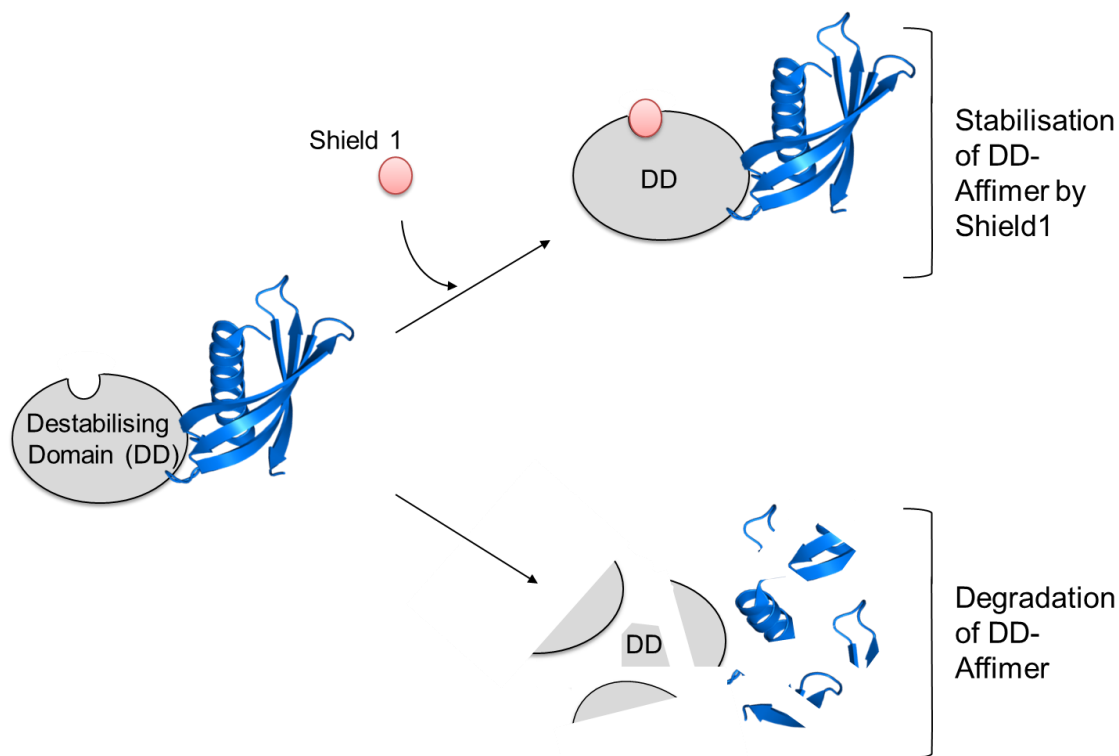
Figure 4.8 Diagram of the ProteoTuner Shield system. A destabilisation domain (DD) is fused to N-terminus of Affimer. In the absence of small molecule ligand Shield1^{TM} (red) the fusion protein is destabilised and degraded by proteasomes. Addition of Shield1^{TM} results in stabilisation of DD-tagged protein. The amount of stabilised fusion protein is proportional to the amount of Shield1^{TM} added, which allows tunable stabilisation/destabilisation of the protein of interest.
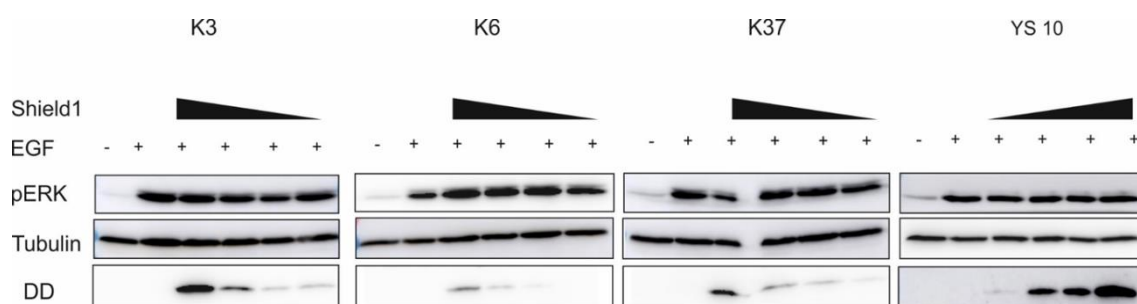
Figure 4.9 Effect of stably expressed Affimers on EGF-induced ERK1/2 phosphorylation in U2OS cells. Retrovirally transduced U2OS cells were seeded into 6-well plate and 2 hours later increasing amounts of Shield1™ were added and the cells were incubated o/n. Cells were then starved in media without serum and with Shield1™ for 1h, then treated with 25 ng/ml EGF for 5 min. Cell lysates were analysed by western blot with anti-phospho-ERK and anti-DD antibodies. Tubulin was used as loading control. Results are representative of three biological replicates (n=3).

4.3 Discussion

The work presented in this chapter characterised anti-KRas Affimers in the cellular context, to further explore their potential to target Ras within the cell. Firstly, binding between anti-KRas Affimers and endogenously expressed Ras in HEK293 cells was investigated. Similarly to anti-Ras DARPins K27 and K55 (Guillard et al., 2017), Affimers successfully engaged with endogenous Ras (Figure 4.3). Noteworthy, the abilities of other anti-Ras scaffold proteins, namely intrabody iDab6 and monobody NS1, to bind to Ras in cell-based assays have been tested; however these assays examined binding to overexpressed recombinant Ras proteins (Tanaka et al., 2007, Spencer-Smith et al., 2017b). Moreover, the anti-Ras intrabody iDab6 was effective only when the iDab6 expression was targeted to the plasma membrane (Tanaka et al., 2007). This therefore, demonstrated the abilities of transiently expressed Affimers to bind to lower levels of endogenously expressed Ras, without the need for subcellular localisation. Furthermore, it showed that Affimers are functional in the reducing environment of the cells.

To test whether the binding of Affimers would result in negative modulation of Ras signalling activity, the effects of downstream ERK phosphorylation were measured. When used as genetically encoded intracellular reagents, Affimers failed to elicit any significant effect on endogenous levels of pERK (Figure 4.5). This could have been due to lower than expected transfection efficiency, in comparison to the efficiency obtained in the transfection optimisation trials (Figure 4.2). As a consequence, any effects of the Affimers would have been concealed as western blotting analysis measures pERK levels from the entire cell population. The observed low transfection efficiency was rather surprising, because the HEK293 cell line, used in these assays, has been extensively characterised for its ability of high efficiency transfection (Thomas and Smart, 2005). Moreover, the transfection protocol has been optimised, and indicated sufficient efficiency (Figure 4.2). As mentioned before, further optimisation trials with varying amounts of DNA and longer incubation time post-transfection could be performed to enhance the transfection efficiency.

To overcome the limitations of low transfection efficiency and assay the levels of ERK phosphorylation in cells producing Affimers, HEK293 cells were transiently co-transfected with plasmids encoding His-tagged Affimers and FLAG-tagged ERK1. This assay has been successfully used to study the effects of NS1 monobody, which was shown to potently inhibit EGF-induced ERK activation (Spencer-Smith et al., 2017b). Similarly here, cells expressing Affimers K6 and K37 showed significantly reduced phosphorylation of the recombinant ERK1, as compared to the EGF-stimulated control cells (Figure 4.6). Interestingly, expression of K3 had no effect on pERK1 levels. This was thought to be due to significantly higher expression of HRas isoform over KRas in HEK293 cell line. Since K3 preferentially inhibited KRas in the nucleotide exchange assay, it was hypothesised that the effects of inhibition of KRas by K3 could have been masked by the signalling from uninhibited HRas. However, further tests would be required to provide definitive answers. For example, co-transfection with the ERK1 plasmid could be coupled with the transfection with individual Ras isoforms, as has been done to assay the isoform specificity of the anti-Ras monobody. As a result, NS1 has been shown to attenuate ERK phosphorylation by inhibition of HRas and KRas but not NRas (Spencer-Smith et al., 2017b).

Having demonstrated that intracellularly expressed Affimers affect the recombinant ERK activation, it was decided to assay the effects on the endogenous pERK levels. An immunofluorescence assay was developed, as this allowed to visualise pERK levels in Affimer-producing cells in comparison to non-transfected cells. All three KRas-binding Affimers, but not the control Affimer YS10, significantly reduced ERK activation (Figure 4.7). This assay has proven to be superior to the western blot analysis employed earlier, as it demonstrated that K3 does have an effect on Ras-mediated signalling and that anti-KRas Affimers are indeed capable of reducing the phosphorylation of endogenous ERK. Noteworthy, Affimers did not rely on localisation to the specific cell compartment to elicit an effect, as this was the case for the anti-Ras intrabody iDab6, which was effective only when targeted to the plasma membrane (Tanaka et al., 2007).

In addition to the immunofluorescence assay described above, the tGFP-tagged Affimer constructs could have been sorted by the fluorescent activated cell sorting (FACS) using flow cytometry, to isolate successfully transfected cells, and perform signalling assay on this population. However, the main limitation of this strategy concerns the decreased cell viability after the sorting, as FACS-mediated induction of oxidative stress can occur, thereby affecting cell metabolism (Llufrio et al., 2018). Nevertheless, FACS sorting has been successfully used to study the effects of anti-Ras DARPins, which were shown to abrogate the pERK response in comparison to the control DARPin (Guillard et al., 2017).

Alternatively to cell sorting, stable transfection has been used, as this ensures 100% transduced population. However, stably expressed Affimers failed to affect ERK phosphorylation (Figure 4.9). As mentioned, this could have been due to low DD-Affimer fusion protein expression detected. Though, analysis with DD-tagged protein standard would be required to quantify the Affimers expression levels. Furthermore, it was hypothesised that the DD-tag interfered with binding to Ras. This has not been directly tested in this study, although it has been demonstrated in the lab that the Grb2 SH2 DD-tagged Affimers failed to bind to theirs target (data not published). One possible optimisation involved cloning the DD-tag at the C-terminus of the Affimer. However, as the ProteoTuner™ system has been shown to work more efficiently with the N-terminally DD-tagged fusion

proteins (Banaszynski et al., 2006), the sub-cloning was not attempted. Conversely, a helical linker peptide sequence was introduced, as this strategy has proven successful in separating domains of bifunctional fusion proteins (Arai et al., 2001). The linker consisted of 20 amino acids containing three helix-forming repeats (EAAAK). However, the introduction of this linker has not resulted in any significant changes to ERK phosphorylation in Affimer-expressing cells (data not shown).

In conclusion, work presented in this chapter demonstrated the ability of Affimers to function in the cytoplasmic environment and to modulate Ras-mediated ERK activation. Since, the effects of other anti-Ras scaffold proteins were not limited to inhibition of ERK activation, but have also shown effects on AKT signalling (Guillard et al., 2017, Spencer-Smith et al., 2017b), future work should concentrate on assaying the Affimers ability to modulate AKT activation. Likewise, it would be interesting to test the effects of Affimers on Ras-effector interactions in cell-based assays, such as the bioluminescent resonance energy transfer (BRET) assay employed to study the Ras-targeting DARPins (Guillard et al., 2017). This would establish whether the inhibition of Ras-Raf interaction observed *in vitro*, could be also observed in the cellular environment. As the Affimers were also shown to be effective against KRas mutants *in vitro*, future work should also involve testing the effects of Affimers in cancer cells harbouring KRas mutations. In addition, the anti-Ras scaffolds, namely iDab6, NS1 and DARPins K27 and K55 were shown to effect Ras-mediated transformation and proliferation (Tanaka et al., 2007, Spencer-Smith et al., 2017b, Guillard et al., 2017). Therefore, it would also be interesting to test how the Affimers would perform in these assays.

Chapter 5

Structural characterisation of the Affimer-KRas complex

Chapter 5

Structural characterisation of the Affimer-KRas complex

5.1 Introduction

Protein function is directly related to its three dimensional structure. Therefore, determining the atomic structure of a protein or protein complex provides significant insights into how they function (McLachlan, 1972, Popp et al., 2018). Moreover, high resolution structures are invaluable for structure-based design of inhibitors that manipulate proteins functions, highlighting the powerful therapeutic potential of structural biology (Watkins and Arora, 2015).

Since the determination of the structure of the myoglobin in 1958, the first high resolution protein crystal structure (Kendrew et al., 1958), significant advances in structural and computational technologies have been made, which have resulted in exponential growth of the number of published structures (Popp et al., 2018, Campbell, 2002). X-ray crystallography was the first method used for structure determination, and it is still one of the most efficient structural technique. However, it relies on the production of protein crystals that diffract to high (enough) resolution. Nuclear magnetic resonance (NMR) is another technique, which can be used to study non-crystalline samples. It is particularly useful for investigating dynamics and conformational changes of the molecules, as the experiments are performed in solution. The main limitation of NMR however, is the protein size, as large molecular weight macromolecules reduce the quality and interpretability of spectra (Yu, 1999). In contrast, electron microscopy (EM) is often used to study large structures. Improvements of EM to achieve better resolution include use of cryogenic temperatures (cryo-EM), higher voltage electron sources and single-particle analysis. Data from EM can often be combined with high resolution information obtained from other methods, thus yielding complementary information about the macromolecule (Murata and Wolf, 2018, Campbell, 2002).

Affimer reagents have been previously shown to inhibit protein function and structural studies have highlighted their mode of action (Hughes et al., 2017, Robinson et al., 2018). For example, the co-crystal structure of Affimer F4 with the Fc gamma receptor IIIa (FcɣRIIIa) revealed an orthosteric mode of inhibition, by binding of the Affimer to the immunoglobulin G (IgG) binding site. Interestingly, the crystal structure of another FcɣRIIIa-targeting Affimer G3 demonstrated binding of the Affimer to the interdomain hinge region of FcɣRIIIa, which did not overlap with the IgG-binding site, therefore indicating allosteric mode of action (Robinson et al., 2018). In another study, structural analysis of Affimer-SUMO complexes also revealed a competitive mode of action, as the Affimer-SUMO interactions used mostly the same residues as the binding between SUMO and SUMO-interacting motifs (SIMs). In addition, structural characterisation, coupled with molecular dynamics simulations allowed definition of the molecular mechanisms that underpin the Affimer S2B3 isoform specificity towards SUMO-2, in contrast to Affimer S1S2D5, which binds both SUMO-1 and SUMO-2 isoforms (Hughes et al., 2017).

Artificial binding proteins tend to identify critical residues, termed 'hot spots', which are amino acids on the target protein that contribute most significantly to binding (Bogan and Thorn, 1998). These hot spots are attractive targets for development of small molecule inhibitors (Modell et al., 2016, London et al., 2013). However, the design of small molecule inhibitors is more likely to succeed when these hot spots are tightly clustered, rather than distributed over an extended interface (Jochim and Arora, 2010). Therefore, scaffold proteins that display smaller interaction surface areas with their target proteins, such as the anti-Ras monobody NS1 (interaction surface area of 568Å^2) (Spencer-Smith et al., 2017a) or Affimers binding to small ubiquitin-related modifier (SUMO) proteins (interface areas in a range of ~610-720Å^2) (Hughes et al., 2017) are more likely to aid small molecule inhibitors design, as opposed to the interactions which occur over relatively large binding interfaces, for example, the HRas-intrabody (interface surface area of 852 Å) or the KRas-DARPins interactions (interface surface area of 950 Å) (Tanaka et al., 2007, Guillard et al., 2017).

This chapter describes the work employed to determine the atomic structures of KRas-bound Affimers via X-ray crystallography, in order to determine the mode

of modulation and identify the intermolecular interactions. Firstly, the Affimers were purified in complex with KRas protein to set up crystallisation trials. Diffraction data from obtained crystals were used to build a KRas-Affimer structure. Analysis of the structure guided further biophysical assays, including loop deletion and alanine scanning, to identify residues essential for function.

5.2 Results

5.2.1 Generation of the Affimer-KRas complex

The affinity tags on KRas structures in the Protein Data Bank (PDB) (Berman et al., 2000) were removed prior to crystallisation because fusion tags are known to hinder the crystal growth (Smyth et al., 2003). The recombinant KRas protein used in the biochemical assays (chapter 3) contained an N-terminal His-tag for affinity purification and C-terminal BAP-tag for *in vitro* biotinylation (Figure 5.1A). To remove these tags, the KRas sequence (without His- and BAP-tag, Figure 5.1A) was amplified by PCR from the bacterial expression vector (as described in chapter 2.2.3.4). Agarose gel analysis of the PCR product indicated band of approximately 500 bp, corresponding to the correct size of tagless KRas sequence, demonstrating successful amplification (Figure 5.1B). The PCR product was then digested with *Nhe I* and *Not I* and ligated back into the bacterial expression vector. Successful cloning was confirmed by sequencing. The tagless KRas was then produced in *E. coli* BL21 Star^{TM} DE3 cells, as described in chapter 2.2.3.2.

A

MHHHHHHTEYKLVVVGAGGVGKSALTIQLIQNHFVDEYDPTIEDSYRKQVVIDGETCLL

DILDTAGQEEYSAMRDQYMRTGEGFLCVFAINNTKSFEDIHHYREQIKRVKDSEDVPMV

LVGNKCDLPSRTVDTKQAQDLARSYGIPFIETSAKTRQGVDDAFYTLVREIRKHKSGLN

DIFEAQKIEWHE

B
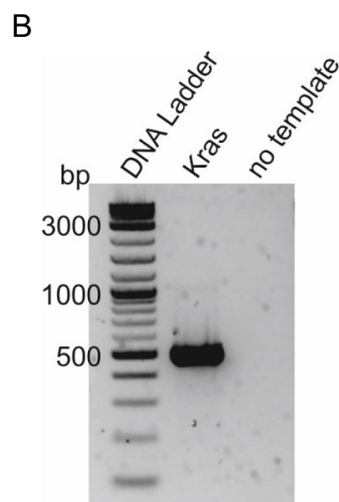
Figure 5.1 Cloning of tagless KRas. A) Protein sequence of wild-type KRas4B residues 1-166, with highlighted His-tag and BAP-tag sequences in red. The black sequence represents the KRas sequence used in crystallisation trials. B) KRas sequence without His-tag and BAP-tag was amplified by PCR (shown in black in A), and the product was analysed on 2% agarose gel. Cloning of tagless KRas was confirmed by sequencing.

The generation of the Affimer-KRas complex is described in chapter 2.2.3.4. Briefly, the purified Affimer was mixed with bacterial cell lysate containing the KRas and incubated overnight to allow for the formation of Affimer-KRas complex. The Affimer-KRas complex was then captured on Ni-NTA resin for purification. After washing the resin, the complex was eluted and samples were analysed by SDS-PAGE and Coomassie staining. Two bands of approximate molecular weights of 18 and 12 kDa, corresponding to tagless KRas and Affimer, respectively, were observed, indicating efficient purification of the Affimer-KRas complex (Figure 5.2A). Moreover, the similar intensity of the bands in each elution suggested a 1:1 stoichiometry.

The eluted complex was further purified by size exclusion chromatography (SEC), to separate any Affimer not in complex with KRas. Additionally, SEC allowed exchange into buffer more suitable for crystallisation trials. A single peak was seen in the A_{280} elution trace (Figure 5.2B), demonstrating that all of the purified proteins were in complex. However, because the molecular weight markers were not analysed, the elution volume of the eluted proteins could not be used to accurately determine the molecular weight of the eluted complex. Therefore, the eluted fractions were analysed by SDS-PAGE and Coomassie staining (Figure 5.2C). Once again, two bands of approximate molecular weights of 18 and 12 kDa, corresponding to tagless KRas and Affimer, respectively, were observed, confirming the purification of the Affimer-KRas complex. The eluted fractions were pooled together and concentrated to 12 mg/ml total protein (see chapter 2.2.3.4), as quantified by BCA protein assay. This protocol has been employed to purify the three Affimers K3, K6 and K37 in complex with KRas, but only the complex purification data for Affimer K6-KRas complex is shown.
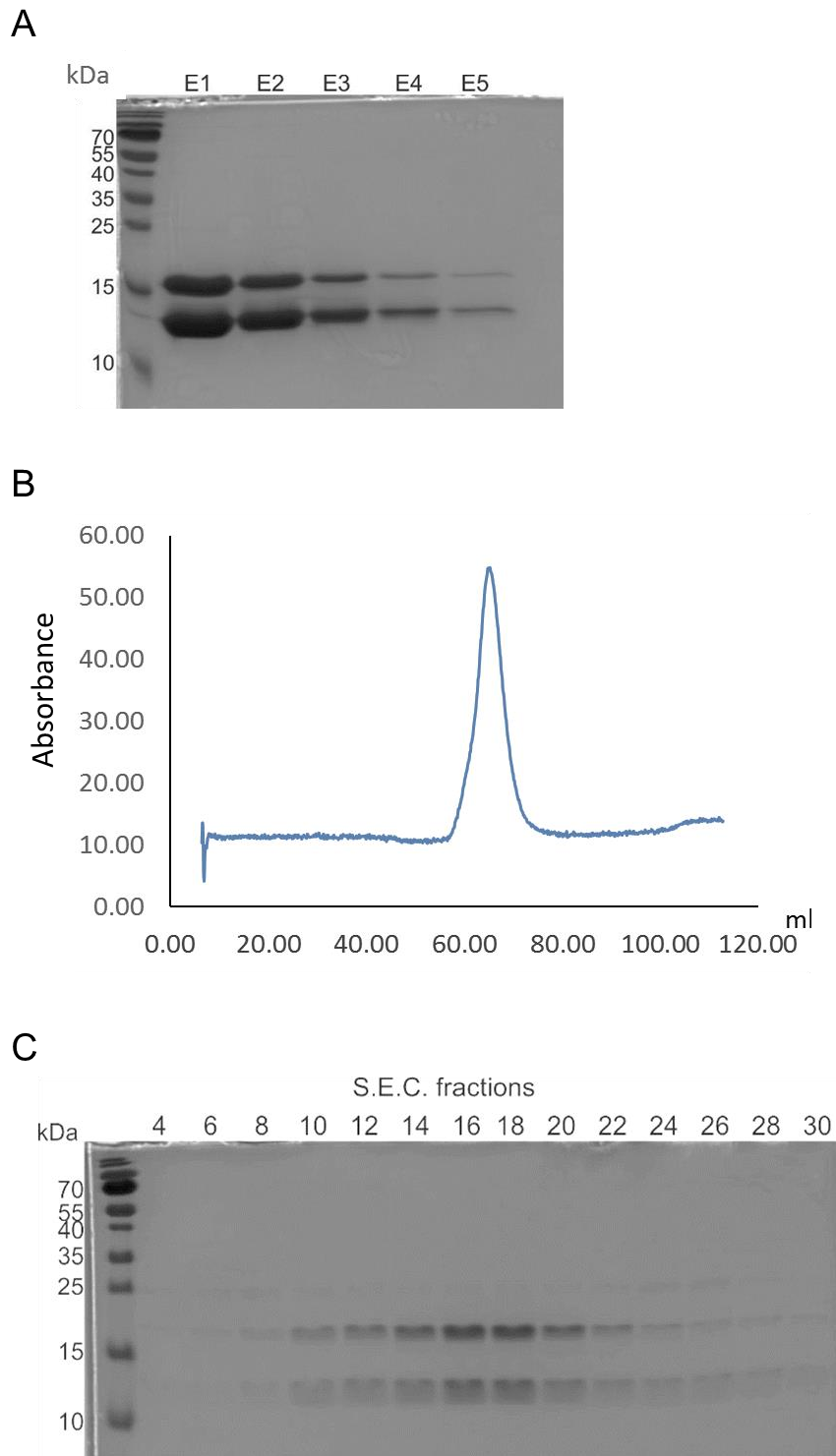
Figure 5.2 Purification of Affimer-KRas protein complex. A) Purified Affimer was mixed with cell lysate containing KRas and incubated overnight. The complex was purified by Ni-NTA affinity chromatography and eluted fractions were analysed by SDS PAGE and Coomassie staining. B) The purified fractions were further purified by size exclusion chromatography (SEC) (B) and fractions were analysed by Coomassie staining (C). Eluted fractions were pooled together and concentrated to 12 mg/ml total protein.
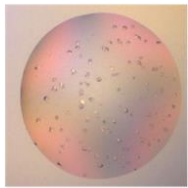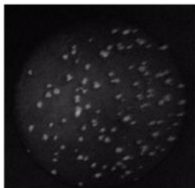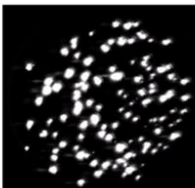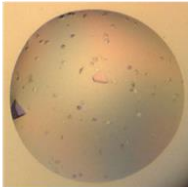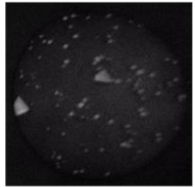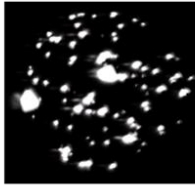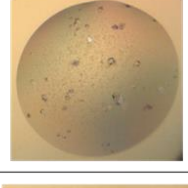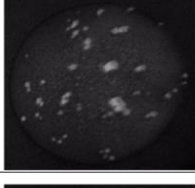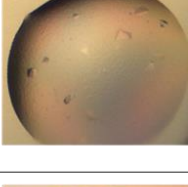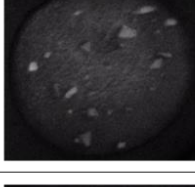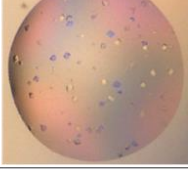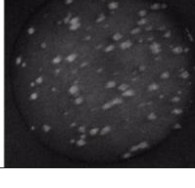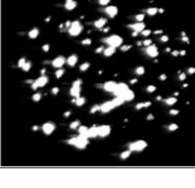
5.2.2 Crystallisation of Affimer-KRas complex

Crystallisation experiments were initiated with commercial crystal screens, JCSG Core I-IV (Qiagen), in order to determine the optimal conditions for crystal growth. A total of 384 conditions, based on a database of successful crystallisation trials (Jancarik and Kim, 1991, Lesley and Wilson, 2005) were used, utilizing the sitting-drop vapor diffusion technique, as described in chapter 2.2.8.1. Crystal formation was monitored with the Rock Imager (Formulatrix) using visible light (vis) microscopy. The absorption of aromatic residues at 280nm (UV) has been also employed in order to confirm the presence of protein. In addition, second-harmonic generation (SHG) microscopy has been used to detect crystal formation, as SHG can only arise from noncentosymmetric ordered structures (Wanapun et al., 2010). Thus visible entities that appear to be crystals that are positive for signal from UV and SHG should be proteins crystals rather than salt crystals on non-crystalline objects.

The crystallisation event occurs during transition from the unsaturated phase, containing the protein of interest below its solubility limit, to the supersaturated phase, which contains the protein in excess of its solubility limit. This drives precipitation or nucleation, which is the process by which molecules pass from disordered state to an ordered one, thus forming crystals. (McPherson and Gavira, 2014). Therefore, optimal protein concentration is essential to obtain the supersaturated state. Protein precipitation has been observed in around 45% of conditions, indicating sufficient protein concentration to obtain supersaturation to drive nucleation (McPherson and Cudney, 2014). Crystals of the Affimer K6-KRas complex started appearing within 24 hours in 5 different conditions. Crystal growth was monitored for 34 days and crystals grew to sizes ranging from 25-75 µm. SHG imaging demonstrated that the observed particles are indeed in crystal forms, and the UV imaging confirmed that these were protein crystals (Table 5.1).

Optimisation of the initial crystallisation conditions was carried out to improve crystal diffraction potential (Chayen and Saridakis, 2002). In addition, upscaling to a larger drop size has been used to produce larger crystals for better diffraction (Chapman et al., 2011). Grid screens, which are one of the most widely used crystal optimisation strategy (Cox and Weber, 1988), have been employed to refine the chemical conditions. The concentration of salt, the precipitating agents

and the pH of the solution in the initial conditions, have been varied in a regular fashion, as outlined in Table 5.2, as optimisation of these factors constitutes the most effective way to induce crystallisation (McPherson and Cudney, 2014). Additionally, some of the optimised screens were supplemented with cryoprotectant agents, such as polyethylene glycol (PEG) 400, ethylene glycol or methyl pentanediol (MPD). These agents were used to prevent ice crystal formation at the cryogenic temperatures used during crystal harvesting and data collection which reduces radiation damage (Farley and Juers, 2014). The crystallisation optimisation plates were incubated at room temperature and crystal formation was observed with a light microscope. Optimisation trials of the original conditions from wells JCSG II C2, D6 and G8 have not yielded any protein crystals. The best crystals were obtained from optimisation of the initial condition from JSCG I well G11, with the final condition of 0.1M Na acetate pH 5, 25% w/v PEG 4K, 0.2M $(NH_4)_2SO_4$, 5% MPD (data not shown). Five crystals from this condition were cryoprotected for data collection in solution containing 30% w/v PEG 4K, 0.1M Na acetate, pH 5, 0.2M $(NH_4)_2SO_4$, 20mM $MgCl_2$, 5% PEG 400, 5% MPD, 5% ethylene glycol and 5% glycerol.
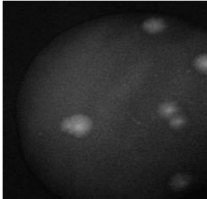
Screen	Well	Vis	UV	SHG	Condition
JCSG I	G11				0.1 M NaOAc 4.6 pH 25 % w/v PEG 4K 0.2 M $(NH_4)_2SO_4$
JCSG II	C2				0.1 M HEPES 7.5 pH 2 %v/v PEG 400 2 M $(NH_4)_2SO_4$
JCSG II	D6				0.1 M Na_3 Cit 5.5 pH 40 %w/v PEG 600
JCSG II	E10				0.1 M Na_3 Cit 5.6 pH 30 %w/v PEG 4K 0.2 M NH_4 Acet
JCSG II	G8				0.16 M $(NH_4)_2SO_4$ 0.08 M Na Acet 4.6 pH 20 %w/v PEG 4K 20 %v/v Glycerol

Table 5.1 Summary of initial crystallisation conditions for obtained Affimer K6-KRas complex crystals. Screen plate names and wells in which the crystals appeared are listed, along with visible light, UV and SHG images of the crystals and components of the mother liquors.
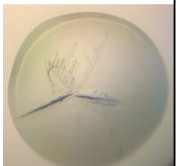
Screen name and well number	Original condition	Optimised conditions
JCSG I - G11	0.1 M Na Acet 4.6 pH, 25 % w/v PEG 4K, 0.2 M $(NH_4)_2SO_4$	• 0.1M Na Acet pH: 4, 4.5, 5 • PEG 4K (%): 15, 20, 25, 30 • +/- 10% PEG 400
JCSG I - G11	0.1 M Na Acet 4.6 pH, 25 % w/v PEG 4K ,0.2 M $(NH_4)_2SO_4$	• 0.1M Na Acet pH: 4.5, 5, 5.5 • PEG 4K (%): 25, 30 • +5% DMSO or 5% PEG 400 or 5% ethylene glycol or 5% MPD
JCSG II - C2	0.1 M HEPES 7.5 pH, 2 %v/v PEG 400, 2 M $(NH_4)_2SO_4$	• 0.1M Hepes pH: 7, 7.5, 8 • $(NH_4)_2SO_4$ (M): 1.8, 2.0, 2.2, 2.4 • +2% PEG 400/ +5% PEG 400
JCSG II - D6	0.1 M Na3 Cit 5.5 pH (Buffer), 40 %w/v PEG 600	• 0.1M Na_3 Cit pH: 5, 5.5, 6 • PEG 600 (%): 30, 35, 40, 45
JCSG II - E10	0.1 M Na3 Cit 5.6 pH, 30 %w/v PEG 4K, 0.2 M NH_4 Acet	• 0.1M Na_3 Cit pH: 5, 5.5, 6 • NH_4 Acet (M): 0.1, 0.2, 0.3, 0.4 • +/- 10% PEG 400
JCSG II - G8	0.16 M $(NH_4)_2SO_4$, 0.08 M Na Acet 4.6 pH, 20 %w/v PEG 4K, 20 %v/v Glycerol	• 0.08M Na Acet pH: 4, 4.5, 5 • Glycerol (%): 15, 20, 25, 30

Table 5.2 Summary of crystallisation optimisation conditions. The original conditions in which crystal growth was observed are shown, along with the concentration and pH ranges of the varied factors in the optimisation trials.

Crystallisation trials of the Affimer K3-KRas and K37-KRas complexes were conducted as described above. Needle clusters crystals of K3-KRas appeared in one condition (Table 5.3), while a cluster of rod-like crystals of K37-KRas was observed in a single condition (Table 5.4). Recently, optimisation of the K3-KRas crystal trials have been performed by Ajinkya Rao from the Tomlinson group and the K3-KRas X-ray co-crystal structure has been solved to 2 Å. The optimisation trials of the K37-KRas condition were also performed, however, these have not yielded any protein crystals.

Screen	Well	Vis	UV	SHG	Condition
JCSG III	D10				0.1 M TRIS 7 pH, 50 %v/v PEG 200

Table 5.3 Summary of crystallisation conditions for obtained Affimer K3-KRas complex crystals. Screen plat name and the well in which the crystals appeared are listed, along with visible light, UV and SHG images of the crystals and components of the mother liquors.

Screen	Well	Vis	UV	SHG	Condition
JCSG III	B5				0.2 M sodium Acetate, 0.1 M Tris pH 8.5, 30% w/v PEG 4000

Table 5.4 Summary of crystallisation conditions for obtained Affimer K37-KRas complex crystals. Screen plat name and the wells in which the crystals appeared are listed, along with visible light, UV and SHG images of the crystals and components of the mother liquors.

5.2.3 Crystal structure of Affimer K6-KRas complex

X-ray diffraction data of the Affimer K6-KRas crystals was collected at the Diamond Light Source and the structure determination was performed as described in chapter 2.2.8.3. Data collection, processing and structure determination were carried out by Dr Chi Trinh.

The crystal structure of Affimer K6 bound to wild type KRas-GDP was solved at 1.9 Å. The co-crystal structure revealed Affimer K6 interacting with KRas switch regions (Figure 5.3). Analysis with PISA (EMBL-EBI) (Krissinel and Henrick, 2007) estimated the total buried surface area of the K6-KRas interaction to be ~475 Å^2, therefore indicating a very small interaction interface. The conformation of the switch regions in the K6-KRas structure most closely resembled that of the previously reported non-liganded, GDP-bound Ras (PDB: 4OBE, (Hunter et al., 2014)), therefore indicating that binding of Affimer did not result in any significant alterations to the KRas structure. Noteworthy, an overlay of the K6-KRas structure with that of the active, GTP-bound KRas (PDB: 5VQ2, (Xu et al., 2017)) did not indicate any steric clashes (Figure 5.4), therefore demonstrating ability of the Affimer K6 to bind to both the inactive and active KRas conformations, which is in agreement with the biochemical data, described in chapter 3.

The Affimer K6 binding site overlapped with that of the nucleotide exchange factor Sos. This therefore, provided structural evidence that K6 works as a competitive inhibitor. However, as mentioned above, binding of K6 did not induce a conformational change in the switch I region, as opposed to the large conformational change in the Ras-Sos structure, resulting from displacement of switch I by α-helix of Sos (Boriack-Sjodin et al., 1998).

Interestingly, comparison of the K6-KRas structure with that of Ras-Raf(RBD) (PDB: 3KUD, (Filchtinski et al., 2010)), indicated a steric clash between the Affimer and RBD (Figure 5.5), suggesting that K6 may block Raf binding to Ras. This however, was not observed in the biochemical assay (see chapter 3.2.4).
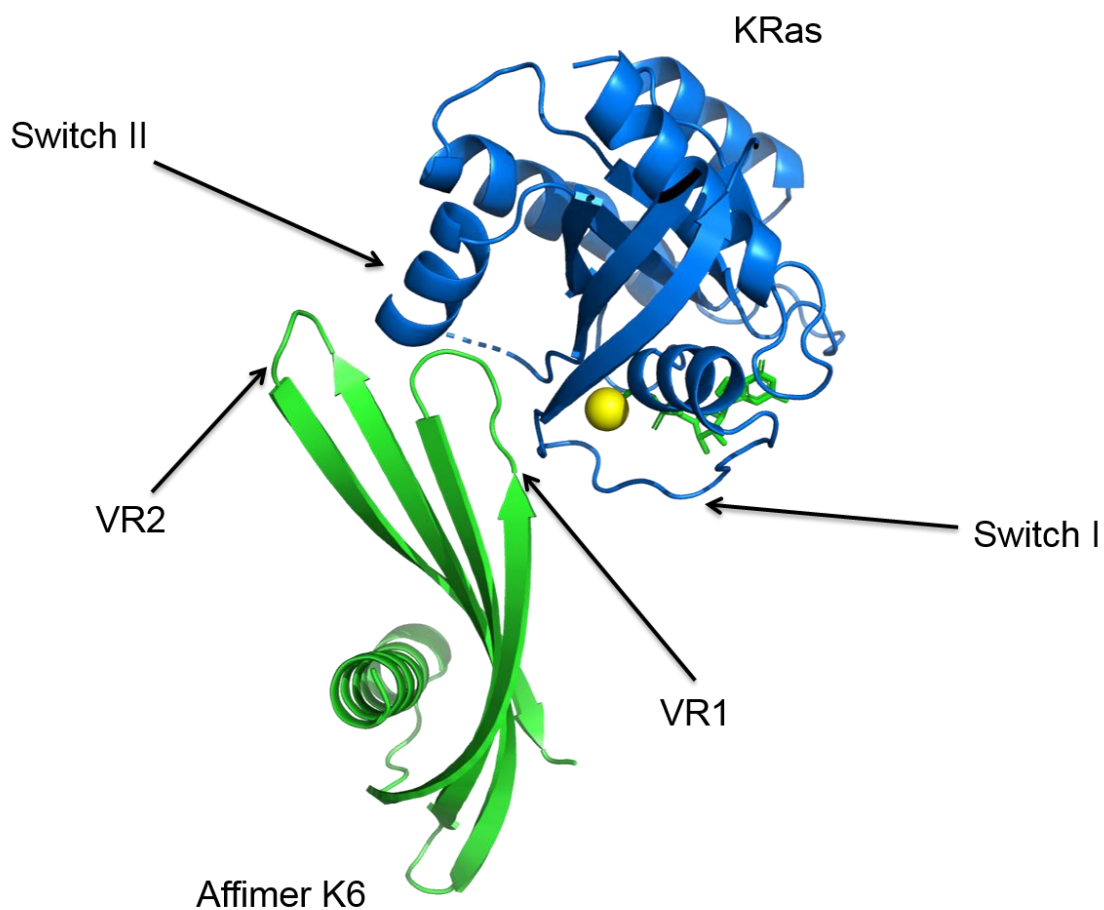
Figure 5.3 The 1.9 Å co-crystal structure of KRas with Affimer K6. Affimer K6 is shown in green and KRas is shown in blue. Magnesium is shown as yellow sphere and GDP as green sticks. Arrows indicate KRas switch I and II regions and Affimer's variable regions 1 and 2. Image was generated in PyMOL.

KRasGDP
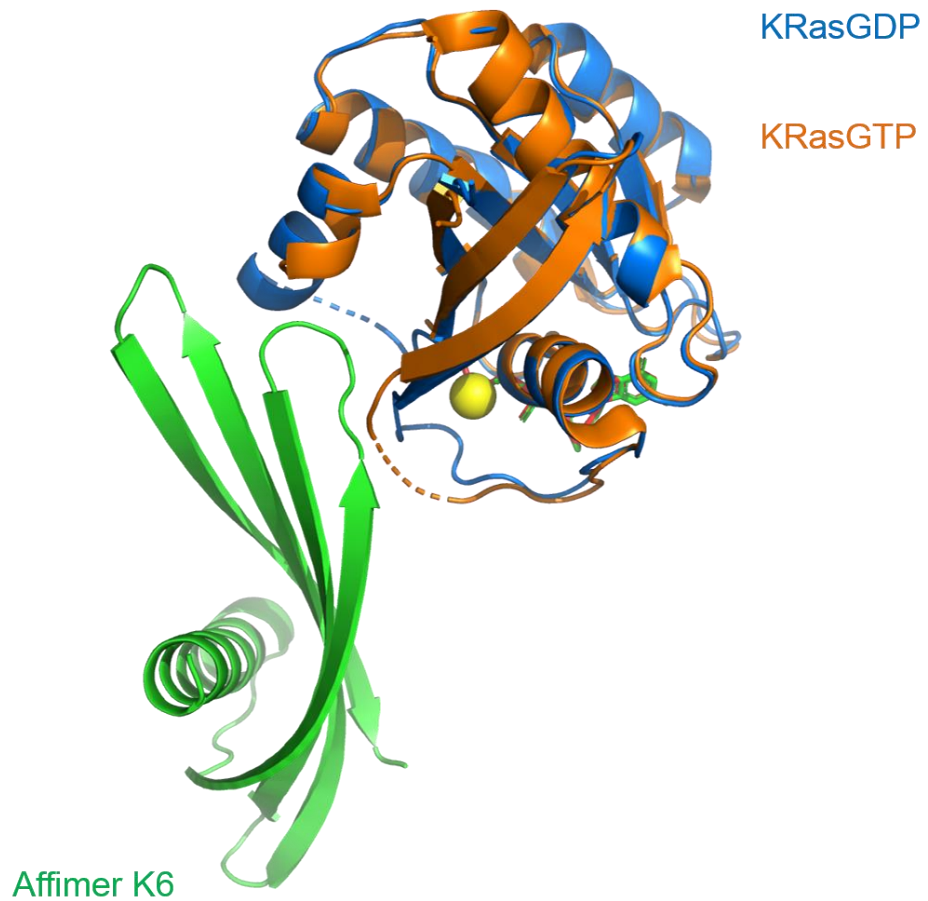
KRasGTP

Affimer K6

Figure 5.4 Comparison of the K6-KRas-GDP structure with the structure of KRas-GTP. An overlay of the K6-KRas-GDP with the KRas-GTP structure (PDB: 5VQ2) indicating no significant steric clashes between the Affimer and GTP-bound KRas, therefore demonstrating that K6 could also bind to the active KRas conformation. Affimer K6 is shown in green. KRas-GDP in blue, KRas-GTP in orange. GDP is shown as green sticks and magnesium as yellow sphere. Image was generated in PyMOL.
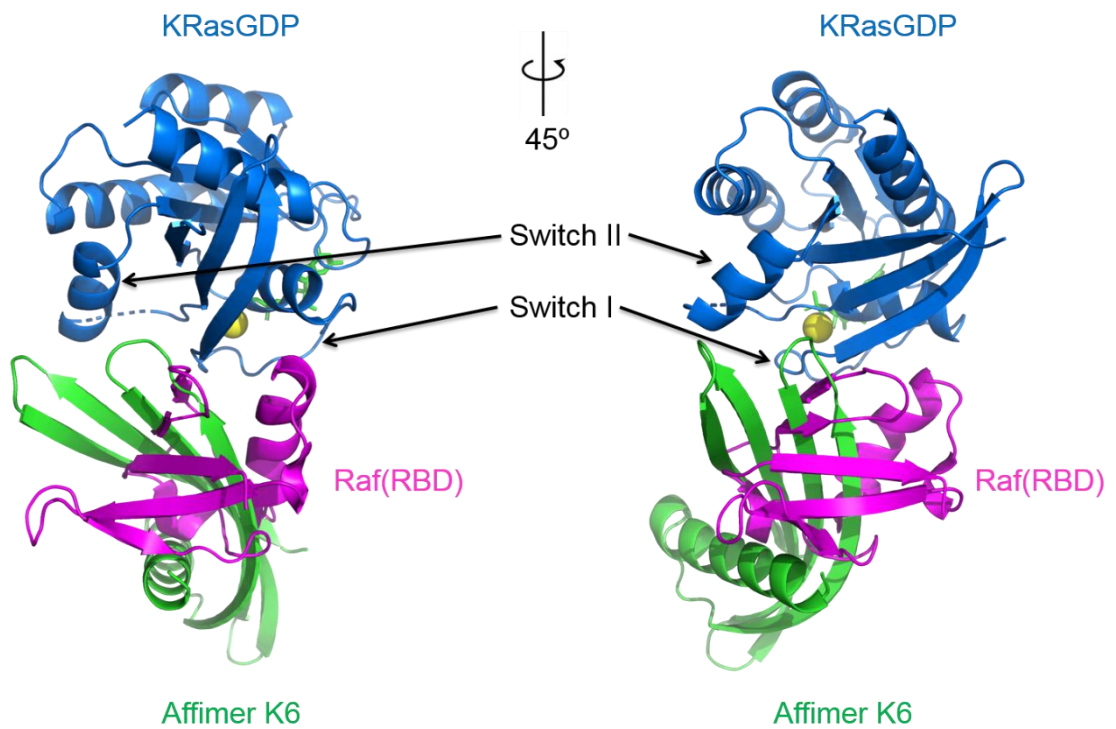
Figure 5.5 Superimposition of the Raf(RBD) structure (PDB:3KUD) onto KRas-K6 complex structure. Significant steric clash has been observed between K6 and Raf binding to KRas. Switch I and II regions are annotated with arrows. Affimer K6 is shown in green, KRas-GDP in blue, and the Ras binding domain (RBD) of Raf is shown in pink. Magnesium is shown as yellow sphere and GDP as green sticks. Images were generated in PyMOL.

5.2.4 Affimer K6ΔVR2 mutant and its effects on binding and inhibition

Protein structures are not static, but rather contain regions displaying different degrees of flexibility. However, in crystal structures, the data is averaged over the time of data collection (Wlodawer et al., 2008). Thus to assay the protein structure's flexibility and dynamics, B-factors can be assessed. A B-factor is a parameter that reflects the fluctuations of an atom about its average position in the crystal structure (Yuan et al., 2005). Large B-factors indicate high mobility of atoms. The B-factors can be shown in a putty tube representation, where the diameter of the tube is correlated with the B-factor of that structure. High B-factors are indicated by orange to red colours and wider tube, while lower B-factors are indicated by blue to green and narrow tube.

The B-factors of the Affimer K6 from the co-crystal K6-KRas structure, were analysed in PyMOL and are shown in Figure 5.6. High B-factors of the variable region two (VR2) were observed, in comparison to the rest of the K6 structure. This therefore, reflected the flexibility of this region. It was then hypothesised that this could be because VR2 was not involved in binding. To test this hypothesis, the residues in VR2 have been replaced with three residues (AAE) of the alanine (Ala) Affimer scaffold, producing a one loop mutant (hereafter referred to as K6ΔVR2). This has been achieved by splice-overlap extension of two PCR products, as described in 2.2.1.9. The first PCR product contained the K6 sequence including the VR1, while the second PCR product contained the alanine Affimer VR2 sequence (Figure 5.7A). These PCR products of approximately 200 bp (Figure 5.7B), where then subjected to SOE, as described in chapter 2.2.1.9, to splice the two fragments together. Agarose gel analysis indicated a product of approximately 300 bp in size, confirming successful splicing of the two PCR fragments (Figure 5.7C). Moreover, a single band indicated that all of the PCR fragments used have been joined together. The product encoding K6ΔVR2 was ligated into bacterial expression vector. Replacement of the K6 VR2 was confirmed by sequencing.
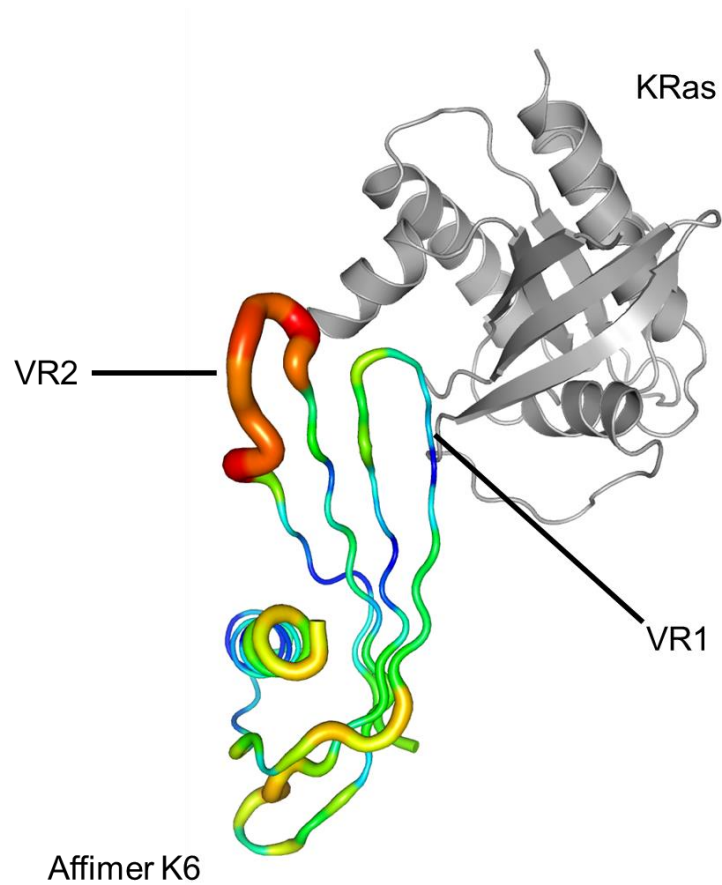
Figure 5.6 B-factor analysis of the Affimer K6 structure. The B-factors of Affimer K6 are shown in a putty tube representation, where high B-factors are indicated by orange to red colours and wider tube, while lower B-factors are indicated by blue to green and narrow tubes. KRas is shown in grey and Affimer's variable regions are indicated. Flexibility of K6 VR2 was observed, as demonstrated by high B-factors. Image was generated in PyMOL.
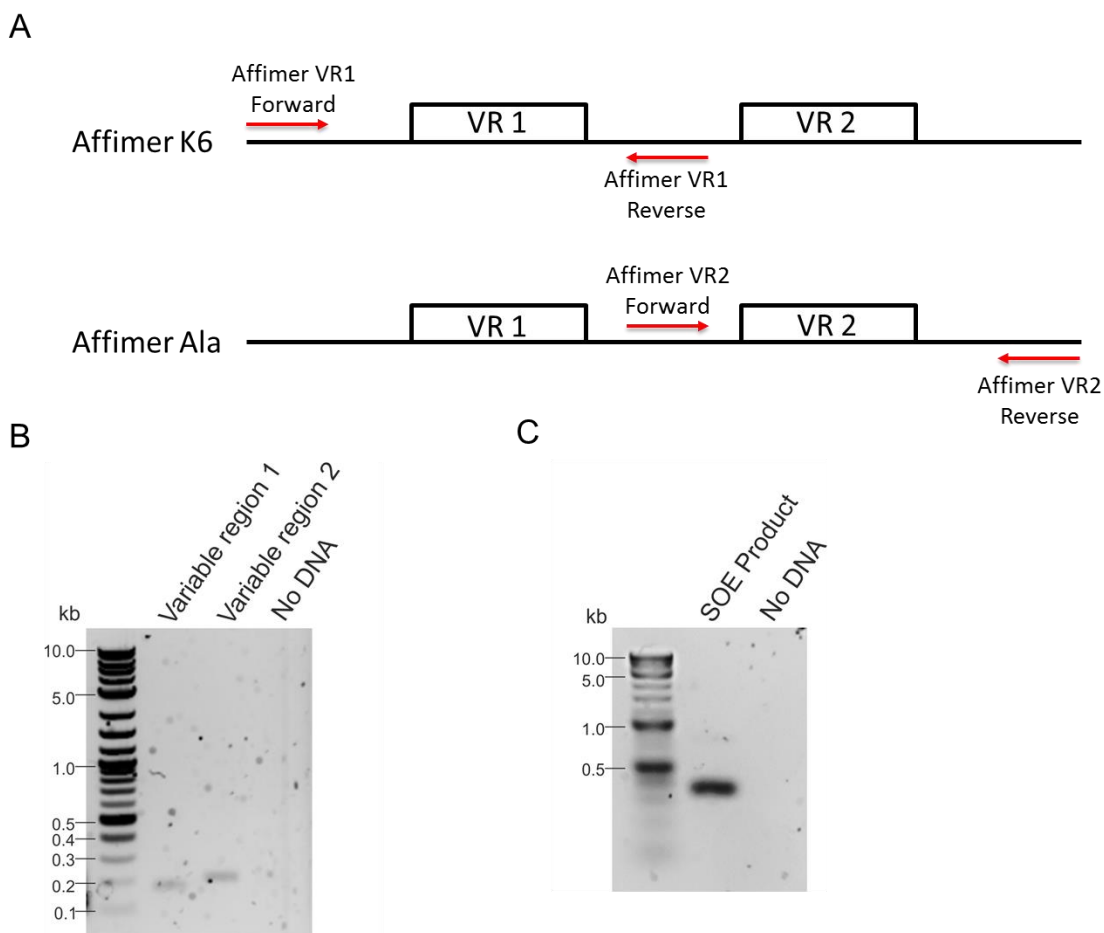
Figure 5.7 Cloning strategy to remove Affimer K6 variable region two. A) Diagram outlining primers (shown as red arrows) used to amplify Affimer K6 variable region one (VR1) and Alanine (Ala) Affimer variable region two (VR2). B) Agarose gel analysis of PCR products, demonstrating two bands of approximately 200 bp size. C) Agarose gel analysis of splice overlap extension (SOE) product, indicating successful splicing of the two PCR products.

The K6ΔVR2 mutant has been produced as described in chapter 2.2.3.1, and its ability to bind and inhibit KRas has been evaluated. Firstly, binding of K6ΔVR2 has been investigated in a pulldown assay. Glutathione S-transferase (GST) tagged KRas has been immobilised on glutathione magnetic Dynabeads™, and incubated either with the wild-type Affimer K6, the K6ΔVR2 mutant or the control YS10 Affimer. K6 was used as a positive control, while YS10 and beads only were used as negative controls. After washing, precipitated proteins were analysed by western blotting with anti-His antibody to detect Affimers and anti-

Ras antibody (Figure 5.8A). Binding to the beads only has not been observed, precluding any non-specific binding. Likewise, the control Affimer YS10 has not been pulled down, indicating that any pulled down proteins are due to specific interactions with KRas-GST. K6 has been pulled down with KRas-GST, as demonstrated by the thick band in the anti-His western blotting analysis. In contrast, only a faint band in the K6ΔVR2 sample has been observed, therefore indicating significantly impaired binding of the K6ΔVR2 to KRas-GST. Noteworthy, the band seen in the K6ΔVR2 sample is of lower molecular weight, when compared to the molecular weight of the K6, due to presence of three rather than nine residues in the VR2.

Next, the effect of VR2 deletion on the inhibitory activity was tested in the nucleotide exchange assay with wild-type KRas-mGDP. The same protocol, which was used to test K6 has been employed. Comparison of the dose-response curves obtained for K6 and the K6ΔVR2 (Figure 5.8B), showed the inability of K6ΔVR2 to inhibit nucleotide exchange on KRas, even at the highest Affimer concentrations. Altogether, these finding established that K6 VR2 is essential for binding and inhibition of KRas.
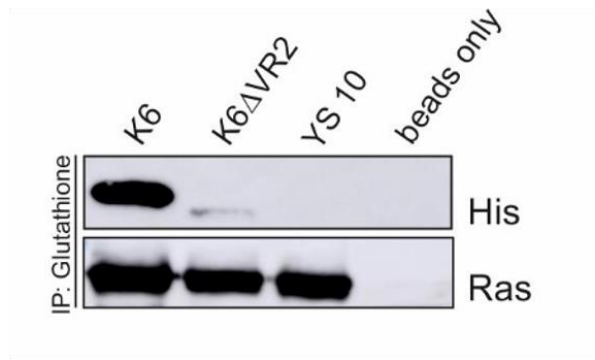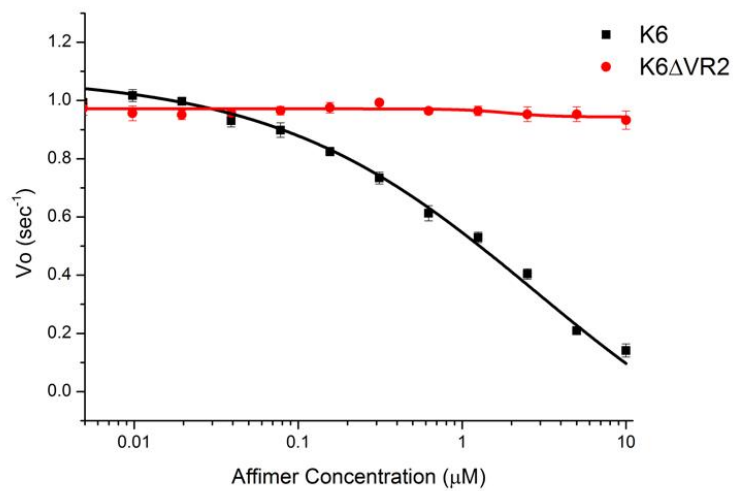
Figure 5.8 Variable region two of Affimer K6 is required for binding and inhibition.
A) KRas-GST wild-type was incubated with either Affimer K6, K6ΔVR2 or YS10, precipitated on glutathione beads and the pulled down proteins were analysed by western blotting with anti-Ras and anti-His antibodies, which demonstrated significantly impaired binding of K6ΔVR2 to KRas-GST. B) K6ΔVR2 has been also tested in nucleotide exchange assay. Dose-response curves for Affimer K6 (black) and K6ΔVR2 (red) demonstrated that K6ΔVR2 mutant did not inhibit nucleotide exchange on wild-type KRas. Results are representative of three biological replicates (n=3). Error bars denote SEM.

5.2.5 Affimer K6 alanine scanning mutants and their effects on binding and inhibition

The three dimensional protein structures yield information about the structural binding epitopes, however they do not address the functional roles of the individual residues within that epitope (Weiss et al., 2000). One strategy for the elucidation of the functional epitope and defining the structure-function relationship is a site-directed mutagenesis. Alanine scanning mutagenesis is one of the most widely used technique for probing functional epitopes (Lefevre et al., 1997). Substitution to alanine eliminates the side chain beyond the β carbon, but without any effects on the conformation of the main chain and without imposing any electrostatic or steric effects (Cunningham and Wells, 1989). This therefore allows mapping of the contribution of individual residues from the structural epitope, to the binding interaction (Weiss et al., 2000).

QuikChange site-directed mutagenesis was used to replace each of the Affimer K6 variable regions' residues to alanine, to determine their contributions to the binding interaction with KRas. The QuikChange method allows efficient site-directed substitution, deletion or insertion in a one-step procedure (Liu and Naismith, 2008). The mutagenesis was performed as described in chapter 2.2.1.10 and diagrammed in Figure 5.9. Reaction without the template DNA was used as a negative control. Following thermal cycling, the mutant plasmids were subjected to agarose gel analysis. No products were observed in the negative control sample, therefore demonstrating that any amplified products were due to the specific annealing of the primers to the template DNA. Products of approximate size of 5.6 kb were detected in all samples but the position 2.9 (Figure 5.10A and B). Although, this did not indicate failure of the position 2.9 mutant strand synthesis. Inability to detect the product in agarose gel analysis could have been due to low DNA concentration, below the detection limit. Nevertheless, all samples were *Dpn I* treated to digest the template DNA and XL-1 Blue cells were transformed with the mutant plasmids for sub-culturing. Mutagenesis was confirmed by sequencing, which demonstrated successful substitution of each residue at a time to alanine (Figure 5.10C and D).
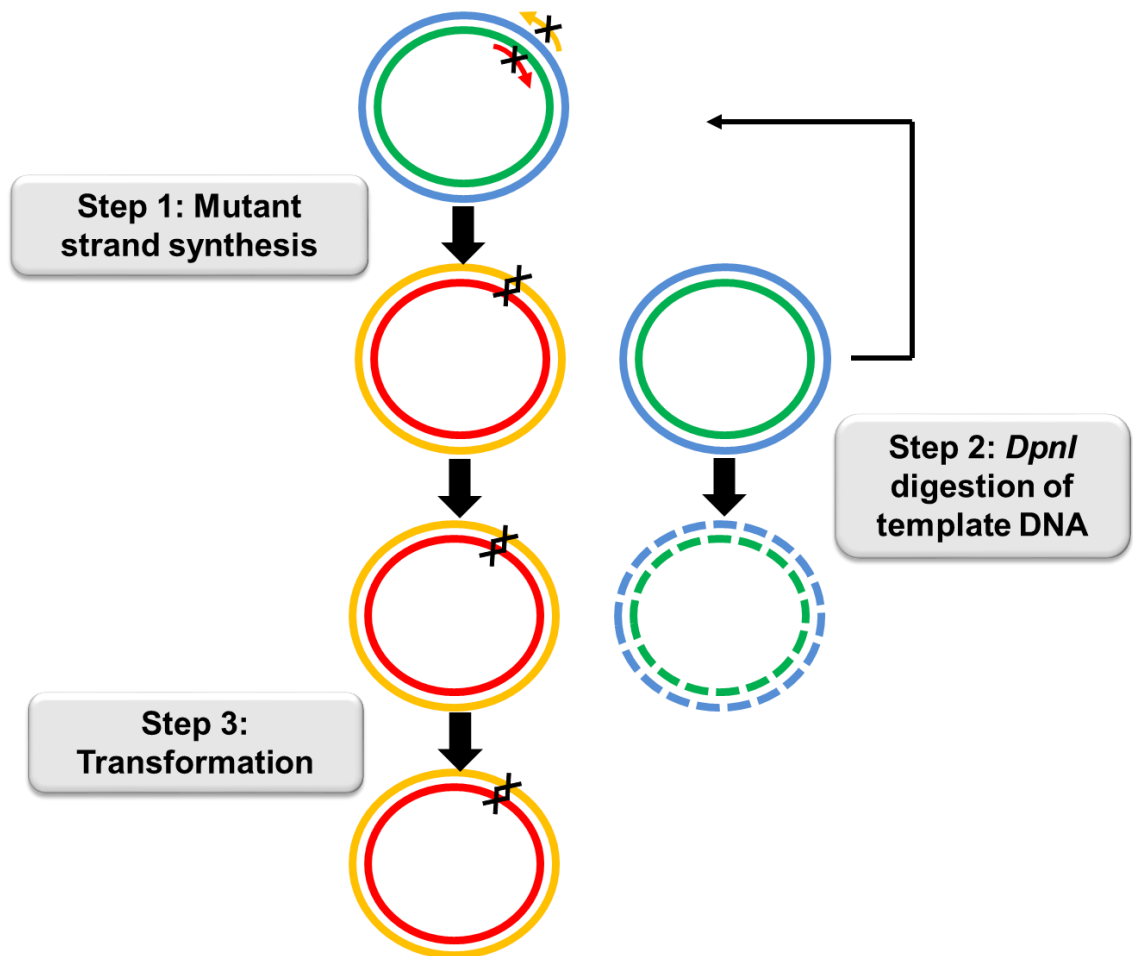
Figure 5.9 Outline of the QuikChange site-directed mutagenesis method. First step consists of thermal cycling to denature template DNA, anneal mutagenic primers and extend primers with DNA polymerase to generate mutated plasmid with staggered nicks. The plasmid is then treated with *Dpn I* endonuclease to digest parental DNA. Finally, XL-1 Blue supercompetent cells are transformed with nicked mutated plasmid.
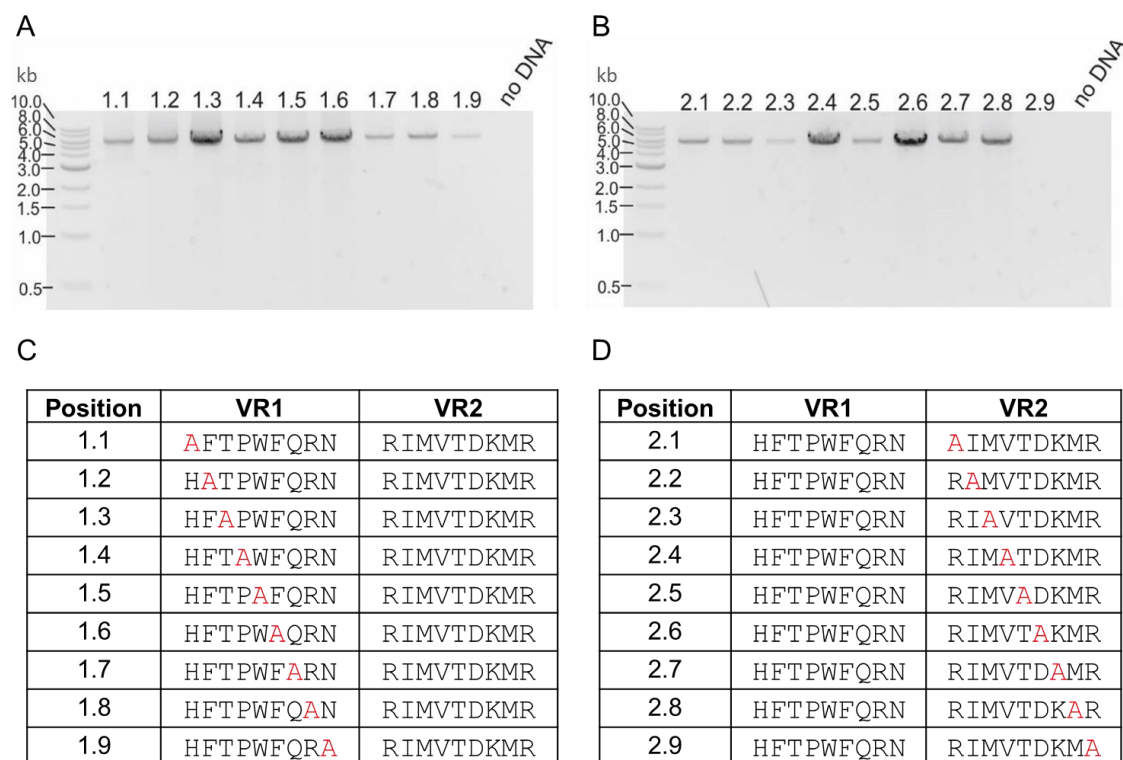
Figure 5.10 Alanine scanning mutagenesis of Affimer K6 variable regions. Thermal cycling with mutagenic primers was performed to mutate each residue of variable regions at a time to alanine and the products for A) variable region 1 mutant plasmids and B) variable region 2 mutant plasmids were analysed on 1% agarose gel. XL1-Blue cells were transformed with mutant plasmids, and mutagenesis was confirmed by sequencing. Variable regions' protein sequences of C) VR1 and D) VR2 mutants are shown with highlighted mutated residues.

The Affimer K6 alanine mutants were produced and purified as described in chapter 2.2.3.1. Coomassie staining indicated sufficient production and purification of Affimer K6 alanine mutants (Figure 5.11). Since the mutagenesis was performed in the Affimer's variable regions, which were previously shown to tolerate insertions into the loop regions, without affecting the structure of the scaffold (Tiede et al., 2014), the structural integrity of these alanine mutants was not assayed.

The ability of the alanine mutants to bind to the recombinant KRas-GST was assessed by ELISA, as described in chapter 2.2.7. Binding of the wild-type

Affimer K6 was used as a positive control. As visualised in Figure 5.12, W43A and F44A mutants had the most significant effect on binding to KRas-GST, with the substitution of phenylalanine resulting in 7 fold reduction in binding. This therefore, demonstrated that these two residues have the biggest contributions to binding. Mutations of residues P42, R46, T77 and M80 had moderate effect at affecting the binding to KRas-GST, suggesting that these could be involved in facilitating the binding to KRas.

To further define the functional epitope, the alanine mutants were tested in the nucleotide exchange with wild-type KRas. The initial reaction rates for each mutant at 10 µM are shown in Figure 5.13, in comparison to the reaction rate of K6 (dashed line). Potent inhibition of the nucleotide exchange is characterised by low initial rate, thus any increase in the reaction rate is indicative of impaired ability to inhibit the reaction. Mutations of residues F40 and Q45 in VR1 and R73 in VR2 significantly impaired ability to inhibit the nucleotide exchange reaction. However, the most profound effects were observed with P42A, W43A and F44A in VR1 and N47A in VR2 mutants, which almost completely abolished the inhibitory effect of Affimer K6. This demonstrated, that these residues are critical for effective inhibition of KRas.
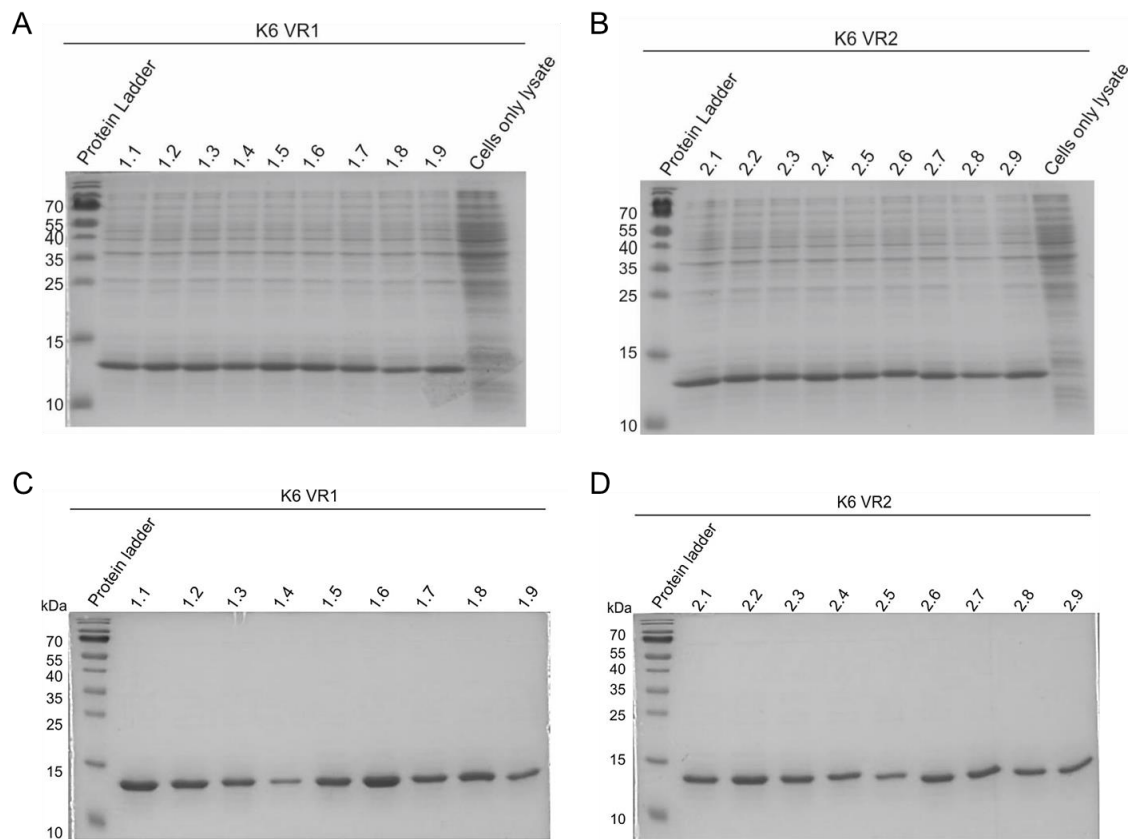
Figure 5.11 Production and purification of Affimer K6 Alanine mutants. Following IPTG-induced production in BL21 Star™ DE3 cells of A) K6 variable region 1 (VR1) alanine mutants and B) K6 variable region 2 (VR2) alanine mutants, whole cell lysates were analysed by Coomassie staining, which demonstrated efficient production of Affimers, as compared to whole cell lysate of non-transfected cells. Affimers were purified by His-tag affinity chromatography, and eluted C) K6 VR1 and D) K6 VR2 mutant proteins were analysed by Coomassie staining, which indicated 95% or more purity of the samples.
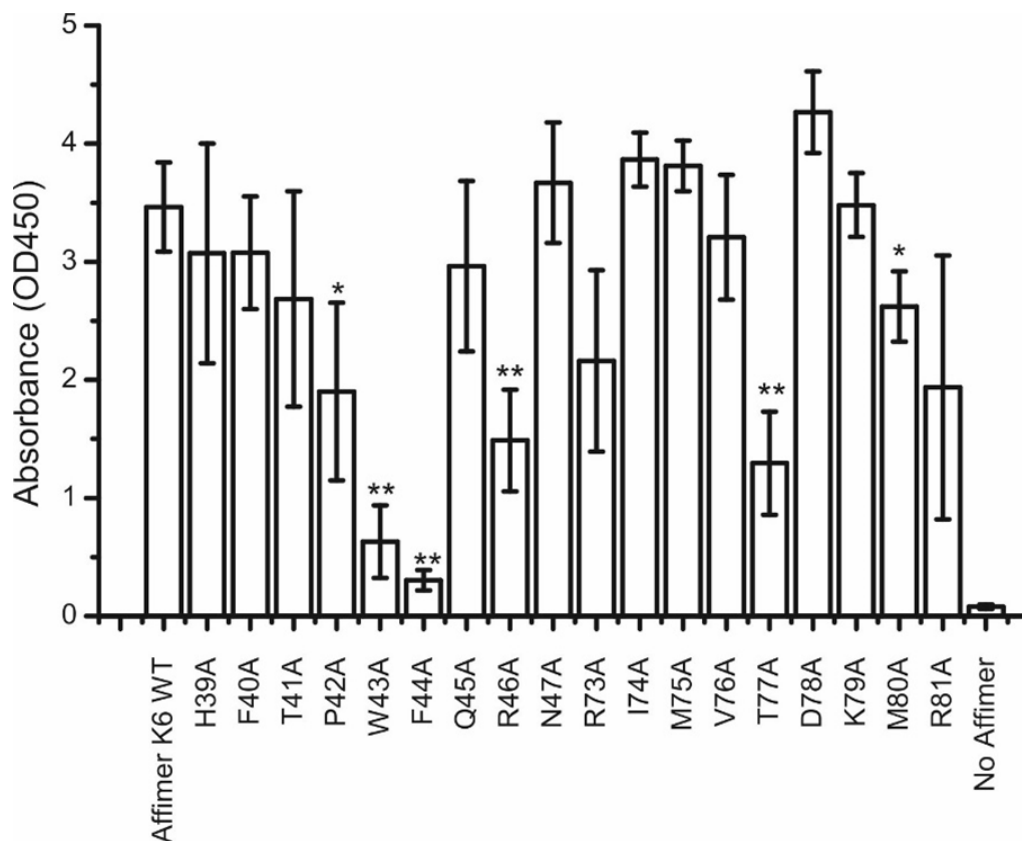
Figure 5.12 Effects of Affimer K6 variable regions alanine mutants on ability to bind to KRas. Enzyme-linked immunosorbent assay (ELISA) was used to test binding of K6 alanine mutants to KRas. GST-tagged wild-type KRas was immobilised on Nunc maxisorp strip plate modules and incubated with either wild-type Affimer K6, alanine mutants or PBS (no Affimer control). Bound Affimers were detected with HRP-conjugated anti-His tag antibody and detected with 3,3',5,5'-tetramethylbenzidine (TMB) substrate. Data is representative of three biological replicates (n=3). Error bars are ± SEM. $p < 0.05$ (*), $p < 0.01$ (**).
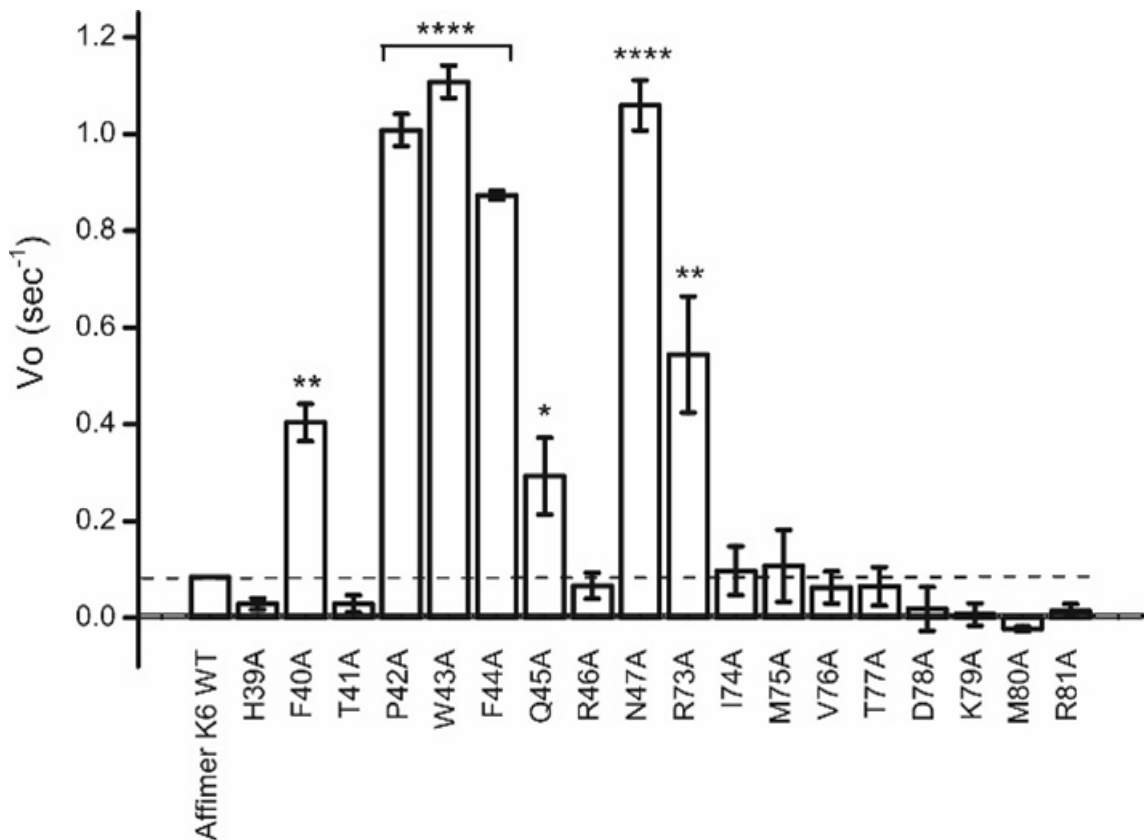
Figure 5.13 Effects of Affimer K6 variable regions alanine mutants on inhibition of nucleotide exchange. Affimer K6 wild-type and alanine mutants were assayed at 10µM in nucleotide exchange reaction with wild-type KRas-mGDP and the initial reaction rates for each protein were plotted. Dashed line indicated reaction rate of wild-type Affimer K6. Results are representative of three biological replicates (n=3). Error bars are ± SEM. $p < 0.05$ (*), $p < 0.01$ (**), $p < 0.0001$ (****).

To determine the structure-function relationship, the residues which mutations had significant effects on binding and inhibition of KRas, were mapped onto the K6-KRas co-crystal structure. The majority of the residues that were shown to be critical for binding and inhibition were involved in intramolecular interactions between the Affimer's variable regions (Figure 5.14). For instance, the F40 interacted via a hydrogen bond (H-bond) with N47 residue, which itself had a H-bond with R73 from variable region two. Mutations of these three residues had significant effect on inhibition of nucleotide exchange. Likewise, glutamine at position 45 interacted via H-bond with P42, F44 and R46 in VR1 and with M75 in

VR2, and the Q45A mutation significantly impaired inhibitory activity. The R46 was also H-bonded with I74 in VR2, however the R46A mutation only affected binding but not inhibition. Binding to KRas-GST was also significantly affected by mutations of the residues T77 and M80, however interactions between these residues and other residues within the Affimer or KRas residues were not observed in the co-crystal structure. This could be because these amino acids are within the variable region two, which was shown to be flexible (Figure 5.6), thus their interactions may not be visible in the structure, or they have a subtle role in stabilising/structuring VR1. Altogether, this data suggested that mutations of the mentioned residues could lead to destabilisation of VR1, resulting in less efficient binding and inhibition. Additionally, this data provided further evidence for the requirement of the variable region two for binding and inhibition, as residues from VR2, although not involved in the direct binding to KRas, are rather involved in the intramolecular interactions within the Affimer structure.

Mutations of the residues P42, W43 and F44 had the most profound effects on binding and inhibitory abilities. Proline residue affects the polypeptide's main chain conformation due to its restricted Phi dihedral angle (MacArthur and Thornton, 1991). Therefore, the effects of P42A mutation could be due to the conformational changes of the polypeptide's backbone. Conversely, the F44 is involved in direct binding to KRas, via a cation-π interaction with Q70 of KRas (Figure 5.15). Thus, substitution of this residue to alanine, disrupts this interaction and abolishes binding and inhibition. Likewise, W44 is also involved in direct interaction with KRas, mainly via the cation-π interaction with K5 from KRas. Other KRas residues surrounding this binding site include V7, L56, Y71 and G75 (Figure 5.16). Therefore, mutation of the tryptophan significantly impairs the binding and inhibitory abilities of the Affimer. Noteworthy, the interacting residues on KRas are identical in H- and NRas (Maurer et al., 2012), which therefore suggests that K6 is likely to be effective on all three isoforms, which is in agreement with the biochemical data (chapter 3). What is the most interesting, is that the W44 displayed binding to the small pocket on KRas, which has been previously targeted with small compounds, such as DCAI (Maurer et al., 2012), compound 13 (Sun et al., 2012) and Abd-7 (Quevedo et al., 2018) (Figure 5.17).

Therefore, highlighting the Affimer's ability to target druggable hot spots on Ras and potentially other proteins.
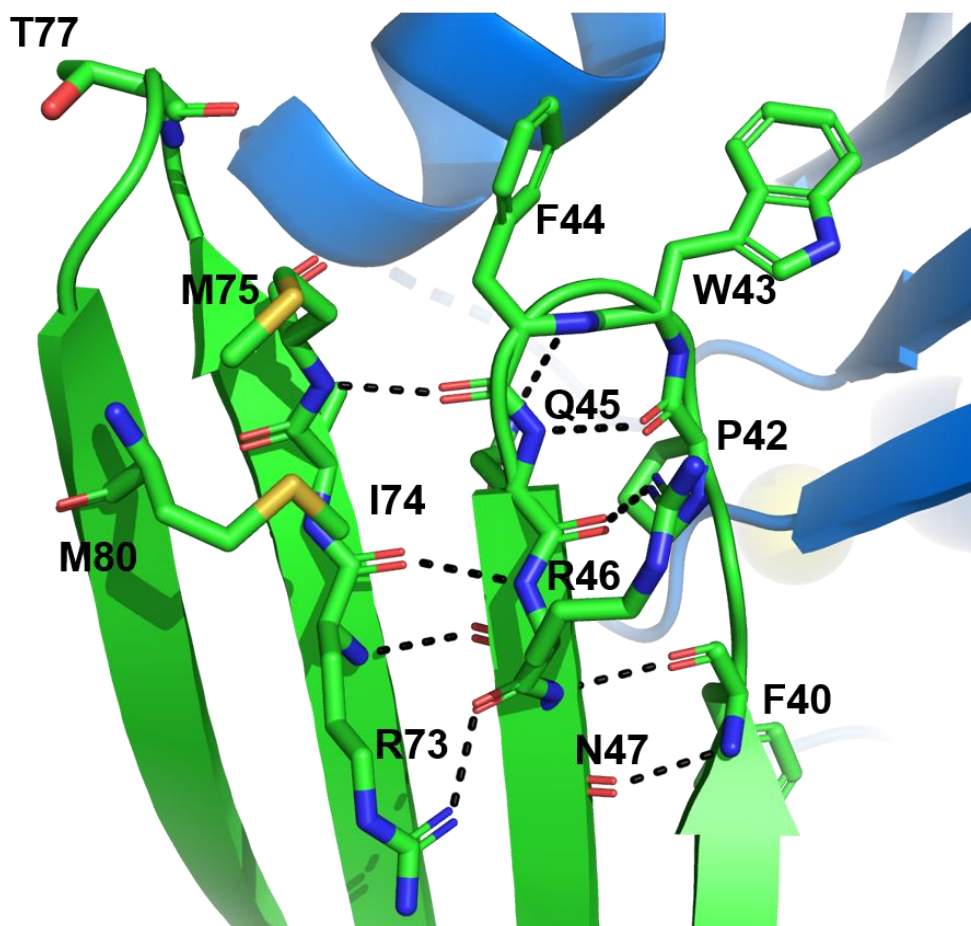
Figure 5.14 Intramolecular interactions in Affimer K6. Structure of Affimer K6, shown in green. The residues of the variable regions, which mutations had significant effect on binding and inhibitory activities are shown as sticks. KRas is shown in blue. H-bond interactions between variable regions' residues were generated in PyMOL and are shown as black dotted lines.
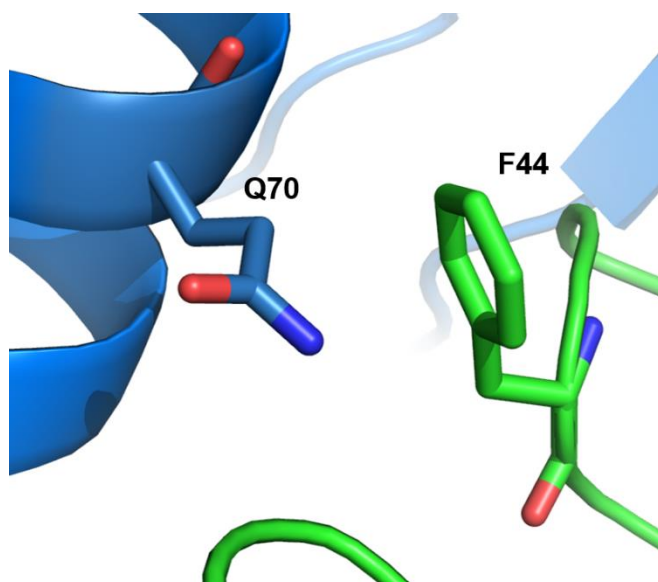
Figure 5.15 The cation- π interaction between Affimer's K6 F44 and Q70 of KRas.
Affimer is shown in green and KRas in blue, with the interacting residues shown as sticks.
Image was generated in PyMOL.
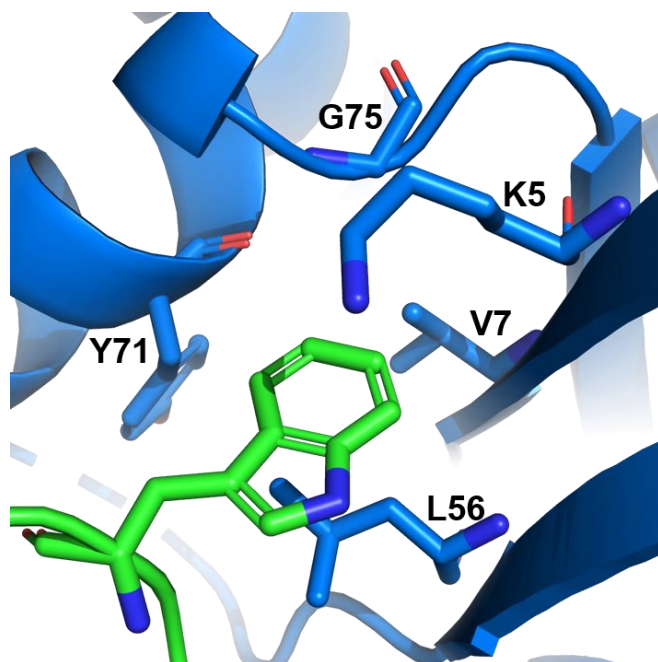
Figure 5.16 The direct interactions between Affimer's K6 W43 and KRas residues.
Affimer is shown in green and KRas in blue, with the interacting residues shown as sticks.
KRas residues are labelled. Image was generated in PyMOL.
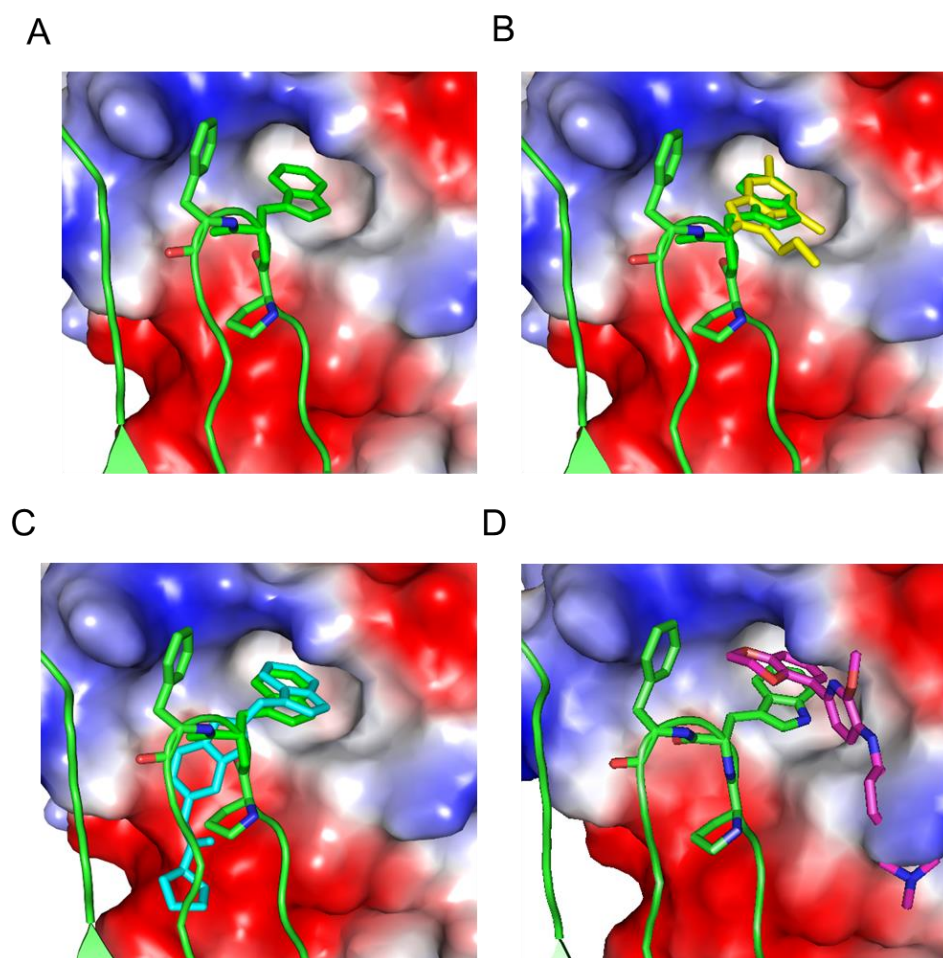
Figure 5.17 Affimer K6 binds to hydrophobic pocket on KRas, previously characterised with small molecules. A) Structure of KRas (shown as surface with electrostatic potential) and Affimer K6 (green) with residues P42, W43 and F44 shown as sticks. Structures of B) DCAI (PDB: 4DST), C) compound 13 (PDB: 4EPY) and D) Abd-7 (PDB: 6FA4) were superimposed onto KRas-Affimer K6 structure. Images were generated in PyMOL.

5.3 Discussion

Atomic structures of proteins or protein complexes deliver valuable information about how these macromolecules function and regulate biological processes (Popp et al., 2018). The most widely used technique for resolving protein structure is crystallisation (Shi, 2014). The most critical step in determination of the crystal structure is obtaining protein crystals. Since crystallisation is dependent on many factors such as protein concentration, temperature, pH, ionic strength and concentration of additives and precipitants, determination of the optimal condition for crystal growth is often a challenging task (Jancarik and Kim, 1991). Therefore, the first stage of crystallisation involves screening of a sparse matrix of conditions, covering a large chemical space, to define conditions which facilitate crystallisation of the sample (Luft et al., 2007). A total of 384 conditions (Jancarik and Kim, 1991, Lesley and Wilson, 2005) was used, which pinpointed conditions under which the Affimer-KRas complexes displayed the propensity to crystallise. The second stage of crystallisation involves optimisation of the initial conditions, to refine the components in order to improve crystal size and diffraction potential (Chayen and Saridakis, 2002). Optimisation of the crystallisation conditions for K6-KRas complex yielded crystals of sufficient quality to obtain diffraction data. Recently, optimisation of the K3-KRas crystal trials have been performed by Ajinkya Rao from the Tomlinson group and the K3-KRas X-ray co-crystal structure has been solved to 2 Å. In contrast, the optimisation of K37-KRas crystal trials have not generated any protein crystals. Therefore, future work should involve further optimisation trials, to achieve crystal growth of that complex. Alternatively, NMR can be employed to determine the Affimer-KRas structures, although this technique is considered to be more labour-intensive than crystallography (Zlomislic et al., 2011).

Structure determination of protein inhibitors allows depiction of the mode of action. For example, crystal structures of Ras-bound intrabody iDab6 and DARPins K27 and K55, demonstrated binding to the switch I and II regions on Ras, which facilitate the binding with GEFs and effectors, therefore providing evidence that these binders act as competitive inhibitors (Tanaka et al., 2007, Guillard et al., 2017). In contrast, the X-ray crystal structure of HRas-bound monobody NS1, suggests an allosteric mode of inhibition by binding to a distal

site to the switch regions, thus describing a previously unrecognised site for inhibiting Ras function (Spencer-Smith et al., 2017a). The Affimer K6-KRas co-crystal structure (Figure 5.3) revealed binding between the KRas switch regions, establishing that K6 functions as a competitive inhibitor, similarly to DARPins K27 and K55 and intrabody iDab6 (Guillard et al., 2017, Tanaka et al., 2007). The structural data also correlates with the results obtained from biochemical assays. For example, DARPin K27 displayed preferential binding to KRas-GDP in biochemical assay, and its inability to bind to the active GTP-bound KRas has been explained by the steric clash between DARPin's phenylalanine residue with the main chain of switch I in the active Ras (Guillard et al., 2017). In contrast, similarly to the recently reported anti-KRas miniprotein 225-11 (McGee et al., 2018), Affimer K6 did not display nucleotide-state selectivity, as demonstrated in chapter 3. The structural data provided an explanation for this, as no significant steric clashes were seen when the K6-KRas co-crystal structure was superimposed with that of the GTP-bound KRas (Figure 5.4). This could have been because, the GTP-bound KRas conformation can exist in two conformations; state 1 in which the switch I displays an open and dynamic conformation and state 2 in which the switch I region is stabilised in the closed conformation (Spoerner et al., 2010). The switch I from the K6-KRas co-crystal structure was in similar conformation to the state 1 conformation of the GTP-bound KRas (PDB:1IAQ) (Spoerner et al., 2001). This therefore indicated that the GTP-bound KRas in state 1 could accommodate Affimer K6 binding. However, it has been recently noted that the state 1 of switch I is significantly higher populated in wild-type KRas, whilst the switch I in the G12D mutant is stabilised in the state 2 (Kauke et al., 2017). Therefore, it would be interesting to study the structure of K6 bound to KRas G12D, to determine if the mutant KRas in the GTP-bound conformation could also accommodate K6 binding. Nevertheless, the Affimer K6 could be used as a valuable tool to study the effects of simultaneous inhibition of the active and inactive wild-type KRas conformations.

In contrast, comparison of the K6-KRas structure to that of Ras-Raf (Figure 5.5), indicated a steric clash between the Affimer and Raf. In the DARPin K55-KRas co-crystal structure, the overlap between K55 and Raf binding sites on KRas provided structural evidence for inhibition of Ras-Raf interaction observed in the

biochemical assays (Guillard et al., 2017). Here however, the inhibition of Raf binding to Ras by K6 was not observed (chapter 3.2.4). This could be because the binding affinity of K6 towards KRas could be lower than that of the Ras-Raf(RBD) (160nM) (Sydor et al., 1998), thus the Affimer could be inefficient at competing with Raf for binding. However, biophysical characterisation of the K6 binding affinity would be necessary to provide evidence for this.

Perhaps the most interesting finding from the investigation of the K6-KRas structure was the discovery of very small functional epitope involved in the direct binding to KRas. This was in agreement with the small interaction interface estimated for the K6-KRas complex (chapter 5.2.3). What is even more interesting, is that the residues of K6 that were shown to be critical for binding and inhibition, bound to the pocket on KRas, which has been previously targeted with small molecule inhibitors (Figure 5.17) (Maurer et al., 2012, Sun et al., 2012, Quevedo et al., 2018). This therefore, indicated that Affimers could be useful tools in the identification of druggable sites on proteins. In addition, the small functional epitope, consisting of three residues, demonstrated a great advantage of Affimers over other Ras-targeting scaffolds, as the Affimer's three residues could be potentially mimicked with compounds to develop Affimer-mimicking small molecule inhibitors. This is not achievable with other scaffolds, such as the intrabodies (Tanaka et al., 2007) or DARPins (Guillard et al., 2017), as these display large interaction surfaces (Figure 5.18). Although, the iDab6 intrabody has been recently used in a competition screen of small molecule library, to isolate so-called antibody-derived compounds - compounds that bound to the same epitope as the intrabody. This therefore bridged the properties of scaffold proteins and small molecules, in the hope of the development of novel anti-Ras inhibitors (Quevedo et al., 2018).

In conclusion, structural studies, combined with biochemical assays provided detailed insights into the mode of action of Affimer K6. Importantly, elucidation of the functional epitope of K6 established a potential new opportunity to exploit the Affimer for the development of new small molecule inhibitors of Ras.

A   **B**

HRas (G12V) – Intrabody iDab6   **KRas – DARPin K27**

Figure 5.18 Ras binding scaffold proteins and their interaction interfaces.
Structures of A) HRas and Intrabody iDab6 complex (PDB: 2UZI) and B) KRas and
DARPin K27 complex (PDB: 5O2S). Ras is shown in blue with switch I and switch II
regions in yellow and orange, respectively. Images were generated in PyMOL.

Chapter 6

Effects of Affimer-derived compounds on Ras activity

Chapter 6

Effects of Affimer-derived compounds on Ras activity

6.1 Introduction

Drug discovery relies on the ability to identify small molecules that interact with the target protein (Chessari and Woodhead, 2009). Despite well-established compound screening strategies to identify hit molecules, such as high throughput screening (HTS), fragment-based, structure-based, virtual or NMR screening (Hughes et al., 2011) (Table 6.1), the number of new drugs approved by FDA is decreasing (Khanna, 2012). This can be attributed to the fact that only around 10% of the human proteome is described as druggable (Hopkins and Groom, 2002). Historically, Ras has been considered as an undruggable protein, because apart from the nucleotide binding pocket, it does not possess any obvious cavities suitable for targeting with small molecules (Cox et al., 2014). Nevertheless, a number of compounds directly targeting Ras have been reported. For example, a SCH-53239 compound, originally designed to compete with GDP, was shown to bind to a novel pocket between switch II and α-helix 3 (Taveras et al., 1997). Fragment-based screens identified small molecules DCAI (Maurer et al., 2012) and 13 (Sun et al., 2012), which bound to previously unidentified pocket between the α-helix 2 and β-strand 3 located between the switch regions. Another pocket, termed the switch II pocket, has been identified with covalent inhibitors of KRas G12C mutant (Gentile et al., 2017). A number of other compounds inhibiting Ras activity were also reported, however, the structural basis of Ras inhibition with these compounds remain elusive (Waldmann et al., 2004, Kato-Stankiewicz et al., 2002). While several of Ras-targeting compounds demonstrated promising preclinical results, none of them have been approved as anti-cancer therapeutics, and only recently the MRTX849 small molecule covalent inhibitor of KRas G12C has entered phase I/II clinical trials (MiratiTherapeutics, 2018).

During the development of protein inhibitors as potential therapeutics, it is important to remember that proteins in their native environment, within the cell,

do not function in isolation, but are rather involved in multi-protein signalling cascades (De Las Rivas and Fontanillo, 2010). These are mediated by protein-protein interactions, which are usually intractable to small molecules, due to large interaction surfaces between two proteins (Cheng et al., 2007, Giordanetto et al., 2014, Chessari and Woodhead, 2009, Nero et al., 2014). This led to the development of macrodrugs, such as peptides (Fosgerau and Hoffmann, 2015), intracellular antibodies (Perez-Martinez et al., 2010) and non-immunoglobulin scaffold proteins (Martin et al., 2018), and these biologics have become the fastest growing class of therapeutics (Aggarwal, 2010). However, while the majority of these biotherapeutics have been effective against extracellular targets, the main limitation is their delivery into cells, thus leaving the intracellular targets out of their reach (Tsomaia, 2015). Moreover, it is unlikely that these will be converted into small molecules, due to large interaction surfaces. Therefore, there is a growing need to develop innovative strategies for novel drug design and discovery. Recently, nanobodies, which are based on single-domain antibody fragments (Bannas et al., 2017), were used to stabilise the functional conformations of G-protein coupled receptors (GPCRs) in order to reveal structural features, that then can be exploited for fragment-based screens and structure-based drug design (Manglik et al., 2017). Antibody fragment has also been used in the development of small molecule inhibitors of Ras, however in a different concept. Quevedo and colleagues used anti-mutant Ras intracellular antibody as a competitor in a small molecule screen to identify compounds that bind to Ras at the same position. Following structure-based optimisation, they identified potent Ras inhibitors that inhibited Ras-effector interactions and Ras-mediated signalling in mammalian cells (Quevedo et al., 2018).

A potential new and previously unexploited strategy for the development of small molecule inhibitors, consists of mimicking the residues of scaffold proteins with compounds. As mentioned above, this is not achievable with most of the scaffold proteins, especially those targeting Ras, as they usually display large interaction interfaces, intractable to small molecules. In contrast, KRas-targeting Affimer K6 has been shown to exploit a smaller binding interface. In addition, elucidation of the functional epitope of K6 revealed binding of K6 residues into the hydrophobic pocket, that has been previously targeted with small molecules (chapter 5). This

led to the hypothesis of whether the Affimer K6 residues could be mimicked with small molecules. Shape-based virtual screening has been employed to select compounds resembling the conformation of the K6 tripeptide (P42-W43-F44) that has been shown to be crucial for binding and inhibitory activity. The selected compounds were then tested in a nucleotide exchange assay to isolate hits with inhibitory activities. Compounds that were effective at inhibiting Sos-mediated KRas activation, were further tested in cell-based assays and their effects on Ras-mediated signalling and cell viability were investigated (Figure 6.1).

Screen	Description
High throughput screen	Screening of a large compound library against the drug target in a suitable assay
Knowledge-based screen	Selecting a subset of molecules from the chemical library, which are likely to have activity at the drug target
Fragment screen	Screening of a small molecular weight compounds against the drug target, which can then be used as a building blocks for larger molecules
Structure-based screen	Use of crystal structures to aid design of molecules
Virtual screen	Screening of the virtual compound library against the crystal structure of the drug target
Physiological screen	Screening of smaller number of compounds againt a tissue sample
NMR screen	Screening of a fragment library against a drug target in NMR spectroscopy

Table 6.1 Summary of the screening strategies employed within pharmaceutical industry and academia to identify hit molecules.
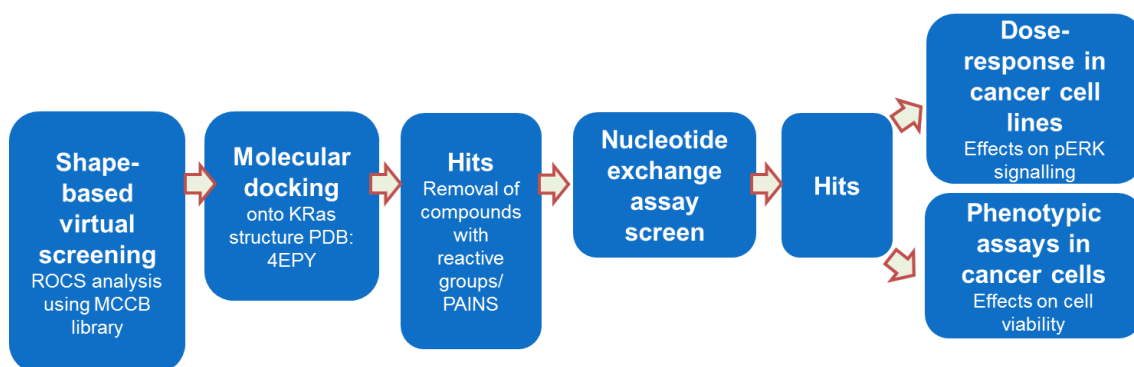
Figure 6.1 Overview of the strategy to identify and test Affimer-derived compounds. The MCCB library of compounds have been screened using the ROCS software to identify molecules similar in shape to the Affimer K6 tripeptide. The identified compounds were then docked onto the KRas structure to predict binding characteristics and narrow down the number of compounds. Selected compounds were screened in nucleotide exchange assay to identify inhibitors. These hits were then further characterised in cellular assays.

6.2 Results

6.2.1 Shape-based virtual screening to isolate Affimer-mimicking compounds

The Affimer K6 tripeptide (P42-W43-F44) has been extracted from the K6-KRas co-crystal structure and the rapid overlay of chemical structure (ROCS) analysis was performed using the small molecule library from the Medical Chemistry and Chemical Biology (MCCB) technology group at University of Leeds, containing 50 000 compounds. The number of generated compounds was limited to 1000, as anything beyond that would likely have a poor structural similarity to the tripeptide. To rank these, the generated compounds were docked onto the previously published KRas crystal structure (PDB: 4EPY). Firstly however, the docking parameters had to be established. This was done by re-docking of the compound 13 (Sun et al., 2012) onto the KRas structure. Re-docking of this compound have been utilised, due to the overlap between compound 13 and Affimer K6 binding site on KRas. A number of different docking parameters have

been tested (data not shown). The quality of reproduction of compound 13 crystallographic binding pose has been measured by root mean square deviation of atomic position (RMSD) analysis. The best docking parameters gave RMSD value of 0.31Å, which was below the preselected threshold of 2 Å (Hevener et al., 2009), confirming that optimal docking parameters have been achieved. These parameters were used for subsequent docking of ROCS results onto the KRas structure. Noteworthy, an attempt was made to use the K6-KRas co-crystal structure for the predictive docking model. However, when the tripeptide was re-docked into the binding site, the pose prediction was poor. This was likely a result of the lack of waters of crystallisation in the protein structure.

The top 400 compounds obtained from ROCS analysis were docked onto the KRas structure. A maximum of 5 poses per ligand were generated during docking. The docking results were then filtered to suggest the best 224 compounds. Pan-assay interference compounds (PAINS) are compounds with defined structures that often lead to false positive results. Therefore, PAINS compounds were removed from the selected list. Likewise, as these compounds have the potential to be developed into therapeutics, any functional groups which would hydrolyse/oxidise in the body (esters/thiols) have been also removed. As a result, 190 compounds were selected for testing in biochemical assay. The virtual screening, docking and filtering of selected compounds was performed by Holly Foster, University of Leeds.

6.2.2 Nucleotide exchange assay to identify Affimer-derived compounds with inhibitory activities

To test if the Affimer-derived compounds possess inhibitory activities, they were tested in a nucleotide exchange assay, as described in chapter 2.2.5. In the initial attempt the compounds were tested at 100μM. The majority of the assayed compounds demonstrated inhibition of nucleotide exchange (data not shown). While conducting the assay at high compound concentration established, that most of the Affimer-derived compounds indeed possess the inhibitory ability, it did not narrow down the number of compounds for further characterisation. Therefore, the assay was repeated at 10-fold lower compound concentration (10μM, data not shown). However, hardly any inhibition was observed. This therefore, indicated that the Affimer-derived compounds are not as potent

inhibitors in comparison to the Affimer K6, which demonstrated the highest inhibition at 10µM. Although, this was expected, as small molecules are often less potent than macrodrugs (Lau and Dunn, 2018). It was then decided, to test the compounds at 30µM, and the initial reaction rate for each compound is shown in Figure 6.2. Notably, 10 compounds displayed auto-fluorescence, and therefore their inhibitory activity could not be determined in this assay. Inhibition of the nucleotide exchange is demonstrated by a low initial rate, therefore a lower reaction rate means a better inhibitor. Dimethyl sulfoxide (DMSO), in which the compounds are dissolved, at the final concentration of 0.3%, was used as negative control and did not show any effect on inhibiting the reaction. Conversely, Affimer K6 at 10µM final concentration was used as a positive control. Noteworthy, a previously reported KRas inhibitor, DCAI (Sigma Aldrich), which bound to the same pocket on KRas has also been tested, to directly compare the effects of Affimer-derived compounds. While the majority of the compounds demonstrated some level of inhibition, only 10 compounds blocked the reaction by 50%. This helped to narrow down the number of compounds to be tested in cell-based assays. Importantly, these compounds displayed significantly better inhibition of the reaction, when compared to DCAI. Thus establishing, that Affimer-derived compounds are more potent inhibitors than this previously published compound.
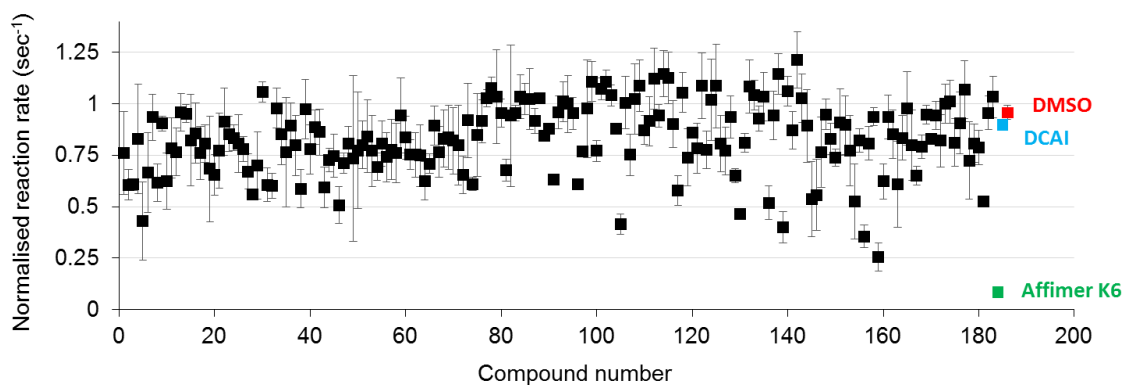
Figure 6.2 Nucleotide exchange assay screen of Affimer-derived compounds.
Hundred and ninety compounds were screened at 30µM in nucleotide exchange assay
with wild-type KRas-mGDP and the reaction rates for each compounds were plotted
(black squares). DMSO was used as negative control (red). Also shown is the reaction
rate at 30µM for known Ras inhibitor DCAI (blue). Reaction rate for Affimer K6 (at 10µM)
is shown in green. Results are representative of two biological replicates. Data
represents mean ± SD.

6.2.3 Effects of Affimer-derived compounds on Ras-mediated signalling in HEK293 and Panc 10.05 cells

The 10 most potent Affimer-derived compounds from the nucleotide exchange
screen were tested in HEK293 cells. In addition, human pancreatic
adenocarcinoma cell line (Panc 10.05), harbouring KRas G12D mutation was
assayed, to investigate the effects of Affimer-derived compounds on mutant
forms of Ras. The compounds were hypothesised to mimic the effects that the
Affimer K6 had on downstream signalling. Therefore, similarly as described in
chapter 4, the levels of ERK phosphorylation were observed, as a measure of
disruption of the Ras-mediated MAPK pathway. The cells were treated with 60µM
compounds, and cell lysates were subjected to western blotting analysis to detect
levels of pERK and tubulin as a control. DMSO at final concentration of 0.6 %
was used as a negative control. Large variability in the effects of compounds on
pERK signalling in HEK293 cells were observed between the two biological
repeats (Figure 6.3 B). This therefore, prohibited to determine the effects of
Affimer-derived compounds on Ras-mediated signalling in HEK293 cells

expressing wt Ras. In contrast, 6 out of the 10 compounds tested, repeatedly reduced pERK levels in Panc 10.05 cells, with compound 7 displaying the most profound effect (Figure 6.3 C and D). Altogether, these results could suggest that the Affimer-derived compounds could show some cell line or Ras mutation specific effects. However, this would need to be further investigated.

A

HEK 293

B

C

Panc 10.05

D
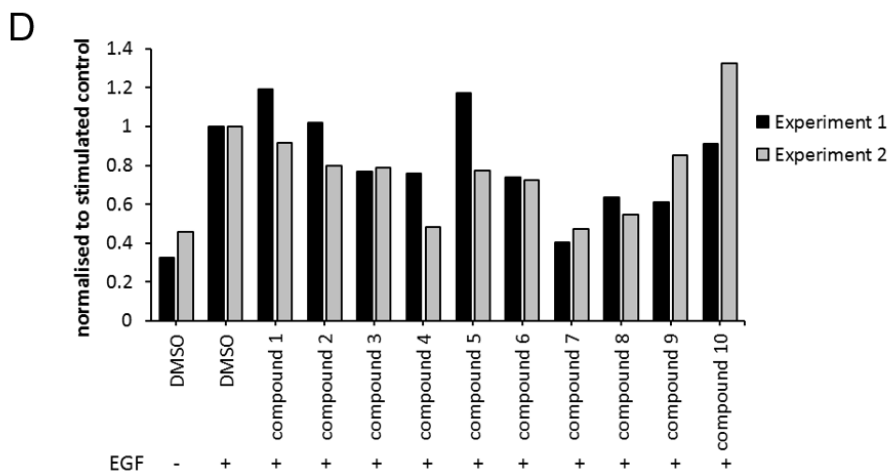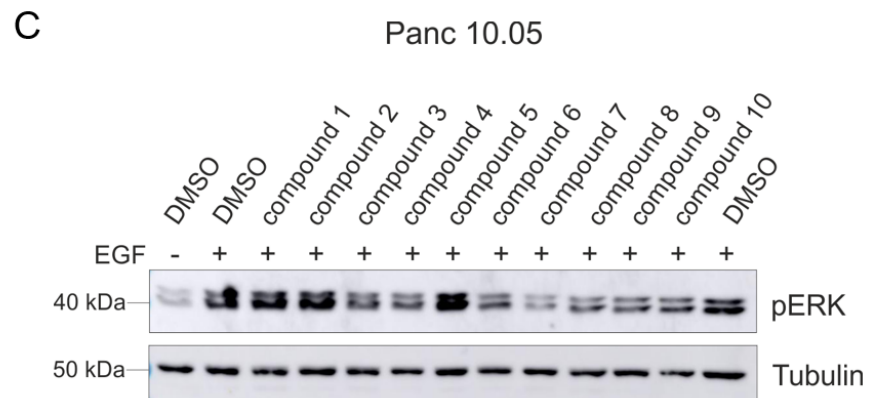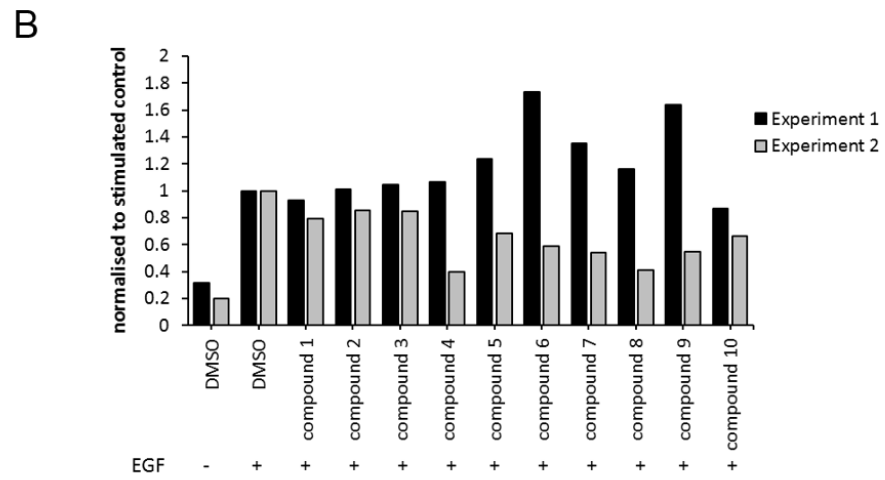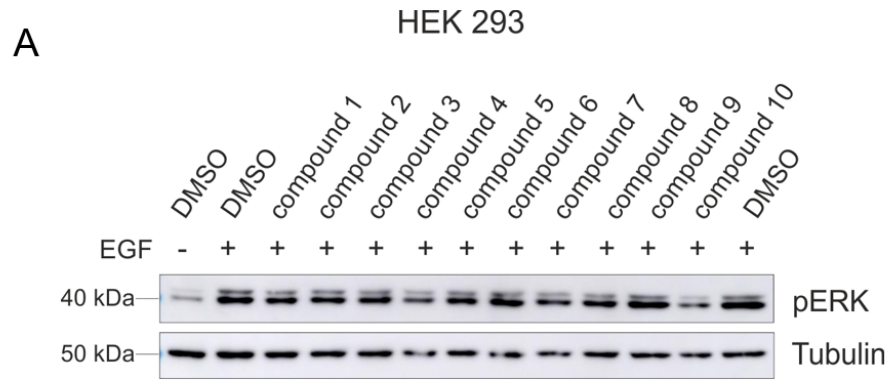
Figure 6.3 Effects of Affimer-derived compounds on EGF-induced ERK phosphorylation in HEK293 and Panc 10.05 cells. HEK293 cells expressing wild-type KRas and Panc 10.05 cells expressing G12D KRas were treated with 60µM of 10 Affimer-derived compounds or 0.6% DMSO for 3h in serum free media. Cell signalling was stimulated with 25 ng/ml EGF for 5min. Lysates of A) HEK293 cells and C) Panc 10.05 cells were analysed by western blotting analysis with phospho-ERK specific antibody. Tubulin was used as loading control. Results are representative of two biological replicates. Data in B) and D) corresponds to quantification of data shown in A) and C), respectively, from two biological replicates (n=2).

To further study the effects of Affimer-derived compounds, which impaired Ras-mediated signalling at 60 µM in Panc 10.05 cells, the cells were treated, as above, with lower compounds concentrations (60, 30, 10 and 1 µM). DMSO at final concentration of 0.6 % was used as a negative control, and the concentration of DMSO in each sample was corrected to be 0.6 %. Compounds 3, 4, 6, 8, and 9 displayed inhibition of pERK only at the highest compound concentration (60 µM, Figure 6.4). Conversely, compound 7 demonstrated dose-dependent impairment of Ras-mediated signalling, with reduced pERK levels even at 10 µM (Figure 6.4). This therefore, established compound 7 as the most cell-potent Affimer-derived compound.
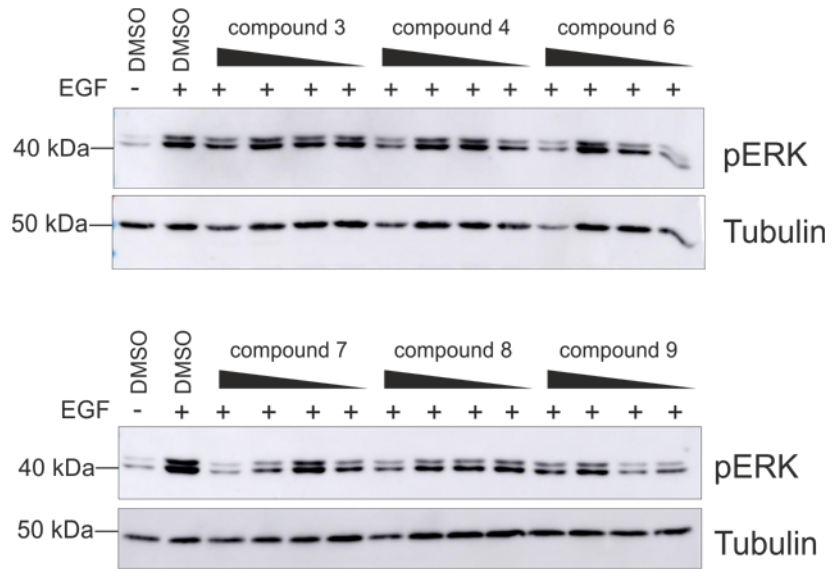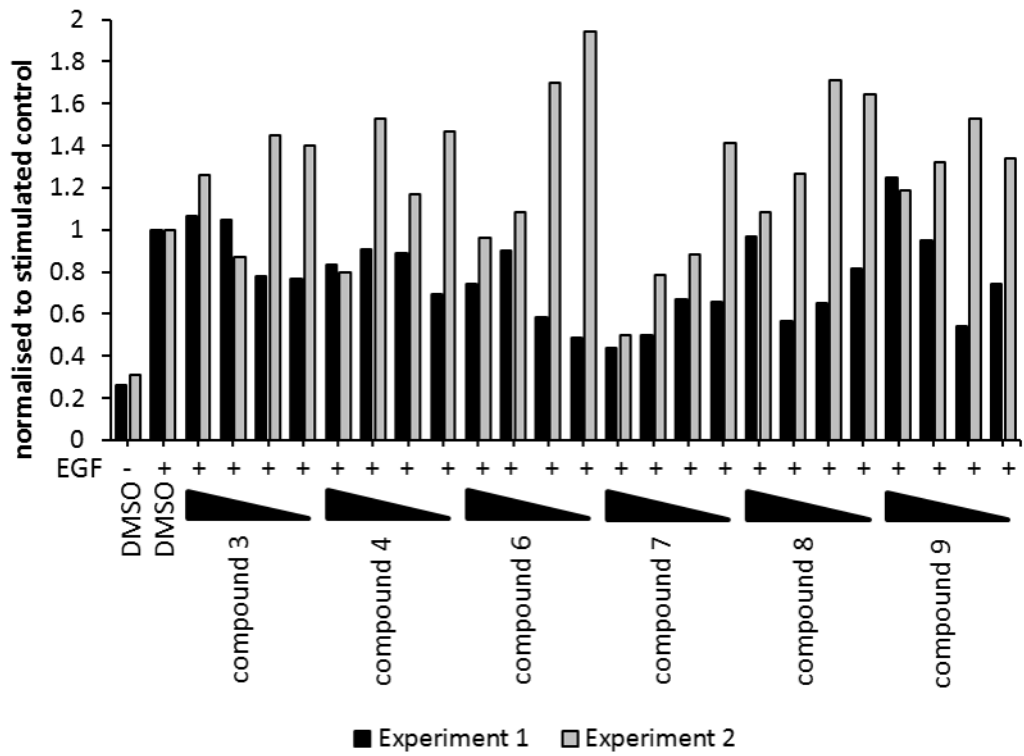
Figure 6.4 Dose-response effects of Affimer-derived compounds on EGF-induced ERK phosphorylation in Panc 10.05 cells. Panc 10.05 cells were treated with 6 Affimer-derived compounds in a concentration range of 1-60 µM or 0.6 % DMSO for 3h in serum free media. Cell signalling was stimulated with 25 ng/ml EGF for 5min. A) Lysates were analysed by western blotting analysis with phospho-ERK specific antibody. Tubulin was used as loading control. Data in B) corresponds to quantification of data shown in A) from two biological replicates (n=2).

6.2.4 Effects on cell viability of Affimer-derived compounds

The effects of 6 Affimer-derived compounds on cell viability of mammalian cells, expressing either wild-type KRas (HEK293) or KRas mutants G12D (Panc 10.05), G13D (DLD-1, human colorectal adenocarcinoma) and G12V (SW620, human colorectal adenocarcinoma), were investigated. The CellTitre-Glo® (Promega) luminescent assay was used, as described in chapter 2.2.16, which measures the number of metabolically active cells, by quantifying the amount of ATP present in a sample (Crouch et al., 1993). Firstly, cell titration was conducted to determine the optimal seeding density to obtain signal within the linear range of the assay. The range of 2500 - 40 000 cells per well were seeded in 96-well plate and incubated for 72h. The cell viability was then measured. Seeding density of 20 000 cells/well has been chosen, as at this plating density, the measured luminescence was within the linear range of the assay after incubation for 72 h (Figure 6.5).
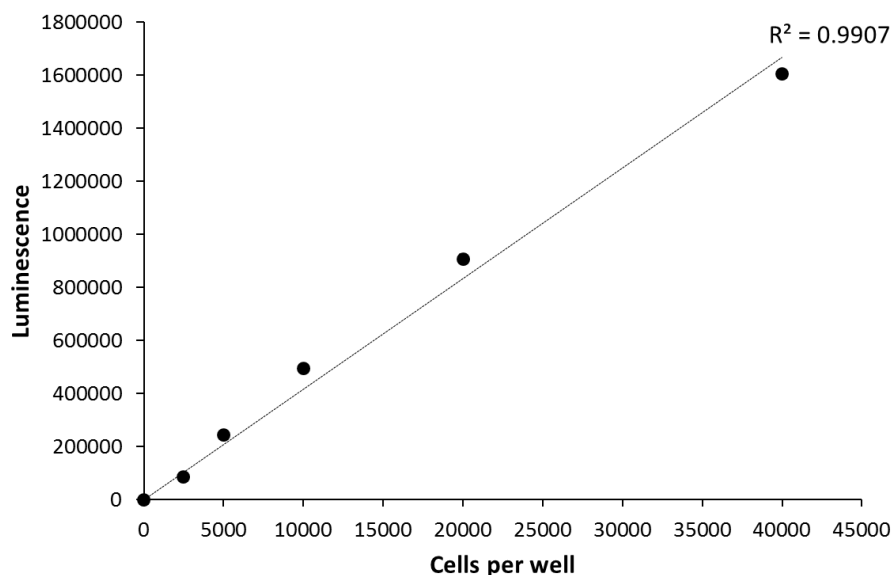
Figure 6.5 Cell number directly correlates with the luminescence signal detected.
The range of 2500 - 40 000 cells per well were seeded in 96-well plate and incubated for
72 h. The CellTitre-Glo reagent was added and the luminescence was measured using
Tecan Spark plate reader. Background luminescence (from DMEM +10% FBS media
only samples) was subtracted from all samples. Values represent mean ± SEM of three
replicates of each cell number. Linear relationship (r^2=0.99) was observed between the
luminescent signal and cell seeding density.

To establish whether inhibition of Ras-mediated signalling would result in reduced
cell viability, the cells were treated with known MEK inhibitor (U0126) (Favata et
al., 1998) for 72 hours and its effects on cell viability were measured. Significant
reduction in viability of all cell lines was observed (Figure 6.6), although less
profound effects of U0126 in HEK293 cells were seen in comparison to the KRas
mutant cell lines. Nevertheless, this confirmed that inhibition of Ras-mediated
signalling, by blocking of MAPK signalling pathway, does indeed affect cell
viability. Therefore, it was hypothesised that inhibition of Ras with the Affimer-
derived compounds could result in reduction in cell viability.
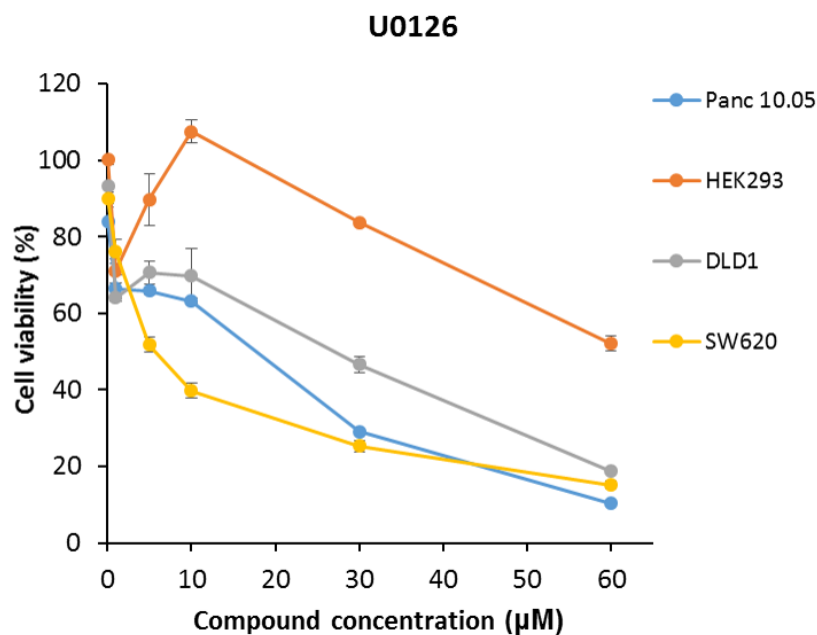
U0126

Figure 6.6 Effects of MEK inhibitor U0126 on cell viability of HEK293, Panc 10.05, DLD-1 and SW620 cells. 20 000 cells were seeded per well of 96 well plate. Following 24 h incubation, cells were treated with increasing concentrations (0.1-60µM) of U0126 or 0.6% DMSO (in growth media) for 72 h and cell viability was then measured. Luminescence from media only was subtracted from all samples, and the luminescence values were normalised to that of DMSO. Data corresponds to mean ± SEM and is representative of two biological replicates.

HEK293, Panc 10.05, SW620 and DLD-1 cells were seeded in 96 well plate and incubated for 24 hr. Cell were then treated with increasing concentrations (1-60µM) of compounds or 0.6% DMSO (in growth media) for 72h and cell viability was measured. Luminescence from media only was subtracted from all samples, and the luminescence values were normalised to that of DMSO. Interestingly, all Affimer-derived compounds reduced cell viability in HEK293 cells (Figure 6.7A). This is in conflict with the data from pERK signalling assays, chapter 6.2.3, as these compounds had no effects on ERK phosphorylation levels. The results seen here however, could be due to prolonged incubation (72 h) in comparison to short treatment (3 h) of the cells with the compounds in the signalling assays. The biggest reduction in cell viability in all cell lines was observed with compound

7, which even at 30 µM reduced the number of viable cells by 97% (Figure 6.7). This therefore, demonstrated compound 7 as the most potent inhibitor, which is in agreement with data from the pERK signalling assays in Panc 10.05 cells. In contrast, compound 6 displayed the least reduction of HEK293, Panc 10.05, SW620 and DLD-1 cell viability, which could be explained by its poor ability at reducing pERK levels in the signalling assays. Therefore, concluding that compound 6 is the least potent Affimer-derived compound. Compounds 3, 4 and 8 demonstrated similar moderate effects on cell viability in tested cell lines and reduction of cell viability in range between 60-80% was observed at the highest compound concentration (Figure 6.7). However, as weak inhibition of ERK phosphorylation was observed with these compounds, especially at lower concentrations, thus some of the effect on cell viability could be due to off-target or cytotoxic effects. Interestingly, effects of compound 9 on cell viability were more profound in KRas-dependent cells lines Panc 10.05 and SW620, in comparison to the KRas-independent DLD-1 cells (Singh et al., 2012). As Panc 10.05 and SW620 cells carry G12 mutants, in comparison to G13D mutation in DLD-1 cell line, these results could potentially indicate mutant specificity of compound 9. Although further investigation would be necessary to confirm this.

A **HEK293**

B **Panc 10.05**

C **SW620**

D **DLD-1**
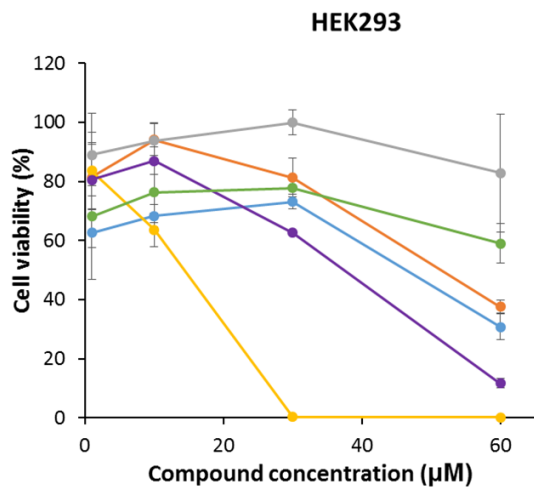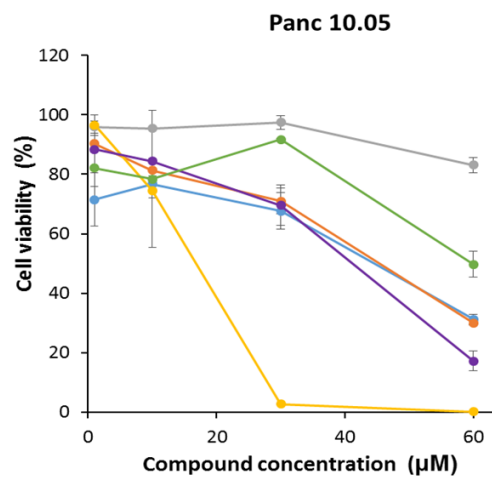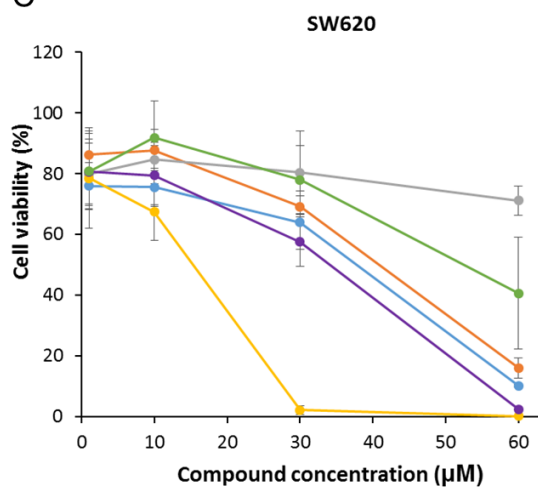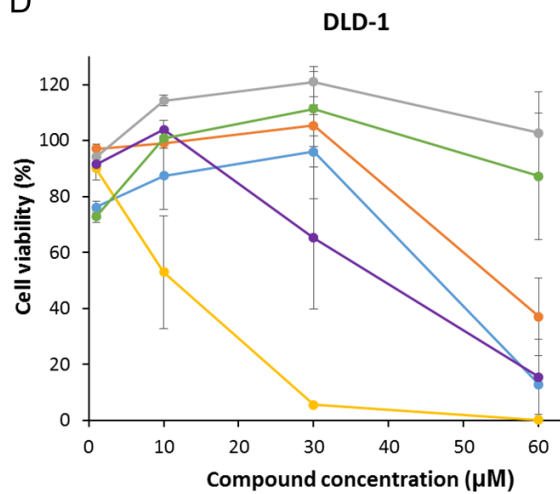
compound 3
compound 4
compound 6
compound 7
compound 8
compound 9

Figure 6.7 Effects of Affimer-derived compounds on cell viability of HEK293, Panc 10.05, DLD-1 and SW620 cells. 20 000 cells were seeded per well of 96 well plate. Following 24h incubation, cells were treated with increasing concentrations (1-60µM) of compounds or 0.6% DMSO (in growth media) for 72h and cell viability was then measured. Luminescence from media only was subtracted from all samples, and the luminescence values were normalised to that of DMSO. Affimer-derived compound displayed differential abilities to effect A) HEK293, B) Panc 10.05, C) SW620 and D) DLD-1 cell viability. Data corresponds to mean ± SEM and is representative of two biological replicates.

6.3 Discussion

Virtual screening (VS) is a powerful technique frequently used in drug discovery, as it reduces the time and costs associated with experimental high-throughput screening (Hawkins et al., 2007). Similarity searching is one of the simplest and easiest method of VS to identify molecules resembling the reference structure, which are the most likely to exhibit biological activity of interest (Lavecchia and Di Giovanni, 2013). Here, the rapid overlay of chemical structures (ROCS) analysis has been used to identify molecules mimicking the three residues of Affimer K6 (P42-W43-F44), which were shown to be critical for binding and inhibitory activity. The identified compounds were tested in the nucleotide exchange assay, to determine whether these demonstrate inhibitory activities comparable to K6. Indeed, most of the Affimer-derived compounds blocked Sos-mediated KRas activation, although with varied potencies (Figure 6.2). While the majority of the compounds inhibited the reaction by 25% at 30 µM, 10 compounds have shown more potent inhibition, with reduction of the reaction rate at least by 50%. Importantly, these compounds displayed significantly better inhibition when compared to the small molecule inhibitor targeting the same pocket on Ras, DCAI, which blocks nucleotide exchange with IC_{50} of 155 ± 36 µM (Maurer et al., 2012). The binding site utilised by Affimer K6 and previously reported compounds DCAI (Maurer et al., 2012), compound 13 (Sun et al., 2012), Abd-7 (Quevedo et al., 2018) and Ch-3 (Cruz-Migoni et al., 2019) is conserved between Ras isoforms and mutants, thus indicating that the Affimer-derived compounds are likely to be effective against KRas mutants and H- and NRas isoforms. However,

investigation of Affimer-derived compounds with those proteins in the nucleotide exchange assays is necessary to confirm this. Notably, 10 of the 190 compounds tested, displayed auto-fluorescence, and therefore their inhibitory activity could not be determined in this assay. Therefore, an alternative assay, such as NMR spectroscopy could be employed to study the effects of these compounds on nucleotide exchange (Vo et al., 2016).

To assess the effects of Affimer-derived compounds on endogenous Ras-mediated signalling, phosphorylation of ERK, a downstream Ras effector, was analysed in HEK293 and Panc 10.05 cells. Similarly to Abd-7 (Quevedo et al., 2018) and Ch-3 (Cruz-Migoni et al., 2019), Affimer-derived compounds reduced pERK levels in mutant KRas human cancer cells (Figure 6.3). However, the effects of Abd-7 and Ch-3 were observed only after optimisation of the initial hits through medicinal chemistry (Quevedo et al., 2018, Cruz-Migoni et al., 2019), whilst one of the initial hit compounds isolated in this study (compound 7), significantly inhibited Ras-mediated signalling at 10 µM. This therefore, demonstrated that Affimer-derived compounds represent a better starting point for the development of more potent molecules, when compared to previously published Ras-targeting compounds. However, further tests are required to determine the effects of Affimer-derived compounds on pERK signalling in HEK293 cells. Moreover, a broader panel of cell lines expressing different Ras isoforms and mutants should be tested, to assay if the Affimer-derived compounds could show some cell line or Ras mutation specific effects. In addition, inhibition of Ras could also lead to impaired PI3K-mediated signalling, as shown with the Abd-7 and Ch-3 compounds (Quevedo et al., 2018, Cruz-Migoni et al., 2019). Therefore, it would be interesting to assay the effects of Affimer-derived compounds on AKT phosphorylation.

In order to determine whether the observed effects of previously reported compounds on biomarker phosphorylation were due to specific inhibition of Ras, the Ras-effector interactions were investigated. Bioluminescence resonance energy transfer (BRET)-based biosensor (Bery et al., 2018) showed that Abd-7 and Ch-3 disrupt the wild-type and mutant Ras interactions with PI3K, CRaf and RALGDS (Quevedo et al., 2018, Cruz-Migoni et al., 2019). Likewise, DCAI was shown to impair the Ras-Raf interaction in a fluorescence-based system (Maurer

et al., 2012). Hence, future work should investigate the effects of Affimer-derived compounds on Ras-effectors binding. To further confirm that the inhibition of phosphorylation is due to direct binding of compounds to Ras, rather than off-target effects, a binding assay with a panel of kinase proteins, such as Raf, MEK and PI3K, could be employed. Likewise, the Affimer-derived compounds could be tested in a BRaf V600E mutant cell lines, in which the MAPK pathway signalling in independent of Ras (Yao et al., 2015). Therefore, any effects of the compounds observed in these cells could be attributed to off-target effects. Additionally, cell permeability assays could be performed to validate, that the observed effects are due to intracellular activities of the compounds.

Similarly to Abd-7 (Quevedo et al., 2018) and Ch-3 (Cruz-Migoni et al., 2019), the Affimer-derived compounds displayed the ability to reduce cell viability, with compound 7 showing the most potent effects (Figure 6.7). Future work should evaluate the IC_{50} values of Affimer-derived compounds to directly compare the potencies of these compounds with the IC_{50} values of Abd-7 and Ch-3 (8.2 µM and 4.5 µM, respectively, (Cruz-Migoni et al., 2019)). In addition, further phenotypic cell assays would be required to establish whether the effects on cell viability were due to induced apoptosis or impaired cell proliferation.

Analysis of the chemical structures of the six Affimer-derived compounds, shown in Figure 6.8, demonstrated that majority contain aromatic groups, which could mimic the indole of tryptophan in binding to the hydrophobic pocket on KRas. However, structural characterisation would be necessary to confirm the binding sites of these compounds. Obtaining the KRas-compounds co-crystal structures could also inform structure-based optimisation of the compounds to achieve better potency or to inform development of new chemical series. Additionally, future work should also investigate the binding affinities of the Affimer-derived compounds towards KRas through, for example surface plasmon resonance (SPR). This would allow comparison of the potency of binding to previously reported anti-Ras compounds and would provide evidence of the direct binding of the compounds to KRas.

In conclusion, the Affimer K6's resides were successfully mimicked with small molecules, to identify initial hit compounds capable of impairing nucleotide exchange, Ras-mediated signalling and cell viability. The Affimer-derived

compounds displayed comparable properties to previously published small molecule inhibitors of Ras, although this was without any optimisation of the compounds. Therefore, these molecules hold great potential for development of even more potent inhibitors through employment of medicinal chemistry.
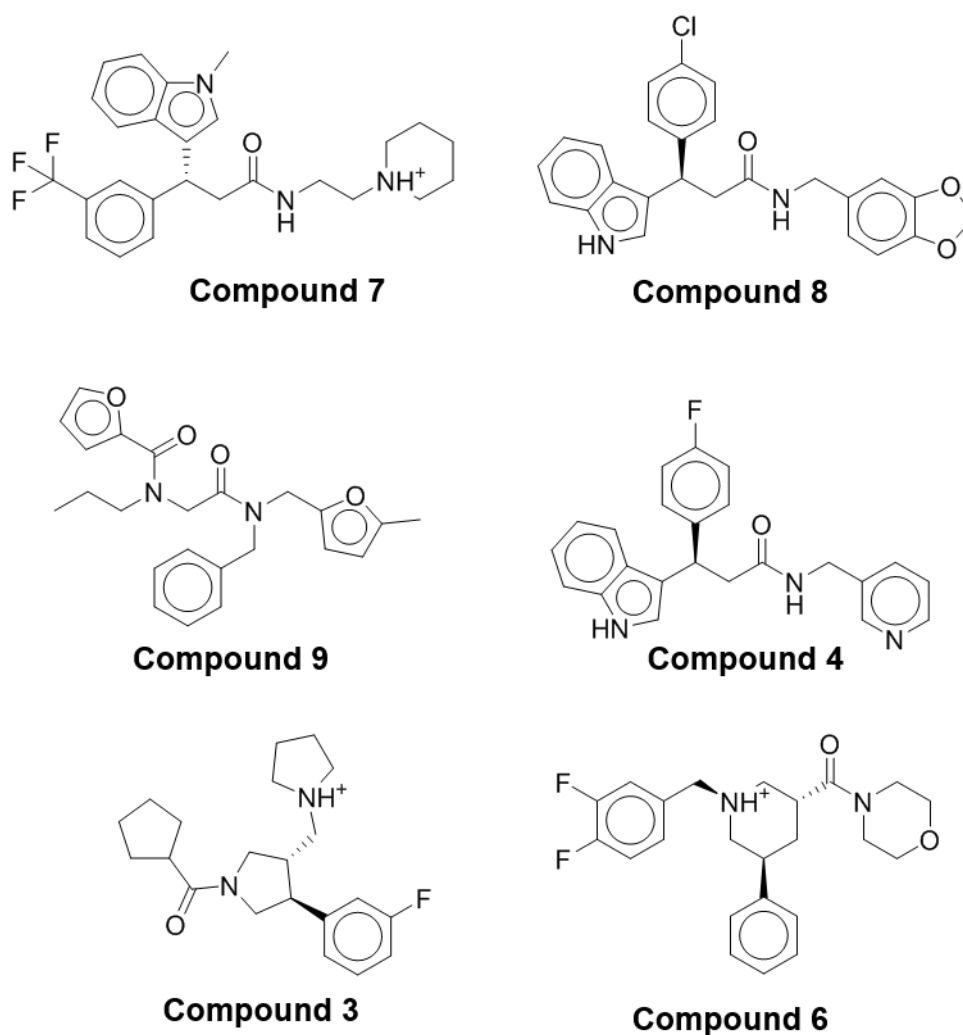
Figure 6.8 The chemical structures of six Affimer-derived compounds.

Chapter 7

Discussion and future perspectives

Chapter 7

Discussion and future perspectives

Work presented in this thesis investigated the suitability of Affimer reagents as a new Ras-targeting molecular biology tool to study Ras function. Ras is a validated cancer target, and is activated by mutation in approximately 30% of all human cancers (Baines et al., 2011, Burns et al., 2014, Friday and Adjei, 2005). However, since more than 30 years of research into development of Ras inhibitors have not yielded clinically relevant compounds, Ras has been considered as an 'undruggable' target (Cox et al., 2014). However, the interest in the development of small molecule Ras inhibitors has recently grown (Ledford, 2015). Virtual, high-throughput and fragment-based screening approaches have identified a number of small molecules targeting Ras. Many of these studies reported previously unknown binding pockets on Ras (Burns et al., 2014, Leshchiner et al., 2015, Maurer et al., 2012, Patgiri et al., 2011, Sun et al., 2012, Shima et al., 2013b, Lim et al., 2014, Ostrem et al., 2013, Welsch et al., 2017, Xiong et al., 2017). While several of these compounds demonstrated promising preclinical results, none of them have been approved as anti-cancer therapeutics, and only one compound has recently reached clinical evaluation stage (MiratiTherapeutics, 2018). A different approach for the development of potent inhibitors used engineered binding proteins, which led to isolation of KRas-binding single domain intrabody (Tanaka and Rabbitts, 2003, Tanaka et al., 2007, Tanaka and Rabbitts, 2010), monobody (Spencer-Smith et al., 2017a) and DARPins (Guillard et al., 2017). These reagents displayed potent inhibition of Ras in biochemical and cellular assays. This inspired the work presented in this thesis to test Affimer reagents as alternative scaffold proteins to target Ras. KRas-binding Affimers were shown to impair Sos-mediated Ras activation, Ras-effector interactions and Ras-mediated signalling in mammalian cells.

7.1 Inhibition of nucleotide exchange as a valid approach to impair Ras function

Historically, oncogenic Ras mutants were considered to be constitutively activated, consequently leading to sustained cell proliferation and tumour formation (Ahmadian et al., 1999). Therefore, inhibition of nucleotide exchange has not been viewed as valid approach for the development of anti-Ras therapeutics. This dogma however, was challenged by studies which provided evidence for cycling of Ras nucleotide states (Patricelli et al., 2016, Smith et al., 2013). As a result, small molecules and peptides, which block nucleotide exchange have been reported. These were shown to inhibit the nucleotide exchange in dose-dependent manner with the half maximal inhibitory concentration (IC_{50}) ranging from mid- to low micromolar. Albeit those inhibitors showed only moderate effects on downstream signalling (Leshchiner et al., 2015, Maurer et al., 2012, Patgiri et al., 2011). Irreversible inhibition of nucleotide exchange on KRas G12C with a covalent inhibitor ARS-853 resulted in reduced levels of active Ras and triggered apoptosis (Patricelli et al., 2016, Lito et al., 2016). Recently, Guillard *et al.* reported potent inhibition of nucleotide exchange with DARPin K27 as an approach to affect active Ras levels and Ras function. DARPin K27 displayed low nanomolar IC_{50} and impaired Ras-mediated signalling and cell proliferation (Guillard et al., 2017). Altogether, these findings re-evaluated the potential of nucleotide inhibition as promising approach to develop novel Ras inhibitors.

Similarly to the inhibitors described above, KRas-binding Affimers were shown to inhibit Sos-mediated nucleotide exchange on wild-type and oncogenic Ras mutants with nanomolar IC_{50} values (chapter 3). Noteworthy, preferential inhibition of some KRas mutants has been observed, which therefore established Affimer reagents as novel tools to study mutant-selectivity.

7.2 Ras-effectors inhibitors

The most universal approach for targeting Ras include interfering with GTPase-effector interaction, as the inhibition of signal propagation would be irrespective of the cause of constitutively active Ras (i.e. mutation, overexpression or loss of GAP activity). However, development of such inhibitors is challenging due to high

affinity binding of effectors to GTPases as well as no well-defined binding pockets (Cromm et al., 2015). Nonetheless, several approaches have yielded GTPase-effector interaction inhibitors, for example: small molecules based on the Kobe family scaffold (Shima et al., 2013a), peptide inhibitors such as cyclorasin 9A5 (Upadhyaya et al., 2015), engineered proteins iDab6 (Tanaka et al., 2007), R11.1.6 (Kauke et al., 2017) and DARPin K55 (Guillard et al., 2017) and organometallic complexes acting as allosteric inhibitors (Cromm et al., 2015). However, due to problems associated with low potency, off-target activity, low binding selectivity and intracellular delivery, none of these agents have reached clinical evaluation (Cox et al., 2014). KRas-targeting Affimers also displayed propensity to inhibit Ras-effector interactions. Interestingly, for the first time dual inhibition of nucleotide exchange and Ras-Raf interaction has been demonstrated with Affimers (chapter 3), which therefore established a novel mode of Ras inhibition. This identified KRas-binding Affimers as new valuable tools that could be further explored for development of novel anti-Ras therapeutics.

7.3 Applications of the Affimers

7.3.1 Affimer reagents as therapeutics

Apart from their use as molecular tools, Affimers could also be used as anti-Ras therapeutics themselves. Other biologics, such as monoclonal antibodies, are already being used as cancer therapeutics, and these biologics have become the fastest growing class of therapeutics (Aggarwal, 2010). However, while the majority of these biotherapeutics have been effective against extracellular targets, the main limitation is their delivery into cells, as, due to their size, biotherapeutics such as peptides and proteins are unable to cross the cell membrane (Walker et al., 2017). Thus leaving the intracellular targets out of their reach (Tsomaia, 2015). Therefore, before the anti-Ras Affimers could be used as therapeutics, an efficient intracellular delivery system would have to be developed. Several strategies already exist to overcome this problem, and these include use of polymerosomes, liposomes and cell penetrating peptides (Anajafi and Mallik, 2015, Lonn et al., 2016). Another hurdle to overcome concerns the immunogenicity of biologics. Administration of protein-based therapeutics could

elicit production of anti-drug antibodies (ADAs), which in turn could impact the pharmacological properties of the therapeutic or may trigger adverse side effects (Garces and Demengeot, 2018). Both Type I and Type II Affimer scaffolds have shown low immunogenicity in *in vitro* peripheral blood mononuclear cells (PBMC) assay, which was comparable to that of the therapeutic antibody Avastin® tested alongside in the assay (Avacta Life Sciences, 2017). This therefore, indicated that Affimer reagents do not possess fundamental immunogenicity problems and could be progressed into therapeutic development.

7.3.2 Affimer reagents as tools for development of small molecule inhibitors

Development of small molecule inhibitors based on the scaffold proteins has not been achieved to date, as these scaffold proteins usually display large interaction surfaces, for example, the HRas-intrabody (interface surface area of 852 Å) or the KRas-DARPins (interface surface area of 950 Å) interactions (Tanaka et al., 2007, Guillard et al., 2017). Ras-targeting intrabody has been recently used in a competition assay to develop small molecule Ras inhibitors (Quevedo et al., 2018). Although these compounds bound to the same site as the intrabody, these did not mimic the intrabody's functional epitope. In contrast, shape-based virtual screen identified compounds resembling Affimer's K6 epitope. These Affimer-derived compounds were shown to be effective in biochemical and cell-based assays, with comparable properties to previously published small molecule inhibitors of Ras without any optimisation of the compounds. Therefore, these molecules hold great potential for development of even more potent inhibitors through employment of medicinal chemistry. This proof of principle study, demonstrated for the first time the direct mimicry of a scaffold protein to yield small molecule inhibitors. Therefore, the work presented in this thesis established a novel use of Affimer reagents as valuable tools for the development of small molecule inhibitors. Most interestingly, this technology could be also applied to other disease related proteins, which are currently intractable to small molecules.

7.4 Continuation of the project

To assess the suitability of use of the Affimer-derived compounds as anti-Ras therapeutics, further characterisation of these molecules is essential.

Crystallisation trials to obtain KRas-compounds co-crystal structures are underway. If successful, this will provide evidence of the direct binding of these compounds to KRas. Moreover, it will confirm whether the binding sites are similar to that of Affimer K6, and therefore establish if the compounds indeed mimic the Affimer's binding. Obtaining the KRas-compounds co-crystal structures could also inform structure-based optimisation of the compounds to achieve better potency or to inform development of new chemical series. Further cell-based studies assaying the effects of compounds on Ras-effector interactions, biomarker phosphorylation, cell proliferation and apoptosis would provide insights into how these molecules function.

Similar approach to the one employed with Affimer K6 could be used to mimic the residues of Affimer K3 with small molecules, as recently obtained Affimer K3-KRas co-crystal structure revealed binding to a different pocket near switch II region. This would be particularly interesting, as K3 has displayed different properties, when compared to K6, notably KRas specificity and simultaneous inhibition of nucleotide exchange and Ras-Raf interaction. This could therefore, yield a set of Ras-targeting compounds with novel properties.

In conclusion, this project described Affimer reagents as new tools to study Ras function, with comparable or improved qualities to other Ras-targeting reagents. Importantly, a novel use of Affimer reagents as precursors for the development of new small molecule inhibitors has been established, and this technology is being exploited in the lab with other targets.

References

AGGARWAL, S. 2010. What's fueling the biotech engine-2009-2010. *Nature Biotechnology,* 28**,** 1165-1171.

AHEARN, I. M., HAIGIS, K., BAR-SAGI, D. & PHILIPS, M. R. 2012. Regulating the regulator: post-translational modification of RAS. *Nat Rev Mol Cell Biol,* 13**,** 39-51.

AHLGREN, S., ORLOVA, A., WALLBERG, H., HANSSON, M., SANDSTROM, M., LEWSLEY, R., WENNBORG, A., ABRAHMSEN, L., TOLMACHEV, V. & FELDWISCH, J. 2010. Targeting of HER2-expressing tumors using 111In-ABY-025, a second-generation affibody molecule with a fundamentally reengineered scaffold. *J Nucl Med,* 51**,** 1131-8.

AHMADIAN, M. R., ZOR, T., VOGT, D., KABSCH, W., SELINGER, Z., WITTINGHOFER, A. & SCHEFFZEK, K. 1999. Guanosine triphosphatase stimulation of oncogenic Ras mutants. *Proc Natl Acad Sci U S A,* 96**,** 7065-70.

ALVAREZ, R. D., BARNES, M. N., GOMEZ-NAVARRO, J., WANG, M., STRONG, T. V., ARAFAT, W., ARANI, R. B., JOHNSON, M. R., ROBERTS, B. L., SIEGAL, G. P. & CURIEL, D. T. 2000. A cancer gene therapy approach utilizing an anti-erbB-2 single-chain antibody-encoding adenovirus (AD21): a phase I trial. *Clin Cancer Res,* 6**,** 3081-7.

ANAJAFI, T. & MALLIK, S. 2015. Polymersome-based drug-delivery strategies for cancer therapeutics. *Ther Deliv,* 6**,** 521-34.

ARAI, R., UEDA, H., KITAYAMA, A., KAMIYA, N. & NAGAMUNE, T. 2001. Design of the linkers which effectively separate domains of a bifunctional fusion protein. *Protein Engineering, Design and Selection,* 14**,** 529-532.

AVACTA LIFE SCIENCES 2017. Affimer Technology: Results of PBMC Immunogenicity. https://www.avacta.com/sites/default/files/resource/Immunogenicity%20Results.pdf.

BAINES, A. T., XU, D. & DER, C. J. 2011. Inhibition of Ras for cancer treatment: the search continues. *Future Med Chem,* 3**,** 1787-808.

BANASZYNSKI, L. A., CHEN, L. C., MAYNARD-SMITH, L. A., OOI, A. G. & WANDLESS, T. J. 2006. A rapid, reversible, and tunable method to regulate protein function in living cells using synthetic small molecules. *Cell,* 126**,** 995-1004.

BANNAS, P., HAMBACH, J. & KOCH-NOLTE, F. 2017. Nanobodies and Nanobody-Based Human Heavy Chain Antibodies As Antitumor Therapeutics. *Front Immunol,* 8**,** 1603.

BARBIE, D. A., TAMAYO, P., BOEHM, J. S., KIM, S. Y., MOODY, S. E., DUNN, I. F., SCHINZEL, A. C., SANDY, P., MEYLAN, E., SCHOLL, C., FROHLING, S., CHAN, E. M., SOS, M. L., MICHEL, K., MERMEL, C., SILVER, S. J., WEIR, B. A., REILING, J. H., SHENG, Q., GUPTA, P. B., WADLOW, R. C., LE, H., HOERSCH, S., WITTNER, B. S., RAMASWAMY, S., LIVINGSTON, D. M., SABATINI, D. M., MEYERSON, M., THOMAS, R. K., LANDER, E. S., MESIROV, J. P., ROOT, D. E., GILLILAND, D. G., JACKS, T. & HAHN, W. C. 2009. Systematic RNA interference reveals that oncogenic KRAS-driven cancers require TBK1. *Nature,* 462**,** 108-12.

BEERLI, R. R., WELS, W. & HYNES, N. E. 1994. Intracellular expression of single chain antibodies reverts ErbB-2 transformation. *J Biol Chem,* 269**,** 23931-6.

BERGLUND, L., BJORLING, E., OKSVOLD, P., FAGERBERG, L., ASPLUND, A., SZIGYARTO, C. A., PERSSON, A., OTTOSSON, J., WERNERUS, H., NILSSON, P., LUNDBERG, E., SIVERTSSON, A., NAVANI, S., WESTER, K., KAMPF, C., HOBER, S., PONTEN, F. & UHLEN, M. 2008. A genecentric Human Protein Atlas for expression profiles based on antibodies. *Mol Cell Proteomics,* 7**,** 2019-27.

BERMAN, H. M., WESTBROOK, J., FENG, Z., GILLILAND, G., BHAT, T. N., WEISSIG, H., SHINDYALOV, I. N. & BOURNE, P. E. 2000. The Protein Data Bank. *Nucleic Acids Res,* 28**,** 235-42.

BERY, N., CRUZ-MIGONI, A., BATAILLE, C. J., QUEVEDO, C. E., TULMIN, H., MILLER, A., RUSSELL, A., PHILLIPS, S. E., CARR, S. B. & RABBITTS, T. H. 2018. BRET-based RAS biosensors that show a novel small molecule is an inhibitor of RAS-effector protein-protein interactions. 7.

BINZ, H. K., STUMPP, M. T., FORRER, P., AMSTUTZ, P. & PLUCKTHUN, A. 2003. Designing repeat proteins: well-expressed, soluble and stable proteins from combinatorial libraries of consensus ankyrin repeat proteins. *J Mol Biol,* 332**,** 489-503.

BLOOM, L. & CALABRO, V. 2009. FN3: a new protein scaffold reaches the clinic. *Drug Discov Today,* 14**,** 949-55.

BOGAN, A. A. & THORN, K. S. 1998. Anatomy of hot spots in protein interfaces. *J Mol Biol,* 280**,** 1-9.

BOLLAG, G. & MCCORMICK, F. 1991. Differential regulation of rasGAP and neurofibromatosis gene product activities. *Nature,* 351**,** 576-9.

BOONE, B. A., ZEH, H. J., 3RD & BAHARY, N. 2018. Autophagy Inhibition in Pancreatic Adenocarcinoma. *Clin Colorectal Cancer,* 17**,** 25-31.

BORDEAUX, J., WELSH, A., AGARWAL, S., KILLIAM, E., BAQUERO, M., HANNA, J., ANAGNOSTOU, V. & RIMM, D. 2010. Antibody validation. *Biotechniques,* 48**,** 197-209.

BORIACK-SJODIN, P. A., MARGARIT, S. M., BAR-SAGI, D. & KURIYAN, J. 1998. The structural basis of the activation of Ras by Sos. *Nature,* 394**,** 337-343.

BOS, J. L. 1989. RAS ONCOGENES IN HUMAN CANCER - A REVIEW. *Cancer Research,* 49**,** 4682-4689.

BOS, J. L., REHMANN, H. & WITTINGHOFER, A. 2007. GEFs and GAPs: critical elements in the control of small G proteins. *Cell,* 129**,** 865-77.

BOURNE, H. R., SANDERS, D. A. & MCCORMICK, F. 1991. The Gtpase Superfamily - Conserved Structure and Molecular Mechanism. *Nature,* 349**,** 117-127.

BRADBURY, A. & PLUCKTHUN, A. 2015. Reproducibility: Standardize antibodies used in research. *Nature,* 518**,** 27-9.

BRITTEN, C. D. 2013. PI3K and MEK inhibitor combinations: examining the evidence in selected tumor types. *Cancer Chemother Pharmacol,* 71**,** 1395-409.

BRUMMELKAMP, T. R., BERNARDS, R. & AGAMI, R. 2002. Stable suppression of tumorigenicity by virus-mediated RNA interference. *Cancer Cell,* 2**,** 243-7.

BUDAY, L. & DOWNWARD, J. 2008. Many faces of Ras activation. *Biochim Biophys Acta,* 1786**,** 178-87.

BURNS, M. C., SUN, Q., DANIELS, R. N., CAMPER, D., KENNEDY, J. P., PHAN, J., OLEJNICZAK, E. T., LEE, T., WATERSON, A. G., ROSSANESE, O. W. & FESIK, S. W. 2014. Approach for targeting Ras with small molecules that activate SOS-mediated nucleotide exchange. *Proceedings of the National Academy of Sciences of the United States of America,* 111**,** 3401-3406.

BUSS, N. A., HENDERSON, S. J., MCFARLANE, M., SHENTON, J. M. & DE HAAN, L. 2012. Monoclonal antibody therapeutics: history and future. *Curr Opin Pharmacol,* 12**,** 615-22.

CAMPBELL, I. D. 2002. Timeline: the march of structural biology. *Nat Rev Mol Cell Biol,* 3**,** 377-81.

CAPON, D. J., SEEBURG, P. H., MCGRATH, J. P., HAYFLICK, J. S., EDMAN, U., LEVINSON, A. D. & GOEDDEL, D. V. 1983. Activation of Ki-ras2 gene in human colon and lung carcinomas by two different point mutations. *Nature,* 304**,** 507-13.

CARTER, P. J. 2011. Introduction to current and future protein therapeutics: a protein engineering perspective. *Exp Cell Res,* 317**,** 1261-9.

CASTELLANO, E. & SANTOS, E. 2011. Functional specificity of ras isoforms: so similar but so different. *Genes & cancer,* 2**,** 216-31.

CASTELLANO, E., SHERIDAN, C., THIN, M. Z., NYE, E., SPENCER-DENE, B., DIEFENBACHER, M. E., MOORE, C., KUMAR, M. S., MURILLO, M. M., GRONROOS, E., LASSAILLY, F., STAMP, G. & DOWNWARD, J. 2013. Requirement for interaction of PI3-kinase p110alpha with RAS in lung tumor maintenance. *Cancer Cell,* 24**,** 617-30.

CHANDHANAYINGYONG, C., KIM, Y., STAPLES, J. R., HAHN, C. & LEE, F. Y. 2012. MAPK/ERK Signaling in Osteosarcomas, Ewing Sarcomas and Chondrosarcomas: Therapeutic Implications and Future Directions. *Sarcoma,* 2012**,** 404810.

CHANDRA, A., GRECCO, H. E., PISUPATI, V., PERERA, D., CASSIDY, L., SKOULIDIS, F., ISMAIL, S. A., HEDBERG, C., HANZAL-BAYER, M., VENKITARAMAN, A. R., WITTINGHOFER, A. & BASTIAENS, P. I. 2011. The GDI-like solubilizing factor PDEdelta sustains the spatial organization and signalling of Ras family proteins. *Nat Cell Biol,* 14**,** 148-58.

CHAPMAN, H. N., FROMME, P., BARTY, A., WHITE, T. A., KIRIAN, R. A., AQUILA, A., HUNTER, M. S., SCHULZ, J., DEPONTE, D. P., WEIERSTALL, U., DOAK, R. B., MAIA, F. R. N. C., MARTIN, A. V., SCHLICHTING, I., LOMB, L., COPPOLA, N., SHOEMAN, R. L., EPP, S. W., HARTMANN, R., ROLLES, D., RUDENKO, A., FOUCAR, L., KIMMEL, N., WEIDENSPOINTNER, G., HOLL, P., LIANG, M., BARTHELMESS, M., CALEMAN, C., BOUTET, S., BOGAN, M. J., KRZYWINSKI, J., BOSTEDT, C., BAJT, S., GUMPRECHT, L., RUDEK, B., ERK, B., SCHMIDT, C., HÖMKE, A., REICH, C., PIETSCHNER, D., STRÜDER, L., HAUSER, G., GORKE, H., ULLRICH, J., HERRMANN, S., SCHALLER, G., SCHOPPER, F., SOLTAU, H., KÜHNEL, K.-U., MESSERSCHMIDT, M., BOZEK, J. D., HAU-RIEGE, S. P., FRANK, M., HAMPTON, C. Y., SIERRA, R. G., STARODUB, D., WILLIAMS, G. J., HAJDU, J., TIMNEANU, N., SEIBERT,

M. M., ANDREASSON, J., ROCKER, A., JÖNSSON, O., SVENDA, M., STERN, S., NASS, K., ANDRITSCHKE, R., SCHRÖTER, C.-D., KRASNIQI, F., BOTT, M., SCHMIDT, K. E., WANG, X., GROTJOHANN, I., HOLTON, J. M., BARENDS, T. R. M., NEUTZE, R., MARCHESINI, S., FROMME, R., SCHORB, S., RUPP, D., ADOLPH, M., GORKHOVER, T., ANDERSSON, I., HIRSEMANN, H., POTDEVIN, G., GRAAFSMA, H., NILSSON, B. & SPENCE, J. C. H. 2011. Femtosecond X-ray protein nanocrystallography. *Nature,* 470**,** 73-77.

CHAYEN, N. E. & SARIDAKIS, E. 2002. Protein crystallization for genomics: towards high-throughput optimization techniques. *Acta Crystallogr D Biol Crystallogr,* 58**,** 921-7.

CHENG, A. C., COLEMAN, R. G., SMYTH, K. T., CAO, Q., SOULARD, P., CAFFREY, D. R., SALZBERG, A. C. & HUANG, E. S. 2007. Structure-based maximal affinity model predicts small-molecule druggability. *Nature Biotechnology,* 25**,** 71-75.

CHENG, C. M., LI, H., GASMAN, S., HUANG, J., SCHIFF, R. & CHANG, E. C. 2011. Compartmentalized Ras proteins transform NIH 3T3 cells with different efficiencies. *Mol Cell Biol,* 31**,** 983-97.

CHENG, Y. & TIAN, H. 2017. Current Development Status of MEK Inhibitors. *Molecules,* 22.

CHESSARI, G. & WOODHEAD, A. J. 2009. From fragment to clinical candidate-a historical perspective. *Drug Discovery Today,* 14**,** 668-675.

COLICELLI, J. 2004. Human RAS superfamily proteins and related GTPases. *Sci STKE,* 2004**,** RE13.

COMMISSO, C., DAVIDSON, S. M., SOYDANER-AZELOGLU, R. G., PARKER, S. J., KAMPHORST, J. J., HACKETT, S., GRABOCKA, E., NOFAL, M., DREBIN, J. A., THOMPSON, C. B., RABINOWITZ, J. D., METALLO, C. M., VANDER HEIDEN, M. G. & BAR-SAGI, D. 2013. Macropinocytosis of protein is an amino acid supply route in Ras-transformed cells. *Nature,* 497**,** 633-7.

COX, A. D. & DER, C. J. 2010. Ras history: The saga continues. *Small GTPases,* 1**,** 2-27.

COX, A. D., FESIK, S. W., KIMMELMAN, A. C., LUO, J. & DER, C. J. 2014. Drugging the undruggable RAS: Mission possible? *Nat Rev Drug Discov,* 13**,** 828-51.

COX, M. J. & WEBER, P. C. 1988. An investigation of protein crystallization parameters using successive automated grid searches (SAGS). *Journal of Crystal Growth,* 90**,** 318-324.

CROMM, P. M., SPIEGEL, J., GROSSMANN, T. N. & WALDMANN, H. 2015. Direct Modulation of Small GTPase Activity and Function. *Angewandte Chemie-International Edition,* 54**,** 13516-13537.

CROUCH, S. P. M., KOZLOWSKI, R., SLATER, K. J. & FLETCHER, J. 1993. The use of ATP bioluminescence as a measure of cell proliferation and cytotoxicity. *Journal of Immunological Methods,* 160**,** 81-88.

CRUZ-MIGONI, A., CANNING, P., QUEVEDO, C. E., BATAILLE, C. J. R., BERY, N., MILLER, A., RUSSELL, A. J., PHILLIPS, S. E. V., CARR, S. B. & RABBITTS, T. H. 2019. Structure-based development of new RAS-effector inhibitors from a combination of active and inactive RAS-binding compounds. *Proc Natl Acad Sci U S A*.

CUNNINGHAM, B. C. & WELLS, J. A. 1989. High-resolution epitope mapping of hGH-receptor interactions by alanine-scanning mutagenesis. *Science,* 244**,** 1081-5.

DE LAS RIVAS, J. & FONTANILLO, C. 2010. Protein–Protein Interactions Essentials: Key Concepts to Building and Analyzing Interactome Networks. *PLOS Computational Biology,* 6**,** e1000807.

DEROO, S., THIOLLOY, S., DESMET, J., BAATZ, F., LOVERIX, S., VANDENBROUCKE, K., LORENT, E., HENDERIKX, P., LEMMENS, I., ALARD, P., LASTERS, I. & MCGRATH, Y. 2016. Abstract 3850: First-in-class cell-penetrating proteins targeting Mcl-1 induce tumor cell apoptosis and inhibition of tumor growth in vivo. *Cancer Research,* 76**,** 3850-3850.

DESHANE, J., SIEGAL, G. P., ALVAREZ, R. D., WANG, M. H., FENG, M., CABRERA, G., LIU, T., KAY, M. & CURIEL, D. T. 1995. Targeted tumor killing via an intracellular antibody against erbB-2. *J Clin Invest,* 96**,** 2980-9.

DOWNWARD, J. 2003. Targeting ras signalling pathways in cancer therapy. *Nature Reviews Cancer,* 3**,** 11-22.

DUFF, M. R., JR., GRUBBS, J. & HOWELL, E. E. 2011. Isothermal titration calorimetry for measuring macromolecule-ligand affinity. *J Vis Exp*.

DUNLEVY, F. K., MARTIN, S. L., DE COURCEY, F., ELBORN, J. S. & ENNIS, M. 2012. Anti-inflammatory effects of DX-890, a human neutrophil elastase inhibitor. *J Cyst Fibros,* 11**,** 300-4.

DUROCHER, Y., PERRET, S. & KAMEN, A. 2002. High-level and high-throughput recombinant protein production by transient transfection of suspension-growing human 293-EBNA1 cells. *Nucleic Acids Res,* 30**,** E9.

DURRANT, D. E. & MORRISON, D. K. 2018. Targeting the Raf kinases in human cancer: the Raf dimer dilemma. *Br J Cancer,* 118**,** 3-8.

DUURSMA, A. M. & AGAMI, R. 2003. Ras interference as cancer therapy. *Semin Cancer Biol,* 13**,** 267-73.

EBERSBACH, H., FIEDLER, E., SCHEUERMANN, T., FIEDLER, M., STUBBS, M. T., REIMANN, C., PROETZEL, G., RUDOLPH, R. & FIEDLER, U. 2007. Affilin-novel binding molecules based on human gamma-B-crystallin, an all beta-sheet protein. *J Mol Biol,* 372**,** 172-85.

EMSLEY, P. & COWTAN, K. 2004. Coot: model-building tools for molecular graphics. *Acta Crystallographica Section D-Biological Crystallography,* 60**,** 2126-2132.

END, D. W., SMETS, G., TODD, A. V., APPLEGATE, T. L., FUERY, C. J., ANGIBAUD, P., VENET, M., SANZ, G., POIGNET, H., SKRZAT, S., DEVINE, A., WOUTERS, W. & BOWDEN, C. 2001. Characterization of the antitumor effects of the selective farnesyl protein transferase inhibitor R115777 in vivo and in vitro. *Cancer Res,* 61**,** 131-7.

ENGELMAN, J. A., CHEN, L., TAN, X., CROSBY, K., GUIMARAES, A. R., UPADHYAY, R., MAIRA, M., MCNAMARA, K., PERERA, S. A., SONG, Y., CHIRIEAC, L. R., KAUR, R., LIGHTBOWN, A., SIMENDINGER, J., LI, T., PADERA, R. F., GARCIA-ECHEVERRIA, C., WEISSLEDER, R., MAHMOOD, U., CANTLEY, L. C. & WONG, K. K. 2008. Effective use of PI3K and MEK inhibitors to treat mutant Kras G12D and PIK3CA H1047R murine lung cancers. *Nat Med,* 14**,** 1351-6.

ESTEBAN, L. M., VICARIO-ABEJON, C., FERNANDEZ-SALGUERO, P., FERNANDEZ-MEDARDE, A., SWAMINATHAN, N., YIENGER, K., LOPEZ, E., MALUMBRES, M., MCKAY, R., WARD, J. M., PELLICER, A. & SANTOS, E. 2001. Targeted genomic disruption of H-ras and N-ras, individually or in combination, reveals the dispensability of both loci for mouse growth and development. *Mol Cell Biol,* 21**,** 1444-52.

EVDOKIMOV, A. G., POKROSS, M. E., EGOROV, N. S., ZARAISKY, A. G., YAMPOLSKY, I. V., MERZLYAK, E. M., SHKOPOROV, A. N., SANDER, I., LUKYANOV, K. A. & CHUDAKOV, D. M. 2006. Structural basis for the fast

maturation of Arthropoda green fluorescent protein. *EMBO Rep,* 7**,** 1006-12.

EVELYN, C. R., DUAN, X., BIESIADA, J., SEIBEL, W. L., MELLER, J. & ZHENG, Y. 2014. Rational design of small molecule inhibitors targeting the Ras GEF, SOS1. *Chem Biol,* 21**,** 1618-28.

FANG, B. 2016. RAS signaling and anti-RAS therapy: lessons learned from genetically engineered mouse models, human cancer cells, and patient-related studies. *Acta Biochim Biophys Sin (Shanghai),* 48**,** 27-38.

FARLEY, C. & JUERS, D. H. 2014. Efficient cryoprotection of macromolecular crystals using vapor diffusion of volatile alcohols. *Journal of structural biology,* 188**,** 102-106.

FAVATA, M. F., HORIUCHI, K. Y., MANOS, E. J., DAULERIO, A. J., STRADLEY, D. A., FEESER, W. S., VAN DYK, D. E., PITTS, W. J., EARL, R. A., HOBBS, F., COPELAND, R. A., MAGOLDA, R. L., SCHERLE, P. A. & TRZASKOS, J. M. 1998. Identification of a novel inhibitor of mitogen-activated protein kinase kinase. *J Biol Chem,* 273**,** 18623-32.

FILCHTINSKI, D., SHARABI, O., RUPPEL, A., VETTER, I. R., HERRMANN, C. & SHIFMAN, J. M. 2010. What makes Ras an efficient molecular switch: a computational, biophysical, and structural study of Ras-GDP interactions with mutants of Raf. *J Mol Biol,* 399**,** 422-35.

FIORUCCI, G. & HALL, A. 1988. All three human ras genes are expressed in a wide range of tissues. *Biochim Biophys Acta,* 950**,** 81-3.

FOSGERAU, K. & HOFFMANN, T. 2015. Peptide therapeutics: current status and future directions. *Drug Discovery Today,* 20**,** 122-128.

FREEMAN, A. K., RITT, D. A. & MORRISON, D. K. 2013. Effects of Raf dimerization and its inhibition on normal and disease-associated Raf signaling. *Mol Cell,* 49**,** 751-8.

FRIDAY, B. B. & ADJEI, A. A. 2005. K-ras as a target for cancer therapy. *Biochim Biophys Acta,* 1756**,** 127-44.

FURTH, M. E., ALDRICH, T. H. & CORDON-CARDO, C. 1987. Expression of ras proto-oncogene proteins in normal human tissues. *Oncogene,* 1**,** 47-58.

GARCES, S. & DEMENGEOT, J. 2018. The Immunogenicity of Biologic Therapies. *Curr Probl Dermatol,* 53**,** 37-48.

GARRAWAY, L. A. & SELLERS, W. R. 2006. Lineage dependency and lineage-survival oncogenes in human cancer. *Nat Rev Cancer,* 6**,** 593-602.

GENTILE, D. R., RATHINASWAMY, M. K., JENKINS, M. L., MOSS, S. M., SIEMPELKAMP, B. D., RENSLO, A. R., BURKE, J. E. & SHOKAT, K. M. 2017. Ras Binder Induces a Modified Switch-II Pocket in GTP and GDP States. *Cell Chem Biol,* 24**,** 1455-1466.e14.

GERA, N., HUSSAIN, M., WRIGHT, R. C. & RAO, B. M. 2011. Highly stable binding proteins derived from the hyperthermophilic Sso7d scaffold. *J Mol Biol,* 409**,** 601-16.

GIORDANETTO, F., SCHAFER, A. & OTTMANN, C. 2014. Stabilization of protein-protein interactions by small molecules. *Drug Discovery Today,* 19**,** 1812-1821.

GIORDANO, G., PANCIONE, M., OLIVIERI, N., PARCESEPE, P., VELOCCI, M., DI RAIMO, T., COPPOLA, L., TOFFOLI, G. & D'ANDREA, M. R. 2017. Nano albumin bound-paclitaxel in pancreatic cancer: Current evidences and future directions. *World journal of gastroenterology,* 23**,** 5875-5886.

GOCHA, T., RAO, B. M. & DASGUPTA, R. 2017. Identification and characterization of a novel Sso7d scaffold-based binder against Notch1. *Sci Rep,* 7**,** 12021.

GORFE, A. A., GRANT, B. J. & MCCAMMON, J. A. 2008. Mapping the nucleotide and isoform-dependent structural and dynamical features of Ras proteins. *Structure,* 16**,** 885-96.

GORMAN, C. M., GIES, D., MCCRAY, G. & HUANG, M. 1989. The human cytomegalovirus major immediate early promoter can be trans-activated by adenovirus early proteins. *Virology,* 171**,** 377-85.

GRADY, W. M. & MARKOWITZ, S. D. 2002. Genetic and epigenetic alterations in colon cancer. *Annu Rev Genomics Hum Genet,* 3**,** 101-28.

GRANT, B. J., LUKMAN, S., HOCKER, H. J., SAYYAH, J., BROWN, J. H., MCCAMMON, J. A. & GORFE, A. A. 2011. Novel allosteric sites on Ras for lead generation. *PLoS One,* 6**,** e25711.

GRAY, G. D., HERNANDEZ, O. M., HEBEL, D., ROOT, M., POW-SANG, J. M. & WICKSTROM, E. 1993. Antisense DNA inhibition of tumor growth induced by c-Ha-ras oncogene in nude mice. *Cancer Res,* 53**,** 577-80.

GREBIEN, F., HANTSCHEL, O., WOJCIK, J., KAUPE, I., KOVACIC, B., WYRZUCKI, ARKADIUSZ M., GISH, GERALD D., CERNY-REITERER, S., KOIDE, A., BEUG, H., PAWSON, T., VALENT, P., KOIDE, S. & SUPERTI-FURGA, G. 2011. Targeting the SH2-Kinase Interface in Bcr-Abl Inhibits Leukemogenesis. *Cell,* 147**,** 306-319.

GRIMALDI, A. M., SIMEONE, E., FESTINO, L., VANELLA, V., STRUDEL, M. & ASCIERTO, P. A. 2017. MEK Inhibitors in the Treatment of Metastatic Melanoma and Solid Tumors. *Am J Clin Dermatol,* 18**,** 745-754.

GRIMM, S., LUNDBERG, E., YU, F., SHIBASAKI, S., VERNET, E., SKOGS, M., NYGREN, P. A. & GRASLUND, T. 2010. Selection and characterisation of affibody molecules inhibiting the interaction between Ras and Raf in vitro. *N Biotechnol,* 27**,** 766-73.

GUILLARD, S., KOLASINSKA-ZWIERZ, P., DEBRECZENI, J., BREED, J., ZHANG, J., BERY, N., MARWOOD, R., TART, J., OVERMAN, R., STOCKI, P., MISTRY, B., PHILLIPS, C., RABBITTS, T., JACKSON, R. & MINTER, R. 2017. Structural and functional characterization of a DARPin which inhibits Ras nucleotide exchange. *Nature Communications,* 8.

GUPTA, S., RAMJAUN, A. R., HAIKO, P., WANG, Y., WARNE, P. H., NICKE, B., NYE, E., STAMP, G., ALITALO, K. & DOWNWARD, J. 2007. Binding of ras to phosphoinositide 3-kinase p110alpha is required for ras-driven tumorigenesis in mice. *Cell,* 129**,** 957-68.

HANAHAN, D. & WEINBERG, R. A. 2011. Hallmarks of cancer: the next generation. *Cell,* 144**,** 646-74.

HANCOCK, J. F. 2003. Ras proteins: different signals from different locations. *Nat Rev Mol Cell Biol,* 4**,** 373-84.

HARVEY, J. J. 1964. UNIDENTIFIED VIRUS WHICH CAUSES RAPID PRODUCTION OF TUMOURS IN MICE. *Nature,* 204**,** 1104-&.

HAUSCHILD, A., DUMMER, R., SCHADENDORF, D., SANTINAMI, M., ATKINSON, V., MANDALA, M., CHIARION-SILENI, V., LARKIN, J., NYAKAS, M., DUTRIAUX, C., HAYDON, A., ROBERT, C., MORTIER, L., SCHACHTER, J., LESIMPLE, T., PLUMMER, R., DASGUPTA, K., HAAS, T., SHILKRUT, M., GASAL, E., KEFFORD, R., KIRKWOOD, J. M. & LONG, G. V. 2018. Longer Follow-Up Confirms Relapse-Free Survival Benefit With Adjuvant Dabrafenib Plus Trametinib in Patients With Resected BRAF V600-Mutant Stage III Melanoma. *J Clin Oncol***,** JCO1801219.

HAWKINS, P. C. D., SKILLMAN, A. G. & NICHOLLS, A. 2007. Comparison of Shape-Matching and Docking as Virtual Screening Tools. *Journal of Medicinal Chemistry,* 50**,** 74-82.

HELMA, J., CARDOSO, M. C., MUYLDERMANS, S. & LEONHARDT, H. 2015. Nanobodies and recombinant binders in cell biology. *J Cell Biol,* 209**,** 633-44.

HEVENER, K. E., ZHAO, W., BALL, D. M., BABAOGLU, K., QI, J., WHITE, S. W. & LEE, R. E. 2009. Validation of molecular docking programs for virtual screening against dihydropteroate synthase. *Journal of chemical information and modeling,* 49**,** 444-460.

HEY, T., FIEDLER, E., RUDOLPH, R. & FIEDLER, M. 2005. Artificial, non-antibody binding proteins for pharmaceutical and industrial applications. *Trends in Biotechnology,* 23**,** 514-522.

HOBBS, G. A., DER, C. J. & ROSSMAN, K. L. 2016a. RAS isoforms and mutations in cancer at a glance. *Journal of Cell Science,* 129**,** 1287-1292.

HOBBS, G. A., DER, C. J. & ROSSMAN, K. L. 2016b. RAS isoforms and mutations in cancer at a glance. *J Cell Sci,* 129**,** 1287-92.

HOCKER, H. J., CHO, K. J., CHEN, C. Y., RAMBAHAL, N., SAGINEEDU, S. R., SHAARI, K., STANSLAS, J., HANCOCK, J. F. & GORFE, A. A. 2013. Andrographolide derivatives inhibit guanine nucleotide exchange and abrogate oncogenic Ras function. *Proc Natl Acad Sci U S A,* 110**,** 10201-6.

HOOPER, A. J. & BURNETT, J. R. 2013. Anti-PCSK9 therapies for the treatment of hypercholesterolemia. *Expert Opin Biol Ther,* 13**,** 429-35.

HOPKINS, A. L. & GROOM, C. R. 2002. The druggable genome. *Nature Reviews Drug Discovery,* 1**,** 727-730.

HUGHES, D. J., TIEDE, C., PENSWICK, N., TANG, A. A., TRINH, C. H., MANDAL, U., ZAJAC, K. Z., GAULE, T., HOWELL, G., EDWARDS, T. A., DUAN, J., FEYFANT, E., MCPHERSON, M. J., TOMLINSON, D. C. & WHITEHOUSE, A. 2017. Generation of specific inhibitors of SUMO-1- and SUMO-2/3-mediated protein-protein interactions using Affimer (Adhiron) technology. *Sci Signal,* 10.

HUGHES, J. P., REES, S., KALINDJIAN, S. B. & PHILPOTT, K. L. 2011. Principles of early drug discovery. *British Journal of Pharmacology,* 162**,** 1239-1249.

HUMAN PROTEIN ATLAS. Available: https://www.proteinatlas.org/ [Accessed].

HUNTER, J. C., GURBANI, D., FICARRO, S. B., CARRASCO, M. A., LIM, S. M., CHOI, H. G., XIE, T., MARTO, J. A., CHEN, Z., GRAY, N. S. & WESTOVER, K. D. 2014. In situ selectivity profiling and crystal structure of SML-8-73-1, an active site inhibitor of oncogenic K-Ras G12C. *Proc Natl Acad Sci U S A,* 111**,** 8895-900.

JACKSON, J. H., LI, J. W., BUSS, J. E., DER, C. J. & COCHRANE, C. G. 1994. Polylysine domain of K-ras 4B protein is crucial for

malignant transformation. *Proc Natl Acad Sci U S A,* 91**,** 12730-4.

JAFFEE, E. M., HRUBAN, R. H., CANTO, M. & KERN, S. E. 2002. Focus on pancreas cancer. *Cancer Cell,* 2**,** 25-8.

JÄGER, V., BÜSSOW, K. & SCHIRRMANN, T. 2015. Transient Recombinant Protein Expression in Mammalian Cells.

JANCARIK, J. & KIM, S.-H. 1991. Sparse matrix sampling: a screening method for crystallization of proteins. *Journal of Applied Crystallography,* 24**,** 409-411.

JANES, M. R., ZHANG, J., LI, L. S., HANSEN, R., PETERS, U., GUO, X., CHEN, Y., BABBAR, A., FIRDAUS, S. J., DARJANIA, L., FENG, J., CHEN, J. H., LI, S., LI, S., LONG, Y. O., THACH, C., LIU, Y., ZARIEH, A., ELY, T., KUCHARSKI, J. M., KESSLER, L. V., WU, T., YU, K., WANG, Y., YAO, Y., DENG, X., ZARRINKAR, P. P., BREHMER, D., DHANAK, D., LORENZI, M. V., HU-LOWE, D., PATRICELLI, M. P., REN, P. & LIU, Y. 2018. Targeting KRAS Mutant Cancers with a Covalent G12C-Specific Inhibitor. *Cell,* 172**,** 578-589 e17.

JOCHIM, A. L. & ARORA, P. S. 2010. Systematic analysis of helical protein interfaces reveals targets for synthetic inhibitors. *ACS Chem Biol,* 5**,** 919-23.

JOHNSON, M. 2013. *Detergents: Triton X-100, Tween-20, and More.*

JONES, M. K. & JACKSON, J. H. 1998. Ras-GRF activates Ha-Ras, but not N-Ras or K-Ras 4B, protein in vivo. *Journal of Biological Chemistry,* 273**,** 1782-1787.

KAELIN, W. G., JR. 2005. The concept of synthetic lethality in the context of anticancer therapy. *Nat Rev Cancer,* 5**,** 689-98.

KANIE, T. & JACKSON, P. K. 2018. Guanine Nucleotide Exchange Assay Using Fluorescent MANT-GDP. *Bio-protocol,* 8**,** e2795.

KATO-STANKIEWICZ, J., HAKIMI, I., ZHI, G., ZHANG, J., SEREBRIISKII, I., GUO, L., EDAMATSU, H., KOIDE, H., MENON, S., ECKL, R., SAKAMURI, S., LU, Y., CHEN, Q.-Z., AGARWAL, S., BAUMBACH, W. R., GOLEMIS, E. A., TAMANOI, F. & KHAZAK, V. 2002. Inhibitors of Ras/Raf-1 interaction identified by two-hybrid screening revert Ras-dependent transformation phenotypes in human cancer cells. *Proceedings of the National Academy of Sciences,* 99**,** 14398-14403.

KAUKE, M. J., TRAXLMAYR, M. W., PARKER, J. A., KIEFER, J. D., KNIHTILA, R., MCGEE, J., VERDINE, G., MATTOS, C. & WITTRUP, K. D. 2017. An engineered protein antagonist of K-Ras/B-Raf interaction. *Sci Rep,* 7**,** 5831.

KENDREW, J. C., BODO, G., DINTZIS, H. M., PARRISH, R. G., WYCKOFF, H. & PHILLIPS, D. C. 1958. A three-dimensional model of the myoglobin molecule obtained by x-ray analysis. *Nature,* 181**,** 662-6.

KHAN, I., SPENCER-SMITH, R. & O'BRYAN, J. P. 2018. Targeting the alpha4-alpha5 dimerization interface of K-RAS inhibits tumor formation in vivo. *Oncogene.*

KHANNA, I. 2012. Drug discovery in pharmaceutical industry: productivity challenges and trends. *Drug Discovery Today,* 17**,** 1088-1102.

KIM, T. K. & EBERWINE, J. H. 2010. Mammalian cell transfection: the present and the future. *Anal Bioanal Chem,* 397**,** 3173-8.

KOHLER, G. & MILSTEIN, C. 1975. Continuous cultures of fused cells secreting antibody of predefined specificity. *Nature,* 256**,** 495-7.

KOIDE, A., BAILEY, C. W., HUANG, X. & KOIDE, S. 1998. The fibronectin type III domain as a scaffold for novel binding proteins. *J Mol Biol,* 284**,** 1141-51.

KOUTSOUMPELI, E., TIEDE, C., MURRAY, J., TANG, A., BON, R. S., TOMLINSON, D. C. & JOHNSON, S. 2017. Antibody Mimetics for the Detection of Small Organic Compounds Using a Quartz Crystal Microbalance. *Analytical Chemistry,* 89**,** 3051-3058.

KRAULIS, P. J., DOMAILLE, P. J., CAMPBELL-BURK, S. L., VAN AKEN, T. & LAUE, E. D. 1994. Solution structure and dynamics of ras p21.GDP determined by heteronuclear three- and four-dimensional NMR spectroscopy. *Biochemistry,* 33**,** 3515-31.

KRISSINEL, E. & HENRICK, K. 2007. Inference of macromolecular assemblies from crystalline state. *Journal of Molecular Biology,* 372**,** 774-797.

KUMAR, M. S., HANCOCK, D. C., MOLINA-ARCAS, M., STECKEL, M., EAST, P., DIEFENBACHER, M., ARMENTEROS-MONTERROSO, E., LASSAILLY, F., MATTHEWS, N., NYE, E., STAMP, G., BEHRENS, A. & DOWNWARD, J. 2012. The GATA2 transcriptional network is requisite for RAS oncogene-driven non-small cell lung cancer. *Cell,* 149**,** 642-55.

KUMMER, L., HSU, C. W., DAGLIYAN, O., MACNEVIN, C., KAUFHOLZ, M., ZIMMERMANN, B., DOKHOLYAN, N. V., HAHN, K. M. & PLUCKTHUN, A. 2013. Knowledge-based design of a biosensor to quantify localized ERK activation in living cells. *Chem Biol,* 20**,** 847-56.

KYLE, H. F., WICKSON, K. F., STOTT, J., BURSLEM, G. M., BREEZE, A. L., TIEDE, C., TOMLINSON, D. C., WARRINER, S. L., NELSON, A., WILSON, A. J. & EDWARDS, T. A. 2015. Exploration of the HIF-1alpha/p300 interface using peptide and Adhiron phage display technologies. *Mol Biosyst,* 11**,** 2738-49.

LACOUTURE, M. E., O'REILLY, K., ROSEN, N. & SOLIT, D. B. 2012. Induction of cutaneous squamous cell carcinomas by RAF inhibitors: cause for concern? *J Clin Oncol,* 30**,** 329-30.

LAU, J. L. & DUNN, M. K. 2018. Therapeutic peptides: Historical perspectives, current development trends, and future directions. *Bioorganic & Medicinal Chemistry,* 26**,** 2700-2707.

LAVECCHIA, A. & DI GIOVANNI, C. 2013. Virtual screening strategies in drug discovery: a critical review. *Curr Med Chem,* 20**,** 2839-60.

LEDFORD, H. 2015. Cancer: The Ras renaissance. *Nature,* 520**,** 278-80.

LEFEVRE, F., REMY, M. H. & MASSON, J. M. 1997. Alanine-stretch scanning mutagenesis: a simple and efficient method to probe protein structure and function. *Nucleic Acids Res,* 25**,** 447-8.

LEHMANN, A. 2008. Ecallantide (DX-88), a plasma kallikrein inhibitor for the treatment of hereditary angioedema and the prevention of blood loss in on-pump cardiothoracic surgery. *Expert Opin Biol Ther,* 8**,** 1187-99.

LEON, J., GUERRERO, I. & PELLICER, A. 1987a. Differential expression of the ras gene family in mice. *Mol Cell Biol,* 7**,** 1535-40.

LEON, J., GUERRERO, I. & PELLICER, A. 1987b. DIFFERENTIAL EXPRESSION OF THE RAS GENE FAMILY IN MICE. *Molecular and Cellular Biology,* 7**,** 1535-1540.

LESHCHINER, E. S., PARKHITKO, A., BIRD, G. H., LUCCARELLI, J., BELLAIRS, J. A., ESCUDERO, S., OPOKU-NSIAH, K., GODES, M., PERRIMON, N. & WALENSKY, L. D. 2015. Direct inhibition of oncogenic KRAS by hydrocarbon-stapled SOS1 helices. *Proc Natl Acad Sci U S A,* 112**,** 1761-6.

LESLEY, S. A. & WILSON, I. A. 2005. Protein production and crystallization at the joint center for structural genomics. *J Struct Funct Genomics,* 6**,** 71-9.

LIM, S. M., WESTOVER, K. D., FICARRO, S. B., HARRISON, R. A., CHOI, H. G., PACOLD, M. E., CARRASCO, M., HUNTER, J., KIM, N. D., XIE, T., SIM, T., JANNE, P. A., MEYERSON, M., MARTO, J. A., ENGEN, J. R. & GRAY, N. S. 2014.

Therapeutic targeting of oncogenic K-Ras by a covalent catalytic site inhibitor. *Angew Chem Int Ed Engl,* 53**,** 199-204.

LITO, P., ROSEN, N. & SOLIT, D. B. 2013. Tumor adaptation and resistance to RAF inhibitors. *Nat Med,* 19**,** 1401-9.

LITO, P., SOLOMON, M., HANSEN, R., LI, L. S. & ROSEN, N. 2016. Allele-specific inhibitors inactivate mutant KRAS G12C by a trapping mechanism. *Cancer Research,* 76.

LIU, H. & NAISMITH, J. H. 2008. An efficient one-step site-directed deletion, insertion, single and multiple-site plasmid mutagenesis protocol. *BMC biotechnology,* 8**,** 91-91.

LLUFRIO, E. M., WANG, L., NASER, F. J. & PATTI, G. J. 2018. Sorting cells alters their redox state and cellular metabolome. *Redox Biol,* 16**,** 381-387.

LOFBLOM, J., FELDWISCH, J., TOLMACHEV, V., CARLSSON, J., STAHL, S. & FREJD, F. Y. 2010a. Affibody molecules: engineered proteins for therapeutic, diagnostic and biotechnological applications. *FEBS Lett,* 584**,** 2670-80.

LOFBLOM, J., FELDWISCH, J., TOLMACHEV, V., CARLSSON, J., STAHL, S. & FREJD, F. Y. 2010b. Affibody molecules: Engineered proteins for therapeutic, diagnostic and biotechnological applications. *Febs Letters,* 584**,** 2670-2680.

LONDON, N., RAVEH, B. & SCHUELER-FURMAN, O. 2013. Druggable protein-protein interactions--from hot spots to hot segments. *Curr Opin Chem Biol,* 17**,** 952-9.

LONN, P., KACSINTA, A. D., CUI, X. S., HAMIL, A. S., KAULICH, M., GOGOI, K. & DOWDY, S. F. 2016. Enhancing Endosomal Escape for Intracellular Delivery of Macromolecular Biologic Therapeutics. *Sci Rep,* 6**,** 32301.

LOWY, D. R. & WILLUMSEN, B. M. 1993. Function and regulation of ras. *Annu Rev Biochem,* 62**,** 851-91.

LUFT, J. R., WOLFLEY, J. R., SAID, M. I., NAGEL, R. M., LAURICELLA, A. M., SMITH, J. L., THAYER, M. H., VEATCH, C. K., SNELL, E. H., MALKOWSKI, M. G. & DETITTA, G. T. 2007. Efficient optimization of crystallization conditions by manipulation of drop volume ratio and temperature. *Protein Sci,* 16**,** 715-22.

LUO, J., EMANUELE, M. J., LI, D., CREIGHTON, C. J., SCHLABACH, M. R., WESTBROOK, T. F., WONG, K. K. & ELLEDGE, S. J. 2009. A genome-wide RNAi screen identifies multiple synthetic lethal interactions with the Ras oncogene. *Cell,* 137**,** 835-48.

MACARTHUR, M. W. & THORNTON, J. M. 1991. Influence of proline residues on protein conformation. *J Mol Biol,* 218**,** 397-412.

MAHER, J., BAKER, D. A., MANNING, M., DIBB, N. J. & ROBERTS, I. A. 1995. Evidence for cell-specific differences in transformation by N-, H- and K-ras. *Oncogene,* 11**,** 1639-47.

MANGLIK, A., KOBILKA, B. K. & STEYAERT, J. 2017. Nanobodies to Study G Protein-Coupled Receptor Structure and Function. *Annu Rev Pharmacol Toxicol,* 57**,** 19-37.

MARSCHALL, A. L., DUBEL, S. & BOLDICKE, T. 2015. Specific in vivo knockdown of protein function by intrabodies. *MAbs,* 7**,** 1010-35.

MARTIN-GAGO, P., FANSA, E. K., KLEIN, C. H., MURARKA, S., JANNING, P., SCHURMANN, M., METZ, M., ISMAIL, S., SCHULTZ-FADEMRECHT, C., BAUMANN, M., BASTIAENS, P. I. H., WITTINGHOFER, A. & WALDMANN, H. 2017. A PDE6 delta-KRas Inhibitor Chemotype with up to Seven H-Bonds and Picomolar Affinity that Prevents Efficient Inhibitor Release by Arl2. *Angewandte Chemie-International Edition,* 56**,** 2423-2428.

MARTIN, H. L., BEDFORD, R., HESELTINE, S. J., TANG, A. A., HAZA, K. Z., RAO, A., MCPHERSON, M. J. & TOMLINSON, D. C. 2018. Non-immunoglobulin scaffold proteins: Precision tools for studying protein-protein interactions in cancer. *New Biotechnology,* 45**,** 28-35.

MASCARENHAS-SARAIVA, M. J. & MASCARENHAS-SARAIVA, M. 2018. Effectiveness and tolerability of linaclotide in the treatment of IBS-C in a "real-life" setting: Results from a Portuguese single-center study. *Neurogastroenterol Motil***,** e13508.

MATALLANAS, D., AROZARENA, I., BERCIANO, M. T., AARONSON, D. S., PELLICER, A., LAFARGA, M. & CRESPO, P. 2003. Differences on the inhibitory specificities of H-Ras, K-Ras, and N-Ras (N17) dominant negative mutants are related to their membrane microlocalization. *J Biol Chem,* 278**,** 4572-81.

MAURER, T., GARRENTON, L. S., OH, A., PITTS, K., ANDERSON, D. J., SKELTON, N. J., FAUBER, B. P., PAN, B., MALEK, S., STOKOE, D., LUDLAM, M. J., BOWMAN, K. K., WU, J., GIANNETTI, A. M., STAROVASNIK, M. A., MELLMAN, I., JACKSON, P. K., RUDOLPH, J., WANG, W. & FANG, G. 2012. Small-molecule ligands bind to a distinct pocket in Ras

and inhibit SOS-mediated nucleotide exchange activity. *Proc Natl Acad Sci U S A,* 109**,** 5299-304.

MCCORMICK, F. 2016. K-Ras protein as a drug target. *Journal of Molecular Medicine-Jmm,* 94**,** 253-258.

MCCOY, A. J., GROSSE-KUNSTLEVE, R. W., ADAMS, P. D., WINN, M. D., STORONI, L. C. & READ, R. J. 2007. Phaser crystallographic software. *Journal of Applied Crystallography,* 40**,** 658-674.

MCGEE, J. H., SHIM, S. Y., LEE, S. J., SWANSON, P. K., JIANG, S. Y., DURNEY, M. A. & VERDINE, G. L. 2018. Exceptionally high-affinity Ras binders that remodel its effector domain. *The Journal of biological chemistry,* 293**,** 3265-3280.

MCLACHLAN, A. D. 1972. Protein Structure and Function. *Annual Review of Physical Chemistry,* 23**,** 165-192.

MCPHERSON, A. & CUDNEY, B. 2014. Optimization of crystallization conditions for biological macromolecules. *Acta Crystallogr F Struct Biol Commun,* 70**,** 1445-67.

MCPHERSON, A. & GAVIRA, J. A. 2014. Introduction to protein crystallization. *Acta Crystallogr F Struct Biol Commun,* 70**,** 2-20.

MIRATITHERAPEUTICS. 2018. *KRAS G12C Inhibitor (MRTX849)* [Online]. https://www.mirati.com/mrtx849/. Available: https://www.mirati.com/mrtx849/ [Accessed 02.01.2019 2019].

MITSUUCHI, Y. & TESTA, J. R. 2002. Cytogenetics and molecular genetics of lung cancer. *Am J Med Genet,* 115, 183-8.

MODELL, A. E., BLOSSER, S. L. & ARORA, P. S. 2016. Systematic Targeting of Protein-Protein Interactions. *Trends in pharmacological sciences,* 37**,** 702-713.

MORRIS, E. J., JHA, S., RESTAINO, C. R., DAYANANTH, P., ZHU, H., COOPER, A., CARR, D., DENG, Y., JIN, W., BLACK, S., LONG, B., LIU, J., DINUNZIO, E., WINDSOR, W., ZHANG, R., ZHAO, S., ANGAGAW, M. H., PINHEIRO, E. M., DESAI, J., XIAO, L., SHIPPS, G., HRUZA, A., WANG, J., KELLY, J., PALIWAL, S., GAO, X., BABU, B. S., ZHU, L., DAUBLAIN, P., ZHANG, L., LUTTERBACH, B. A., PELLETIER, M. R., PHILIPPAR, U., SILIPHAIVANH, P., WITTER, D., KIRSCHMEIER, P., BISHOP, W. R., HICKLIN, D., GILLILAND, D. G., JAYARAMAN, L., ZAWEL, L., FAWELL, S. & SAMATAR, A. A. 2013. Discovery of a novel ERK inhibitor with activity in models of acquired resistance to BRAF and MEK inhibitors. *Cancer Discov,* 3**,** 742-50.

MULLARD, A. 2012. Cholesterol-lowering blockbuster candidates speed into Phase III trials. *Nat Rev Drug Discov,* 11**,** 817-9.

MURATA, K. & WOLF, M. 2018. Cryo-electron microscopy for structural analysis of dynamic biological macromolecules. *Biochim Biophys Acta Gen Subj,* 1862**,** 324-334.

MURSHUDOV, G. N., VAGIN, A. A. & DODSON, E. J. 1997. Refinement of macromolecular structures by the maximum-likelihood method. *Acta Crystallographica Section D-Structural Biology,* 53**,** 240-255.

NERO, T. L., MORTON, C. J., HOLIEN, J. K., WIELENS, J. & PARKER, M. W. 2014. Oncogenic protein interfaces: small molecules, big challenges. *Nature Reviews Cancer,* 14**,** 248-262.

NOH, K., KIM, K. O., PATEL, N. R., STAPLES, J. R., MINEMATSU, H., NAIR, K. & LEE, F. Y. 2011. Targeting inflammatory kinase as an adjuvant treatment for osteosarcomas. *J Bone Joint Surg Am,* 93**,** 723-32.

O'HAGAN, R. C. & HEYER, J. 2011. KRAS Mouse Models: Modeling Cancer Harboring KRAS Mutations. *Genes Cancer,* 2**,** 335-43.

OMEROVIC, J., HAMMOND, D. E., CLAGUE, M. J. & PRIOR, I. A. 2008. Ras isoform abundance and signalling in human cancer cell lines. *Oncogene,* 27**,** 2754-2762.

OSTREM, J. M., PETERS, U., SOS, M. L., WELLS, J. A. & SHOKAT, K. M. 2013. K-Ras(G12C) inhibitors allosterically control GTP affinity and effector interactions. *Nature,* 503**,** 548-51.

PAPKE, B. & DER, C. J. 2017. Drugging RAS: Know the enemy. *Science,* 355**,** 1158-1163.

PATGIRI, A., YADAV, K. K., ARORA, P. S. & BAR-SAGI, D. 2011. An orthosteric inhibitor of the Ras-Sos interaction. *Nat Chem Biol,* 7**,** 585-7.

PATRICELLI, M. P., JANES, M. R., LI, L. S., HANSEN, R., PETERS, U., KESSLER, L. V., CHEN, Y. C., KUCHARSKI, J. M., FENG, J., ELY, T., CHEN, J. H., FIRDAUS, S. J., BABBAR, A., REN, P. D. & LIU, Y. 2016. Selective Inhibition of Oncogenic KRAS Output with Small Molecules Targeting the Inactive State. *Cancer Discovery,* 6**,** 316-329.

PEREZ-MARTINEZ, D., TANAKA, T. & RABBITTS, T. H. 2010. Intracellular antibodies and cancer: New technologies offer therapeutic opportunities. *Bioessays,* 32**,** 589-598.

PETERS, W. B., FRASCA, V. & BROWN, R. K. 2009. Recent developments in isothermal titration calorimetry label free screening. *Comb Chem High Throughput Screen,* 12**,** 772-90.

PIRKMAJER, S. & CHIBALIN, A. V. 2011. Serum starvation: caveat emptor. *Am J Physiol Cell Physiol,* 301**,** C272-9.

PLANCHARD, D., SMIT, E. F., GROEN, H. J. M., MAZIERES, J., BESSE, B., HELLAND, A., GIANNONE, V., D'AMELIO, A. M., JR., ZHANG, P., MOOKERJEE, B. & JOHNSON, B. E. 2017. Dabrafenib plus trametinib in patients with previously untreated BRAF(V600E)-mutant metastatic non-small-cell lung cancer: an open-label, phase 2 trial. *Lancet Oncol,* 18**,** 1307-1316.

PLUCKTHUN, A. 2015. Designed ankyrin repeat proteins (DARPins): binding proteins for research, diagnostics, and therapy. *Annu Rev Pharmacol Toxicol,* 55**,** 489-511.

POPP, D., KOH, F., SCIPION, C. P. M., GHOSHDASTIDER, U., NARITA, A., HOLMES, K. C. & ROBINSON, R. C. 2018. Advances in Structural Biology and the Application to Biological Filament Systems. *BioEssays,* 40**,** 1700213.

PULCIANI, S., SANTOS, E., LONG, L. K., SORRENTINO, V. & BARBACID, M. 1985. ras gene Amplification and malignant transformation. *Mol Cell Biol,* 5**,** 2836-41.

QUEVEDO, C. E., CRUZ-MIGONI, A., BERY, N., MILLER, A., TANAKA, T., PETCH, D., BATAILLE, C. J. R., LEE, L. Y. W., FALLON, P. S., TULMIN, H., EHEBAUER, M. T., FERNANDEZ-FUENTES, N., RUSSELL, A. J., CARR, S. B., PHILLIPS, S. E. V. & RABBITTS, T. H. 2018. Small molecule inhibitors of RAS-effector protein interactions derived using an intracellular antibody fragment. *Nature Communications,* 9**,** 3169.

RAINA, M., SHARMA, R., DEACON, S. E., TIEDE, C., TOMLINSON, D., DAVIES, A. G., MCPHERSON, M. J. & WALTI, C. 2015. Antibody mimetic receptor proteins for label-free biosensors. *Analyst,* 140**,** 803-10.

RAWLINGS, A. E., BRAMBLE, J. P., TANG, A. A. S., SOMNER, L. A., MONNINGTON, A. E., COOKE, D. J., MCPHERSON, M. J., TOMLINSON, D. C. & STANILAND, S. S. 2015. Phage display selected magnetite interacting Adhirons for shape controlled nanoparticle synthesis. *Chemical Science,* 6**,** 5586-5594.

RICHTER, A., EGGENSTEIN, E. & SKERRA, A. 2014. Anticalins: exploiting a non-Ig scaffold with hypervariable loops for the engineering of binding proteins. *FEBS Lett,* 588**,** 213-8.

ROBINSON, J. I., BAXTER, E. W., OWEN, R. L., THOMSEN, M., TOMLINSON, D. C., WATERHOUSE, M. P., WIN, S. J., NETTLESHIP, J. E., TIEDE, C., FOSTER, R. J., OWENS, R.

J., FISHWICK, C. W. G., HARRIS, S. A., GOLDMAN, A., MCPHERSON, M. J. & MORGAN, A. W. 2018. Affimer proteins inhibit immune complex binding to FcgammaRIIIa with high specificity through competitive and allosteric modes of action. *Proc Natl Acad Sci U S A,* 115**,** E72-E81.

RODENHUIS, S. & SLEBOS, R. J. 1992. Clinical significance of ras oncogene activation in human lung cancer. *Cancer Res,* 52**,** 2665s-2669s.

RODON, J., OMLIN, A., HERBSCHLEB, K. H., GARCIA-CORBACHO, J., JAN STEINER, I. D., CHRISTOF ZITT, D. F., TURNER, D., DAWSON, K. M., STUMPP, M. T., GILBOY, P., HARSTRICK, A., AZARO, A., ACKERMANN, C. J., MIDDLETON, M. R. & BAIRD, R. D. 2015. First-in-human Phase I study to evaluate MP0250, a DARPin® blocking HGF and VEGF, in patients with advanced solid tumors. *AACR-NCI-EORTC International Conference on Molecular Targets and Cancer Therapeutics.* Boston, MA.

ROSKOSKI, R., JR. 2012. ERK1/2 MAP kinases: structure, function, and regulation. *Pharmacol Res,* 66**,** 105-43.

RYAN, M. B. & CORCORAN, R. B. 2018. Therapeutic strategies to target RAS-mutant cancers. *Nature Reviews Clinical Oncology,* 15**,** 709-720.

S SMITH, H. & DEER, T. 2009. *Safety and efficacy of intrathecal ziconotide in the management of severe chronic pain*.

SAAFAN, H., FOERSTER, S., PARRA-GUILLEN, Z. P., HAMMER, E., MICHAELIS, M., CINATL, J., VÖLKER, U., FRÖHLICH, H., KLOFT, C. & RITTER, C. A. 2016. Utilising the EGFR interactome to identify mechanisms of drug resistance in non-small cell lung cancer – Proof of concept towards a systems pharmacology approach. *European Journal of Pharmaceutical Sciences,* 94**,** 20-32.

SAMATAR, A. A. & POULIKAKOS, P. I. 2014. Targeting RAS-ERK signalling in cancer: promises and challenges. *Nature Reviews Drug Discovery,* 13**,** 928-+.

SCOLNICK, E. M. 1982. Hyperplastic and Neoplastic Erythroproliferative Diseases Induced by Oncogenic Murine Retroviruses. *Biochimica Et Biophysica Acta,* 651**,** 273-283.

SCOLNICK, E. M., PAPAGEORGE, A. G. & SHIH, T. Y. 1979. Guanine Nucleotide-Binding Activity as an Assay for Src Protein of Rat-Derived Murine Sarcoma-Viruses. *Proceedings of the National Academy of Sciences of the United States of America,* 76**,** 5355-5359.

SEBAUGH, J. L. 2011. Guidelines for accurate EC50/IC50 estimation. *Pharm Stat,* 10**,** 128-34.

SHA, F., GENCER, E. B., GEORGEON, S., KOIDE, A., YASUI, N., KOIDE, S. & HANTSCHEL, O. 2013. Dissection of the BCR-ABL signaling network using highly specific monobody inhibitors to the SHP2 SH2 domains. *Proceedings of the National Academy of Sciences,* 110**,** 14924-14929.

SHAGIN, D. A., BARSOVA, E. V., YANUSHEVICH, Y. G., FRADKOV, A. F., LUKYANOV, K. A., LABAS, Y. A., SEMENOVA, T. N., UGALDE, J. A., MEYERS, A., NUNEZ, J. M., WIDDER, E. A., LUKYANOV, S. A. & MATZ, M. V. 2004. GFP-like proteins as ubiquitous metazoan superfamily: evolution of functional features and structural complexity. *Mol Biol Evol,* 21**,** 841-50.

SHAH, B. H., FARSHORI, M. P., JAMBUSARIA, A. & CATT, K. J. 2003. Roles of Src and epidermal growth factor receptor transactivation in transient and sustained ERK1/2 responses to gonadotropin-releasing hormone receptor activation. *J Biol Chem,* 278**,** 19118-26.

SHARMA, R., DEACON, S. E., NOWAK, D., GEORGE, S. E., SZYMONIK, M. P., TANG, A. A. S., TOMLINSON, D. C., DAVIES, A. G., MCPHERSON, M. J. & WALTI, C. 2016. Label-free electrochemical impedance biosensor to detect human interleukin-8 in serum with sub-pg/ml sensitivity. *Biosensors & Bioelectronics,* 80**,** 607-613.

SHI, Y. 2014. A glimpse of structural biology through X-ray crystallography. *Cell,* 159**,** 995-1014.

SHIMA, F., YOSHIKAWA, Y., YE, M., ARAKI, M., MATSUMOTO, S., LIAO, J., HU, L., SUGIMOTO, T., IJIRI, Y., TAKEDA, A., NISHIYAMA, Y., SATO, C., MURAOKA, S., TAMURA, A., OSODA, T., TSUDA, K., MIYAKAWA, T., FUKUNISHI, H., SHIMADA, J., KUMASAKA, T., YAMAMOTO, M. & KATAOKA, T. 2013a. In silico discovery of small-molecule Ras inhibitors that display antitumor activity by blocking the Ras-effector interaction. *Proc Natl Acad Sci U S A,* 110**,** 8182-7.

SHIMA, F., YOSHIKAWA, Y., YE, M., ARAKI, M., MATSUMOTO, S., LIAO, J. L., HU, L. Z., SUGIMOTO, T., IJIRI, Y., TAKEDA, A., NISHIYAMA, Y., SATO, C., MURAOKA, S., TAMURA, A., OSODA, T., TSUDA, K., MIYAKAWA, T., FUKUNISHI, H., SHIMADA, J., KUMASAKA, T., YAMAMOTO, M. & KATAOKA, T. 2013b. In silico discovery of small-molecule Ras inhibitors that display antitumor activity by blocking the Ras-effector

interaction. *Proceedings of the National Academy of Sciences of the United States of America,* 110**,** 8182-8187.

SHIMIZU, K., GOLDFARB, M., PERUCHO, M. & WIGLER, M. 1983. ISOLATION AND PRELIMINARY CHARACTERIZATION OF THE TRANSFORMING GENE OF A HUMAN NEURO-BLASTOMA CELL-LINE. *Proceedings of the National Academy of Sciences of the United States of America-Biological Sciences,* 80**,** 383-387.

SILACCI, M., LEMBKE, W., WOODS, R., ATTINGER-TOLLER, I., BAENZIGER-TOBLER, N., BATEY, S., SANTIMARIA, R., VON DER BEY, U., KOENIG-FRIEDRICH, S., ZHA, W., SCHLERETH, B., LOCHER, M., BERTSCHINGER, J. & GRABULOVSKI, D. 2016. Discovery and characterization of COVA322, a clinical-stage bispecific TNF/IL-17A inhibitor for the treatment of inflammatory diseases. *MAbs,* 8**,** 141-9.

SILVERMAN, J., LIU, Q., BAKKER, A., TO, W., DUGUAY, A., ALBA, B. M., SMITH, R., RIVAS, A., LI, P., LE, H., WHITEHORN, E., MOORE, K. W., SWIMMER, C., PERLROTH, V., VOGT, M., KOLKMAN, J. & STEMMER, W. P. 2005. Multivalent avimer proteins evolved by exon shuffling of a family of human receptor domains. *Nat Biotechnol,* 23**,** 1556-61.

SIMEONE, E., GRIMALDI, A. M., FESTINO, L., VANELLA, V., PALLA, M. & ASCIERTO, P. A. 2017. Combination Treatment of Patients with BRAF-Mutant Melanoma: A New Standard of Care. *BioDrugs,* 31**,** 51-61.

SINGH, A., SWEENEY, M. F., YU, M., BURGER, A., GRENINGER, P., BENES, C., HABER, D. A. & SETTLEMAN, J. 2012. TAK1 inhibition promotes apoptosis in KRAS-dependent colon cancers. *Cell,* 148**,** 639-50.

SINGH, M., LIMA, A., MOLINA, R., HAMILTON, P., CLERMONT, A. C., DEVASTHALI, V., THOMPSON, J. D., CHENG, J. H., BOU RESLAN, H., HO, C. C., CAO, T. C., LEE, C. V., NANNINI, M. A., FUH, G., CARANO, R. A., KOEPPEN, H., YU, R. X., FORREST, W. F., PLOWMAN, G. D. & JOHNSON, L. 2010. Assessing therapeutic responses in Kras mutant cancers using genetically engineered mouse models. *Nat Biotechnol,* 28**,** 585-93.

SKERRA, A. 2007. Alternative non-antibody scaffolds for molecular recognition. *Current Opinion in Biotechnology,* 18**,** 295-304.

SMITH, M. J., NEEL, B. G. & IKURA, M. 2013. NMR-based functional profiling of RASopathies and oncogenic RAS mutations. *Proc Natl Acad Sci U S A,* 110**,** 4574-9.

SMYTH, D. R., MROZKIEWICZ, M. K., MCGRATH, W. J., LISTWAN, P. & KOBE, B. 2003. Crystal structures of fusion proteins with large-affinity tags. *Protein Sci,* 12**,** 1313-22.

SON, J., LYSSIOTIS, C. A., YING, H., WANG, X., HUA, S., LIGORIO, M., PERERA, R. M., FERRONE, C. R., MULLARKY, E., SHYH-CHANG, N., KANG, Y., FLEMING, J. B., BARDEESY, N., ASARA, J. M., HAIGIS, M. C., DEPINHO, R. A., CANTLEY, L. C. & KIMMELMAN, A. C. 2013. Glutamine supports pancreatic cancer growth through a KRAS-regulated metabolic pathway. *Nature,* 496**,** 101-5.

SONDERMANN, H., SOISSON, S. M., BOYKEVISCH, S., YANG, S. S., BAR-SAGI, D. & KURIYAN, J. 2004. Structural analysis of autoinhibition in the Ras activator Son of sevenless. *Cell,* 119**,** 393-405.

SPENCER-SMITH, R., KOIDE, A., ZHOU, Y., EGUCHI, R. R., SHA, F., GAJWANI, P., SANTANA, D., GUPTA, A., JACOBS, M., HERRERO-GARCIA, E., COBBERT, J., LAVOIE, H., SMITH, M., RAJAKULENDRAN, T., DOWDELL, E., OKUR, M. N., DEMENTIEVA, I., SICHERI, F., THERRIEN, M., HANCOCK, J. F., IKURA, M., KOIDE, S. & O'BRYAN, J. P. 2017a. Inhibition of RAS function through targeting an allosteric regulatory site. *Nat Chem Biol,* 13**,** 62-68.

SPENCER-SMITH, R., KOIDE, A., ZHOU, Y., EGUCHI, R. R., SHE, F., GAJWANI, P., SANTANA, D., GUPTA, A., JACOBS, M., HERRERO-GARCIA, E., COBBERT, J., LAVOIE, H., SMITH, M., RAJAKULENDRAN, T., DOWDELL, E., OKUR, M. N., DEMENTIEVA, I., SICHERI, F., THERRIEN, M., HANCOCK, J. F., IKURA, M., KOIDE, S. & O'BRYAN, J. P. 2017b. Inhibition of RAS function through targeting an allosteric regulatory site. *Nature Chemical Biology,* 13**,** 62-68.

SPOERNER, M., HERRMANN, C., VETTER, I. R., KALBITZER, H. R. & WITTINGHOFER, A. 2001. Dynamic properties of the Ras switch I region and its importance for binding to effectors. *Proceedings of the National Academy of Sciences of the United States of America,* 98**,** 4944-4949.

SPOERNER, M., HOZSA, C., POETZL, J. A., REISS, K., GANSER, P., GEYER, M. & KALBITZER, H. R. 2010. Conformational states of human rat sarcoma (Ras) protein complexed with its natural ligand GTP and their role for effector interaction and GTP hydrolysis. *The Journal of biological chemistry,* 285**,** 39768-78.

SPOERNER, M., WITTINGHOFER, A. & KALBITZER, H. R. 2004. Perturbation of the conformational equilibria in Ras by

selective mutations as studied by 31P NMR spectroscopy. *FEBS Lett,* 578**,** 305-10.

STADLER, L. K., HOFFMANN, T., TOMLINSON, D. C., SONG, Q., LEE, T., BUSBY, M., NYATHI, Y., GENDRA, E., TIEDE, C., FLANAGAN, K., COCKELL, S. J., WIPAT, A., HARWOOD, C., WAGNER, S. D., KNOWLES, M. A., DAVIS, J. J., KEEGAN, N. & FERRIGNO, P. K. 2011. Structure-function studies of an engineered scaffold protein derived from Stefin A. II: Development and applications of the SQT variant. *Protein Eng Des Sel,* 24**,** 751-63.

STECKEL, M., MOLINA-ARCAS, M., WEIGELT, B., MARANI, M., WARNE, P. H., KUZNETSOV, H., KELLY, G., SAUNDERS, B., HOWELL, M., DOWNWARD, J. & HANCOCK, D. C. 2012. Determination of synthetic lethal interactions in KRAS oncogene-dependent cancer cells reveals novel therapeutic targeting strategies. *Cell Res,* 22**,** 1227-45.

STUMPF, M. P., THORNE, T., DE SILVA, E., STEWART, R., AN, H. J., LAPPE, M. & WIUF, C. 2008. Estimating the size of the human interactome. *Proc Natl Acad Sci U S A,* 105**,** 6959-64.

STUMPP, M. T., BINZ, H. K. & AMSTUTZ, P. 2008. DARPins: a new generation of protein therapeutics. *Drug Discov Today,* 13**,** 695-701.

SU, A. I., WILTSHIRE, T., BATALOV, S., LAPP, H., CHING, K. A., BLOCK, D., ZHANG, J., SODEN, R., HAYAKAWA, M., KREIMAN, G., COOKE, M. P., WALKER, J. R. & HOGENESCH, J. B. 2004. A gene atlas of the mouse and human protein-encoding transcriptomes. *Proc Natl Acad Sci U S A,* 101**,** 6062-7.

SU, F., VIROS, A., MILAGRE, C., TRUNZER, K., BOLLAG, G., SPLEISS, O., REIS-FILHO, J. S., KONG, X., KOYA, R. C., FLAHERTY, K. T., CHAPMAN, P. B., KIM, M. J., HAYWARD, R., MARTIN, M., YANG, H., WANG, Q., HILTON, H., HANG, J. S., NOE, J., LAMBROS, M., GEYER, F., DHOMEN, N., NICULESCU-DUVAZ, I., ZAMBON, A., NICULESCU-DUVAZ, D., PREECE, N., ROBERT, L., OTTE, N. J., MOK, S., KEE, D., MA, Y., ZHANG, C., HABETS, G., BURTON, E. A., WONG, B., NGUYEN, H., KOCKX, M., ANDRIES, L., LESTINI, B., NOLOP, K. B., LEE, R. J., JOE, A. K., TROY, J. L., GONZALEZ, R., HUTSON, T. E., PUZANOV, I., CHMIELOWSKI, B., SPRINGER, C. J., MCARTHUR, G. A., SOSMAN, J. A., LO, R. S., RIBAS, A. & MARAIS, R. 2012. RAS mutations in cutaneous squamous-cell carcinomas in

patients treated with BRAF inhibitors. *N Engl J Med,* 366**,** 207-15.

SUBEDI, G. P., JOHNSON, R. W., MONIZ, H. A., MOREMEN, K. W. & BARB, A. 2015. High Yield Expression of Recombinant Human Proteins with the Transient Transfection of HEK293 Cells in Suspension. *J Vis Exp,* e53568.

SUN, J., QIAN, Y., HAMILTON, A. D. & SEBTI, S. M. 1995. Ras CAAX peptidomimetic FTI 276 selectively blocks tumor growth in nude mice of a human lung carcinoma with K-Ras mutation and p53 deletion. *Cancer Res,* 55**,** 4243-7.

SUN, Q., BURKE, J. P., PHAN, J., BURNS, M. C., OLEJNICZAK, E. T., WATERSON, A. G., LEE, T., ROSSANESE, O. W. & FESIK, S. W. 2012. Discovery of small molecules that bind to K-Ras and inhibit Sos-mediated activation. *Angew Chem Int Ed Engl,* 51**,** 6140-3.

SYDOR, J. R., ENGELHARD, M., WITTINGHOFER, A., GOODY, R. S. & HERRMANN, C. 1998. Transient kinetic studies on the interaction of Ras and the Ras-binding domain of c-Raf-1 reveal rapid equilibration of the complex. *Biochemistry,* 37**,** 14292-9.

TANAKA, T., LOBATO, M. N. & RABBITTS, T. H. 2003. Single domain intracellular antibodies: a minimal fragment for direct in vivo selection of antigen-specific intrabodies. *J Mol Biol,* 331**,** 1109-20.

TANAKA, T. & RABBITTS, T. H. 2003. Intrabodies based on intracellular capture frameworks that bind the RAS protein with high affinity and impair oncogenic transformation. *Embo Journal,* 22**,** 1025-1035.

TANAKA, T. & RABBITTS, T. H. 2010. Interfering with RAS-effector protein interactions prevent RAS-dependent tumour initiation and causes stop-start control of cancer growth. *Oncogene,* 29**,** 6064-6070.

TANAKA, T., WILLIAMS, R. L. & RABBITTS, T. H. 2007. Tumour prevention by a single antibody domain targeting the interaction of signal transduction proteins with RAS. *Embo Journal,* 26**,** 3250-3259.

TAVERAS, A. G., REMISZEWSKI, S. W., DOLL, R. J., CESARZ, D., HUANG, E. C., KIRSCHMEIER, P., PRAMANIK, B. N., SNOW, M. E., WANG, Y. S., DEL ROSARIO, J. D., VIBULBHAN, B., BAUER, B. B., BROWN, J. E., CARR, D., CATINO, J., EVANS, C. A., GIRIJAVALLABHAN, V., HEIMARK, L., JAMES, L., LIBERLES, S., NASH, C., PERKINS, L., SENIOR, M. M., TSARBOPOULOS, A.,

WEBBER, S. E. & ET AL. 1997. Ras oncoprotein inhibitors: the discovery of potent, ras nucleotide exchange inhibitors and the structural determination of a drug-protein complex. *Bioorg Med Chem,* 5**,** 125-33.

THOMAS, P. & SMART, T. G. 2005. HEK293 cell line: a vehicle for the expression of recombinant proteins. *J Pharmacol Toxicol Methods,* 51**,** 187-200.

THOMPSON, H. 2013. US National Cancer Institute's new Ras project targets an old foe. *Nat Med,* 19**,** 949-50.

TIEDE, C., BEDFORD, R., HESELTINE, S. J., SMITH, G., WIJETUNGA, I., ROSS, R., ALQALLAF, D., ROBERTS, A. P. E., BALLS, A., CURD, A., HUGHES, R. E., MARTIN, H., NEEDHAM, S. R., ZANETTI-DOMINGUES, L. C., SADIGH, Y., PEACOCK, T. P., TANG, A. A., GIBSON, N., KYLE, H., PLATT, G. W., INGRAM, N., TAYLOR, T., COLETTA, L. P., MANFIELD, I., KNOWLES, M., BELL, S., ESTEVES, F., MAQBOOL, A., PRASAD, R. K., DRINKHILL, M., BON, R. S., PATEL, V., GOODCHILD, S. A., MARTIN-FERNANDEZ, M., OWENS, R. J., NETTLESHIP, J. E., WEBB, M. E., HARRISON, M., LIPPIAT, J. D., PONNAMBALAM, S., PECKHAM, M., SMITH, A., FERRIGNO, P. K., JOHNSON, M., MCPHERSON, M. J. & TOMLINSON, D. C. 2017. Affimer proteins are versatile and renewable affinity reagents. *eLife,* 6**,** e24903.

TIEDE, C., TANG, A. A. S., DEACON, S. E., MANDAL, U., NETTLESHIP, J. E., OWEN, R. L., GEORGE, S. E., HARRISON, D. J., OWENS, R. J., TOMLINSON, D. C. & MCPHERSON, M. J. 2014. Adhiron: a stable and versatile peptide display scaffold for molecular recognition applications. *Protein Engineering Design & Selection,* 27**,** 145-155.

TOLCHER, A. W., SWEENEY, C. J., PAPADOPOULOS, K., PATNAIK, A., CHIOREAN, E. G., MITA, A. C., SANKHALA, K., FURFINE, E., GOKEMEIJER, J., IACONO, L., EATON, C., SILVER, B. A. & MITA, M. 2011. Phase I and pharmacokinetic study of CT-322 (BMS-844203), a targeted Adnectin inhibitor of VEGFR-2 based on a domain of human fibronectin. *Clin Cancer Res,* 17**,** 363-71.

TRAXLMAYR, M. W., KIEFER, J. D., SRINIVAS, R. R., LOBNER, E., TISDALE, A. W., MEHTA, N. K., YANG, N. J., TIDOR, B. & WITTRUP, K. D. 2016. Strong Enrichment of Aromatic Residues in Binding Sites from a Charge-neutralized Hyperthermostable Sso7d Scaffold Library. *J Biol Chem,* 291**,** 22496-22508.

TSAI, F. D., LOPES, M. S., ZHOU, M., COURT, H., PONCE, O., FIORDALISI, J. J., GIERUT, J. J., COX, A. D., HAIGIS, K. M. & PHILIPS, M. R. 2015. K-Ras4A splice variant is widely expressed in cancer and uses a hybrid membrane-targeting motif. *Proceedings of the National Academy of Sciences of the United States of America,* 112**,** 779-784.

TSE, E., LOBATO, M. N., FORSTER, A., TANAKA, T., CHUNG, G. T. & RABBITTS, T. H. 2002. Intracellular antibody capture technology: application to selection of intracellular antibodies recognising the BCR-ABL oncogenic protein. *J Mol Biol,* 317**,** 85-94.

TSOMAIA, N. 2015. Peptide therapeutics: Targeting the undruggable space. *European Journal of Medicinal Chemistry,* 94**,** 459-470.

TSUCHIDA, N., RYDER, T. & OHTSUBO, E. 1982. Nucleotide-Sequence of the Oncogene Encoding the P21 Transforming Protein of Kirsten Murine Sarcoma-Virus. *Science,* 217**,** 937-939.

UHLEN, M., ZHANG, C., LEE, S., SJOSTEDT, E., FAGERBERG, L., BIDKHORI, G., BENFEITAS, R., ARIF, M., LIU, Z., EDFORS, F., SANLI, K., VON FEILITZEN, K., OKSVOLD, P., LUNDBERG, E., HOBER, S., NILSSON, P., MATTSSON, J., SCHWENK, J. M., BRUNNSTROM, H., GLIMELIUS, B., SJOBLOM, T., EDQVIST, P. H., DJUREINOVIC, D., MICKE, P., LINDSKOG, C., MARDINOGLU, A. & PONTEN, F. 2017. A pathology atlas of the human cancer transcriptome. *Science,* 357.

UPADHYAYA, P., QIAN, Z., SELNER, N. G., CLIPPINGER, S. R., WU, Z., BRIESEWITZ, R. & PEI, D. 2015. Inhibition of Ras Signaling by Blocking Ras-Effector Interactions with Cyclic Peptides. *Angewandte Chemie-International Edition,* 54**,** 7602-7606.

VENKATESAN, K., RUAL, J. F., VAZQUEZ, A., STELZL, U., LEMMENS, I., HIROZANE-KISHIKAWA, T., HAO, T., ZENKNER, M., XIN, X., GOH, K. I., YILDIRIM, M. A., SIMONIS, N., HEINZMANN, K., GEBREAB, F., SAHALIE, J. M., CEVIK, S., SIMON, C., DE SMET, A. S., DANN, E., SMOLYAR, A., VINAYAGAM, A., YU, H., SZETO, D., BORICK, H., DRICOT, A., KLITGORD, N., MURRAY, R. R., LIN, C., LALOWSKI, M., TIMM, J., RAU, K., BOONE, C., BRAUN, P., CUSICK, M. E., ROTH, F. P., HILL, D. E., TAVERNIER, J., WANKER, E. E., BARABASI, A. L. & VIDAL,

M. 2009. An empirical framework for binary interactome mapping. *Nat Methods,* 6**,** 83-90.

VISINTIN, M., SETTANNI, G., MARITAN, A., GRAZIOSI, S., MARKS, J. D. & CATTANEO, A. 2002. The intracellular antibody capture technology (IACT): towards a consensus sequence for intracellular antibodies. *J Mol Biol,* 317**,** 73-83.

VO, U., VAJPAI, N., FLAVELL, L., BOBBY, R., BREEZE, A. L., EMBREY, K. J. & GOLOVANOV, A. P. 2016. Monitoring Ras Interactions with the Nucleotide Exchange Factor Son of Sevenless (Sos) Using Site-specific NMR Reporter Signals and Intrinsic Fluorescence. *Journal of Biological Chemistry,* 291**,** 1703-1718.

VOICE, J. K., KLEMKE, R. L., LE, A. & JACKSON, J. H. 1999. Four human Ras homologs differ in their abilities to activate Raf-1, induce transformation, and stimulate cell motility. *Journal of Biological Chemistry,* 274**,** 17164-17170.

WALDMANN, H., KARAGUNI, I.-M., CARPINTERO, M., GOURZOULIDOU, E., HERRMANN, C., BROCKMANN, C., OSCHKINAT, H. & MÜLLER, O. 2004. Sulindac-Derived Ras Pathway Inhibitors Target the Ras–Raf Interaction and Downstream Effectors in the Ras Pathway. *Angewandte Chemie International Edition,* 43**,** 454-458.

WALKER, B. J., STAN, G. V. & POLIZZI, K. M. 2017. Intracellular delivery of biologic therapeutics by bacterial secretion systems. *Expert Rev Mol Med,* 19**,** e6.

WANAPUN, D., KESTUR, U. S., KISSICK, D. J., SIMPSON, G. J. & TAYLOR, L. S. 2010. Selective detection and quantitation of organic molecule crystallization by second harmonic generation microscopy. *Anal Chem,* 82**,** 5425-32.

WANG, T., YU, H., HUGHES, N. W., LIU, B., KENDIRLI, A., KLEIN, K., CHEN, W. W., LANDER, E. S. & SABATINI, D. M. 2017. Gene Essentiality Profiling Reveals Gene Networks and Synthetic Lethal Interactions with Oncogenic Ras. *Cell,* 168**,** 890-903 e15.

WATKINS, A. M. & ARORA, P. S. 2015. Structure-based inhibition of protein–protein interactions. *European Journal of Medicinal Chemistry,* 94**,** 480-488.

WEISS, G. A., WATANABE, C. K., ZHONG, A., GODDARD, A. & SIDHU, S. S. 2000. Rapid mapping of protein functional epitopes by combinatorial alanine scanning. *Proc Natl Acad Sci U S A,* 97**,** 8950-4.

WELSCH, M. E., KAPLAN, A., CHAMBERS, J. M., STOKES, M. E., BOS, P. H., ZASK, A., ZHANG, Y., SANCHEZ-MARTIN, M.,

BADGLEY, M. A., HUANG, C. S., TRAN, T. H., AKKIRAJU, H., BROWN, L. M., NANDAKUMAR, R., CREMERS, S., YANG, W. S., TONG, L., OLIVE, K. P., FERRANDO, A. & STOCKWELL, B. R. 2017. Multivalent Small-Molecule Pan-RAS Inhibitors. *Cell,* 168**,** 878-+.

WENNERBERG, K., ROSSMAN, K. L. & DER, C. J. 2005. The Ras superfamily at a glance. *J Cell Sci,* 118**,** 843-6.

WHEELER, Y. Y., CHEN, S. Y. & SANE, D. C. 2003. Intrabody and intrakine strategies for molecular therapy. *Mol Ther,* 8**,** 355-66.

WILLUMSEN, B. M., CHRISTENSEN, A., HUBBERT, N. L., PAPAGEORGE, A. G. & LOWY, D. R. 1984. The P21 Ras C-Terminus Is Required for Transformation and Membrane Association. *Nature,* 310**,** 583-586.

WINTER, J. J., ANDERSON, M., BLADES, K., BRASSINGTON, C., BREEZE, A. L., CHRESTA, C., EMBREY, K., FAIRLEY, G., FAULDER, P., FINLAY, M. R., KETTLE, J. G., NOWAK, T., OVERMAN, R., PATEL, S. J., PERKINS, P., SPADOLA, L., TART, J., TUCKER, J. A. & WRIGLEY, G. 2015. Small molecule binding sites on the Ras:SOS complex can be exploited for inhibition of Ras activation. *J Med Chem,* 58**,** 2265-74.

WITTINGHOFER, A. 2014. *Ras Superfamily Small G Proteins: Biology and Mechanisms 1*, Springer-Verlag Wien.

WLODAWER, A., MINOR, W., DAUTER, Z. & JASKOLSKI, M. 2008. Protein crystallography for non-crystallographers, or how to get the best (but not more) from published macromolecular structures. *Febs j,* 275**,** 1-21.

WOJCIK, J., HANTSCHEL, O., GREBIEN, F., KAUPE, I., BENNETT, K. L., BARKINGE, J., JONES, R. B., KOIDE, A., SUPERTI-FURGA, G. & KOIDE, S. 2010. A potent and highly specific FN3 monobody inhibitor of the Abl SH2 domain. *Nature Structural &Amp; Molecular Biology,* 17**,** 519.

WOLF, S., SOUIED, E. H., MAUGET-FAYSSE, M., DEVIN, F., PATEL, M., WOLF-SCHNURRBUSCH, U. E., STUMPP, M. & GROUP, M. P. W. A. M. D. S. 2011. Phase I Mp0112 Wet AMD Study: Results Of A Single Escalating Dose Study With DARPin® MP0112 In Wet AMD. *Investigative Ophthalmology & Visual Science,* 52**,** 1655-1655.

WURCH, T., PIERRE, A. & DEPIL, S. 2012. Novel protein scaffolds as emerging therapeutic proteins: from discovery to clinical proof-of-concept. *Trends in Biotechnology,* 30**,** 575-582.

XIE, C., TIEDE, C., ZHANG, X., WANG, C., LI, Z., XU, X., MCPHERSON, M. J., TOMLINSON, D. C. & XU, W. 2017a.

Development of an Affimer-antibody combined immunological diagnosis kit for glypican-3. *Sci Rep,* 7**,** 9608.

XIE, C. M., TIEDE, C., ZHANG, X. Y., WANG, C. R., LI, Z. X., XU, X., MCPHERSON, M. J., TOMLINSON, D. C. & XU, W. W. 2017b. Development of an Affimerantibody combined immunological diagnosis kit for glypican-3. *Scientific Reports,* 7.

XIONG, Y., LU, J., HUNTER, J., LI, L. B., SCOTT, D., CHOI, H. G., LIM, S. M., MANANDHAR, A., GONDI, S., SIM, T., WESTOVER, K. D. & GRAY, N. S. 2017. Covalent Guanosine Mimetic Inhibitors of G12C KRAS. *Acs Medicinal Chemistry Letters,* 8**,** 61-66.

XU, S., LONG, B. N., BORIS, G. H., CHEN, A., NI, S. & KENNEDY, M. A. 2017. Structural insight into the rearrangement of the switch I region in GTP-bound G12A K-Ras. *Acta Crystallogr D Struct Biol,* 73**,** 970-984.

YAN, J., ROY, S., APOLLONI, A., LANE, A. & HANCOCK, J. F. 1998. Ras isoforms vary in their ability to activate Raf-1 and phosphoinositide 3-kinase. *Journal of Biological Chemistry,* 273**,** 24052-24056.

YANG, S., WANG, X., CONTINO, G., LIESA, M., SAHIN, E., YING, H., BAUSE, A., LI, Y., STOMMEL, J. M., DELL'ANTONIO, G., MAUTNER, J., TONON, G., HAIGIS, M., SHIRIHAI, O. S., DOGLIONI, C., BARDEESY, N. & KIMMELMAN, A. C. 2011. Pancreatic cancers require autophagy for tumor growth. *Genes Dev,* 25**,** 717-29.

YAO, Z., TORRES, N. M., TAO, A., GAO, Y., LUO, L., LI, Q., DE STANCHINA, E., ABDEL-WAHAB, O., SOLIT, D. B., POULIKAKOS, P. I. & ROSEN, N. 2015. BRAF Mutants Evade ERK-Dependent Feedback by Different Mechanisms that Determine Their Sensitivity to Pharmacologic Inhibition. *Cancer cell,* 28**,** 370-383.

YING, H., KIMMELMAN, A. C., LYSSIOTIS, C. A., HUA, S., CHU, G. C., FLETCHER-SANANIKONE, E., LOCASALE, J. W., SON, J., ZHANG, H., COLOFF, J. L., YAN, H., WANG, W., CHEN, S., VIALE, A., ZHENG, H., PAIK, J. H., LIM, C., GUIMARAES, A. R., MARTIN, E. S., CHANG, J., HEZEL, A. F., PERRY, S. R., HU, J., GAN, B., XIAO, Y., ASARA, J. M., WEISSLEDER, R., WANG, Y. A., CHIN, L., CANTLEY, L. C. & DEPINHO, R. A. 2012. Oncogenic Kras maintains pancreatic tumors through regulation of anabolic glucose metabolism. *Cell,* 149**,** 656-70.

YU, H. 1999. Extending the size limit of protein nuclear magnetic resonance. *Proceedings of the National Academy of Sciences,* 96**,** 332-334.

YUAN, Z., BAILEY, T. L. & TEASDALE, R. D. 2005. Prediction of protein B-factor profiles. *Proteins,* 58**,** 905-12.

ZEEH, J. C., ZEGHOUF, M., GRAUFFEL, C., GUIBERT, B., MARTIN, E., DEJAEGERE, A. & CHERFILS, J. 2006. Dual specificity of the interfacial inhibitor brefeldin a for arf proteins and sec7 domains. *J Biol Chem,* 281**,** 11805-14.

ZENG, M., LU, J., LI, L., FERU, F., QUAN, C., GERO, T. W., FICARRO, S. B., XIONG, Y., AMBROGIO, C., PARANAL, R. M., CATALANO, M., SHAO, J., WONG, K. K., MARTO, J. A., FISCHER, E. S., JANNE, P. A., SCOTT, D. A., WESTOVER, K. D. & GRAY, N. S. 2017. Potent and Selective Covalent Quinazoline Inhibitors of KRAS G12C. *Cell Chem Biol,* 24**,** 1005-1016 e3.

ZIMMERMANN, G., PAPKE, B., ISMAIL, S., VARTAK, N., CHANDRA, A., HOFFMANN, M., HAHN, S. A., TRIOLA, G., WITTINGHOFER, A., BASTIAENS, P. I. & WALDMANN, H. 2013. Small molecule inhibition of the KRAS-PDEdelta interaction impairs oncogenic KRAS signalling. *Nature,* 497**,** 638-42.

ZLOMISLIC, M. R., CORRADI, V. & TIELEMAN, D. P. 2011. Protein Modeling. *Reviews in Cell Biology and Molecular Medicine.*